The transcription factor STAT5 catalyzes Mannich ligation reactions yielding inhibitors of leukemic cell proliferation

Inaugural-Dissertation

to obtain the academic degree

Doctor rerum naturalium (Dr. rer. nat.)

submitted to the Department of Biology, Chemistry and Pharmacy of
Freie Universität Berlin

by

Ee Lin Wong

From Kuala Lumpur, Malaysia

2019

This thesis was done from December 2013 to June 2017 under the supervision of Prof. Dr. Jörg Rademann, at the Institute of Pharmacy, Freie Universität Berlin.

Research of the present study was conducted from December 2013 till June 2017 under the supervision of Prof. Dr. Jörg Rademann at the Institute of Pharmacy of the Freie Universität Berlin.

1st reviewer : Prof. Dr. Jörg Rademann
2nd reviewer : Prof. Dr. Gerhard Wolber

Date of defense: 04-12-2019

Statement

I hereby declare that I completed the doctoral thesis independently based on the stated resources and aids. I have not applied for a doctoral degree elsewhere and do not have a corresponding doctoral degree. I have not submitted the doctoral thesis, or parts of it, to another academic institution and the thesis has not been accepted or rejected. Furthermore, I declare that no collaboration with commercial doctoral degree supervisors took place, and that the principles of Freie Universität Berlin for ensuring good academic practice were abided by.

Date / signature

Parts of the present work have already been published in:

Wong, E.L., Nawrotzky, E., Arkona, C., Kim, B.G., Beligny, S., Wang, X., Wagner, S., Lisurek, M., Carstanjen, D. and Rademann, J. The transcription factor STAT5 catalyzes Mannich ligation reactions yielding inhibitors of leukemic cell proliferation. *Nat. Commun.* **10**, 66 (2019).

Acknowledgements

My deep and sincere gratitude goes first to my supervisor, Prof. Dr. Jörg Rademann, who introduced me to the field of medicinal chemistry and drug discovery and expertly guided me through my research studies with encouragement support. Our discussions have been enlightening and motivating, and this thesis would not have been possible without your openness to new idea and new experiments which afforded me the opportunity to develop my scientific curiosity. I would also like to express my sincere appreciation to Berlin School of Integrative Oncology (BSIO) for their generous financial support. I must also thank members of my PhD committee: Prof. Dr. Gerhard Wolber for generously allowing me to explore the field of computational drug design by providing accessibility of molecular modelling software and Dr. Stephan Mathas for having the foresight that my thesis was a viable PhD project.

Spending majority of my time in the lab like most of the PhD. students do will not be fun without a bunch of friendly coworkers and conducive working environment. Firstly, I would like to thank Dr. Christoph Arkona for sharing his intriguing view in Science and also his life experiences. I am especially grateful to Silke for going beyond the role of research assistant, often acting as a friend, teacher and above all, a listener of all the difficulties of graduate school and life-in-general. I would also like to express my gratitude to past and present members of the Rademann's lab: most notably Eric, Christina, Sebastian, Iwona, Franzi, Matteo, Mike, Lisa, Joanna, Caro, Yuwen, Marc, Xinning, Enaam, Daniel, Stefan, Péter and Markus. Some of them have contributed scientifically to this thesis but all of them have made it fun to work in the lab.

Other people who I must sincerely acknowledge for contributing to this thesis are Isabel for her guidance on Fluorescence Polarization Assay, Eric and Thomy for

For my parents, who embrace my quirkiness and never quit supporting me.

Abstract

Biological processes are often regulated by signal transduction pathway via transcription factor through protein-protein interactions (PPIs). Aberrant activation of transcription factor deregulates the cell signaling pathway which contributes to disease progression. Cancer is well characterized as a result of over activation of transcription factor and/or loss of an essential protein-protein interaction. Therefore, transcription factor have become attractive molecular target for drug development.

Protein-templated fragment ligations have been established as a powerful method for the assembly and detection of optimized protein ligands. Initially developed for reversible ligations, the method has been expanded to irreversible reactions enabling the formation of super-additive fragment combinations. In this thesis, protein-induced Mannich ligations are introduced and discovered as a biocatalytic reaction furnishing inhibitors of the transcription factor STAT5. STAT5 protein was employed to catalyze multicomponent reactions of a phosphate mimetic, formaldehyde, and 1H-tetrazoles yielding protein ligands with greatly increased binding affinity and ligand efficiency. Reactions are induced under physiological conditions selectively by native STAT5 but not by other proteins. Formation of ligation products and (auto-) inhibition of the reaction are quantified and the mechanism is investigated.

Inhibitors assembled by STAT5 were further validated using functional biochemical assay and were proven to block specifically the phosphorylation of this protein in a cellular model of acute myeloid leukemia (AML), DNA-binding of STAT5 dimers, expression of downstream targets of the transcription factor, and the proliferation

of cancer cells in mice. In addition, STAT5 inhibitors also exert strong synergistic effect with tyrosine kinase inhibitor, PKC412 in targeting leukemic cells.

Throughout our effort in establishing highly selective STAT5 inhibitor, a first class of inhibitors that assembled through protein induced Mannich ligation reported to date have been successfully identified. STAT5 assembled inhibitors have proven to exhibit favorable potency and selectivity profile against STAT5 and possess the potential to become candidate for combination therapy with tyrosine kinase inhibitor for pre-clinical trials as STAT5 targeted therapeutic. Last but not least, these small molecules STAT5 inhibitors well served as a research tool to study the effect of knocking down of STAT5 function at the protein level on cancer prognosis and progression.

Zusammenfassung

Biologische Prozesse werden häufig über Signaltransduktionswege durch Transkriptionsfaktoren gesteuert und werden durch Protein-Protein-Interaktion (PPIs) vermittelt. Die abweichende Aktivierung eines Transkriptionsfaktors verändert den zellulären Signalweg, was zur Entwicklung oder zum Fortschreiten von Krankheiten beitragen kann. Krebs ist gut charakterisiert als das Ergebnis einer Überaktivierung von Transkriptionsfaktoren und/oder des Verlustes von essentiellen Protein-Protein-Interaktionen. Daher sind Transkriptionsfaktoren ein attraktives molekulares Ziel für die Arzneimittelentwicklung

Protein-templierte Fragment-Ligationen wurden als leistungsfähiges Verfahren zur Gewinnung und zur Erkennung von optimierten Protein-Liganden eingeführt. Ursprünglich entwickelt für reversible Ligationen wurde die Methode auf irreversible Reaktionen ausgeweitet und ermöglicht die Bildung von super-additiven Fragmentkombinationen. In dieser Arbeit werden protein-induzierte Mannich-Ligationen als eine biokatalytische Reaktion entdeckt, die Inhibitoren für den Transkriptionsfaktor STAT5 liefern. STAT5-Protein katalysiert Multikomponenten-Reaktionen eines Phosphat-Mimetikums, von Formaldehyd und von 1*H*-Tetrazolen, die Proteinliganden mit stark erhöhter Bindungsaffinität und Ligandeneffizienz liefern. Reaktionen werden unter physiologischen Bedingungen selektiv durch natives STAT5, aber nicht durch andere Proteine ausgelöst. Die Bildung von Ligationsprodukten und die (Auto-)Inhibition der Reaktion werden gemessen und der Mechanismus wird erforscht.

Durch STAT5 gebildeten Inhibitoren werden weiter in funktionellen biochemischen Assays validiert und es wird gezeigt, dass sie spezifisch die Phosphorylierung dieses Proteins in einem zellulären Modell der akuten myeloischen

Leukämie (AML), die DNA-Bindung von STAT5-Dimern, die Expression von Zielproteinen des Transkriptionsfaktors und die Proliferation von Krebszellen in Mäusen blockieren. Zusätzlich haben STAT5-Inhibitoren zusammen mit dem Tyrosinkinase-Inhibitor PKC412 eine starke synergistische Wirkung auf Leukämiezellen.

Wir haben die erste bisher bekannte Klasse von Inhibitoren identifiziert, die durch eine Protein-induzierte Mannich-Ligation gebildet wurden. Die durch STAT5 entstandenen Inhibitoren zeigen günstige Wirkungen und ein vorteilhaftes Selektivitätsprofil gegenüber STAT5 und besitzen das Potential, Kandidaten für eine Kombinationstherapie mit Tyrosinkinase-Inhibitoren für vorklinische Versuche als gezielte STAT5-Therapien zu werden.

Zu guter Letzt dienten diese kleinen STAT5 Inhibitor-Moleküle als geeignete Forschungswerkzeuge, um die Effekte der Ausschaltung von STAT5-Funktionen auf die Prognose und den Verlauf von Krebserkrankungen zu untersuchen.

Contents

Chapter 1

Introduction

Scientists have been on a long mission to halt cancer progression and hunt down the most effective remedies to cure cancer. Despite many new anti-cancer agents have been designed to improve the current treatment regime, there is still a gap to be filled in targeted drug therapy. It is cleared that the future of cancer treatments is directing towards specific treatment which target different cancer pathways, rather than a universally applicable therapy across cancer.

Traditional universal chemotherapeutic drugs are well described as jack of all trades but master of none due to their lack of specificity. Research findings have proven that cancer cells can outsmart universally applicable therapy such as tyrosine kinase inhibitor (TKI) by developing genetic alterations, resulting in DNA and protein mutations in tumor cells. This eventually leads to the development of chemotherapeutic resistance.[2,3]

1.1   Overview of traditional chemotherapeutic approaches and their limitations

Anticancer agents can be classified according to their biological target either from antimetabolites, DNA targeting agent or tumor targeted monoclonal antibodies (mAbs), just to name a few. Antimetabolites have similar structure to essential metabolites but are limited to participate in the biochemical process or reaction. They are designed to replace essential metabolites and their structures are generally based on pyrimidine or purine DNA bases or folic acid.[4] This class of chemotherapeutic drugs inhibits and deplete the important building block required for DNA synthesis. One of the most commonly used antimetabolites in clinical practice is 5-fluorouracil (5-FU).[5] It is designed through bioisosteric replacement by substituting one of the key hydrogen in uracil to fluorine. This bioisosteric replacement makes 5-FU a powerful cancer drug. It is administered as a prodrug which is then converted to active metabolite 5-fluorodeoxyuridine monophosphate and is proven to irreversibly inhibits the enzyme thymidylate synthase that play vital roles in the DNA synthesis (Figure

1.0).[6] Over the years, there has been significant development of new antimetabolites which improve and expand this class of chemotherapeutic agents ranging from gemcitabine, capecitabine, permetrexed, fludarabine and to the most recent FDA approved pralatrexate.[7]

Although antimetabolites are widely used as chemotherapeutic agents in the clinic to target cellular metabolism, their anti-cancer effects are exhibited mainly through cytotoxic effect. Patients that undergo antimetabolites-based chemotherapeutic regime suffer from severe side effects.[6] Previous studies have proven that the treatment outcome of antimetabolites in patients varies dramatically and the causes of heterogeneity are yet to be found.[8]
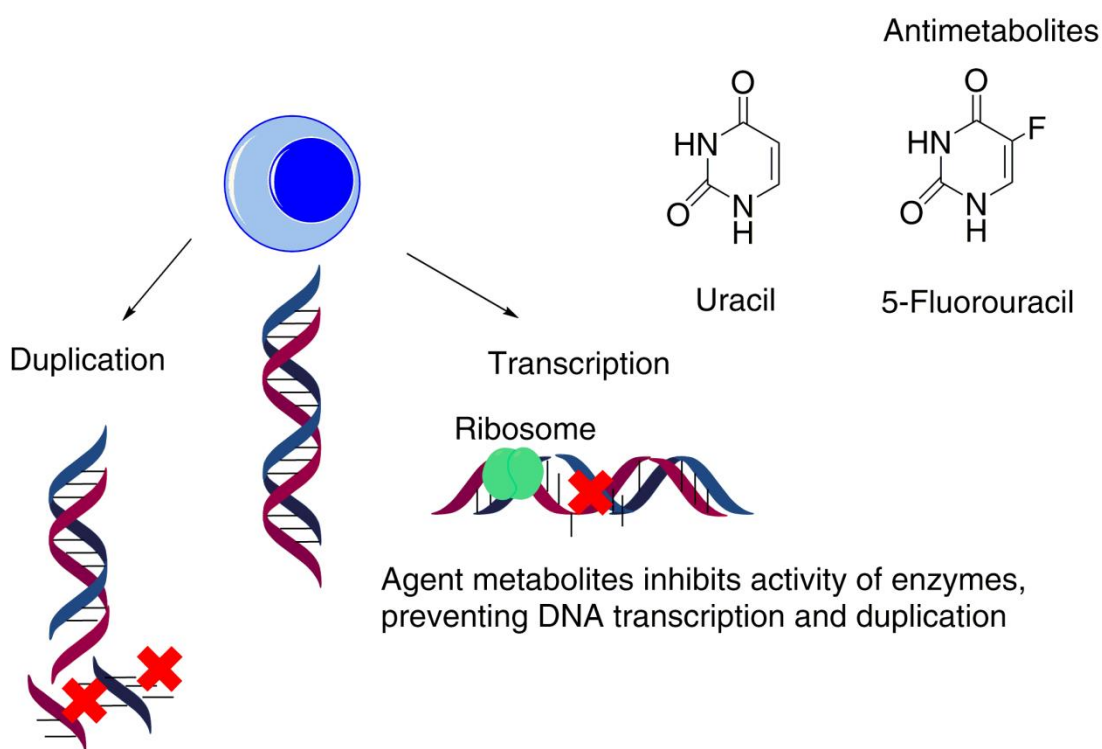
Figure 1.0: Antimetabolites interfere with normal synthesis of nucleic acid and prevent the DNA duplication and transcription in rapidly dividing cancer cells.[3]

Another class of chemotherapeutic agents involves targeting DNA and their mode of action heavily depends on the exact interactions with DNA. This class of anti-cancer agents are classified into intercalators, minor groove binding agents, alkylating agents and antimitotic agents.[9] Doxorubicin and daunomycin are two intercalators that are commonly used in treating cancer for many years. They are able to form stable, non-covalent complexes with DNA which inhibit the availability of DNA for replication and transcription around the point of intercalation. These agents heavily rely on the increased replication of rapidly dividing cells for their anti-cancer action and are generally non selective.[10] This has resulted in adverse side effects and general cytotoxicity in patient but these drugs are still being used in clinical setting until a safer treatment alternative is identified.[11]
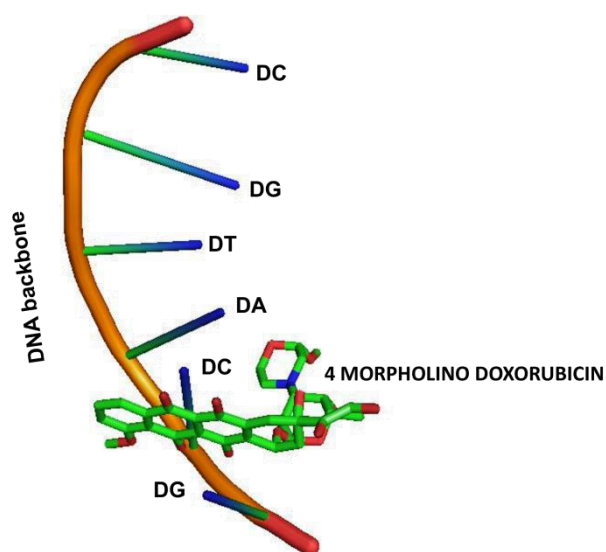
Figure 1.1: Crystal structure of the anti-cancer drug 4-morpholino-doxorubicin complexed with DNA sequence D (CGTACG) showing the mode of action of this DNA-binding drug via DNA-intercalation.[11]

On the other hand, minor groove binding agents bind to the sugar phosphate backbone of the DNA double helix. It started to gain interest recently when trabectedin, a marine natural product, which binds to the minor groove of DNA backbones was approved in Europe for anti-cancer chemotherapy.[12] Similarly, this class of drugs leads to severe toxicity due to low drug selectivity and specificity. Unlike other minor groove binding agents, trabectedin exhibits antitumor activity in multidrug resistant tumors and was found to selectively bind the AT-rich region of DNA.[13]

The long term effects of universal chemotherapeutic drugs which lack target specificity allow cancer cell to manipulate their genomes and metabolism to halt further drug influx and increase efflux of accumulated drugs. This escape mechanism is also known as "the neostrategy of cancer cells and tissues". Chemotherapy resistance occured due to several host or tumor related factors whereby genes that handle efflux pumps will be up regulated to reduce drug accumulation inside malignant cells. Surprisingly, drug-target interaction could also evolve somatically to promote drug resistancy. For example, long term chemotherapeutic treatment with thymidylate synthetase inhibitor, 5-fluorouracil lead to over expression of thymidylate synthetase genes postulating mode of resistance.

Another limitation of universal chemotherapeutic drugs is the possibility of activation or amplification of alternative pathway. As signalling pathways are complex network, blocking one pathway in cell will turn on the associated alternative pathway to maintain tumor cell proliferation and survival. Cancer cell will activate alternative pathway to establish chemoresistance when upstream targets are blocked in the cell signaling pathway by conventional universal drugs. Current treatments still rely on universal chemotherapeutic drugs but unfortunately, local recurrence and metastasis occurs in approximately 40% of patients. Therefore, new and targeted therapies are urgently needed for better cancer treatment regime. [8,14]

1.2 Establishing fragment-based approaches

Over the past decade, drug discovery experts and research scientists are making effort in finding alternative starting point for the discovery of high quality lead candidates that is less time consuming. A key approach that has garnered the most interest among researchers is the fragment-based drug discovery (FBDD) which potentially acts as an alternative starting point for lead discovery in drug development.

Fragment based drug discovery undertakes a rather different route compared to the conventional approaches such as high throughput screening (HTS). In FBDD, a small collection of very small compounds that comprised of > 20 non-hydrogen atoms or "heavy atoms" was employed which furnish lower number but better streamlined possible fragments hits. Therefore, fragments libraries are comprised of few thousand of miniscule molecules.[15,16]

Small fragments are much more favorable because they form fewer interactions with a protein target thus are foreseen to bind easily to more sites on a wide range of targets, which in turn translates to a greater number of "hits". On the other hand, larger molecules are less favorable as they pose greater molecular complexity and greater interactions with protein target as this limits the number of hits found.[17] To put it into perspective- it is preferable to start with a small, weak affinity hit as it provides better structural insight for lead optimization in comparison to a larger, more potent compound.[18] (Figure 1.2)
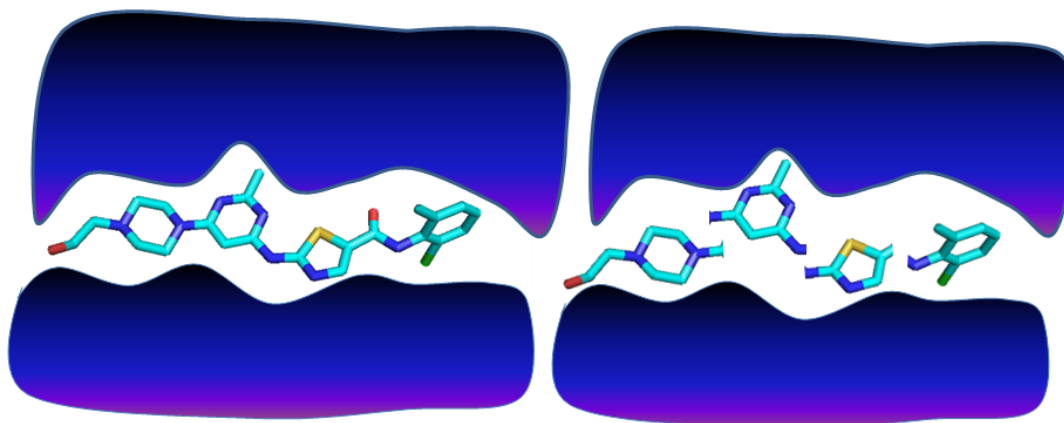
Figure 1.2: Comparison of HTS and fragment binding to a protein target.[18,19]

The fragment based approach was initially introduced on a theoretical basis before FBDD was put into practice physically. The idea was first tested using computational and structural biology method to study the binding of small molecules or fragments to the active site of protein. This theoretical findings was strengthen when studies have shown that intrinsic binding energy of each functional groups can be determined as " goodness of fit" of a drug to its molecular target.[15,19]

Fragment based method was first practically applied in the field of drug discovery in 1996 by two Abbott scientists, Fesik and Halduk. Both of them used a nuclear magnetic resonance (NMR)-based method to detect and identify fragments that could possibly bind to the proximal subsites of the targeted protein.[20] In the following years, researchers have jumped on the bandwagon of X-ray crystallographic screening for clinical compound discovery. Both methods have been tailored to be widely applicable in drug discovery field by numerous pharmaceutical companies. [18]

Upon primary fragments detection, they proceed with further optimization and fragment linking by attaching additional functional groups to achieve high affinity ligands.

Medicinal chemist applied three main methods for fragment elaboration, i.e. fragment

growing, linking and merging to improve the primary fragments.[21](Figure 1.3)
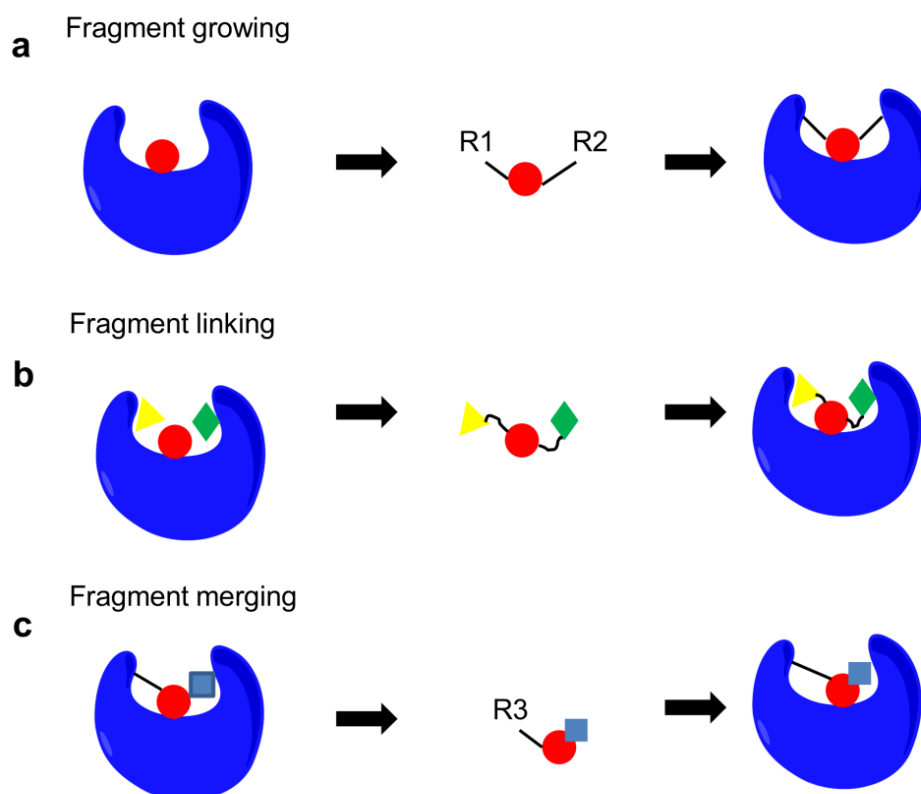
Figure 1.3: Fragment elaboration methods commonly applied for fragment based drug design.

Upon identification of suitable binding fragment in the binding pocket of a targeted protein,

fragment can be modified to increase the receptor-ligand interactions. **(a)** fragment growing is

a process of expanding the initial fragment to increase lead likability in order to enhance

binding affinity of ligand .(b) fragment linking is useful in order to link multiple fragments

that portray affinity towards different sub regions in the protein binding pocket. By

introducing linkers to connect potential fragment hits increase the lead likability and novel

class of compound can be discovered. **c**, fragment merging started off with a known lead that

partially occupy the binding pocket. The initial lead is used as a probe to screen for suitable

fragments to fit the remaining space in the protein binding pocket. Linkers can then be used to merge both fragments to enhance the strength of receptor-ligand interactions.[18,22]

FBDD has been driven by several screening technologies but its application in more complex biological targets remains a challenge[22] (Figure 1.4). One of the biggest issue that limit the development and full exploitation of fragment-based methods in drug discovery is the detection of protein-binding fragments which require further advancement in biophysical techniques. So often, protein binding fragments are present in high concentration due to their low affinity in nature which in turn saturates the detection signal. The detectability and identification of fragment hits heavily depends on the sensitivity and robustness of the biophysical techniques used. Therefore, several other approaches have been adapted from FBDD besides NMR and X-ray-crystallography.[20] For instance, there are assays that apply high protein concentrations to overcome the bottle neck of ligand saturation such as fluorescence anisotropy or saturation transfer difference (STD) NMR.
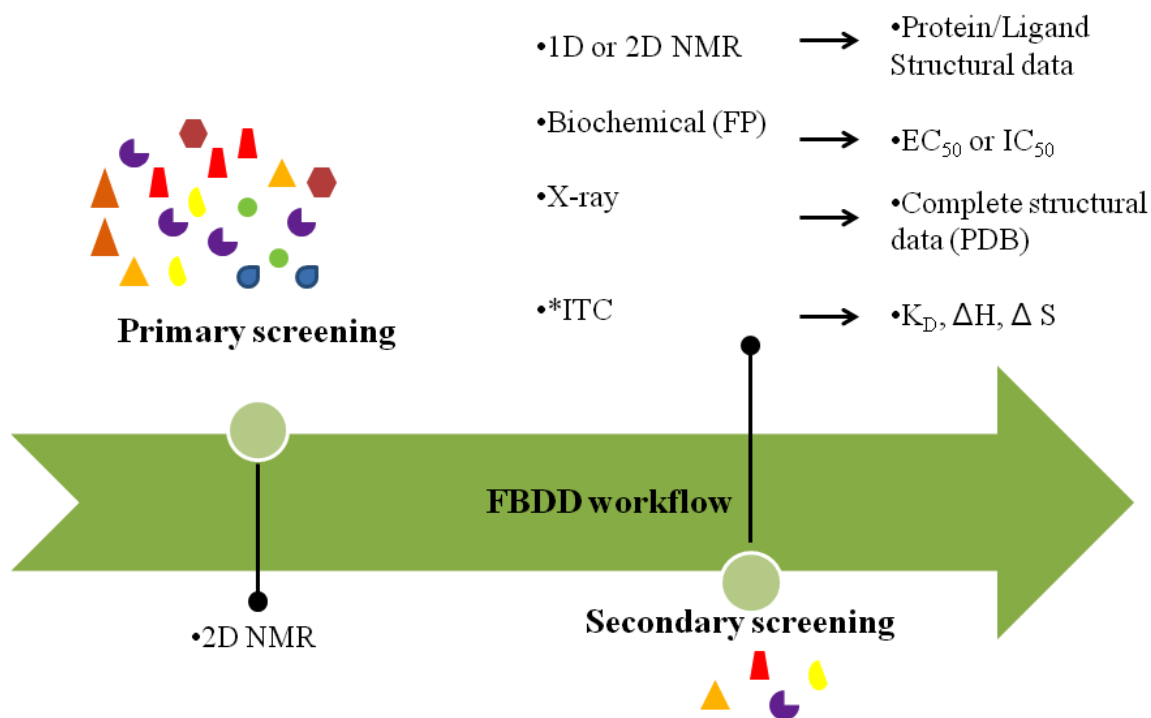
Figure 1.4: A glimpse on the typical FBDD screening workflow. The workflow composes of important route in both primary and secondary screening in the drug discovery journey. The hierarchy is provide an overview but does not represent all drug discovery programs. Screening options at the primary and secondary screening stages were shown in bullet points. Fragments proceeded to secondary screening will eventually acquired structural information using NMR or X-ray crystallography to be progressed for hit generation. In secondary screening, fragment hits will be ranked using ITC technique (*).[23]

Over the last decade, several approaches such as mass spectrometry (LC-MS)[24-27], nuclear magnetic resonance (NMR)[28-30], saturation transfer difference-NMR (STD-NMR), microscale thermophoresis (MST), X-ray crystallography[31-33], isothermal titration calorimetry[34], differential scanning fluorimetry (DSF)[35] a.k.a thermal shift assay (TSA), fluorescence polarization (FP)[36,37] and surface plasmon resonance (SPR)[38] have been seen as core technologies in numerous pharmaceutical and biotechnology-based industries settings for the identification of low affinity fragment compounds.[39] (Figure 1.5)
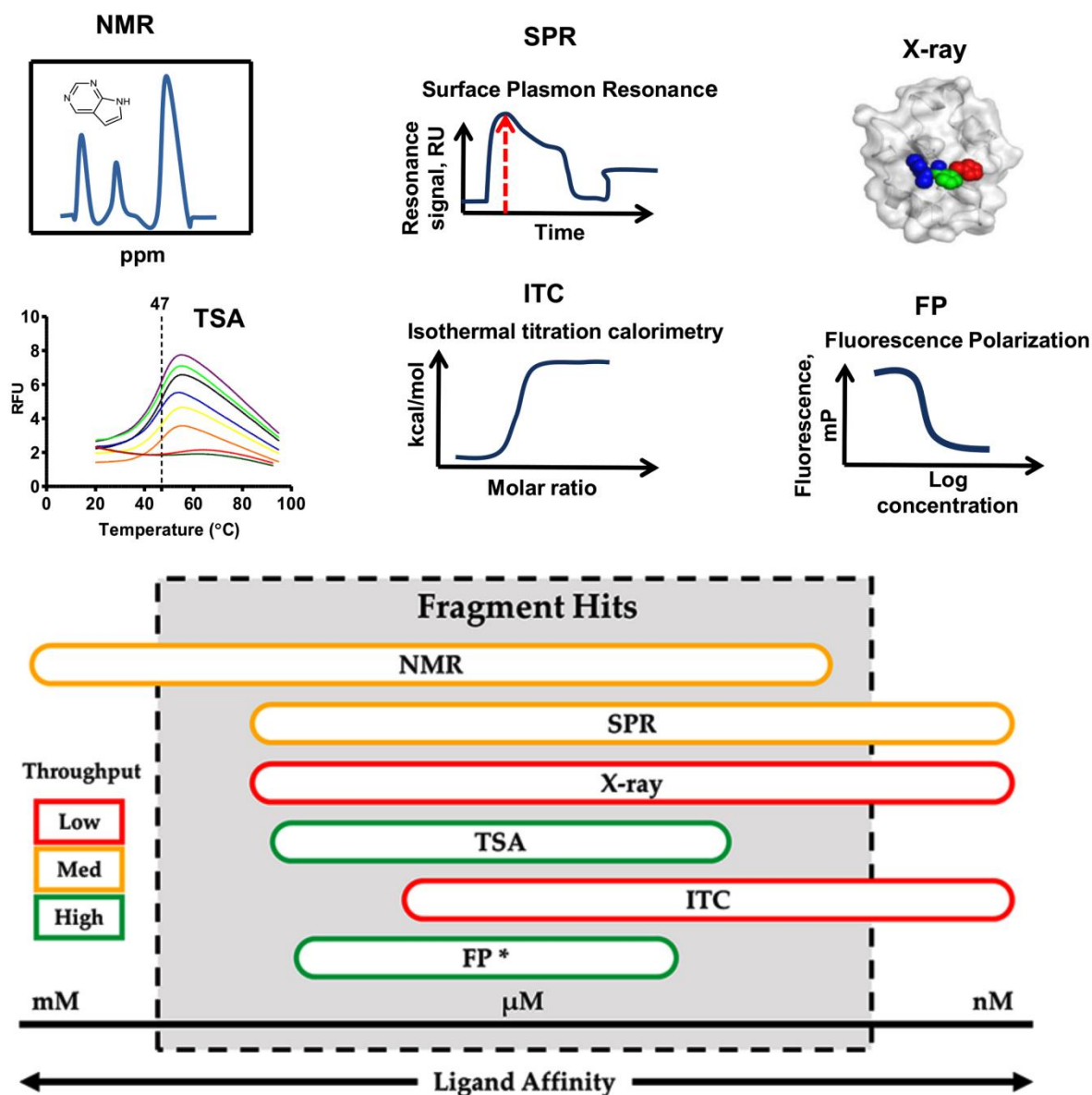
Figure 1.5: Biophysical techniques fitted to a range of fragment affinities. Each technique was ranked based on how often they were applied in FBDD. NMR is mostly applicable in medium-throughput method, but can also be considered in low throughput based method depending on the protein availability. Another biochemical technique that has broad application in FBDD is highly dependent on probe affinity and most suitable to be used for high throughput screening (HTS).[23]

1.3 Protein Templated Fragment Ligation

Protein Templated Fragment Ligation (PTFL) is defined as chemical reactions that involved two or more small molecules / fragments that employ the protein's surface as catalyst to generate protein ligands with higher binding affinity. The chemical reactions in the definition include both reversible and irreversible ligation reactions. (Figure 1.6) In reversible PTFL, chemically reactive small fragments adapt on the molecular level and optimize to form thermodynamically favoured ligand through recleavage of covalent chemical bonds. This adaptive and self-optimizing system is considered as an example of molecular learning.. It is often observed that reversible ligation reaction yield unstable products before isolation but could achieve better stability after isolation while products of irreversible ligation reaction are mostly stable. PTFL has been widely applied in FBDD by combining both chemical synthesis of protein ligands and protein activity modulation in one single step[24,40-42] to achieve both time and cost efficiency.
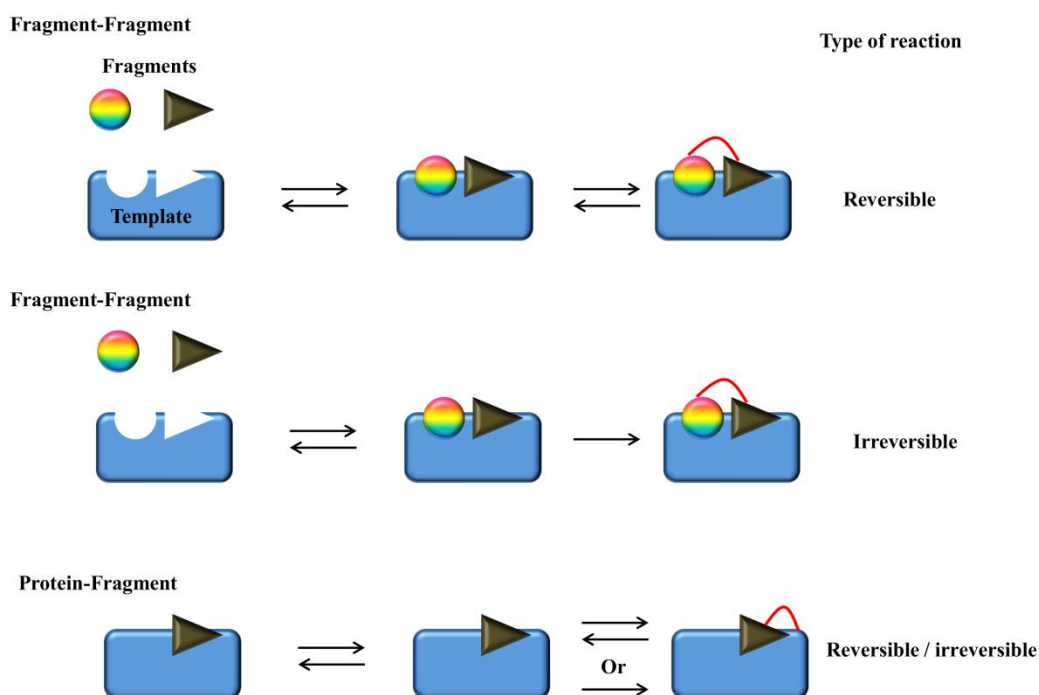
Figure 1.6: Protein template fragment ligation methods for ligand discovery. Binding of small fragments to protein binding site reversibly escalate the formation of reversible or irreversible chemical bonding. On a side note, bound fragment can interact with the protein template itself by forming reversible/ irreversible chemical reaction. [43]

Fragment based ligation method has an added advantage in ligand detection due to their higher affinity of the fragments ligation product formed. In principle, starting fragments concentration is presence at a lower concentration to achieve partial inhibition which can then be saturated through the latter formation of stronger binding ligation product. This has overcome the shortcomings of concentration limits in other fragment assays as even low affinity fragments can be identified. Undoubtedly, challenges still remain due to several reasons. Fragment ligation method yields higher binding affinity ligation products than the starting fragments and their formation are auto inhibitory. Thus, the concentration of protein template added has become the limiting factor in ligation product formation. Eventually, the fragment ligation product needs to be fished out from a pool of excess non reacted fragments.[40]

Another challenge that has been widely discussed arises from the reactivity of the starting fragments in the fragment ligation assays. In some occasion, the less reactive fragments acquired activation by electrophiles in fragment ligation assay. Unavoidably, fragments might react with protein nucleophiles as reaction partner which intentionally serve as a template for the assays. Consequently, control tests need to be carried out to distinguish the effect of one fragment from the effect of a fragment combination to avoid false positive results. In addition, it is also advisable to carry out independent secondary assays to eliminate false positive hit fragments.[40]

1.4 Detection of fragment binding and fragment ligation product

In recent years, medicinal chemist has been exploring the possibility of directly examined the bioactivity of fragment combination prior to product isolation and purification. So far, several bioassays have been developed to adapt bioactivity-guided fragment ligations that include both substrate competition and substrate enhancement assays. Substrate competition assay require the presence of a fluorogenic or chromogenic substrate such as FRET (Fluorescence Resonance Energy Transfer) substrate to be replaced by the fragment combination product. On the other hand, in substrate enhancement assay the substrate affinity is increased via reversible ligation leading to higher turnover rate of the substrate. Our group has reported the application of substrate competition assay in SARS coronavirus main protease for the discovery of potent non-peptidic inhibitors via dynamic ligation screening (DLS). (Figure 1.7) A fluorogenic tetrapeptidyl-7-amino-4-methyl courmarinyl 2-acetamide (AMCA) was used as a fluorogenic substrate to detect bioactive fragment combination.
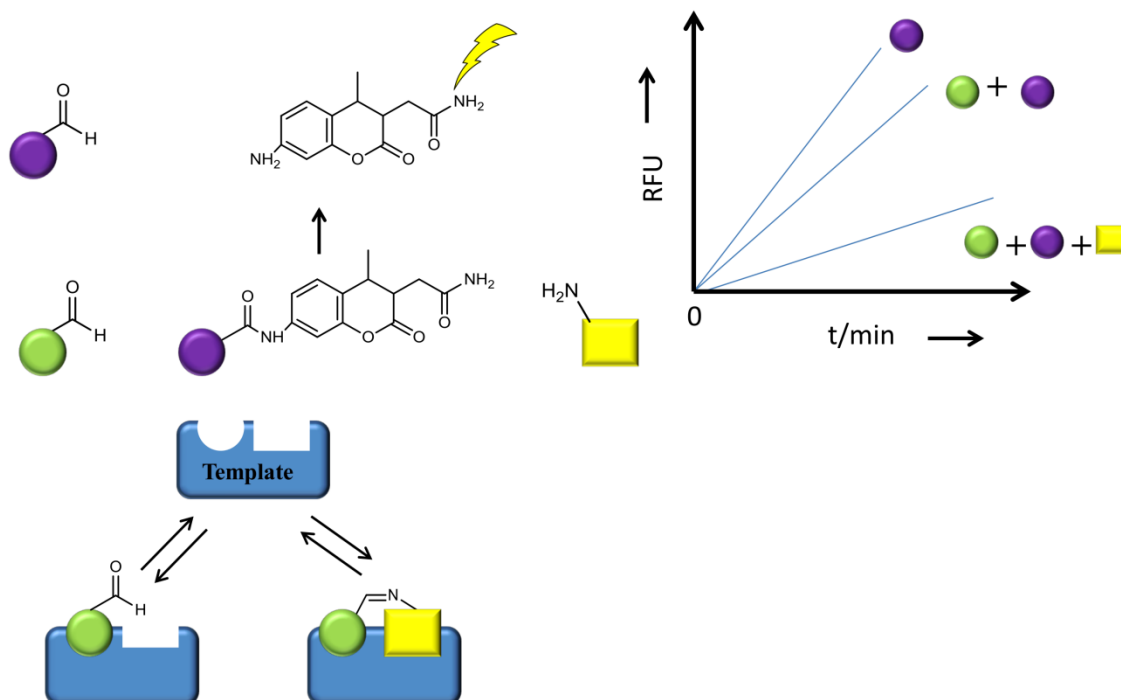
Figure 1.7: Schematic representation of dynamic ligation screening. Aldehyde and amine fragments react in an equilibrium reaction to form imine ligation product. The binding of

fragments into neighbouring pockets of the target protein (template) shifted the equilibrium towards imine ligation product formation, which known as template-assisted fragment ligation. Both fragments and fragment ligation product will then compete with the fluorescence substrate for protein binding for the enzyme. The formation of a fragment ligation product is detected by a significant reduction in substrate turnover, resulting in superadditive inhibition compared to the binding of single fragments alone.

Furthermore, fragment ligation product can also be detected via protein binding assay using fluorescence polarization. By attaching carboxy-fluorescein which serves as a fluorophore to the protein binding fragment, A distinctly determines the binding of secondary fragment B to be either additive or cooperative binding. The best cooperative binding of B elevates the binding affinity of A resulting in higher fluorescence polarization ($FP_{AB} < FP_A$). Both fragments A and B will then link covalently to generate potent inhibitor.

Another approach that was applied in ligand detection for protein template fragment ligation is through protein-saturation transfer difference NMR spectroscopy (^{1}H-STD-NMR). This approach enables the detection of less stable ligation product in aqueous solution such as hemiacetals and hemithioacetals. ^{1}H-STD-NMR works by exploiting the selective transfer of proton magnetization from protein to reversibly bound ligand and allow site-specific identification of protein binding fragments as well as the functional characterization of enzymatic sites.

Nonetheless, medicinal chemist has also adapted label free method to detect bioactive fragment ligation product in homogenous protein binding assays. For instance, thermal shift assay were used to detect protein-ligand complexes. This method examined the protein defolding at increasing temperature by adding external fluorophores (dyes) such as Sypro Orange that shows increased fluorescence when they bound to the hydrophobic region of denatured, unfolded protein. Fragment binding increased protein stability through
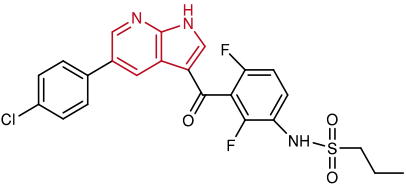
enhancement of the protein's melting temperature due to the free binding energy of ligand. However, the method provides initial clue on protein-ligand binding and detailed thermodynamic information is acquired by carrying out isothermal titration calorimetry.
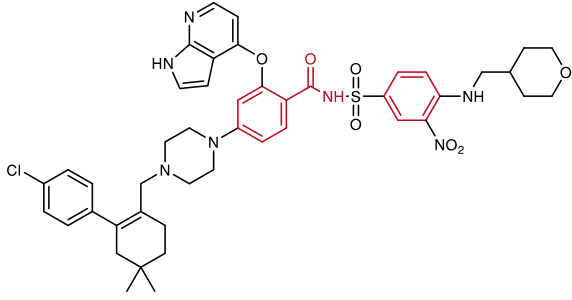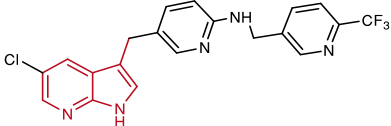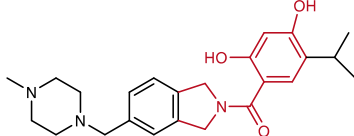
The discovery of various bioactivity based method compared to classical detection approach has accelerated the identification of bioactive fragment ligations products in protein-binding, enzymatic, and cellular assays.

1.5   Drugs derived from Fragment-based methods (FBDD)

In the past, fragment based drug discovery (FBDD) was often seen as an alternative approach to high throughput screening (HTS). However, in recent years both methods are complementing each other and adopting both strategies would bring distinct advantage. When FBBD and HTS are applied in parallel, FBDD facilitates the characterization of target druggability while HTS allows for the identification of structural moieties. As most pharmaceutical companies have adopted both methods in the discovery of potent inhibitors, their success stories of advancing weak fragment hits to potent lead candidates for a selection of proteins are shared in Table 1. [44,45]

Table 1: Successful examples of FBDD-derived drug.

Structure	Drug	Drug target	Status
	Vemurafenib	BRAF-V600E	FDA approved

	Venetoclax	BCL-2	FDA approved
	Pexidartinib	FMS, KIT and FLT3-ITD	Phase III clinical trial
	Onalespib	HSP90	Phase II clinical trial

1.6 Transcription factors

Transcription factors are proteins that bind to the DNA-regulatory regions to initiate and modulate the rate of gene transcription. Thus, the regulation of transcription factor availability and activity is the core parameters for gene expression. The availability of transcription factors is highly regulated by their level of production, degradation and subcellular localization.[46] On the other hand, the activity of transcription factor is modulated by post-translational modifications e.g. phosphorylation, acetylation, methylation, ubiquitylation or SUMOylation.[47]

The most common and rapid alterations in transcription factor activity involves protein phosphorylation and dephosphorylation, but it is proven that lysine acetylation also

posed tremendous impact on transcription factor activity. So often, acetylation of transcription factors modulates activity involving protein stabilization, cellular localization, and DNA-protein or protein- protein interaction. In addition, extracellular signaling molecules also play significant roles in triggering changes in gene expression that lead to appropriate physiological responses. [48]

1.7   Transcriptional control

Transcriptional control was established in bacterial systems[49] half a century ago. Subsequent studies from the pioneering work revealed that DNA-binding transcription factors in eukaryotic system recognize and occupy distinct DNA sequences at control elements[50] (CIS regulatory elements) and recruit transcription apparatus for gene expression.[51,52] Transcriptional activation of protein is described as a combinatorial interplay between site - specific transcriptions factors and cofactors involved. (Figure 1.6) In addition, gene transcription is also core regulated by both tissue-specific gene expression and specific stimuli (both intra and extracellular).[46] Gene regulation often occurs at the transcription level while deciding which genes will be transcribed to primary RNA transcript even though some cases of regulations after transcription do exist. Once the gene transcription has occurred, the following stages of gene expression such as RNA splicing will take place resulting in the production of corresponding protein. [48]

1.8   Signal transducer and activator (STAT) family

There are seven members in the STAT family including STAT1, STAT2, STAT3, STAT4, STAT5A, STAT5B and STAT6 (Figure 1.7).[53] Of all the seven mammalian STAT proteins, STAT5a and STAT5b isoforms are particularly similar with approximately 91%

identical in amino acid albeit encoded by separate genes.[53-57] The variability between STAT5a and STAT5b is primarily in the 12 C-terminal amino acids which contribute to subtle difference in molecular weight of 94 and 92kDa respectively. All STATs protein share conserved domains that play vital roles in phosphotyrosines binding, protein-protein interactions (PPI), DNA binding ability, and transactivation once bound to the promoter region of target genes.[58,59] Interestingly, seven different STATs are known to share several conserved functional domains, but the transactivation domain at the C-terminus is the most diverse part.

STAT1 and STAT2 are critical for interferon response and mice lacking STAT1 have impaired innate immunity with remarkably sensitivity to viral infections and other pathological agents. The role of STAT2 in interferon signaling was also confirmed through generation of knockout mice.[53,54] Similar to STAT1 deficient mice, STAT2 null mice are prone to viral infections and less responsive to interferon signaling. In addition, double knockout of STAT1 and STAT2 has profound defects on interferon response consistent with the concept that STAT2 facilitates tyrosine phosphorylation of STAT1 in order to activate interferon α/β complex.[60]

STAT4 is predominantly activated in response to IL-12 and play crucial role in IL-12 signaling. In addition, STAT4 knockout mice reveal its deficiency causes defects in T helper cell differentiation along the Th1 pathway while STAT6 deficient mice are defective for IL-4 induced T-cell proliferation and differentiation.[54,61]

STAT3 is found to be constitutively active in several types of solid tumors, leukemia, and lymphoma. In myeloma and prostate malignant cells, IL-6 autocrine or paracrine loops was recognized as the main culprit for STAT3 over activation. Nevertheless, STAT3 was also reported to have multiple complex roles in hematopoiesis and immune tolerance. STAT3

knockdown mice have been shown to develop colitis and higher response towards T-cell, indicating that STAT3 proteins are directly implicated in oncogenesis and inflammation.[57,61,62]

STAT5 is essential for competitive repopulation and proliferative responses towards cytokines in normal hematopoietic stem cells. Constitutive activation of STAT5 has also been closely associated with hematologic malignancies and cancer progression in chronic myelogenous leukemia (CML). Knocking down both STAT5a and STAT5b isoforms lead to infertility in female mice. In addition, STAT5 plays significant role in IL-2 signaling via gammaC and T cell proliferation for natural killer (NK) cells productions.[62,63]

However, not all members in STAT proteins are involved in promoting cancer progression. In fact, activation of STAT1 has been associated with pro-apoptotic and anti-proliferative effect as knocking out STAT1 in mice lead to greater risk of tumor development compared to controls.[55]
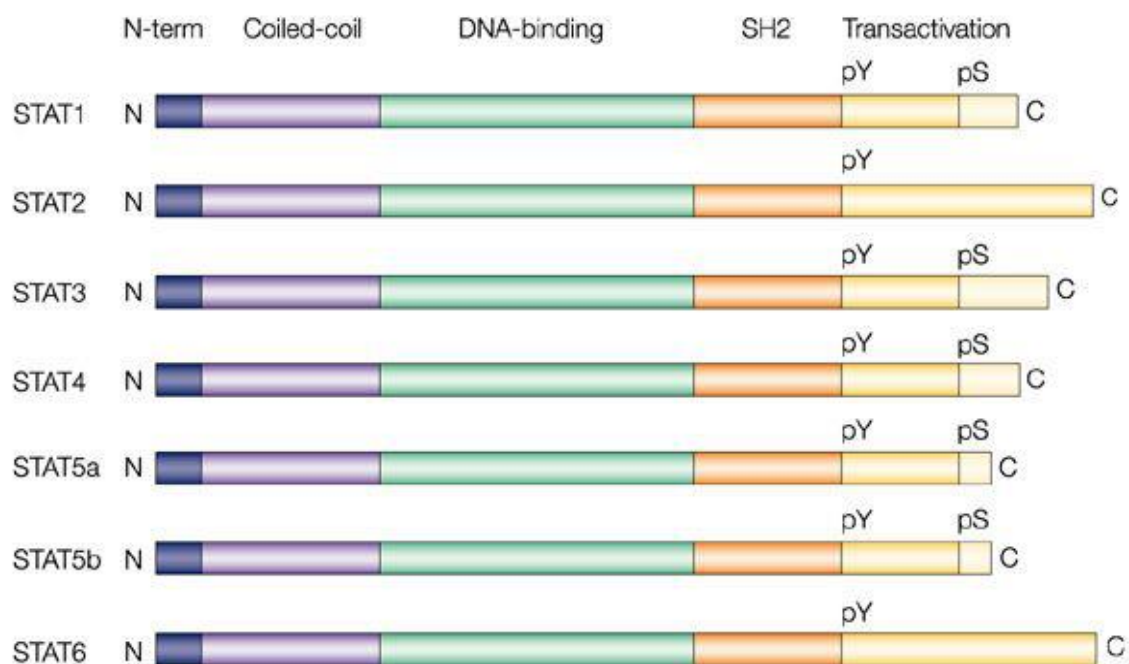
Figure 1.8: STAT protein domain structure. STAT protein domains comprise a short N-terminal structure which involved in STAT dimerization and tetramerization. The adjacent coiled-coil domain interacts with other transcription factors while the DNA binding domain makes direct interactions with the promoter regions in gene transcription. Nevertheless, the DNA binding domain also defines the DNA-binding specificity and mediates distinct signals for specific interacting ligands. [55]

On the other hand, the SH2 domain mediates binding to the phosphotyrosines on neighboring STAT molecules. The transactivation domain activates the expression of the target genes by interacting with DNA remodeling enzymes such as histone acetyltransferases. A carboxyterminal phosphoserines regulate the transcriptional process by enhancing the transcriptional activity in some STATs. STAT5a and STAT5b are closely related proteins but encoded by different genes.[54,55]

1.9 STAT5 protein structure and specificity

Crystal structure of STAT5a (pdb: 1Y1U) was first revealed by Becker and colleagues in 2005. Like all members in STAT family, STAT5 has a modular structure of seven conserved protein domains comprised of a N-terminal domain, coiled-coil domain, DNA-binding domain, Src-homology-2-domain (SH2), linker domain, phosphotyrosines tail segment and last but not least the transactivation domain. Structural and functional information of STATs is deduced mainly from crystallographic data as well as mutagenic and biochemical studies (Figure 1.9).[64]

The structure of both STAT5 proteins is similar to the other members of the STAT family. The N-terminal domain stands as an independently folded structure and is required for protein interactions[65], nuclear export and also mediates STAT5 tetramerization.

Apparently, N-terminal interactions between STAT5 dimers are found to facilitate STAT5 tetramerization and thus promote cooperativity upon binding to tandem response element in STAT5 dependent gene regulation.[66-69]

The SH2 domain, also known as phosphotyrosines binding domain is the most conserved domain that mediates specific interactions between STAT5 receptor, STAT5-JAK and STAT5-STAT5. The SH2 domain recruits STAT5 to the phosphorylated receptor for subsequent formation of transcriptionally active STAT dimers. Tyrosine residue (Y694 of STAT5A and Y699 of STAT5B) which located between SH2 and transactivation domains will undergo phosphorylation in order for STAT5 dimerization to occur. (Figure 1.8) Reciprocal interactions between the SH2 domains of one STAT5 monomer and the phosphotyrosines of the other monomer led to the formation of STAT5 dimers.[63]
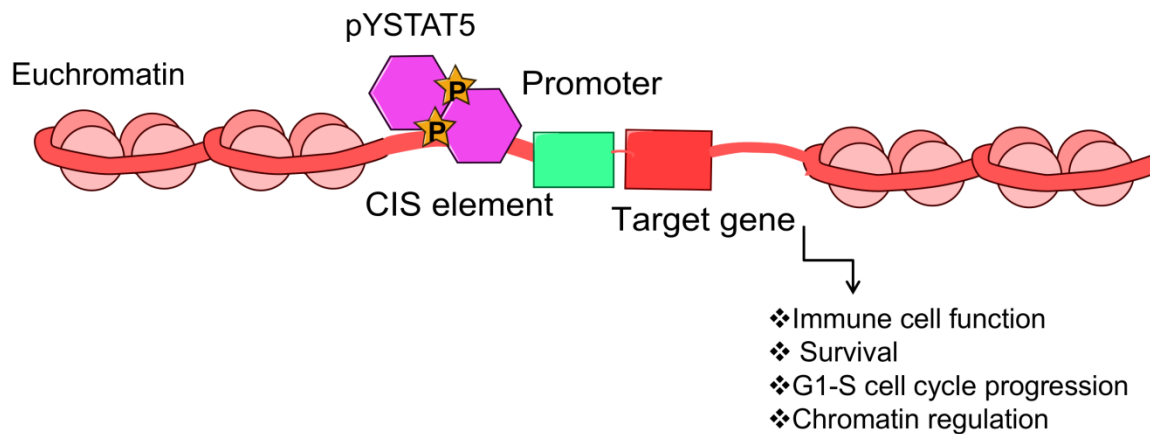
Figure 1.9: STAT5 dimers enter the nucleus and bind to a distinct DNA sequence (CIS element) and activate gene transcription for cell survival, regulate immunity and chromatin regulation.[50]

Drug selectivity between the two variants STAT5a and STAT5b has always gain interest and attention in the field of drug discovery as the selectivity problem is hard to tackle for the two STAT5 variants as compared with other members in STAT family. Interestingly, STAT5 isomers show non-redundant functions despite their high degree of sequence and structure similarity and overlapping roles. [56,62,70,71]
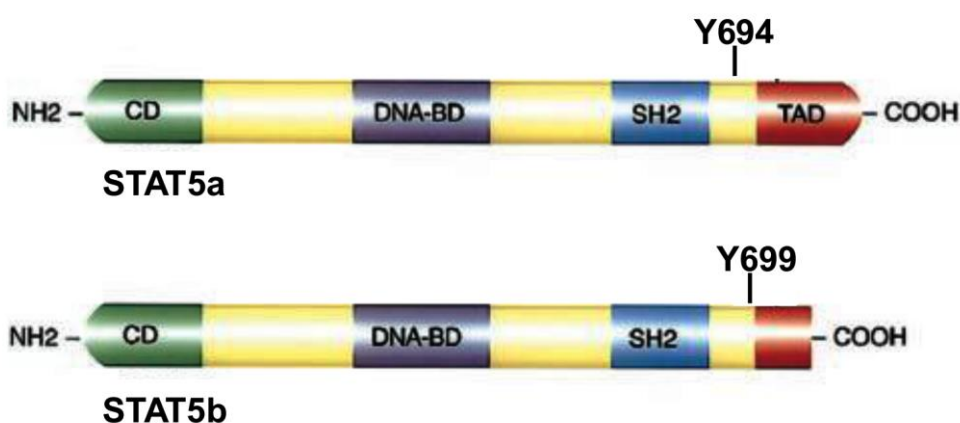
Figure 1.10: STAT5 isomers functional domains and key tyrosine residue. The conserved tyrosine residue (Y694 of STAT5A and Y699 of STAT5B) is located between the SH2 and transactivation domains. Phosphorylation of the conserved residue in STAT5 is essential for STAT5 dimerization. NH2 indicates amino terminal, COOH, carboxyl terminal; CD, cooperative domain, DNA-BD, DNA-binding domain; TAD, transactivation domain.[64]

The c-terminal transactivation domain is the most divergent domain between the members of the STAT family and is required for induction of gene expression by medicating interactions of STATs with other components of the transcription machinery. In addition, c-terminally truncated STAT5 isoforms are dominant-negative transcriptional regulators and have been found in the bone marrow of AML patients. Previous research has demonstrated that genetically engineered c-terminal STAT3 mutants can cause neoplastic transformation

thus provide evidence that c-terminal transactivation domain of STAT protein play causative role in oncogenesis. [55]

a

αA α7
αA α7 α6 α4 N-terminal α2
A α7' α6'
C B α8 α4'
αD g' a g
αC a' b c α3 α1
αB e
  x
C-terminal

b

┌╴╴╴╴╴╴╴╴╴╴╴╴┐
╎**SH2 domain**╎
└╴╴╴╴╴╴╴╴╴╴╴╴┘
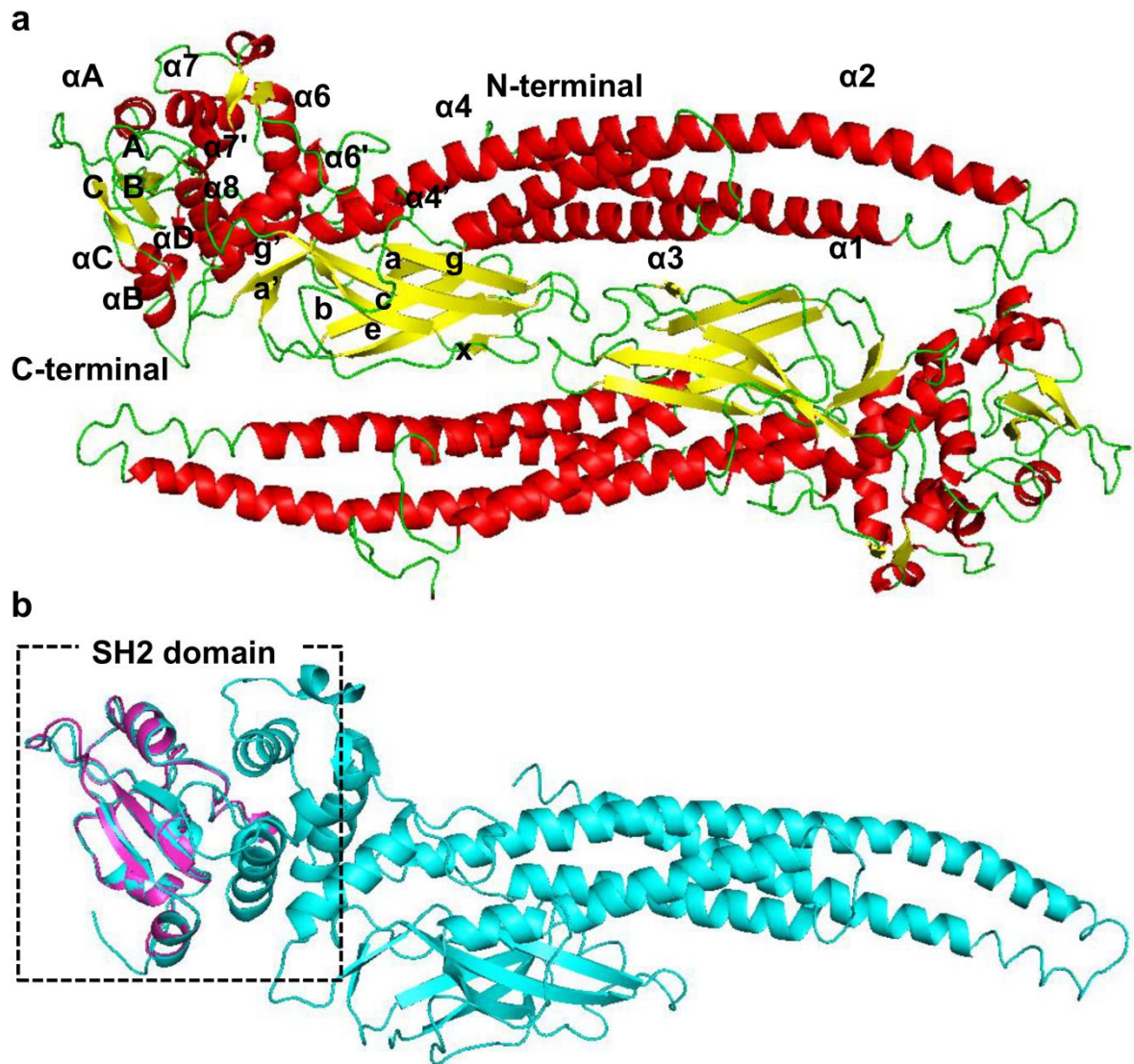
Figure 1.11: Crystal structure of STAT5a. (a) 3D conformational structure of STAT5a dimer color coded according to the domain shown in ribbon: the N-terminal (Nterm) four helix bundles (red), the β-barrel domain (yellow) and the SH2 domain (green). Secondary elements are attributed according to the program PyMOL. Cterm, c-terminal. (b) Overlapping of the

crystal structure STAT5a-SH2 domain with homology modeled of STAT5b-SH2 domain using Sybyl8.1 with RMSD= 0.598 show structural similarity of both STAT5 isomers.[64]

1.10   Activation and function of STAT5

1.10.1 The JAK-STAT signalling pathway

Signal transducers and activators of transcription (STAT proteins) play essential roles in cellular functions and are critical for developments as they modulate gene expression in response to various growth factors, cytokines and interferons. STAT5 activation is largely carried out by tyrosine phosphatase. Signalling is initiated upon ligand binding at the cytokines and growth factor receptor, exuding a signal from the cell membrane to the nucleus.[54] Throughout evolutions, the Janus kinase/ signal transducer and activator of transcription (JAK/STAT) signaling pathway is highly conserved and the activation of JAKs lead to activation and tyrosine phosphorylation of STATs. [72]

Sequentially, signaling molecules bind and activate JAK kinase and phophorylates key tyrosine residues on their receptors which allow the binding of STAT5 protein to the phosphotyrosines docking site via their SH2 domain. The STAT5 protein in turn are phosphorylated and dimerized before entering the nucleus to initiate gene transcription. The two variants of STAT5 isomers (STAT5A/B) are activated by more than 20 different cytokines, hormones and growth factors. Cytokines that often associated are interleukin (IL)-2, 3, 4, 5,7,9,15,21, erythropoietin (EPO), thrombopoietin (TPO), prolactin (PRL), and granulocyte macrophage colony-stimulating factors (GM-CSF) and growth hormones (GH).[55,63] The cellular model used in this work, murine pro-B cell line BaF3depends on interleukin-3 (IL-3) to activate STAT5 signalling for cell proliferation and survival. (Figure 1.12)
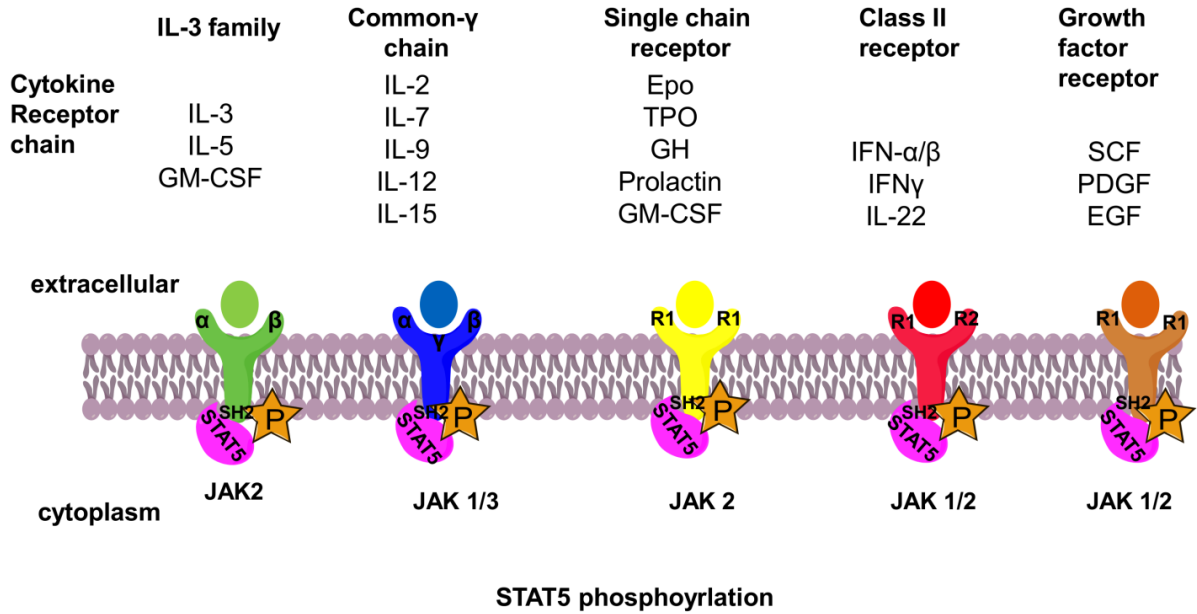
Figure 1.12: Non-redundant JAK/STAT signaling. Schematic showing the preferential cytokine/growth factor usage of different JAKS for STAT5 phosphorylation based on gene-targeting studies in mice.[73]

A handful of small molecules inhibitors that aim to target JAK2 activity have been identified. Cardama and coworkers discovered a JAK1/2 inhibitor named ruxolitinib that proven to increase apoptosis in patient with JAK2-V617F mutation.[74] Ruxolitinib shows promising results in preclinical evaluation and has progressed forward for clinical used.[75] Another JAK inhibitor, CYT387 (momelotinib) which is an ATP mimetic has also proven to inhibit JAK2 activity in BaF3/ JAK2-V615F cell lines with IC_{50} in submicromolar range (IC_{50}=1.5 μM).[55,76] In addition, TG101348[77] was found to inhibit JAK2 in low nanomolar range (IC_{50}=3 nM) with surprising high selectivity (334 fold) over JAK3. (Figure 1.13)
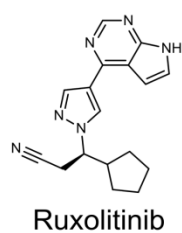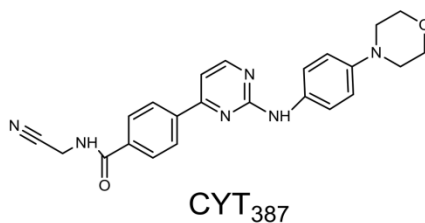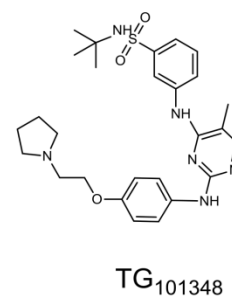
Figure 1.13: Chemical structures of JAK2 inhibitors that potently inhibit JAK2 and its mutant JAK 2-V617F. [75,77]

1.10.2 The FLT3-STAT5 signalling pathway

Constitutive activation of STAT5 in the signal transduction pathways resulting from mutations confer proliferative and survival advantage of leukemic cells. Mutations activates receptor tyrosine kinases and have been widely studied are FMS-like tyrosine kinase 3 (FLT-3) followed by JAK2, RAS, C-KIT and SHP-2.[54,78] Previous studies have proven that these mutations contribute to poor prognosis and high relapse rate in leukemia patients. Furthermore, statistics have shown that intensive chemotherapy can only achieved a cure rate of 30-40%.[79,80] On the same page, acute myeloid leukemia (AML) patients carrying FLT3 internal tandem duplication (FLT3-ITD) somatic mutation have experienced high relapse rate and lower survival rate. FLT3 –ITD mutation is a form of in-frame duplication that disrupt the negative regulatory function of juxtamembrane domain causing aberrant activation of tyrosine kinase activity and other closely related pathways such as the JAK2-STAT5, mitogen-activated protein kinase/ extracellular signal-regulated kinase (MAPK/ERK), PI3K/AKT/mTOR and RAS/Raf/MEK/ERK.. These have resulted in up regulation of their downstream effectors like Bcl-xl, c-Myc, pim-1, JAB and p21 that are essential for anti-

apoptic and cell survival. Similar to other tyrosine kinase mutation, FLT3- ITDs constitutively activates FLT3, independence from its ligand and capable of stabilizing the 3D conformation of the activation loop for ATP binding.[79] Gene translocation, FLT3-ITD leads to deregulation of signal transduction pathway causing excessive proliferation. (Figure 1.14)
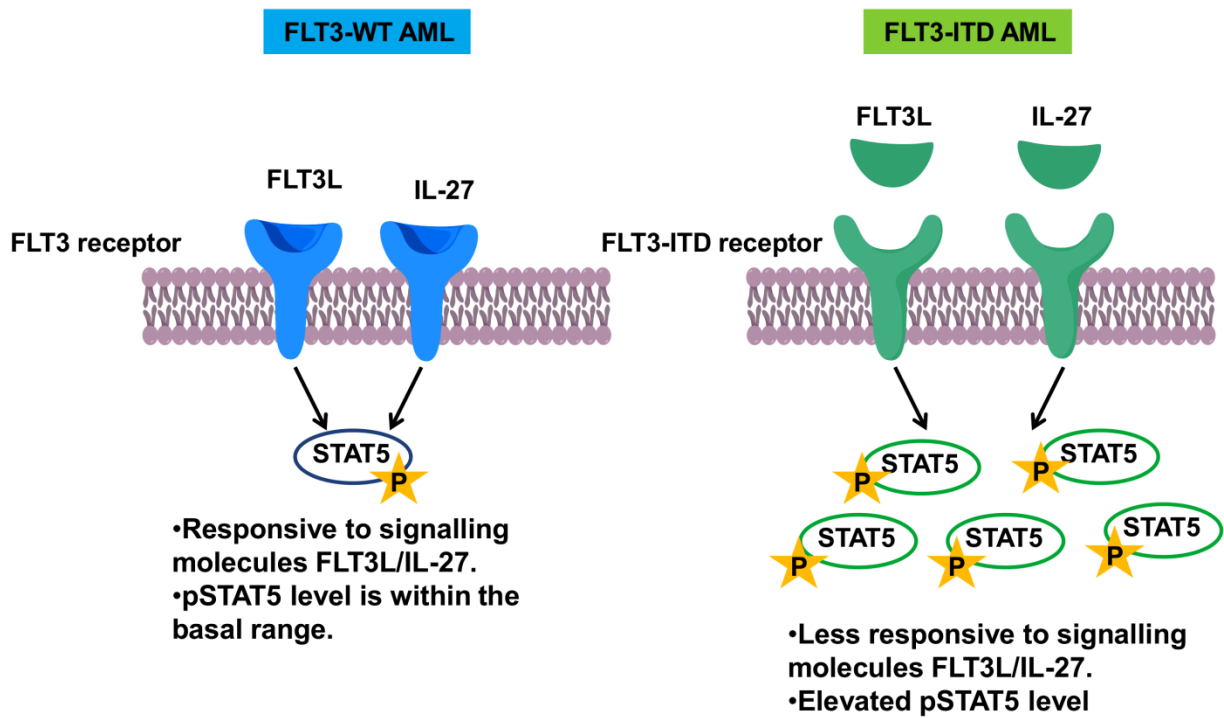
Figure 1.14: Overview of the difference observed between FLT3-ITD and FLT3-WT in AML patient. Wild type FLT3 is responsive towards modulators (FLT3 and IL27) whereas mutated FLT3-ITD is constitutively active and less responsive towards modulators.[80]

Up to date, there are more than 20 small molecule inhibitors against FLT3 reported but only few that have advanced through the clinical trial phases (Figure 1.15). Lestaurtinib, a first generation FLT3 inhibitor exhibits nanomolar inhibition towards both FLT3 and JAK2 while also potently inhibit FLT3-ITD expressing AML samples.[81] Another promising molecule worth mentioning is Sorafenib, a multiple kinase inhibitor exhibits 15 folds more potency in AML patient bearing FLT3-ITD mutation compared to wild type FLT3.[82] Most of

the small molecules inhibitors were initially identified through high throughput screening of existing compound libraries. Disappointingly, not all hits fulfilled the pharmacokinetic and pharmacodynamic requirements and were halted in the early phase of clinical trials. In general, most of the inhibitors suffer from short *in vivo* half life and mediocre target specificity in vivo. Therefore, researchers approach alternative ways by targeting the downstream target of FLT3, i.e STAT5 in order to provide one-two punch effect in combination therapy to fight leukemia.[83,84]

a
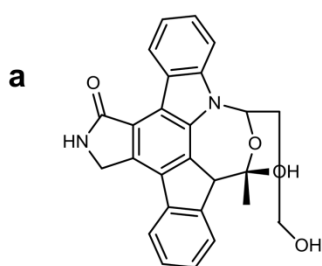
Lestaurtinib

$IC_{50\ (FLT3)}$: 3 nM

b
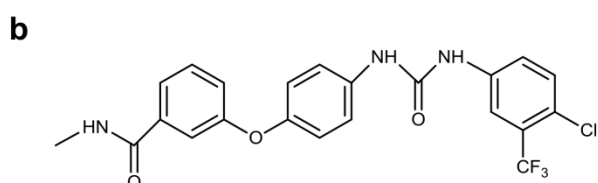
Sorafenib

$IC_{50\ (FLT3)}$: 0.29 nM

c
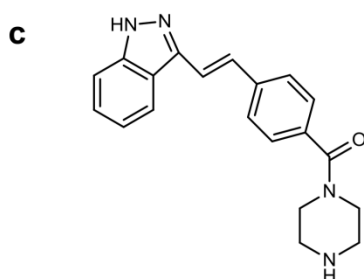
KW 2449

$IC_{50\ (FLT3)}$: 1 nM

d
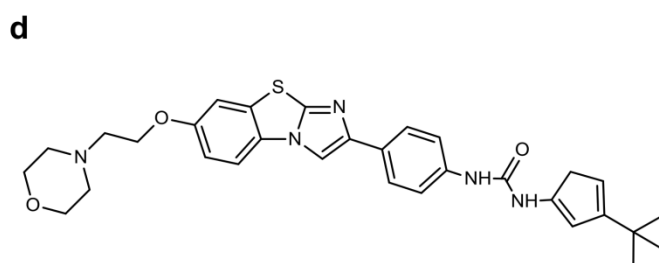
AC 220

$IC_{50\ (FLT3)}$: 1.1 nM

Figure 1.15: FLT3 inhibitors used in clinical trials.[85,86]

1.10.3 The BCR-ABL signal transduction pathway

BCR-ABL is a unique fusion gene and is found in chronic myeloid leukemia (CML) patient. CML is a characterized by the Philadelphia (Ph) chromosome, which results from the reciprocal translocation of chromosome 9 and 22. This translocation leads to the fusion of ABL gene from chromosome 9 and the Breakpoint Cluster Region (BCR) gene from chromosome 22 thus generating the oncogenic BCR-ABL fusion gene. The expression of chimeric BCR-ABL oncoprotein constitutively activates kinase activity and enhances leukemic cell survival and proliferation.[87-89] (Figure 1.16)
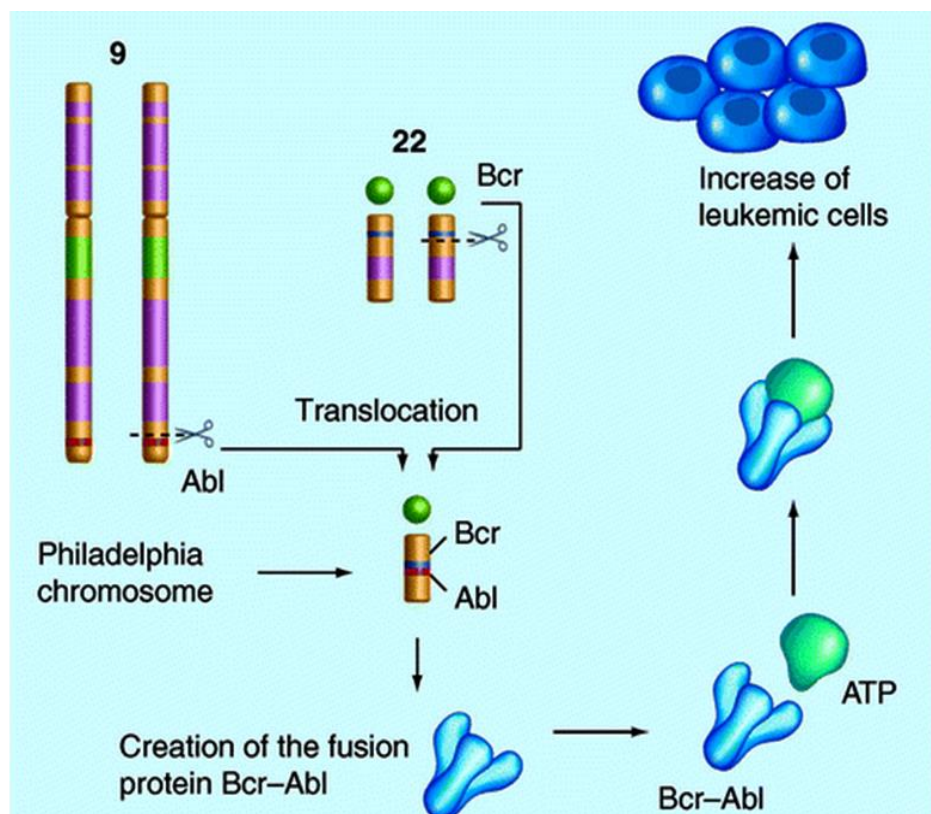
Figure 1.16: Schematic illustration of Philadelphia (Ph) chromosome formation leading to Chronic Myeloid Leukemia (CML).[89]

Before gene translocation, ABL protein physiological shuttles between nucleus and cytoplasm. Intriguingly, it was found mainly in the cytoplasm after fused to BCR in order to

ease interaction with protein involved in oncogenic pathway. BCR-ABL crosstalk with several growth-promoting signalling pathways such as RAS/RAF/MEK, PI3K and also JAK-STAT pathway.[89]

Pharmaceutical company sees BCR-ABL as an attractive target for therapeutic invention. Novartis have carried out high throughput screening (HTS) and identified Gleevec (imatinib mesylate) as a potent kinase inhibitor. Imatinib has successfully in treating patient inducing complete remission and being classified as gold standard for CML treatment. However, even with high success rate of curing CML, surprisingly there are subsets of CML cells that are non-sensitive and resistance towards imatinib which urge scientist to search for an alternative therapeutic target.[90] A second generation derivative of imatinib, named nilotinib[91,92] was designed and synthesized to tackle secondary resistance but was again faced with the same bottle neck issues. CML patients detected with BCR-ABL[T315I] mutation hardly response to both imatinib and nilotinib. A third generation tyrosine kinase inhibitor, Dasatinib[93] was designed to target resistance in BCR-ABL[T315I] but the dispersion of mutations across kinase domain limits the effectiveness of TKIs.[94] (Figure 1.17)

First generation
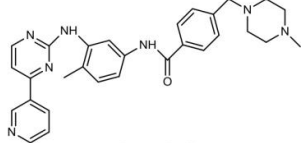
Imatinib

$IC_{50 \text{ Bcr-Abl}}$: 350 nM
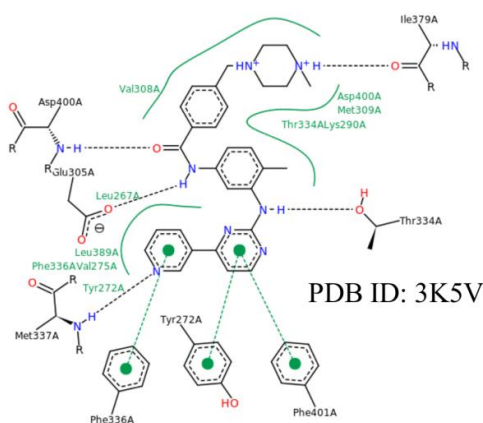
PDB ID: 3K5V

Second generation
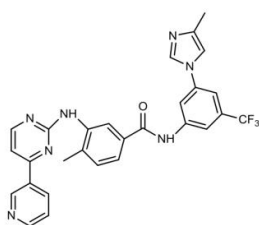
Nilotinib

$IC_{50 \text{ Bcr-Abl}}$: 30 nM
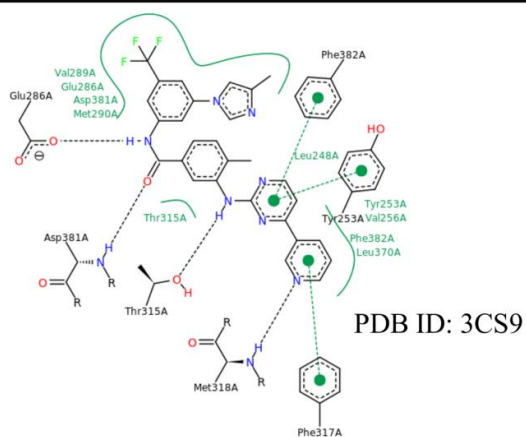
PDB ID: 3CS9

Third generation
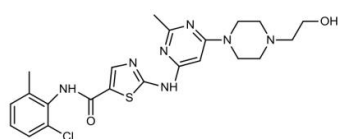
Dasatinib

$IC_{50 \text{ Bcr-Abl}}$: 0.8 nM
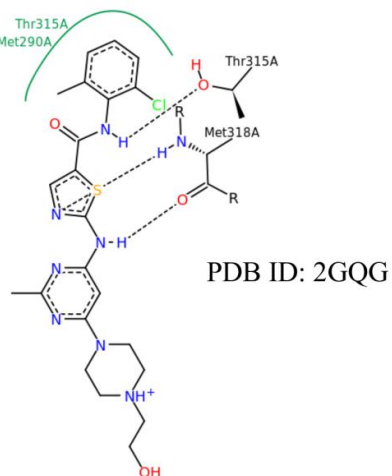
PDB ID: 2GQG

Figure 1.17: Three different generations of small molecule inhibitors for Bcr-Abl protein and key interacting residues involves in binding. [90,91,94]

Studies have also proven STAT5 inhibition decrease the survival and proliferation of CML cell bearing BCR-ABL mutations. This clearly indicates that STAT5 acts as an important downstream mediator of BCR-ABL in the oncogenic pathway. In addition, Hantschel et al. observed that STAT5 inhibition is much more efficient in treating CML cells with BCR-ABL than targeting other downstream target of BCR-ABL. On the same page, STAT5 overactivation is observed in CML mutants and causing relapsed and resistance towards 2nd and 3rd generations tyrosine kinase inhibitors.[89,93,94]

Undoubtedly, STAT5 is among the few genes that initiates and drives leukemia, therefore making it a potential therapeutic target in blood cancer.[57,87,95]
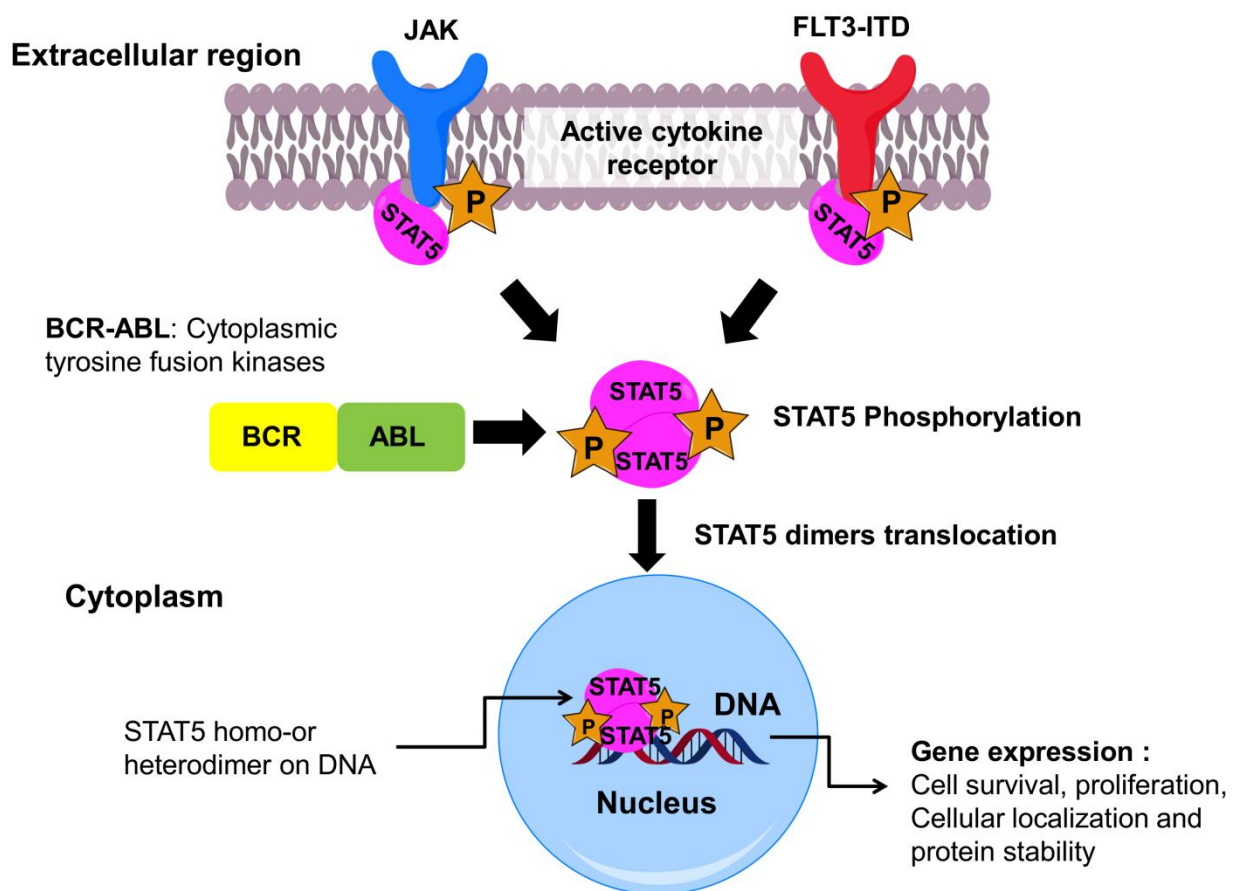
Figure 1.18: STAT5-the central hub in signalling node of aggressive leukemia. Canonical activation of STAT5 is initiated by cytokine binding to specific kinase receptor. Upon cytokines binding, receptors are activated through conformational changes followed by pY phosphorylation. Activated kinase receptor mediates phosphorylation of their downstream targets at the cytoplasmic end at specific sites. STAT5 bounds to the activated receptors JAK2 and FLT3-ITD as preformed parallel or anti-parallel dimers and is activated through SH2 domain phosphorylation. The activated STAT5 proteins form homo or hetero dimers via their SH2 domain and translocate to the nucleus to bind to the DNA and resulted in elevated target gene expression for leukemic cell survival and proliferation. On the contrary, BCR-ABL is a constitutive active cytoplasmic tyrosine fusion kinase with a translocation between chromosomes 9 and 22 which able to phophorylate STAT5 directly making JAK2 signalling dispensable. (Figure 1.16)[72,95,96]

1.11   Negative regulation of STAT5 signalling

STAT5 activity is tightly regulated to maintain appropriate signal intensity and duration in cell. In a healthy cell, STAT5 phosphorylation is regulated by constitutively expressed regulator such as phophateses and suppressors of cytokine signalling (SOCs) protein family.[97] Furthermore, STAT5 signal will experience gradual decay via ubiquitin-proteasome pathway and receptor down-regulation. [98]

There are three important negative regulators in JAK/STAT pathway and all of them come from different protein families. Src homology phosphatases SHP-1 and SHP-2 negative regulate STAT5 either by direct STAT5 dephosphorylation or acted on its upstream JAK receptor. The other common negative regulator composed of phosphotyrosines phosphatase IB (PTP1B) family. T cell protein tyrosine phosphatase (TC-PTP) regulates cellular STATs

activity through direct dephosphorylation of STATs or JAK kinase. The transmembrane phosphotyrosines phosphatase CD45 is known to down regulate STAT5 signaling by inactivating JAKs. [99,100]

Besides that, protein inhibitor of activated STAT3 (PIAS3) also plays vital role in repressing STAT5 activity. PIAS is found to interacts with STAT5 and interfere with STAT5-DNA binding. Nonetheless, cytokine-induced SH2-domain-containing protein (CIS) and SOCS1, SOCS2 and SOCS3 are well discussed STAT5 regulator among the SOCS family. They are known to be downstream target of STAT5 and attenuate STAT5 signaling via negative feedback inhibition. Studies also proven that they compete with STAT5 for binding sites at the receptor kinase to inhibit their activity. [101,102]

1.12   Role of STAT5 in cancer and resistance in cancer

Anti-leukemic treatment often encounters a huge bottle neck of chemoresistance that prone to develop over the course of chemotherapeutic treatments which provides a useful hindsight that leukemic stem cell pool is not a static population and is hardly eradicate using universal chemotherapeutic drugs. [3]

Overactivation of STAT5 are commonly linked to development of various type of hematologic malignancies as well as solid tumor cancers such as breast cancer, prostate cancer, head and neck cancer, hepatocellular carcinoma and melanoma. Aberrant STAT5 activation is often associated with constitutively active oncogenic tyrosine kinases and non-receptor tyrosine kinases such as BCR-ABL[87] (breakpoint cluster region protein and Abelson murine leukemia viral oncogene homology 1), $JAK2_{v617F}$[72,73] and FLT3-ITD.[98]

FLT3-ITD mutation is found in 30-50% AML patient, leading to persistent activation of STAT5 for cell survival and proliferation. Overactivation of STAT5 is extremely crucial

for leukemic stem cell (LSC) self renewal, making AML patient prone to develop resistancy towards tyrosine kinase inhibitor. Surprisingly, the mechanism of STAT5 activation by mutant FLT3 are seen and labeled as non-canonical signaling which absence in normal cells. This criterion portrayed added advantage in the therapeutic index sparing normal hematopoietic cells and leukemic cells by using drug targeting STAT5.[79]

A driver mutation, $STAT5_{N642H}$ found in leukemia/ lymphoma patients has been extensively studied by Moriggl and colleagues. Previous studies have shown that $STAT5_{N642H}$ drives cancer progression by stabilizing activated STAT5-dimer and prolonged their activation state.[103] (Figure 1.19) This STAT5b mutation is found in 2% of large lymphocytic leukemia (LGL) while no STAT5a mutation is detected. A few rare mutations in STAT5b were also reported namely E438K, G492C, P702A, I704L, and Q706L but their effect towards STAT5 are yet to be explored.[104] Transgenic mice expressing human $STAT5_{N642H}$ show enhance STAT5 tyrosine phosphorylation even in the presence of low dose cytokines. This has further proven that $STAT5_{N642H}$ majorly contributes to the leukemicT-cell proliferation and survival in T-cell ALL (acute lymphoblastic leukemia) and T-cell lymphoma.[105,106]
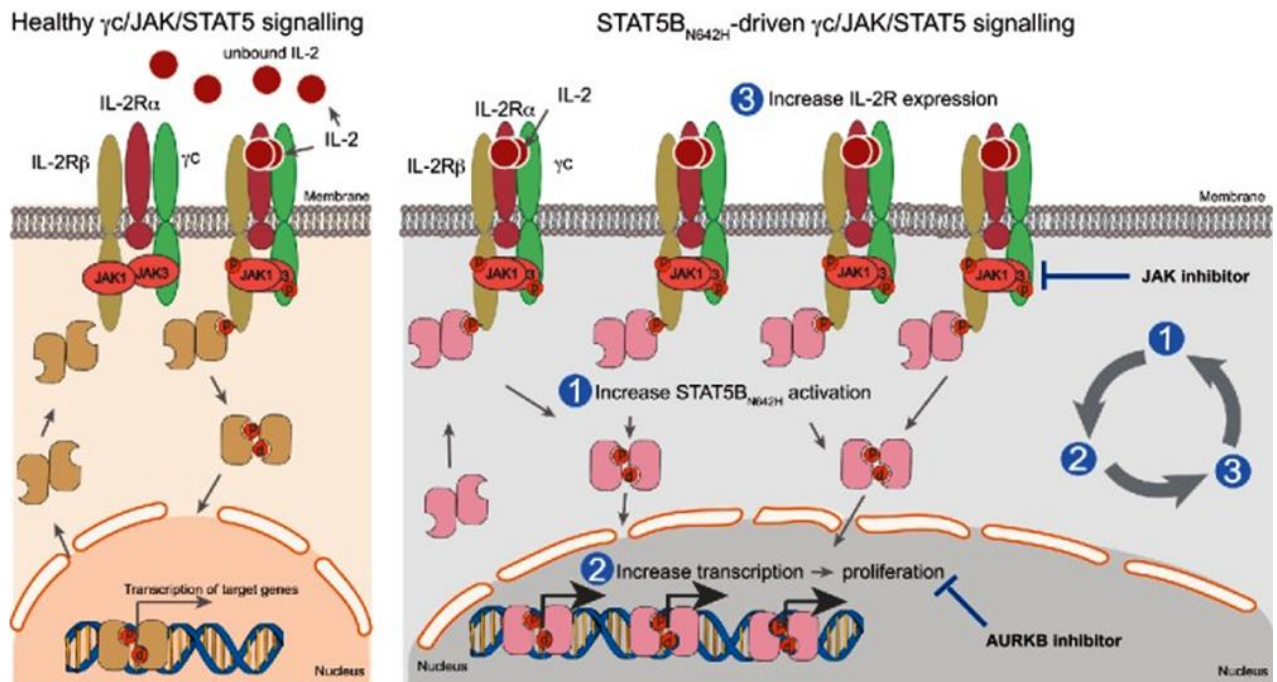
Figure 1.19: STAT5$_{N642H}$ acts as a driver mutation enhance proliferation of T-cell leukemia and lymphoma via JAK-STAT signalling. 1-2, prolonged activation of STAT5$_{N642H}$ leads to sustain DNA binding which increased transcription of STAT5 target genes. 3, STAT5$_{N642H}$ amplified cytokine receptor signalling through up regulation of interleukin 2 receptor alpha (IL-2Rα). Vicious cycle (1-3) leads to cancer cell survival and progression. Development of specific inhibitors that directly block SH2 domain is urgent need to halt STAT5 overactivation.[106]

1.13   Drugging the STAT5 pathway

STAT5 protein, carrying major roles in driving leukemia has been validated as potential therapeutic target. In the past, chemotherapeutic treatment using multiple tyrosine kinase inhibitors has brought severe side effects in patients due to their off target cytotoxicity, therefore it is useful to target their downstream transcription factors in order to reduce the adverse side effects.[56,57,107]

By taking a closer look in to transcription factor STAT5, this protein does not possess enzymatic activities thus making it a challenging target for the development of small molecules inhibitors that are specific and effective with high cell permeability. The most promising approach in targeting STAT5 protein is through functional inhibition of the protein-protein interaction (STAT5 dimerization) and Src homology 2 (SH2 domain). Phosphopeptide mimetics was initially shown to bind STAT5-SH2 domain, disrupting STAT5 dimerization but was failed to provide significant cellular activity.[62,71,108]

The most discussed challenge in targeting STAT5 lay in finding the workable therapeutic window for leukemia cells while having minimal side effects in normal cells. STAT5 inhibition using tyrosine kinase inhibitor (TKI) often leads to long term off target toxicity and TKI resistance. Even though TKIs obtained the most clinical success, many patients are dealing side effects from off-target binding due to the multi-targeted natured of TKIs as well as secondary resistance which often increase the chance of relapse. Targeting STAT5 using TKIs lead to targets amplification or mutation of target as an escape mode to prevent action of the inhibitor. In addition, drug-efflux proteins are up regulated to reduce the intra-cellular concentration of inhibitors or amplification of complementary pathway such as STAT3 to compensate the lost of functional STAT5 protein.

Due to the critical role of STAT5 in mediating various mutated tyrosine kinase (TK) pathways, it is worth to discover selective and specific STAT5 inhibitors as an alternative to target cancer development. Hence, target inhibition of STAT5 pose great potential to eradicate cancer cells without causing resistance. Up to date, a handful of direct STAT5 inhibitors have been developed, mostly only show activity in binding assays and cellular assays such as chromone based compounds, fosfosal, salicylic acid-based, an adenosine-5-monophosphoate derivative, osmium complex and catechol bisphosphates derivatives.[58,109] Most of the STAT5 inhibitors were discovered through high throughput screening (HTS) of

chemical libraries and fragment based drug discovery. In addition, many of the reported STAT5 inhibitor still posed indirect effect on JAK/STAT or BCR-ABL signaling pathway due to unverified target specificity. Stafib-2, a biphosphate-containing small molecule was reported to inhibit STAT5 at nanomolar range and selective towards STAT5b over STAT5a.[71] Another STAT5 specific inhibitor, AC-3-19, a salicylic-based STAT5 SH2 domain inhibitor was also developed to selectively targeted STAT5.[56] More recently, an improved salicylic-based STAT5 SH2 domain inhibitor, AC-4-130 was reported to bind STAT5b in 1D ^{19}F NMR and also show potent inhibitory effect in cellular assay as well as in vivo animal studies, , but none of the inhibitors above were potent and selective enough to be translated into clinical use.[110]

Undeniably, there is progress in development of STAT5 inhibitor but finding inhibitor that could target STAT5 specifically remains challenging. This is mainly due to the nature of transcription factor which exert most of their functions through protein-protein interactions and DNA-protein interactions. The key interacting pockets are often lack of well-defined hydrophobic pockets which typically serve as a starting point for the identification of small molecule inhibitors.[62,71] Nonetheless, SH2 domain shows high degree of structural homology across STAT family making it harder to develop inhibitor that target STAT5 SH2 domain specifically.

1.14   The application of FBDD and protein templated ligand formation of STAT5

Transcription factors play vital role in regulating target gene transcription to achieve precise and balance regulation of cellular phenotype. STAT5 (STAT=signal transducers and activator of transcription factor) was chosen as target protein due to their critical role in mediating the effect of upstream kinases in signalling pathway, making them an attractive

protein for the development of targeted anti-cancer therapeutic agents. Aberrant activation of STAT5 is observed in various types of cancers but is majorly found to be activated in myeloid malignancies, lead to the development of leukaemia.[54,56] As we gained better understanding of STAT5 signalling in cancer cells, direct inhibition of STAT5 might contribute to personalized medicine approach in the hope of lessening the side effect in treating cancer patients.

At the present time, there is still room for further exploration in the chemical space by protein-templated reactions. Most of the PTFL reactions reported are mainly reversible, i.e., dynamic ligation reactions and only few are irreversible[111-114], and therefore it is worthwhile to explore the possibility of using multicomponent reactions for protein dependent reaction. Given that the transcription factor STAT5 is a target for tumor therapy, protein-catalyzed reaction such as PTFL is a great attempt to explore site-specific identification of protein binding fragments since there is insufficient X-ray structural information on STAT5 protein-ligand complexes.

Chapter 2

Aim of the Thesis

Aim of thesis

Conventional chemotherapy are always seen as a universally applicable therapy that target bulk population of cells with high cytotoxic effect but still remains as the standard regime for treating myeloid leukemias. The major downside of this treatment approach is the lack of drug specificity and selectivity which in turns leads to large number of side effect. Such approach, hardly discriminate rapidly dividing non malignant and cancer cells.

As targeting the upstream kinases in the signal transduction pathways has its own limitation, it is worth to explore the downstream target which has smaller niche and involved lesser crosstalk in multiple transductions pathway, It is foreseeable that by designing targeting therapeutics for downstream target has more limited nonspecific mechanism. Over activation of STAT5 due to deregulated signalling pathways often leads to oncogenic transformation proofing that transcriptional factor activity have powerful consequences. Therefore, it is worthwhile to take a closer look into finding inhibitors that could target transcription factor and to halt the over expression of oncoproteins.

The goal of this thesis was to develop a novel experimental strategy that based upon protein-templated fragment assembly reaction for the discovery of highly potent STAT5 inhibitors. In this strategy, a protein-binding phosphate mimetic, which was identified earlier by the AG Rademann from screening of a fragment library was used as a starting point. Aim of the research was to investigate, if and how this initial fragment could be extended to more potent inhibitors of the STAT5-SH2 domain by using a protein-templated three-component Mannich ligation.

In our studies, we attempt to take a rather different approach where STAT5 protein is recruited to catalyze multicomponent reactions of a phosphate mimetic, formaldehyde and 1H-tetrazole to furnish potent protein ligands that equipped with high selectivity and specificity as well as ligand efficiency. As proof of concept, several methods for monitoring

of the protein-templated reaction ought to be developed. The formed ligation product from protein-catalyzed reaction will be investigated using binding assays such as fluorescence polarization assay and also thermal shift assay as well as high-performance liquid chromatography-mass spectrometry (HPLC-MS) analysis.

We will also take a closer look on the feasibility of the reaction by testing the protein templated Mannich ligation under physiological conditions and also in a range of pH. In addition, the templated reaction and the formed inhibitors will then be tested with STAT5 closely related proteins such as STAT1 and STAT3 to determine the drug specificity and selectivity as STAT family shares high structural homology of SH2 domain. Nevertheless, the formed inhibitors will be examined against phosphatases like SHP2 and PTPIB to prevent non selective binding and inhibition.

In order to study the binding of potent inhibitors formed via templated reaction, molecular modeling and docking will be carried out. Nevertheless, binding analysis software, BINANA will be use to provide insight on the binding mechanism of the formed inhibitors with STAT5 while also identified the key binding residues in protein binding pocket.

To assess the possible implications on formed inhibitors in targeting STAT5 in leukemic cells, in vivo and in vitro studies were carried out. The formed inhibitors are carefully investigated in both leukemia and other cancer cell lines for cell cytotoxicity studies. The activity of the formed inhibitor in blocking cell proliferation and survival were determined in a xenograft mouse model. Biochemical studies will be carried out to verify the ability of formed inhibitors in blocking phosphorylation of STAT5, disrupting DNA-binding and halt gene transcription that drives cancer cell proliferation and survival. We were also keen to examine the synergistic effect of our STAT5 inhibitor with a staurosporine-derived

FLT3-inhibitor PKC412 which inhibits the upstream tyrosine kinase receptor to gain insight on new therapeutic approaches in tackling leukemia and potentially other cancers.

Together this study will explore the formation and identification of a specific protein-binding ligand via protein templated reaction. Furthermore, it also contributes to a better understanding on how the ligand bound and inhibits the target proteins, STAT5. Ultimately, it should broaden the application of protein templated reactions and also provide molecular basis for the development of potent protein ligands in numerous protein targets.

Chapter 3

Results

3.1 Discovery and validation of a phosphate-mimetic fragment targeting STAT5 via HTS

A robust, high throughput assay fluorescence polarization (FP) assay is employed for an accurate assessment of STAT5 inhibitor. Berg et al. applied the same biochemical technique to identify specific STAT5b inhibitors whereas Gunning et al. set up a complementary high throughput FP assay for STAT5a. To date, only one crystal structure of STAT5a isoform is available on the protein data bank (PDB: 1Y1U) and no resolved crystal structure of STATb. The lack of structural data impedes the use of structure based drug design (SBDD) to identify selective STAT5b inhibitors. [56,58,62,71,115]

In addition, target validation against STAT5b-SH2 domain is extremely crucial since selective STAT5b-SH2 domain inhibitors can block aberrant dimerization and transcriptional activity without interfering with other essential cellular functions mediated by other structural domain of STAT5. For instance, the C-terminal domain in STAT5 acts as a physiological substrate for insulin receptor. This highlights the need for setting up FP assay targeting STAT5b-SH2 domain in order to develop STAT5 inhibitors that could potentially STAT5b dimerization and halt aberrant STAT5 signaling in leukemia.[62,108]

3.1.1 High Throughput STAT5b Fluorescence Polarization assay

High-throughput screening (HTS) assays enable the testing of huge numbers of chemical substances for activity in diverse areas of biology. The biological responses measured in HTS assays span isolated biochemical systems containing purified receptors or enzymes to signal transduction pathways and complex networks functioning in cellular environments. Biochemical based high-throughput screening is widely used to discover small molecule drugs that modulate protein-protein or protein-peptide interactions.[70] Here, we

utilized fluorescence polarization (FP) assay for high throughput screening of large small-molecules libraries for modulators of the activity of the SH2 domain of STAT5b (Figure 3.1).[116] Strong affinity binding of STAT5b to either its upstream receptor or reciprocally to itself requires the key pY-SH2 domain interactions. A high affinity phosphotyrosine octapeptide, 5-CF-GpYLSLPPW **1** derived from Granulocyte-Macrophage Colony-Stimulating Factor (GM-CSF) receptor has been developed as a fluorescent probe for the STAT5-SH2 domain ($K_D = 55$ nM) to be used in the fluorescence polarization assay. [117]
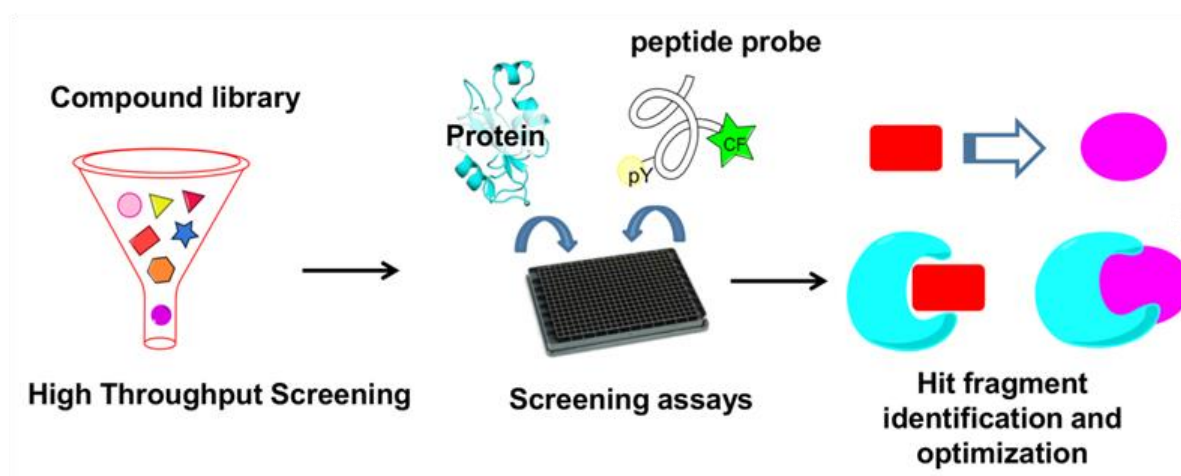
Figure 3.1: High throughput screening using fluorescence polarization assay is a robust way to screen for inhibitors. A schematic view of the different stages which came upon a drug discovery process based on traditional HTS.

A collection of 17,000 fragments and fragment combinations composed in accordance with the substructure composition of the World Drug Index (WDI) was screened for inhibitor of the phosphopeptide-STAT5b interaction. Primary amine fragments were tested in the FP assay in the presence of electrophilic phosphotyrosine mimetic **2** as described earlier for protein tyrosine phosphatases (PTP) in order to distinguish secondary site binders that

enhance the inhibition of **2** from inhibitors that are not affected by **2** (Figure 3.2, unpublished work by Dr. Samuel Beligny).
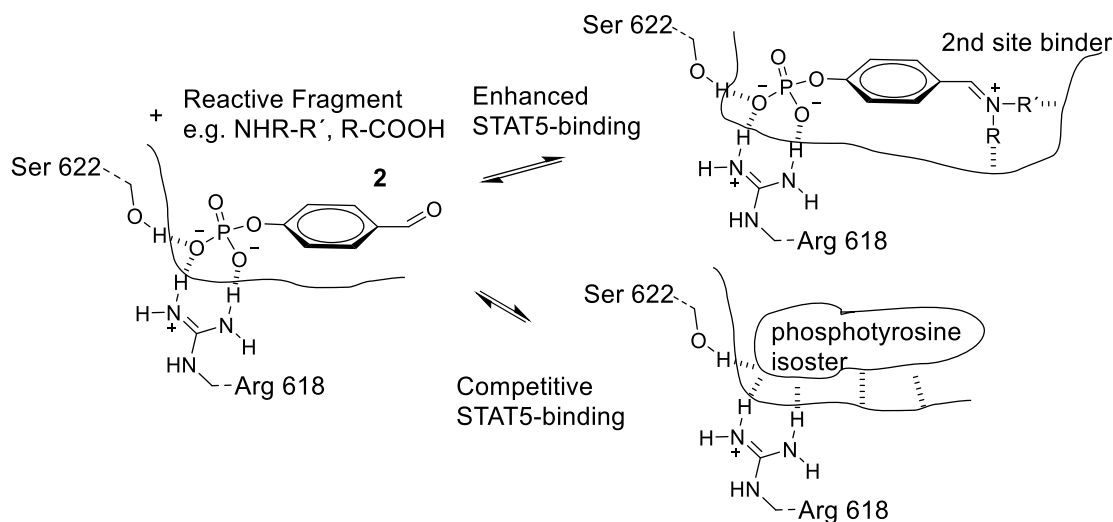
Figure 3.2: Fragment ligation assay for detecting nucleophilic fragments, which can either enhance the binding of 4-formyl-phenyl phosphate **2**, or replace **2** competitively. (Unpublished work by Dr. Samuel Beligny)

The assay was adapted to the 384-well microtiter plate format with high statistical reliability ($Z' = 0.75$) which is appropriate for high throughput screening. Potential hits can be recognized by a decrease in the fluorescence polarization through displacement of fluorescent probe **1**, which initially bounded to the STAT5 protein In addition, the non-labeled phosphotyrosine peptide AcpYLSLPPW was included as a positive control.

Binding of fragments to the recombinantly expressed STAT5b-SH2 domain fused to maltose binding protein (MBP) as affinity tag was recorded by measuring fluorescence polarization (FP) of the carboxyfluoresceine-labeled phosphotyrosine octapeptide **1** (Figure 3.3).
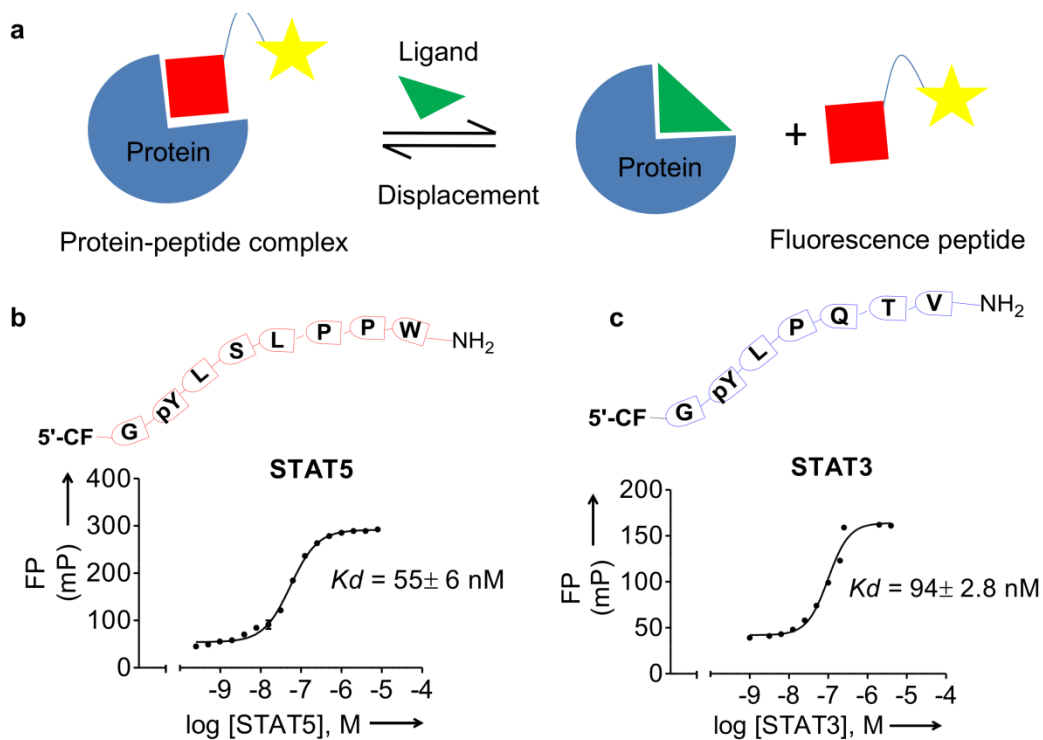
Figure 3.3: (a) Schematic illustration of the fluorescence polarization (FP) binding assay. Binding curves of carboxyfluorescein phosphopeptides 5-CF-GpYLSLPPW (**1**) for STAT5b (b) and 5-CF-GpYLPQTV for STAT3 (**c**) The dissociation constants (K_D) of the peptides were determined to be 55 ±6 nM for STAT5b and 94 ±2.8 nM for STAT3.

The library was then subjected to a high-throughput MBP-STAT5b fluorescence polarization (FP) assay to determine their binding affinity towards STAT5b-SH2 domain. The competitive displacement assay examines the small molecule displacement of a high affinity STAT5b-SH2 domain fluorescence phosphopeptide **1**, resulting in reduced polarization of the fluorescence emission due to rotational movement of the free, and unbound fluorescence phosphopeptide **1**.

Among the primary amine fragments tested, one fragment, 4-amino-furazan-3-carboxylic acid **3** (M = 129 g/mol) displayed a K_D value of 420 μM, corresponding to the ligand efficiency of 2.1 kJ/mol per non-hydrogen atom, higher than that of the nanomolar phosphopeptide **1**, the phosphotyrosine mimetic **2**, and the best reported STAT5 inhibitors

(Figure 3.4). Ligands with such high ligand efficiency are rather found for enzymatic binding pockets than for protein-protein interaction sites and thus fragment **3** was selected for further validation.

*Fluorescence Probe 1= 5-CF-GpYLSLPPW-NH2
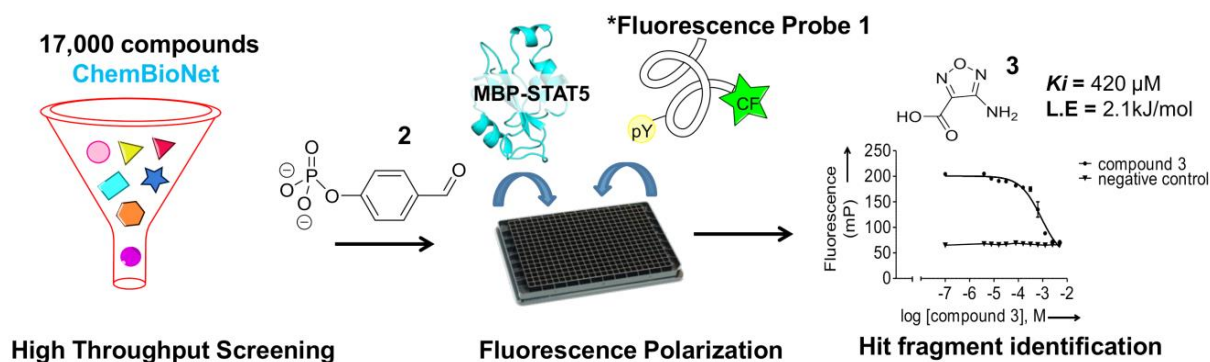
Figure 3.4: High throughput fluorescence polarization assay against a collection of 17,000 fragments in the ChemBioNet using fluorescence probe, **1** in the presence of phosphotyrosines mimetic, **2** give rises to one potent fragment, 4-amino-furazan-3-carboxylic acid **3** displayed a K_D value of 420 μM with high ligand efficiency (2.1 kJ/mol per non-hydrogen atom).

3.1.2 Thermal Shift Assay

3.1.2.1 Determination of melting temperature, *Tm* of MBP-STAT5b protein

The fluorescence-based thermal shift assay is a general method for identification of inhibitors of target proteins from compound libraries.[70,118] Using an environmentally sensitive fluorescent dye to monitor protein thermal unfolding, the ligand-binding affinity can be accessed from the shift of the unfolding temperature (ΔT_m) obtained in the presence of ligands relative to that obtained in the absence of ligands. The thermal unfolding of MBP-STAT5 protein monitored by LightCycler is shown in Figure 3.5. The fluorescence intensity

increases on protein unfolding because the fluorescent dye Sypro orange has a higher quantum yield in a lower dielectric medium and protein unfolding exposes the hydrophobic region corresponding to a lower dielectric environment. However, after reaching the plateau, the fluorescence intensity starts to decrease, mainly due to aggregation of the denatured protein–dye complexes.[118]
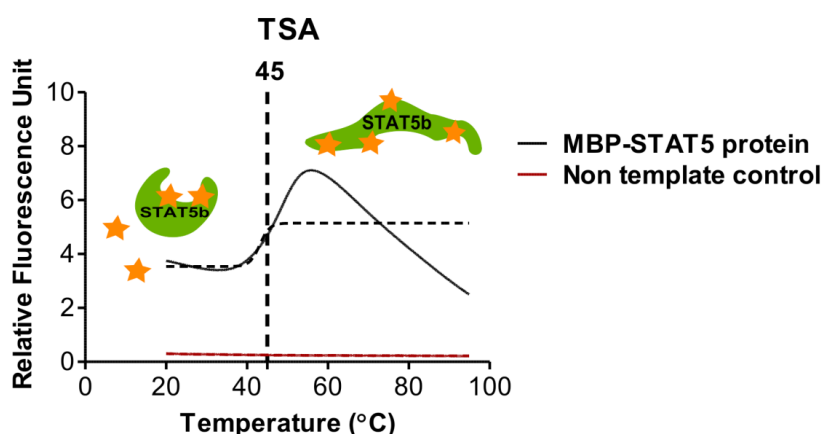
Figure 3.5: MBP-STAT5 protein melting temperature measured in Thermal Shift Assay (TSA).

3.1.2.2 Fragment 3 thermally stabilizes MBP-STAT5

A ligand bound to the active site of a protein, has the propensity to increase its thermal stability (*Tm*) through newly formed protein-ligand interactions. The difference in melting temperature (ΔTm) of the protein and of the ligand-protein complex has been shown previously to correlate to ligand's concentration and binding affinity. In this manner, a melting curve is generated, the *Tm* determined, and changes in *Tm* (ΔTm) induced by prospective binding ligands can be calculated. The midpoint temperature changes ($\Delta T_m = T_m - T_0$) in the presence of fragments **3**, **25** and **26** at 0.156mM -2mM are shown in Figure 3.6.

Binding of **3** to STAT5b-SH2 was confirmed using the thermofluor assay, a thermal

shift assay (TSA), as an independent biophysical assay. Binding of fragment **3** augmented the

melting point of STAT5 by ΔT_m of 3 °C (Figure 3.6).
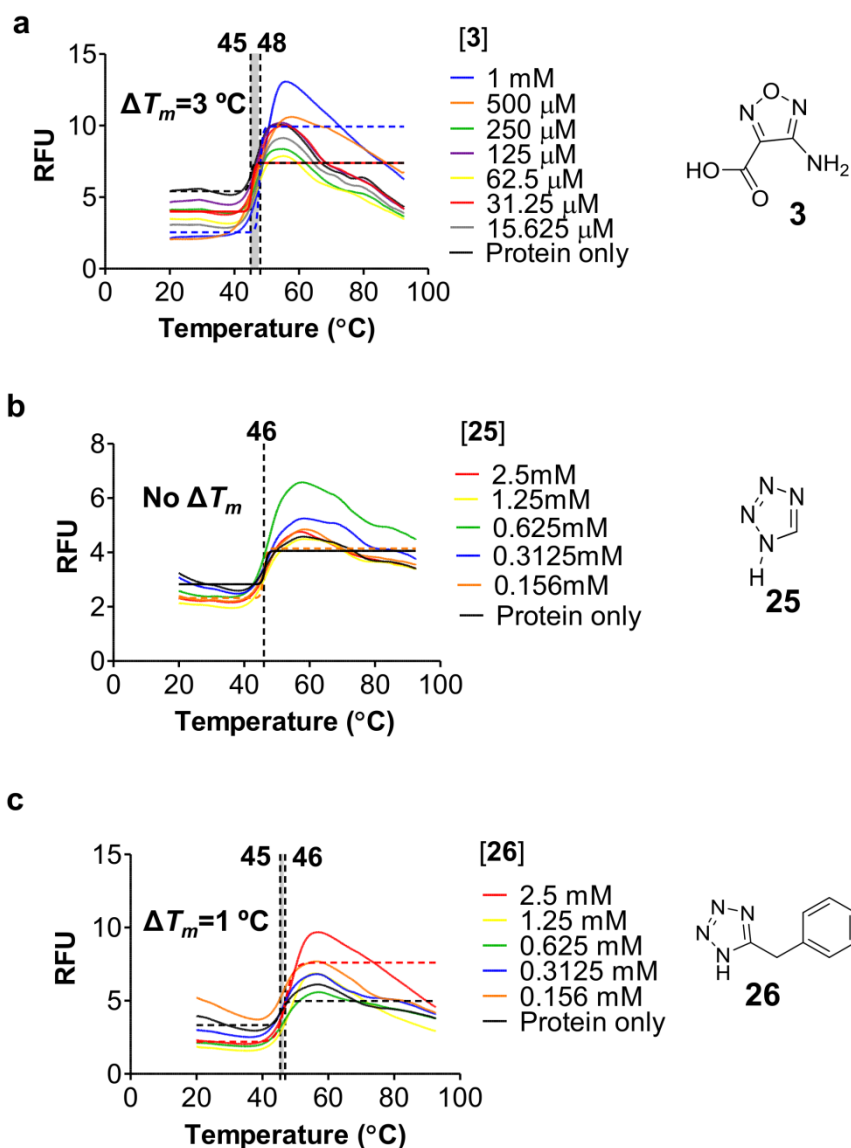
Figure 3.6: Melting temperature of MBP-STAT5b in the presence of fragments **3**, **25** and **26**.

(a) Fragment **3** induced a significant shift in the melting temperature (ΔT_m=3 °C) of MBP-

STAT5b protein at 1mM. (b-c) Fragments **25** and **26**, respectively, show no or minute T_m

shift (1 °C) in the thermal denaturation curves of MBP-STAT5b. The fluorescence changes

shown in the plot with increasing temperature were fitted to the Boltzmann equation by non-linear regression to obtain the melting temperature, T_m.

Potential binding modes of the phosphotyrosine **2** and the fragment hit **3** were scrutinized using a homology model of STAT5b derived from the crystal structure of STAT5a (pdb: 1Y1U) due to the absence of STAT5b crystal structure for molecular docking.[64] Sequence alignment of mouse STAT5a to human STAT5b were adopted from Lin et al. as shown in Figure 3.7 using Sybyl8.1. As illustrated in figure 3.7, the residues spanning the SH2 domain of both STAT5a and STAT5b are highly conserved with exception of 7 amino acid.[119]

```
MuSTAT5A (aa589)  WNDGAILGFV NKQQAHDLLI NKPDGTFLLR FSDSEIGGIT IAWKDFSPDR
HuSTAT5B (aa589)  .......... .......... .......... .......... .......QE.

MuSTAT5A (aa639)  NLWNLKPFTT RDFSIRSLAD RLGDLNYLIY VFPDRPKDEV FA
HuSTAT5B (aa639)  MF...M.... .......... .......... .......... YS
```

Figure 3.7: Alignment of SH2-domains mouse STAT5a (MuStat5a) to human STAT5b (HuSTAT5b)[119]

The phosphotyrosine binding site in the STAT5-SH2 domain is shallow compared to the deeper binding pockets of PTP coordinating phenyl phosphate **2** by only two amino acid residues, Arg618 and Ser622.[120,121] As a result, the benzene ring of **2** is not buried in a cavity like in the case of PTPs but rather exposed to the solvent at the protein surface. Binding of fragment **3** is mediated by the Coulomb interaction between the carboxylate anion and the cation of protonated Arg618 and H-bonds involving Arg618, Ser622, and Asn642 (Figure 3.8).
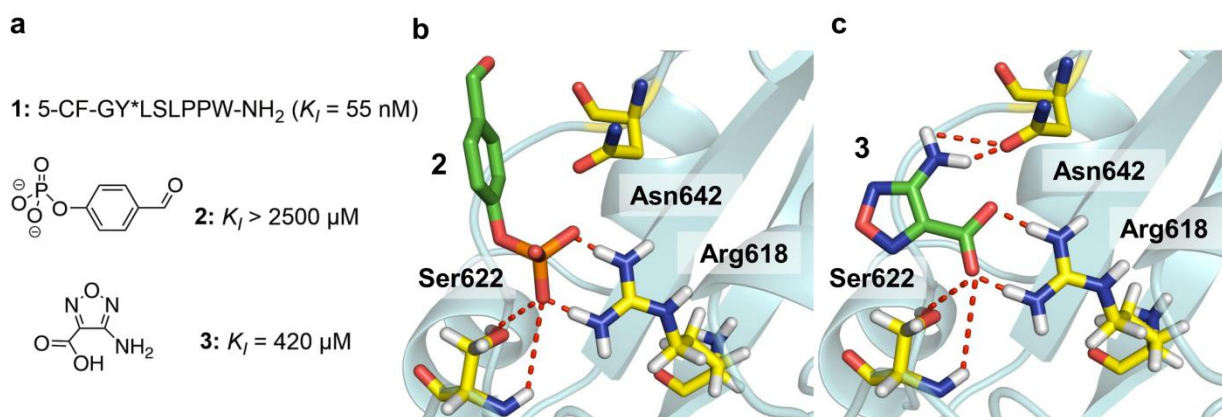
Figure 3.8: Discovery of phosphate-mimetic fragment **3.** (a) Fluorescently labeled phosphotyrosine peptide **1** was used in an FP assay for the screening of a fragment library furnishing 4-amino-furazan-3-carboxylic acid **3** as a phosphate-mimetic. Phosphotyrosine-mimetic fragment 4-formyl-phenyl phosphate **2** was employed to investigate fragment hits for second site binding. (b‑c) Molecular docking results of fragments **2** and **3** into homology model of human STAT5b-SH2 domain, generated from the published structure of STAT5a (PDB accession codes, 1Y1U). Hydrogen bonds with key residues in the hydrophilic binding pocket of the STAT5-SH2 domain were illustrated as red dashed lines.[116]

3.2   Hit-to-lead optimization of selective STAT5 inhibitors

Fragment **3** was identified as an attractive starting point to initiate chemistry. Although fragment **3** has moderate activity in the fluorescence polarization and thermal shift assay with $Ki = 420$ µM, it contains exceptionally high ligand efficiency and a novel core from which further modifications can be generated. In general, the smaller the fragment hits the lesser the observational activity of the inhibitors. Notably, in silico molecular docking of fragment **3** illustrated its binding in the STAT5b-SH2 domain forming two essential hydrogen bonds with Arg 618 and Ser 622. Surprisingly, fragment 3 also form and additional H-bond with Asn642 which allow it to bind stronger to the STAT5b-SH2 domain.

Derivatives of fragment **3** were synthesized and tested in order to investigate structure-activity relations and thus to challenge and substantiate the binding hypothesis. [116]

3.2.1 Fragment expansion through protein-induced Mannich ligations.

First, the novel phosphate mimetic **3** was expanded by amidation (Figure 3.9a), a reaction recently introduced to protein-templated fragment ligations. The N-acetyl derivative **4** and all other tested amides including **5**, however, were inactive in the FP assay (Figure 3.10). In order to reduce the steric demand from a carbonyl to the more flexible methylene linkage, the Mannich ligation was investigated as fragment expansion method (Figure 3.9b). Fragment **3** was found to react readily with formaldehyde (FA) and various N-heterocycles in aqueous buffer at pH 5.0 at room temperature yielding Mannich ligation products while no reaction was observed without protein at pH 7.4.

.
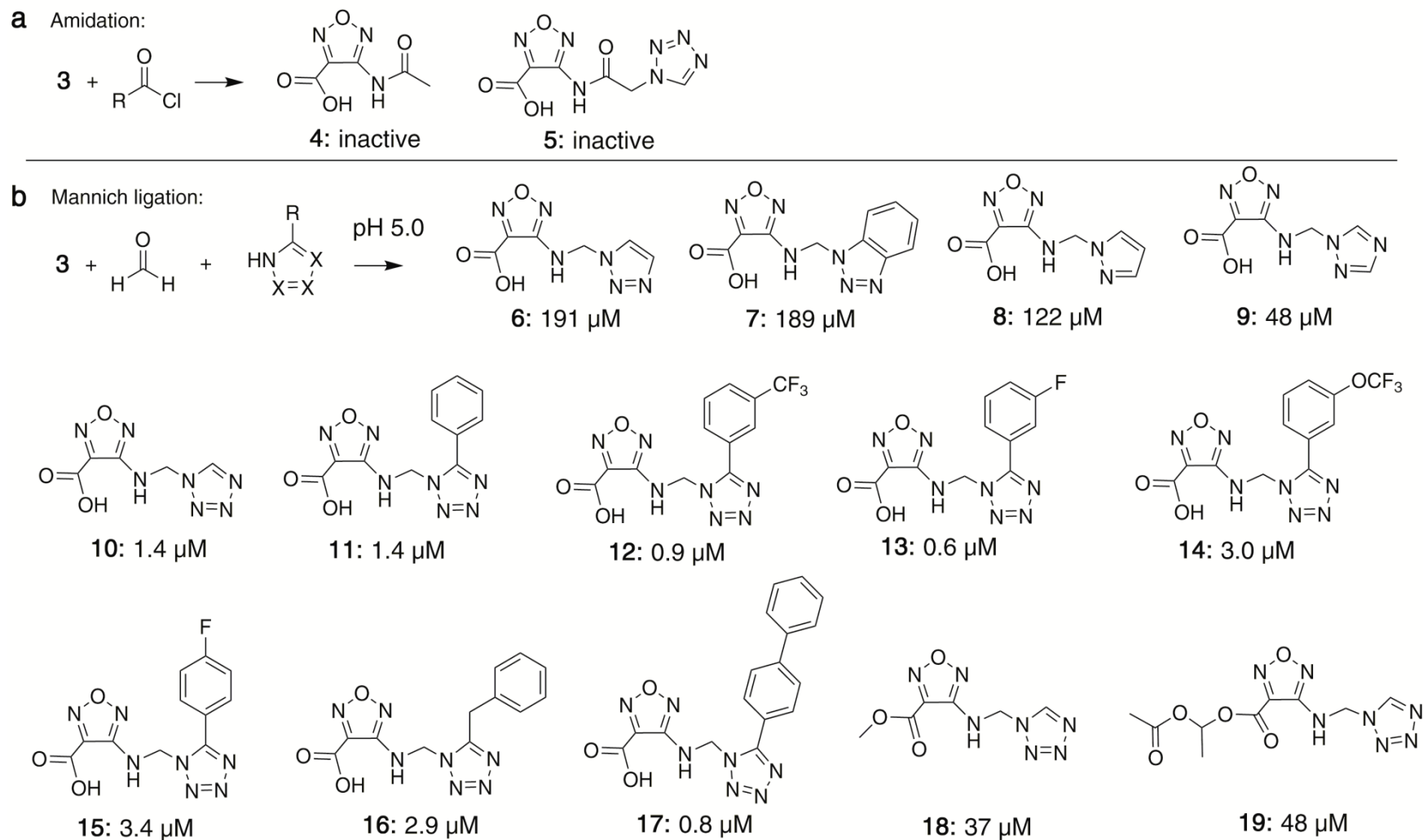
Figure 3.9: Expansion of fragment **3** through protein-induced reactions. (**a**) Amidation of **3** yielded compounds **4** and **5** which were inactive in the FP assay. (**b**) Mannich ligation was investigated as an alternative fragment expansion method to obtain the active compounds **6-19** containing a linker with reduced steric hindrance and better structural flexibility.
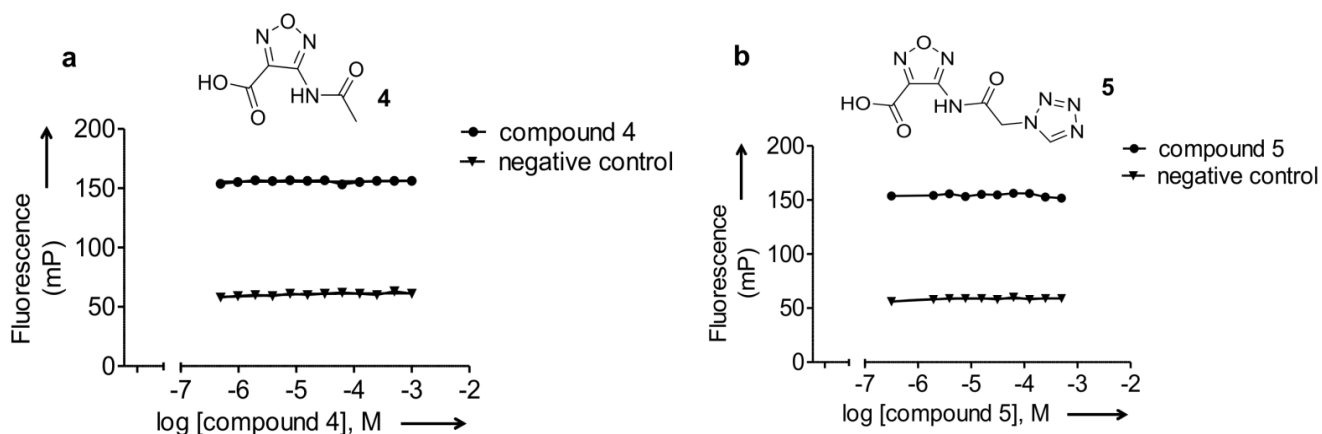
Figure 3.10: Fluorescence polarization curve for the binding of compound **4** (**a**) and **5** (**b**) to recombinant STAT5-SH2 domain shows no improvement in binding upon structure expansion by amidation

3.2.1.1 Mechanistic analysis of the protein-induced reactions

In order to implement protein-dependent Mannich ligations, the compatibility of the reaction with the protein MBP-STAT5b-SH2 and with the FP assay was investigated. 3-(N-Morpholino)-propane sulfonic acid (MOPS, 50 mM, pH 7.4) was used as a buffer containing no primary and secondary amines that could interfere with the reaction. FP of MBP-STAT5b-SH2 (125 nM) with peptide **1** (10 nM) was recorded in the presence of increasing concentrations of FA at pH 7.4. No change of FP was observed at concentrations up to 250 μM FA, while at higher concentrations FP values increased considerably (Figure 3.11a). Likewise, up to 250 μM no effect of FA on the melting point of STAT5b-SH2 was recorded in the TSA, although higher FA concentrations reduced the intensity of the fluorescence signal suggesting interference of FA with the fluorescent dye (Figure 3.11c).

Protein induced Mannich ligation:

3 + HCHO (formaldehyde) + HN-tetrazole **25** →(MOPS, pH7.4, MBP-STAT5)→ **10**

a Effect of FA on FP assay

250 µM

FP (mP) vs log [FA], mM

- MBP-STAT5-SH2 + **1** + [FA]
- **1** + [FA]

b Protein-induced formation of **10** in FP

250 µM

FP (mP) vs log [FA], mM

- MBP-STAT5-SH2 + **1** + **3** + **25** + [FA]
- **1** + **3** + **25** + [FA]

c Effect of FA on TSA

47

RFU vs Temperature (°C)

[FA]
— 0
— 50 µM
— 100 µM
— 150 µM
— 200 µM
— 250 µM
— 500 µM
— 1000 µM

d Protein-induced formation of **10** in TSA

47 54

$\Delta T_m = 7°C$

RFU vs Temperature (°C)

a

[FA]
— 0
— 50 µM
— 100 µM
— 125 µM
— 150 µM
— 200 µM
— 250 µM
— Protein only

Figure 3.11: Assembly of STAT5 inhibitor **10** through protein-induced Mannich ligations. (a) FA was tolerated at up to 250 µM in the FP assay of MBP-STAT5b-SH2. (b) FA did not affect the STAT5b protein stability in the TSA at ≤ 250 µM. (c) Protein-induced formation of **10** in the FP assay with increasing FA concentrations. (d) Protein-induced formation of **10** from fragments **3** and 1*H*-tetrazole **25** with increasing FA concentrations in the TSA ($\Delta T_m =$ 7° C).

For in-situ Mannich ligation assays, fragment **3** was incubated with one hetaryl nucleophile and FA (all 250 µM) per microtiter-plate-well in water resulting in pH 5.0. After 12 h incubation at room temperature, protein MBP-STAT5b (125 nM in 50 mM MOPS

buffer pH 7.4) with the peptide probe **1** were added and further incubated for 15 min before FP was recorded. Several of the added heterocycles led to substantially decreased FP values – suggesting the formation of a Mannich ligation product as inhibitor of STAT5b with increased affinity. Active Mannich ligation products were re-synthesized, purified, and tested in the FP assay (Appendix Table 2-3).

Remarkably, the addition of five-membered N-heterocycles ("azoles") to the formimine of fragment **3** led to strongly enhanced inhibition of STAT5b. The 1, 2, 3-triazol-1-yl product **6** as well as the benzo-1, 2, 3-triazol-1-yl (**7**) increased the affinity by a factor of >2, pyrazol-1-yl **8** >3-fold, 1, 2, 4-triazol-1-yl **9** > 9-fold and tetrazol-1-yl **10** 300-fold resulting in a K_I of 1.4 μM (Figure 3.12). The reaction with 5-substituted tetrazoles yielded strongly active inhibitors **11-17**, some even with sub-micromolar affinities, including 4-(5-phenyl-tetrazol-1-yl-methylamino)-furazane-3-carboxylate **11** (1.4 μM), 5-(3-trifluoromethyl-phenyl)- **12** (0.9 μM), 5-(3-fluorophenyl) **13** (0.6 μM), 5-benzyl **16** (2.9 μM), and 5-biphenyl **17** (0.8 μM). Esters of the furazane carboxylic acid (**18, 19**) were prepared as prodrug derivatives. 4-(Tetrazolyl-1-methyl-amino)-furazan-3-carboxylic acid **10** is the STAT5 inhibitor with the highest ligand efficiency of 2.23 kJmol^{-1} per non-hydrogen atom.

All starting azoles like tetrazole **25** were completely inactive at concentrations of 5 mM, thus the inhibitors constitute examples of super-additive fragment combinations. As a consequence, the observed protein-dependent ligation reaction did not proceed as a protein-templated reaction that requires the binding of both reacting fragments to the protein.
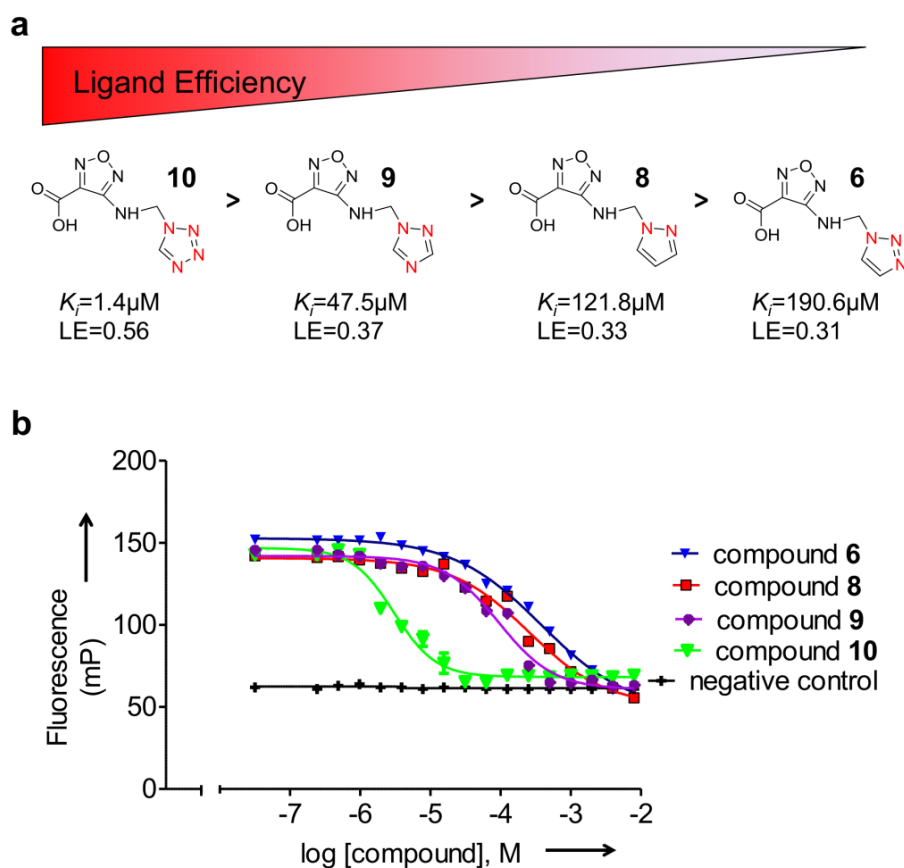
Figure 3.12: Compound **10** has the highest ligand efficiency (LE) of all inhibitors. (a) *Ki* values and ligand efficiencies of compounds **6**-**10**. (b) Fluorescence polarization curve for the binding of compound **6**, **8, 9**, and **10** to recombinant STAT5-SH2 domain.

3.3 Quantitative analysis of the protein induced Mannich reaction

Protein-dependent reactions of fragment **3** with FA and 1*H*-tetrazole **25** were investigated by using the binding assays (FP, TSA), and HPLC-MS analysis. Incubation of fragments **3** and **25** (250 μM each) with MBP-STAT5b-SH2 (250 nM) with increasing concentrations of FA at pH 7.4 led to decreased FP values, suggesting the formation of an inhibitor (Figure 3.11b). The protein-dependent formation of a STAT5 inhibitor was confirmed in the TSA: Incubation of fragments **3** and **25** with increasing concentrations of

FA and the protein resulted in a shift of the protein´s melting point ΔT_m by 7 °C (Figure 3.11d).
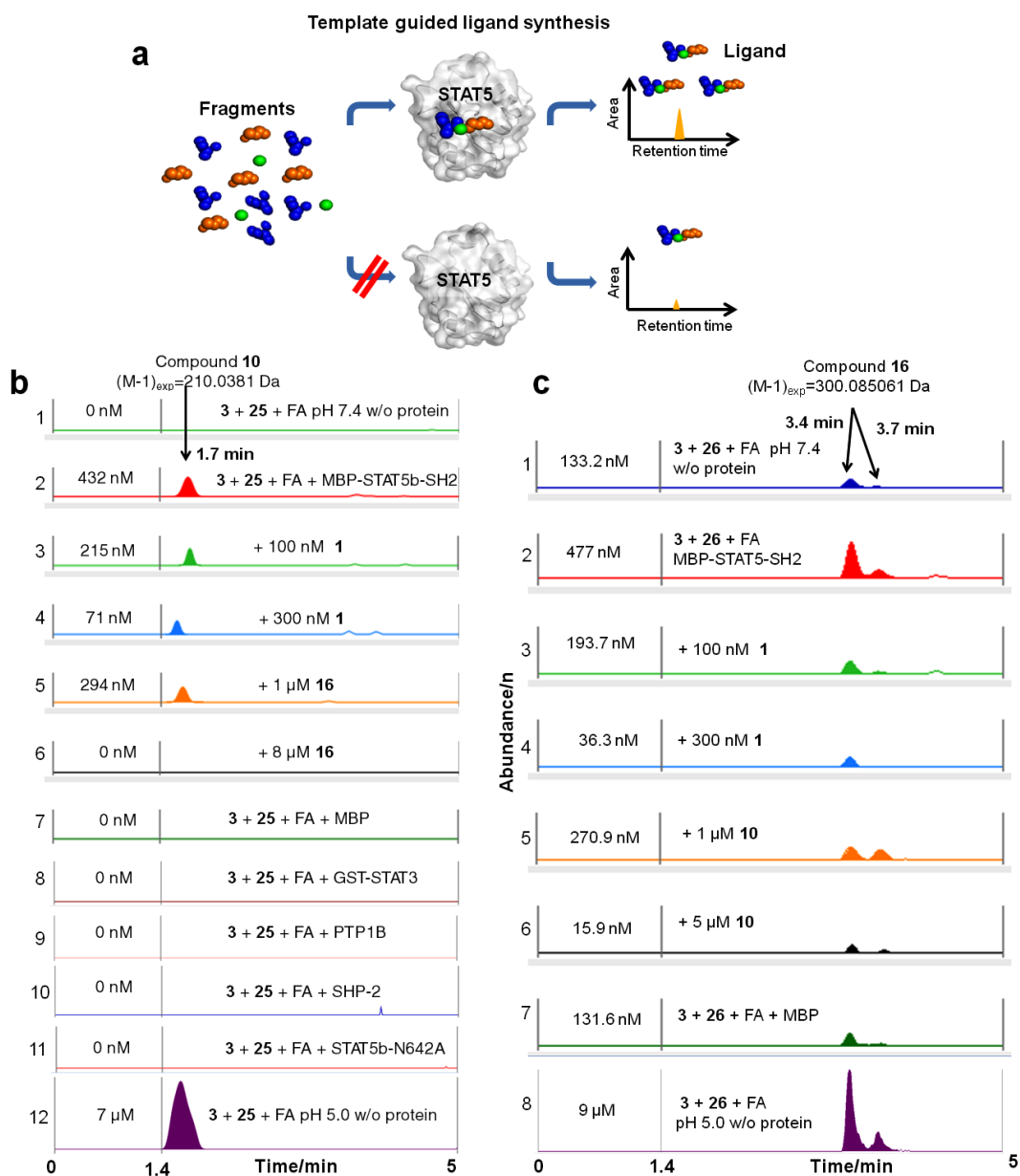
Figure 3.13: Protein-induced ligand formation through Mannich ligations**.** (a) Schematic illustration of protein-induced formation of ligand. (b) Formation of **10** detected in the HPLC-QTOF-MS (average of three independent experiments). 1: No formation of **10** from FA, fragments **3** and **25** (all 250 μM) at pH 7.4 in MOPS buffer without protein. 2: Protein-

- 61 -

induced formation of compound **10** with protein MBP-STAT5b-SH2 (250 nM) at pH 7.4. 3-6: Inhibition of protein-induced formation of **10** by peptide **1** (3, 4) or inhibitor **16** (5, 6). 7, 8: No formation of compound **10** in the presence of Maltose Binding Protein (1 μM) or GST-STAT3 (250 nM). 9-11: Compound **10** was not formed in the presence of phosphatases, SHP-2 (250 nM) and PTP1B (250 nM) nor in the presence of mutant STAT5b-N642A at pH7.4 in MOPS buffer. 12: Formation of compound **10** at pH 5.0 without protein. (c) Formation of compound **16** detected in the HPLC-QTOF-MS. Lane 1: Negative control: formation of **16** from FA, fragments **3** and **26** at pH 7.4 in MOPS buffer without MBP-STAT5b-SH2. 2: Protein-induced formation of compound **16** at pH 7.4. Lanes 3-6: Protein-induced formation of compound **16** blocked by peptide **1** (3, 4) or inhibitor **10** (5,6). 7: Formation of compound **16** in the presence of Maltose Binding Protein. 8: Formation of compound **16** at pH 5.0 without protein.

High resolution HPLC-QTOF-MS analysis was employed to quantify Mannich ligation product **10** formed with or without protein present (Figure 3.13). At pH 7.4 absolutely no inhibitor was formed from **3**, **25**, and FA, if MBP-STAT5-SH2 protein was not present (trace 1). With 250 nM MBP-STAT5-SH2 in the buffer at pH 7.4, 432 nM of **10** were formed over 24 h (average of three independent experiments). The protein-dependent reaction was saturated after 24 h, no significant changes in product concentration were observed between 24 and 48 h reaction time suggesting product inhibition of the ligation reaction. Addition of phosphopeptide **1** or inhibitor **16** to the protein-induced reaction suppressed the formation of **10** completely or partly in a concentration-dependent manner (traces 3-6). If instead of the MBP-STAT5-SH2 protein only the protein tag MBP (1 μM) or the catalytic domains of tyrosine phosphatases SHP2 or PTP1B (250 nM) were added, no product was formed at all (traces 7, 9, 10). In contrast, incubation of reagents **3**, **25**, and FA at pH 5.0 led

with or without protein to the formation of 7 μM of inhibitor **10** in a protein-independent background reaction (trace 12). Similar data were obtained for the protein-dependent reaction of fragments **3**, FA, and benzyl-tetrazole **26** although traces of a background reaction were observed in this case (Figure 3.13c). In contrast, no protein-dependent reaction was observed when replacing the 1H-tetrazoles by 1, 2, 4-triazole (Figure 3.14c), most likely due to its lower acidity compared to 1H-tetrazoles (Figure 3.15).
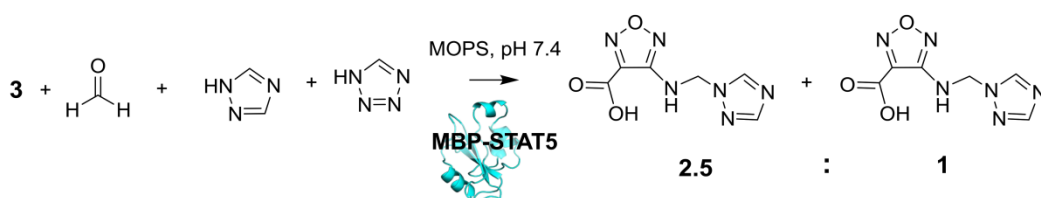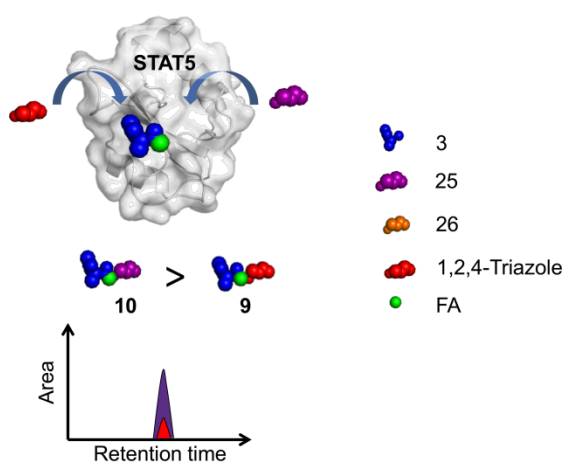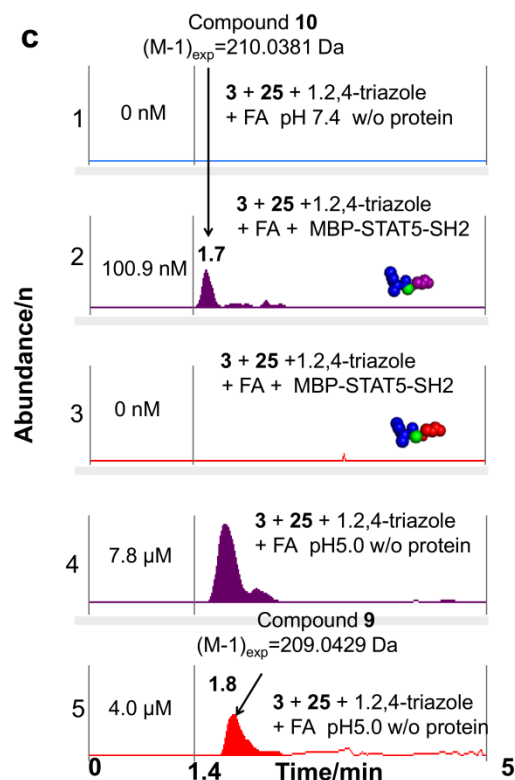
Figure 3.14: (a) Schematic illustration of competitive protein-induced ligand formation. (b) Compound **10** formed predominantly over **9** when fragment mixtures (**3**, **25**, and **1, 2, 4-triazole**) were incubated with FA in the presence of MBP-STAT5b-SH2. (c) Formation of

compound **9** and **10** were detected in the HPLC-QTOF-MS. Lane 1: negative control, no

formation of **9** or **10** from FA, fragments **3, 25** and 1, 2, 4-triazole at pH 7.4 in MOPS buffer

without MBP-STAT5b-SH2. 2: Formation of compound **10** with protein at pH 7.4. 3: No

formation of compound **9** was detected with protein at pH 7.4. 4: Formation of compound **9**

and **10** at pH 5.0 without protein; formation of compound **10** is 2.5x higher compared to **9**.
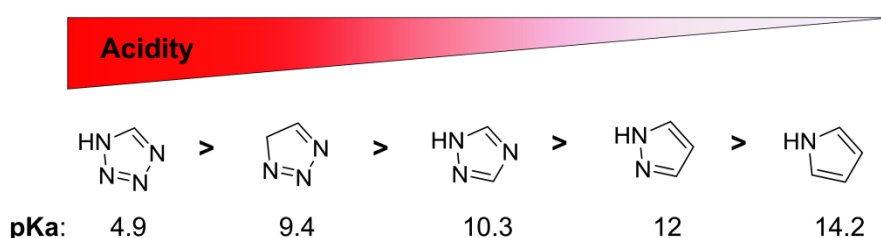
Figure 3.15: pKa value of pentazoles (pyrrole, diazoles, triazoles and tetrazoles)

3.4 Identification of Asn642 as key binding residue for STAT5 –inhibitor interactions

Protein-ligand docking plays an integral part in drug discovery spanning from the

initial target identification and validation through lead discovery and optimization. It is

beneficial to employed protein-ligand docking to accurately predict ligand conformation

bound to a target molecules active site and speed up the crucial hit-to-lead optimization

process. Nevertheless, computational tools such as molecular docking allows chemist to

explore a wider chemical space while reducing the number of compounds being synthesized

and tested in vitro which are more cost effective and less time consuming.[58,62,71]

Autodock version 4.2 docking software has been employed to evaluate the ligand

binding within the STAT5-SH2 domain. Autodock combines a grid-based method for binding

energy evaluation and pre-calculate ligand-protein interaction energy in order for subsequent

simulation with a Lamarckian Genetic Algorithm (LGA)/ Monte Carlo search for optimal ligand binding conformation.[122,123]

Using AutoDock4.2, we performed global searches of the conformational space along with careful local searches to derive the best conformational fit within the STAT5b-SH2 domain. Docking simulations were carried out with a rigid protein structure, allowing for ligand flexibility using a Lamarckian Genetic Algorithm (LGA) with the global and adaptive local search parameters through 100 trials of the "long" GA runs. Upon run completion, confirmation were specifically populated with the most favorable free energy of binding (ΔG) and is ready to chosen for further analysis. In short, the free energy is an important indication to distinguish the protein-ligand binding affinity as it is defined as the summation of all the terms of dispersion/ repulsion, hydrogen bonding, electrostatics, desolvation and torsional energy.

Molecular docking suggested that the large increase in binding affinity of compound **10** was contributed by expansion of the binding interaction into the adjacent amphiphilic pocket containing residues Trp641, Leu643 and Met639 via hydrophobic contacts. The H-bond, between the 4-amino group of **10** and the carbonyl of Asn642 was retained and possibly enforced by the higher polarity of the NH-bond[56,58,71,110] in **10** (Figure 3.16). An additional H-bond was proposed by BINding ANALyzer (BINANA)[124] between the tetrazole ring and the amide-NH_2 of Asn642 and strengthened the binding of compound **10** in the binding pocket. Similarly, compound **16** which has shows stronger inhibitory effect in cells binds to STAT5 by forming H-bond with key residues Asn642, Ser622 and Arg618 and hydrophobic interactions with residues Trp631 and Trp641.Other tetrazoles derivates (compound **11**-**14**) were docked and bound to STAT5-SH2 domain by forming essential hydrogen bonds with Asn642, Ser622 and Arg618 (Figure 3.17).
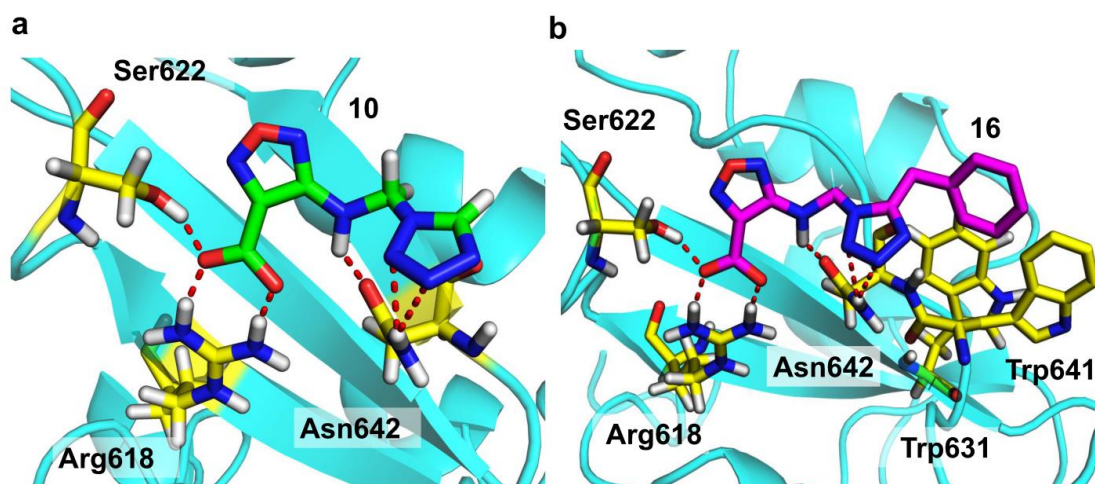
Figure 3.16: 3D-binding model of compound **10** and **16** bound to STAT5b. Hydrogen bonds are illustrated as red dashed lines and key interacting residues in yellow stick. Figures were drawn using PyMOL.
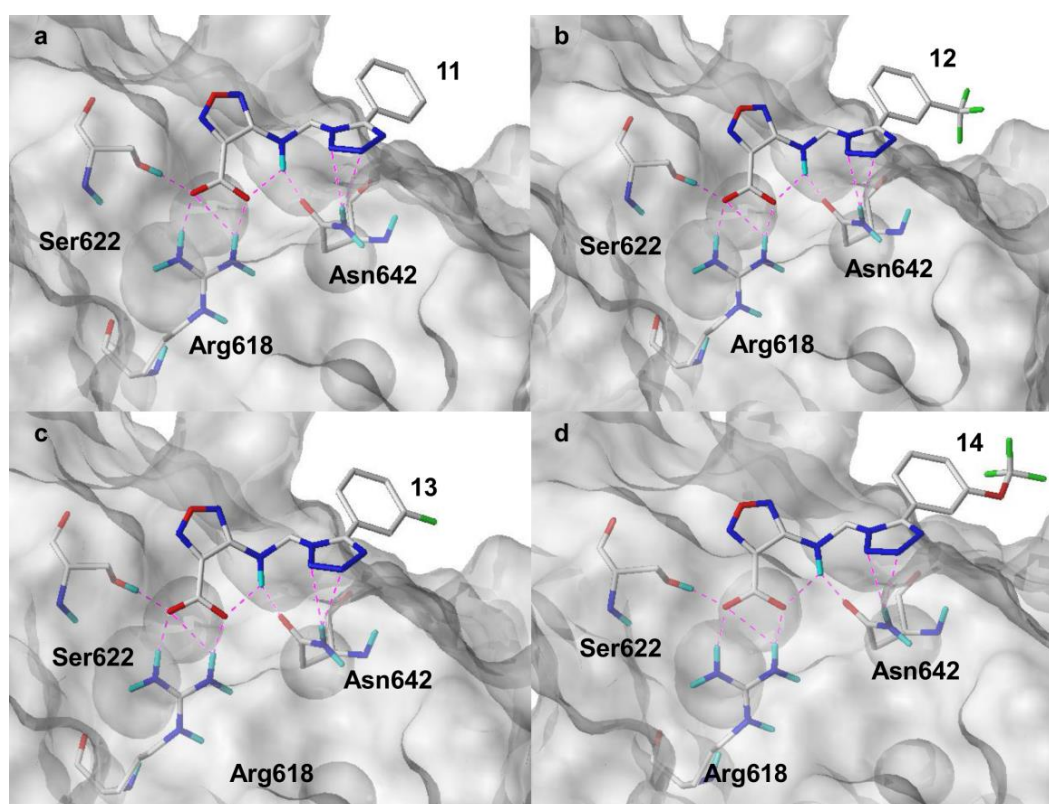
Figure 3.17: Molecular docking results of compound into STAT5a-SH2 domain (pdb: 1YIU). Stereoview of compounds 11(a), 12(b), 13(C) and 14 (D) coordination in the binding pocket showing hydrogen bond forming residues. Protein is represented as cyan surface. All compounds were bound to STAT5a-SH2 domain by forming hydrogen bonds with side chains of Asn642, Arg618 and Ser622. Protein was displayed as grey surface with key interacting residues and ligands shown as sticks. Hydrogen bonds were shown as red, dashed lines. Color-coded by element: N in blue, O in red and carbon in white. Pictures were generated with Sybyl-X 1.3.
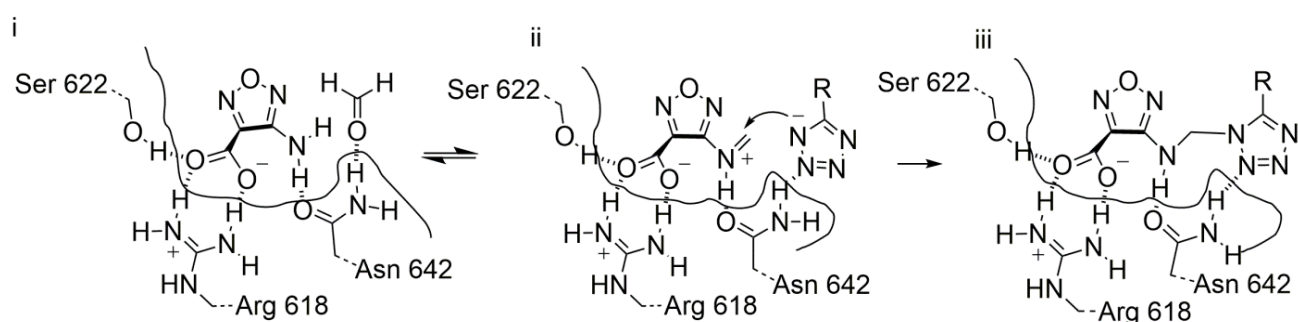
Scheme 3.1: Mechanism of the protein-induced formation of **10** from **3** with FA and **25** (R=H). (**i**) Binding of **3** via Arg618, Ser622, and Asn642, activation of FA with Asn642. (**ii**) Activation of the forminium cation of **3**, coordination of the incoming tetrazolium anion of **25** by Asn642 leads to formation of Mannich ligation product **10** (**iii**)

The proposed binding mechanism and binding mode of fragment **3** to STAT5b-SH2 domain was based on molecular docking in STAT5b homology model. This proposed binding mode highlights the importance of residue Asn642 in protein-ligand binding. In order to challenge the postulated importance of Asn642 for the reactivity of fragment **3** with

STAT5b-SH2, the fragment ligation of **3**, FA, and 1*H*-tetrazole at pH 7.4 was investigated with GST-STAT3, a protein without Asn in the otherwise similar phosphotyrosine recognition site (Figure 3.13, trace 8). With STAT3 instead of STAT5b absolutely no fragment ligation product was formed. In addition, the mutant MBP-STAT5b-SH2 N642A was generated by site-directed mutagenesis to address its significant contribution in binding to STAT5b-SH2 domain. To our surprise, the mutant protein displayed a strongly binding affinity to peptide **1** with ca. 5 µM (instead of 55 nM for the wildtype) and bound inhibitor **10** with 31 µM (instead of 1.5 µM for the wildtype). The affinity of MBP-STAT5b-SH2 N642A for **10** was significantly lower (20 fold) compared to the wild type STAT5b (Figure 3.19).

Accordingly, the conditions of the fragment ligation reaction yielded no product with the mutant protein as well (Figure 3.13). Plausibly, the side chain carbonyl group of Asn642 binds to the amino group of compound **3** via accepting an H-bond (Scheme 3.1). As a result, the amide-NH_2 of Asn642 is free to coordinate and activate the incoming FA as an H-bond donor, leading to the formation of the formiminium derivative of **3**, which is again stabilized by its H-bond to the Asn-carbonyl. Next, the amide-NH_2 could coordinate the incoming 1*H*-tetrazolium ion which reacts to the observed ligation product **10**. These data illustrate key residues Asn642 as the determining factor for selectivity for protein-ligand binding. [116]

a

```
>40310924.seq - ID: Klon40_5-GATC-Stat5B_intern1-2623426 on 2018/7/17-
6:17:24 automatically edited with PhredPhrap, start with base no.: 10
Internal Params: Windowsize: 20, Goodqual: 19, Badqual: 10,
Minseqlength: 50, nbadelimit: 1
TannGCCaGATGGGACCTTCCTCCTGAGATTCAGTGACTCAGAAATTGGCGGCATCACCATTGCTTGGAAG
                             A
TTTGATTCTCAGGAAAGAATGTTTTGGGCTCTGATGCCTTTTACCACCAGAGACTTCTCCATTCGGTCCCT
                             642
AGCCGACCGCTTGGGAGACTTGAATTACCTTATCTACGTGTTTCCTGATCGGCCAAAAGATGAAGTATACT
CCAAATACTACACACCAGTTCCCTGCGAGTCTGCTACTGCTAAAGCTGTTGATGGATACGTGAAGCCACAG
ACCCCGGCGCGCCGATCCAGATCTCATCACCATCACCATCACTAAGCTTGGCACTGGCCGTCGTTTTACAA
CGTCGTGACTGGGAAAACCCTGGCGTTACCCAACTTAATCGCCTTGCAGCACATCCCCCTTTCGCCAGCTG
GCGTAATAGCGAAGAGGCCCGCACCGATCGCCCTTCCCAACAGTTGCGCAGCCTGAATGGCGAATGGCAGC
TTGGCTGTTTTGGCGGATGAGATAAGATTTTCAGCCTGATACAGATTAAATCAGAACGCAGAAGCGGTCTG
ATAAAACAGAATTTGCCTGGCGGCAGTAGCGCGGTGGTCCCACCTGACCCCATGCCGAACTCAGAAGTGAA
ACGCCGTAGCGCCGATGGTAGTGTGGGGTCTCCCCATGCGAGAGTAGGGAACTGCCAGGCATCAAATAAAA
CGAAAGGCTCAGTCGAAAGACTGGGCCTTTCGTTTTATCTGTTGTTTGTCGGTGAACGCTCTCCTGAGTAG
GACAAATCCGCCGGGAGCGGATTTGAACGTTGCGAAGCAACGGCCCGGAGGGTGGCGGGCAGGACGCCCgc
cAtAacggCcaGgCATC
```

642

```
TTTTGG AAT CTG
         N
```

```
TTTTGG GCT CTG
         A
```

b Ala642 3 Arg618 Ser622

c Ala642 10 Arg618 Ser622

Figure 3.18: Site-directed mutagenesis N642A was performed on the STAT5b sequence. (**a**) Sanger sequencing data confirmed that the AAT codon (Asn) is replaced to GCT (Ala) at the amino acid site 642. Molecular illustration of key binding residues, Asn642 substituted with alanine and affected the ligand binding for compound 3 (**b**) and 10 (**c**) by losing essential H-bonds. STAT5 protein was shown as cyan ribbon; key interacting residues were depicted as yellow stick; Residue subjected to alanine mutation was shown as purple sticks; hydrogen bonds with key residues in the hydrophilic binding pocket of the STAT5-SH2 domain were illustrated as red dashed lines.
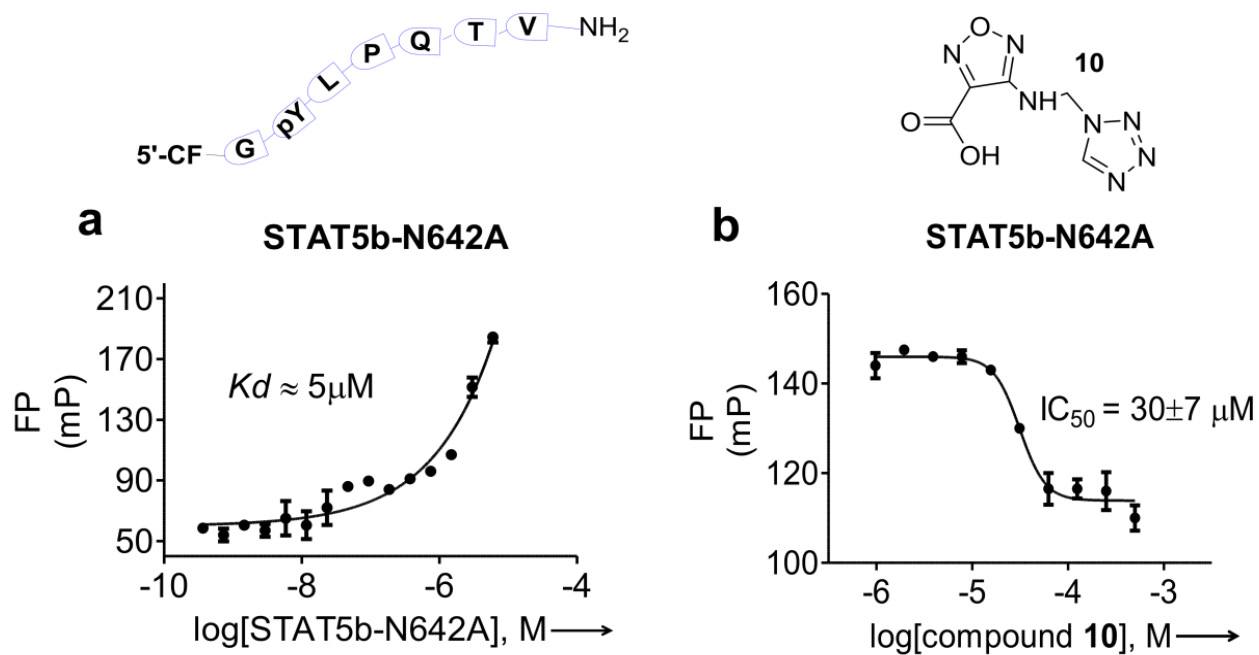
Figure 3.19: Compound **10** shows 30-fold reduction in affinity towards STAT5b protein when key binding residue Asn642 is mutated to Ala642. (a) Binding curve of phosphopeptide **1** to STAT5b-N642A. (b) Fluorescence polarization curve for the binding of compound **10** to recombinant STAT5b-N642A domai

Summary Protein induced Mannich ligation in STAT5 and ligand detection methods.
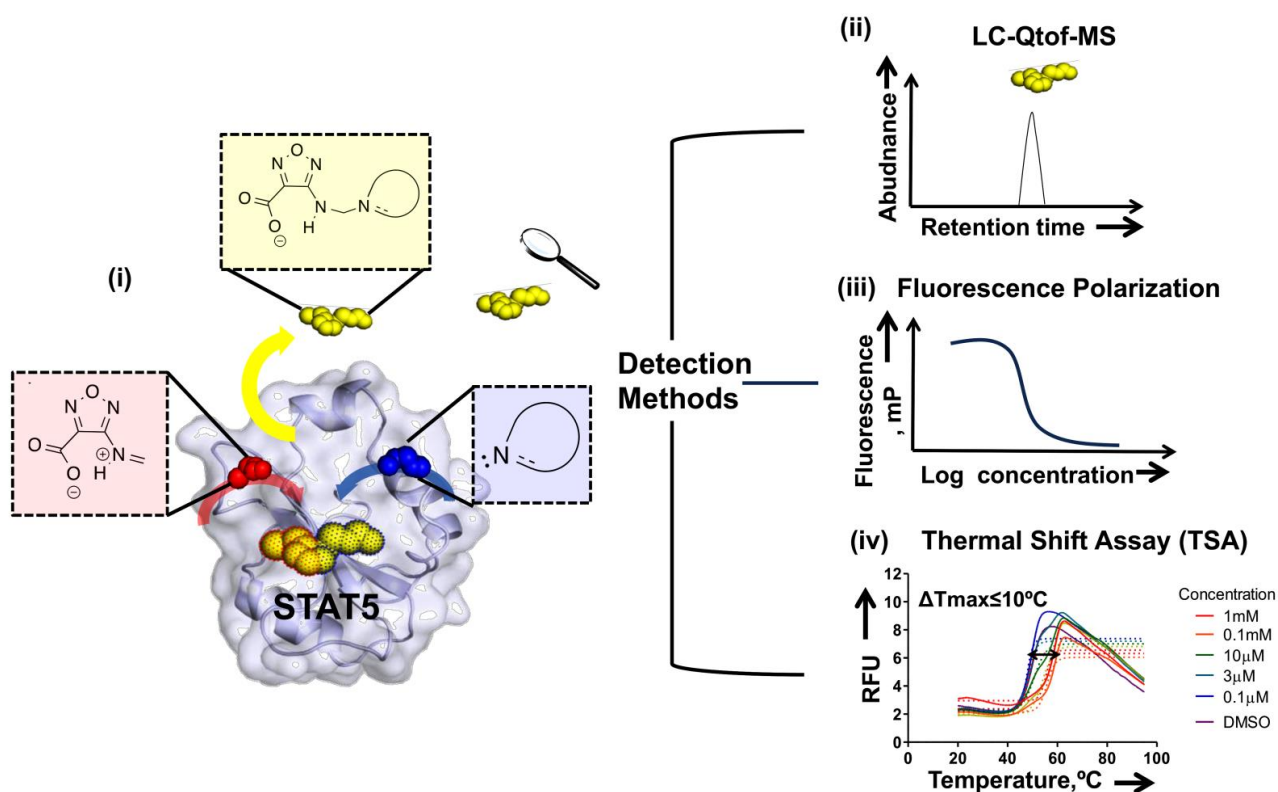
Figure 3.20: (i) Template-assisted formation of highly selective STAT5 inhibitor via Mannich reaction. Ligated product can be detected via (ii) LC-Qtof-MS, (iii) Fluorescence polarization and (iv) Thermal Shift Assay.

3.5 Specificity of STAT5 inhibitors with isolated proteins and in cell lysates

Selectivity and specificity of compound **10** for STAT5b protein was tested against STAT3 and SHP2 protein. To comprehensively determine the potential off-target effects, compound **10** was tested with closely related STAT3 and the catalytic domain of protein tyrosine phosphatase SHP2 (PTPN10) and at concentrations up to 1 mM no binding or inhibition was observed (Figure 3.21). Encouragingly, **10** portrayed negligible effects against the closely related proteins and suggested that inhibition of pSTAT5 is solely due to interaction with STAT5b-SH2 domain and not via non specific interactions with other cellular proteins.
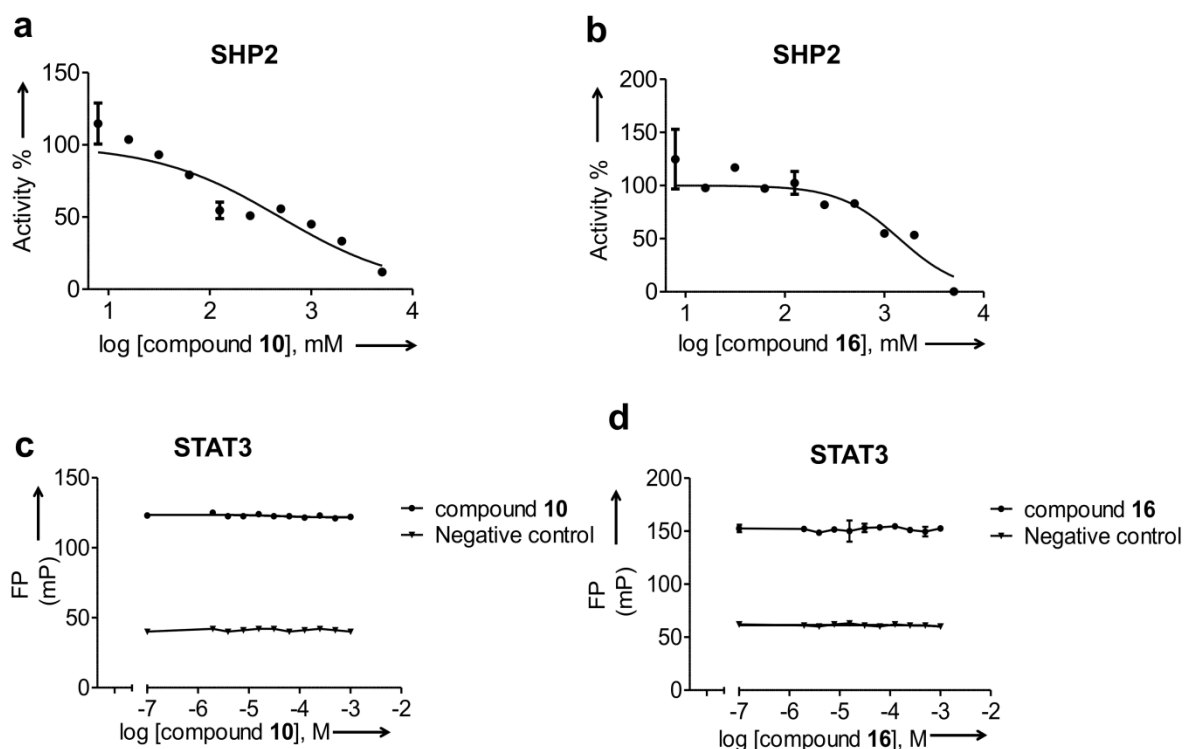
Figure 3.21: STAT5 inhibitors **10** and **16** were inactive towards SHP2. Enzyme kinetic assays of compound **10** (a) and **16** (b) with SHP2 protein. Both compounds show no significant inhibitory effects on the enzymatic activities of SHP2 protein. Dose-response

fluorescence polarization curve illustrates no binding of compound **10** (c) and **16** (d) to recombinant STAT3 protein.

In order to examine the potential effect of compounds on STAT5b activity, a STAT5-DNA binding assays was performed. Firstly, phosphorylated STAT-dimers were extracted from nuclei of BaF3/FLT3-ITD cells and were pre-treated by incubating with a serial concentration (10-1000 μM) of compounds **3**, **10** and **16** respectively. Then, a double-stranded oligonucleotide containing STAT5b consensus site was added into each mixtures before the binding of STAT1, 3, 5a, and 5b to DNA was detected using an ELISA specific for the respective protein-DNA-complexes.[58,125,126] Intriguingly, **10** inhibited STAT5b-DNA binding by more than 50% at 30 μM. We also tested the effect of **10** on STAT5a DNA binding activity and found out that the inhibitory effect is 20% lesser under comparable conditions. Compounds **3**, **10**, and **16** inhibited formation of the DNA-complex of STAT5a and STAT5b (Figure 3.22a), but not of STAT1 and STAT3 (Figure 3.22c). This result also suggests that **10** selectively block the interaction of STAT5b and DNA over other STATs in the family.

Furthermore, we also carried out EMSA analysis to further validate the inhibitory of compound **10** in the formation of STAT5: DNA complex. In EMSA analysis, STAT5: DNA complexes have a higher molecular weight therefore migrate slower than protein-free DNA. The STAT5: DNA complexes were then identified using STAT5 specific antibody. Importantly, nuclear extract of BaF3:FLT3/ITD was used for evaluation since they produced larger quantity of the STAT5 dimer/tetramer complex and ease the detection by providing more pronounced effects. Compound **10** was then added into the STAT5-DNA complex mixture before running on gel electrophoresis. Likewise, inhibition of the STAT5: DNA complex by compound **10** was detected in the Electro Mobility Shift Assay (EMSA) (Figure

3.22b).The gel electrophoresis show a clear reduction of STAT5-DNA complex when treated

with serial concentration of compound **10**. [58,125]
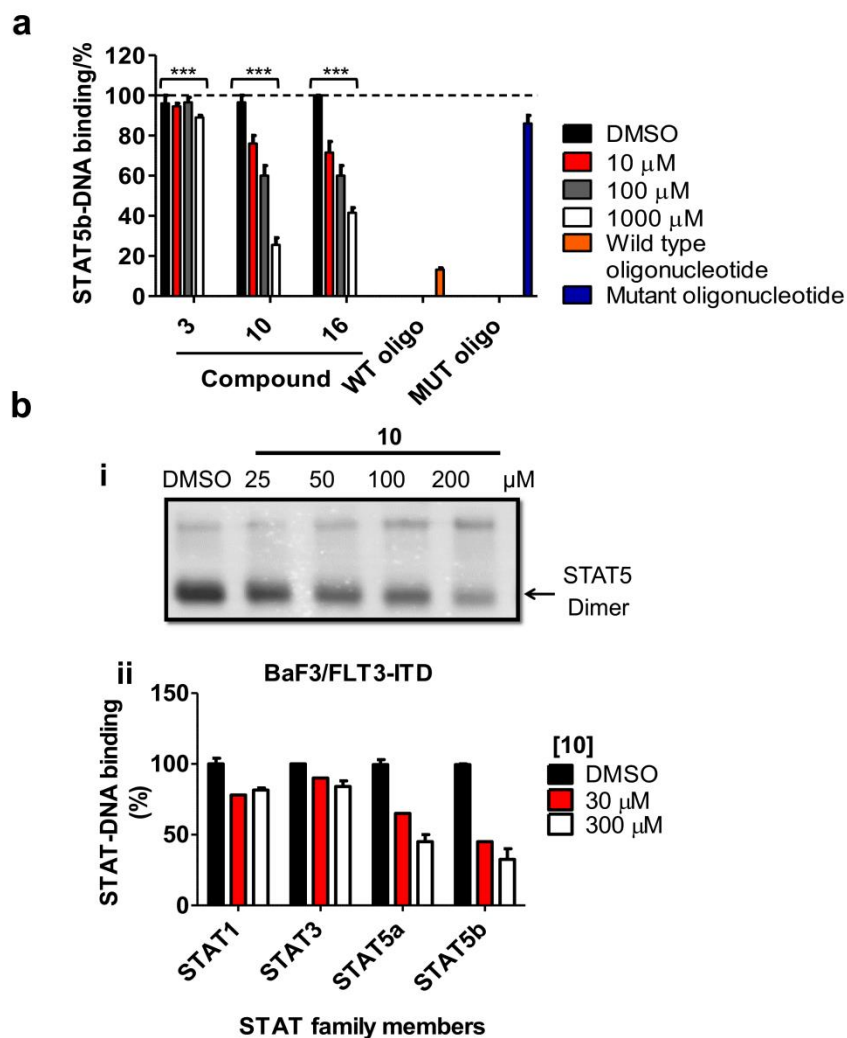
Figure 3.22: STAT5 inhibitor **10** blocks STAT5 dimerization in BaF3/FLT3-ITD nuclear

lysates. (a) **10** and **16** inhibit formation of trimeric $(STAT5b)_2$-DNA complexes in an ELISA.

(b) (i) **10** inhibits binding of STAT5 dimers, isolated from nuclear extracts of BaF3/FLT3-

ITD cells, to its target DNA in the ElectroMobility Shift Assay (EMSA) and (ii) shows

selectivity for disrupting STAT5a,b-DNA complexes in the TransAM® STAT family ELISA.
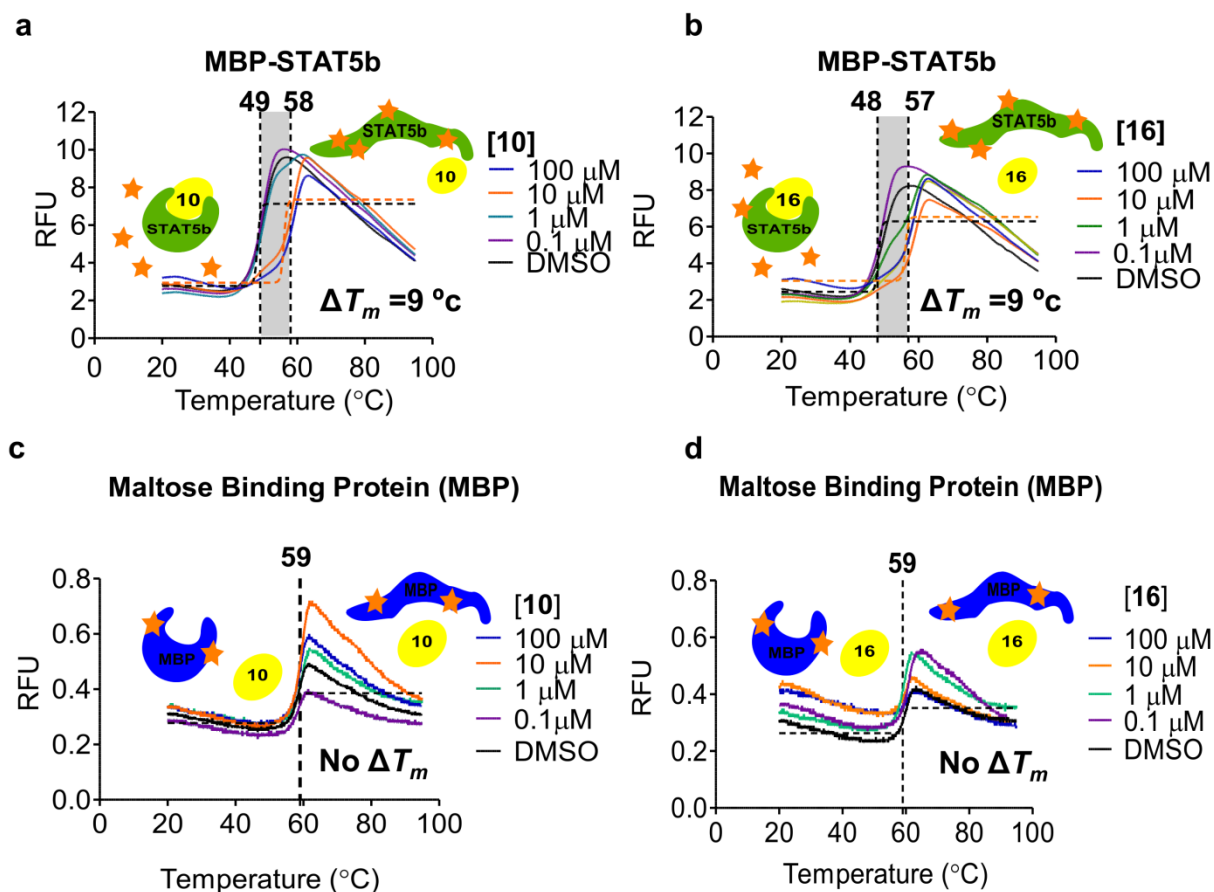
Figure 3.23: Compound **10** (a) and **16** (b) stabilized STAT5 protein shifting the melting temperature (ΔT_m) of MBP-STAT5b-SH2 protein by 9 ℃ in the thermal shift assay (TSA) but did not bind to maltose binding protein (MBP)(c-d).

Compound **10** and **16** bound to isolated MBP-STAT5b-SH2 shifting the melting temperature (T_m) by 9 ℃ (Figure 3.23). The specificity of compound **10** was further investigated in complex cell lysates using cellular thermal shift assays (CETSA).[127] We first performed cellular thermal shift assay to investigate STAT5a and STAT5b melting temperature in cell lysates in order to investigate inhibitor engagement of STAT5 (Figure 3.25). BaF3/FLT3-ITD cell lysates were incubated with **10** and exposed to a temperature gradient from 43-73°C.
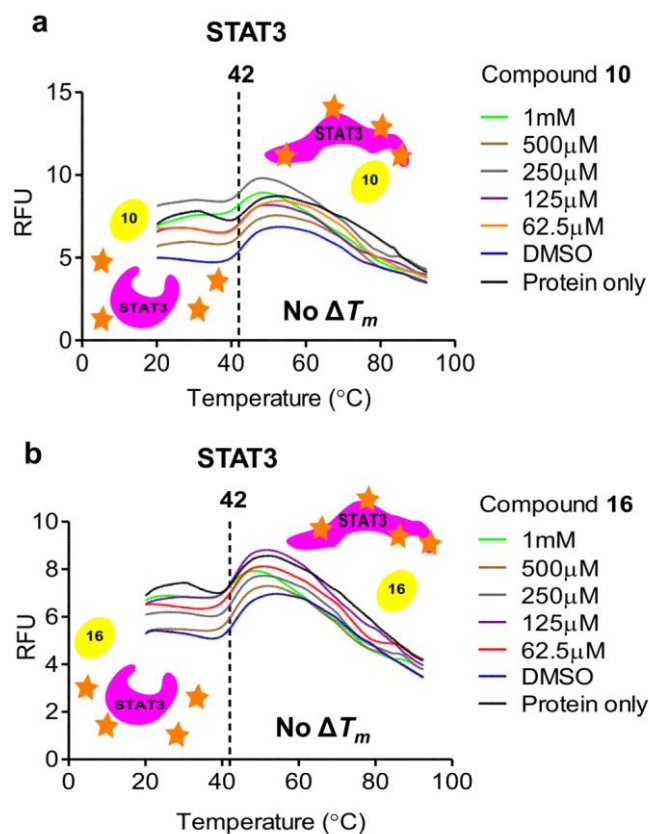
Figure 3.24: Compound **10** (a) and **16** (b) did not induce thermal stability even at high concentration in STAT3 protein indicating binding specificity of both compounds towards STAT5 protein.

Supernatants were analyzed by gel electrophoresis and immunoblotting was performed with STAT5a/b antibodies. Inhibitor **10** shifted the melting temperatures of STAT5a/b by 5 and 8 °C, respectively, indicating the thermal stabilization of STAT5 proteins through ligand binding in cell lysates (Figure 3.26).
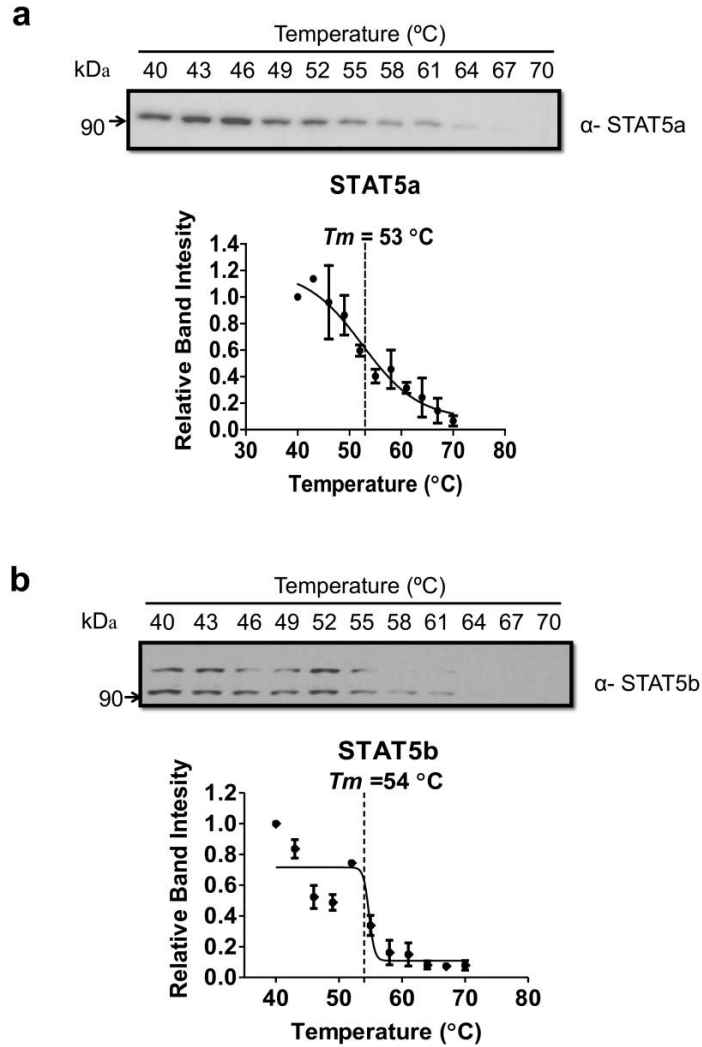
Figure 3.25: (a-b) CETSA-melting curve of STAT5a and b. Representative Western-blot signals corresponding to STAT5a and b show a decrease in intensity at elevated temperatures Band intensities obtained from Western blot-analysis were related to the highest Western blot signal which has been set to 100%. Relative band intensities were plotted against incubation temperatures and fitted to Boltzmann sigmoidal curve.
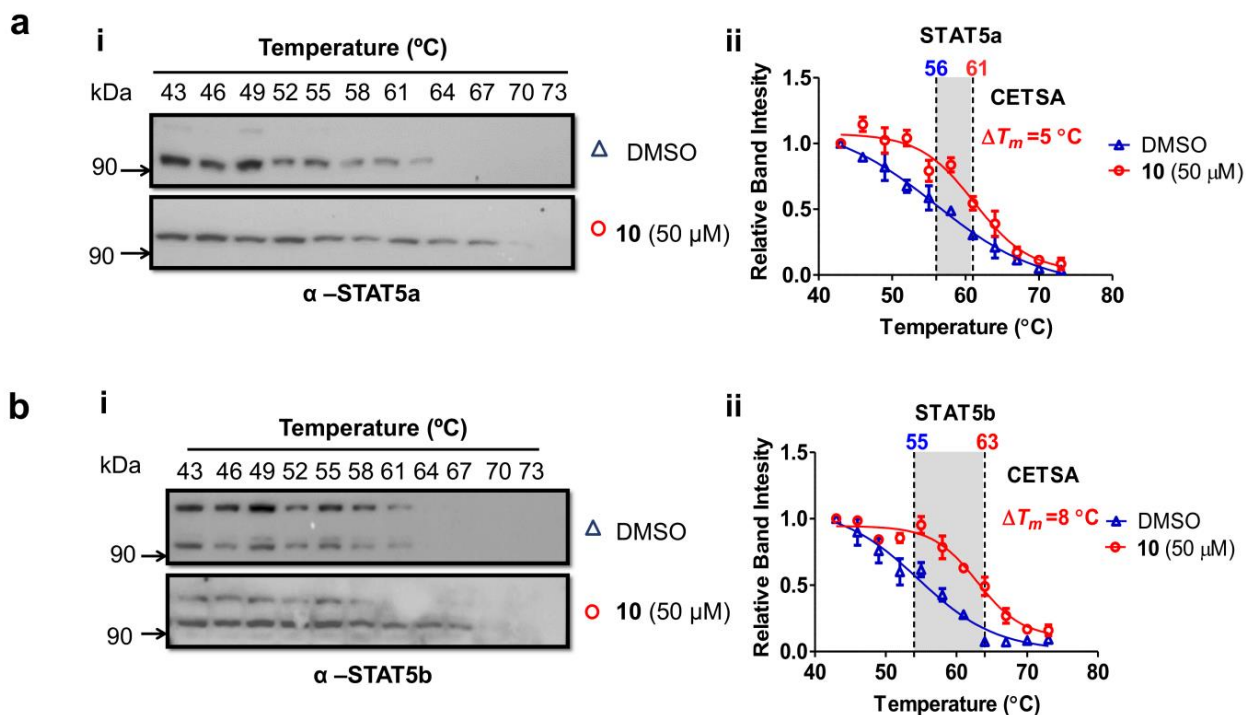
Figure 3.26: Compound **10** binds to STAT5a (a) and STAT5b (b) in complex cellular lysates as demonstrated by cellular TSA (CETSA) resulting in shifted melting curves at 50 µM compared to vehicle (DMSO). Relative STAT5a and STAT5b band intensities were plotted against corresponding incubation temperatures and fitted to Boltzmann sigmoidal curve.

3.5.1 Determination of STAT5 inhibitors target specificity using peptide 27 in neutravidin pulldown.

The most commonly used method to identify interaction partners of a specific peptide sequence is to employ the peptide as a bait to be used in affinity pull-down experiment and potential binding partners could be directly detected. Furthermore, pull-down assay can also help to confirm the existence of protein-protein interaction which has been determined via other research techniques such as co-immunoprecipitation (co-IP). Here, we designed and applied a dual label peptide, **27** to distinguish and verify postulated protein-protein interactions by competitive displacement of bindings. Peptide **27** is designed with two different tags i.e. biotin and carboxyfluorescein tag at each terminal. Biotin tag is chosen for affinity purification purposes due to its high binding affinity and its small size whereas carboxyfluorescein tag help to monitor bait protein binding, purification and localization.[128] Peptide **27** binds STAT5 at submicromolar concentration and could be used as bait to fish out potential STAT5 interaction partners or/ and determine the selectivity of STAT5 inhibitors using competitive displacement assay.

As shown in Figure 3.28, peptide **27** was added to bovine serum albumin (BSA) as control experiment to evaluate non-specific bindings. Predictably, peptide **27** does not bind and cross linked with BSA and therefore show non product in neutravidin pull down as anticipated. In addition, a serial concentration of peptide **27** was added to 25 μM of recombininat MBP-STAT5b to determine protein-peptide saturation point. Peptide **27** was shown to bind and photo-crosslinked STAT5 in a concentration dependent manner and reached a saturation point at 25μM (Figure 3.29).

M: Protein Marker
1,2,3 : BSA   (negative control)
4,5,6 : BSA   (+100μM Peptide 27)
7,8,9 : Biotin BSA
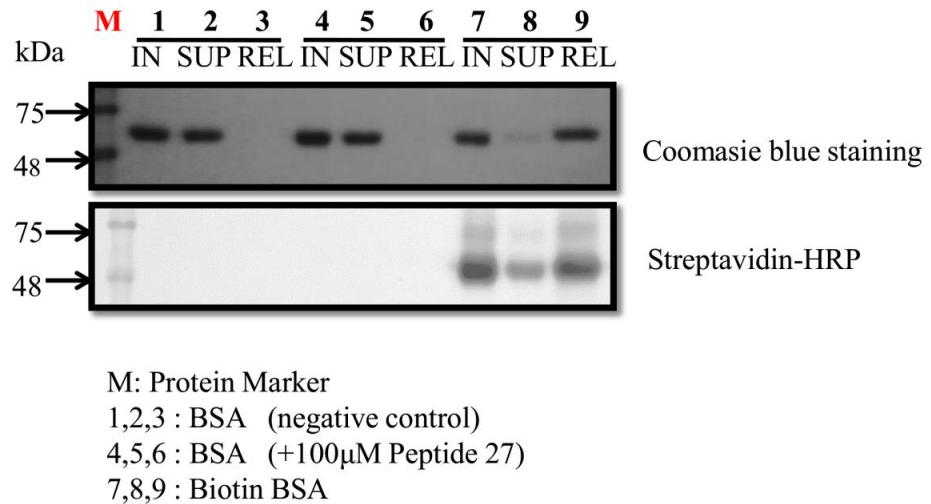
Figure 3.27: Peptide **27** does not interact and photocrosslinked with bovine serum albumin (BSA) and neutravidin pull down only allows purification of Biotinylated Bovine Serum Albumin (BSA) which acts as a positivie control.
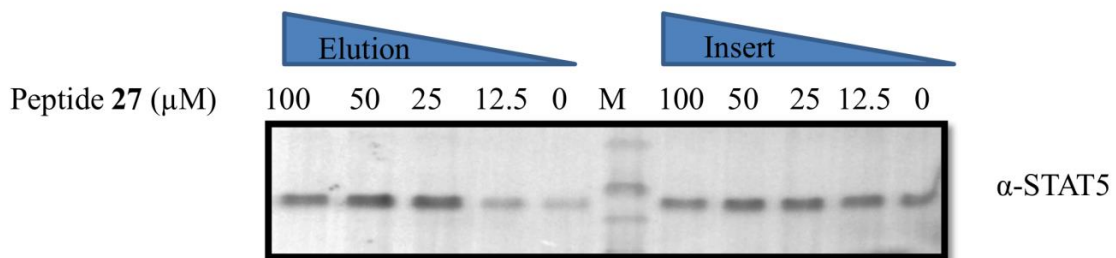
Figure 3.28: A serial concentration of peptide **27** (0-100 μM) were incubated and photocrosslinked with MBP-STAT5 (25 μM) before subjected to neutravidin beads pull down.

Binding of biotinylated MBP-STAT5 to Neutravidin beads increased proportionally with the amount of peptide **27** added as indicated in the elution fraction on western blotting.

3.5.2 Competitive displacement of peptide 27 using STAT5 inhibitors

We further employed peptide **27** to verify the target selectivity and specificity of STAT5 inhibitor, **10**. As a control experiment, we used a non fluorescent phosphotyrosine peptide, 5-Ac-GpYLSLPPW-NH2 to displace peptide **27** in STAT5 binding. We observed reduction in the photocrosslinking efficiency of peptide **27** affecting the final readout in both fluorescence intensity and band intensity in streptavidin blot (Figure 3.29b-c). Then, we substituted the Ac-peptide with the STAT5 inhibitor, **10** and observed reduction in both fluorescence intensity and pull down yield in a concentration dependent manner. This strongly indicates that small molecule **10** binds competitively to STAT5-SH2 domain by displacing high affinity peptide **27**, proving its high selectivity towards STAT5.

On the same page, peptide **1**[117] which possess strong affinity (Kd= 55 nM) towards STAT5 was also shown to interfere with the photocrosslinking event and biotinylation by competitively displace peptide **27** (Figure 3.30). As shown in Figure 3.30b, photocrosslinking event of peptide1 is concentration dependent and is affected when high affinity peptide 1 was added. Both peptide **1** and **27** compete for the same binding site, STAT5-SH2 domain indicating the high selectivity of both peptide towards STAT5. Therefore, dual labeled peptide **27** can be used as a bait to fish out specific STAT5 interaction partners for cellular signaling studies.

We then tested out the same experiment in a much complex environment using BaF3:FLT3/ITD cell lysates. Peptide **27** (100 µM) was added into the cell lysates and incubated for an hour before photocrosslinking for 15 minutes. The mixture was then subjected to neutravidin pulldown to fish out potential interaction partners. To our surprise, peptide **27** acts as bait and interacts with a range of proteins in the complex cell lysates enhancing the neutravidin pulldown yield and noticeable bandshift. It is worth looking into and identifies potential interaction partners using LC-MS/MS (Figure 3.31). Quantitative,

high resolution MS results facilitates the identification of specific peptide-protein interactions from crude cell extracts in a single-step affinity purification using neutravidin beads at near physiological conditions. This one step purification method is superior but required stringent washing conditions follow by SDS PAGE, in order to distinguish high abundant and high affinity binders, avoiding unwanted bias. The specific interaction partners are then quantified by a SILAC ratio of 1:1, to distinguish them as real binders of peptide **27**. In addition, using quantitative MS has two major advantages the determination of binding partners of peptide **27**. Firstly, unwanted bias can be easily avoided by normalizing the total amount of background binders in bait pull-down and control. Secondly, it is much easier to distinguish specific interaction candidates even in the presence of highly abundant background binders. Therefore, a near physiological buffer can be used during peptide incubation and washing which helps to preserve less stable but specific interaction.
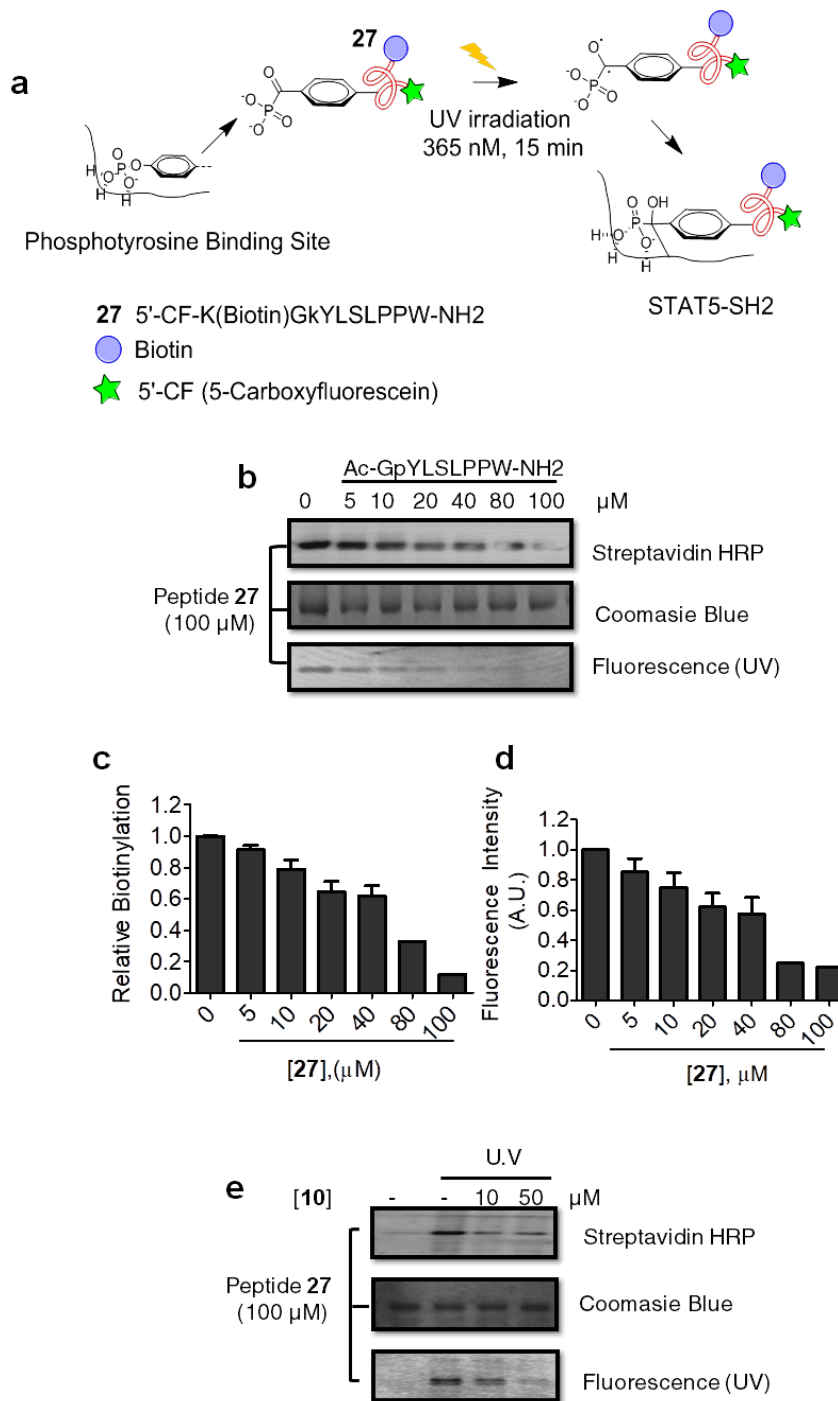
Figure 3.29: (a) Schematic illustration of the dual-labeled STAT5-binding peptide, 5-CF - K(biotin)GpcFLSLPPW-NH2 **27** (CF= carboxyfluorescein, pcF=phosphonocarboxy-phenylalanine) photo-crosslink STAT5b upon UV irradiation. (b) Photo-crosslinking of peptide **27** to STAT5 protein was displaced by the non-fluorescent; phosphotyrosines containing control peptide, 5-Ac-GpYLSLPPW-NH2 affecting fluorescence intensity and

biotinylation in a concentration dependent manner. (**c-d**) Relative STAT5 biotinylation and fluorescence intensity level were plotted using GraphPad Prism 5[129] after quantification using Image J[130] software to reflect the efficiency of photo-crosslinking of peptide **27**. Experiments were repeated twice; errors bars represent SD. (**e**) Compound **10** was able to interfere the photo-crosslinking event of peptide **27** indicating specific interaction of **10** with STAT5.
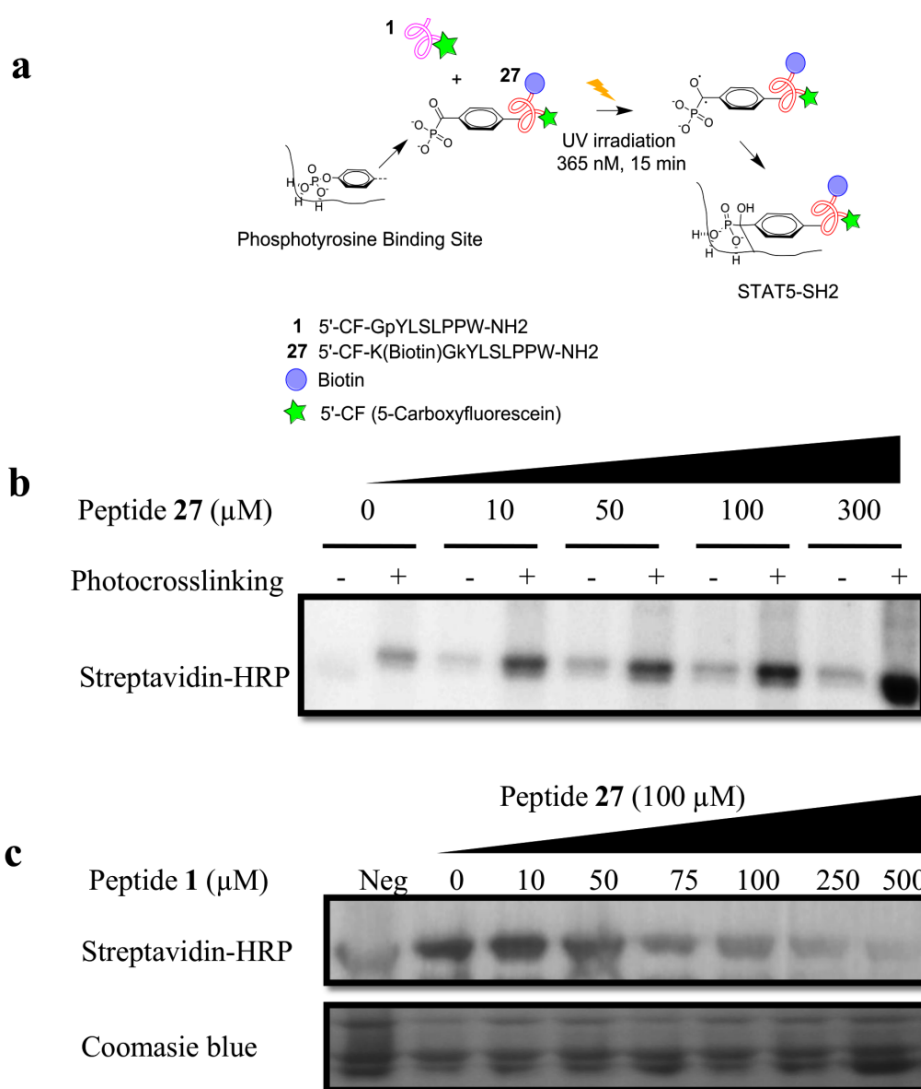
Figure 3.30: (a) Schematic illustration of competitive displacement of the dual-labeled STAT5-binding peptide, 5-CF-K(biotin)GpcFLSLPPW-NH2 **27** (CF= carboxyfluorescein, pcF=phosphonocarboxy-phenylalanine) by high affinity peptide probe **1** in MBP-STAT5b-

SH2 photo-crosslinking upon UV irradiation. (**b**) Photo-crosslinking of peptide **27** to MBP-STAT5b-SH2 in a concentration dependent manner. (**c**) Photo-crosslinking of peptide **27** to STAT5 protein was displaced by peptide **1** affecting biotinylation in a concentration dependent manner.

Coomasie Blue Staining:
M: Protein Marker
1,2,3 : MBP-STAT5 (-Peptide)
4,5,6 : MBP-STAT5 (+100µM Peptide)
7,8,9 : BaF3 FLT3:ITD (-Peptide)
10,11: BaF3 FLT3:ITD (+100µM Peptide)

Western Blot (Anti-Streptavidin-POD):
M: Protein Marker
1,2,3 : MBP-STAT5 (-Peptide)
4,5,6 : MBP-STAT5 (+100µM Peptide)
7,8,9 : BaF3 FLT3:ITD (-Peptide)
10,11: BaF3 FLT3:ITD (+100µM Peptide)
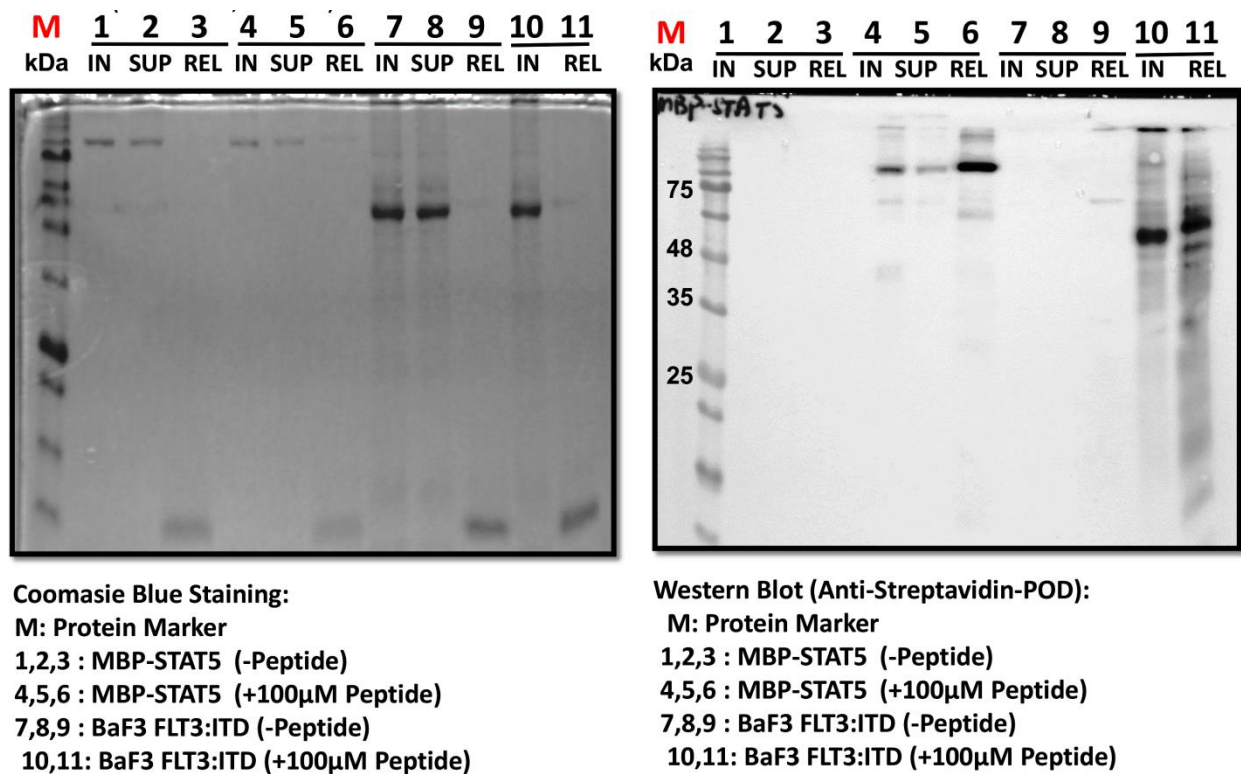
Figure 3.31: Photocrosslinking of peptide **27** to MBP-STAT5-SH2 protein followed by neutravidin beads pulldown. Peptide **27** bounds and photocrosslinks recombinant MBP-STAT5 protein and shows successfully pulldown of other STAT5 interaction partner in complex BaF3/FLT3-ITD cell lysates. It is worth to study STAT5 interaction partner using LC-MS/MS by excising eluent gel bands on the coomasie blue staining.

3.5.3   SILAC-based peptide protein interactions identify candidate bindings to peptide 27.

Stable Isotope Labelling of Amino acids in cell culture (SILAC) is carried out by culturing two cell population in heavy ($^{13}C_6$)and light ($^{12}C_6$) medium respectively.[131] Therefore, these two cell populations are metabolically encoded with either heavy or light amino acids. Background protein presents in similar amount in control and bait eluate, and the SILAC peptide pairs (heavy and light) will have 1:1 intensity ratio.[132] On the other hand, specific interaction partners to peptide **27** is easily distingush as they will possess heavy/light ratio(vice versa) significantly differ from 1:1. This significant difference is beneficial to detect interactions of protein to peptides.

To identify the possible interaction partner from our previous finding in BaF3:FLT3/ITD cell lysates, we carried out SILAC quantiitative proteomics method using peptide **27** as bait protein for photocrosslinking. After culturing both heavy and light BaF3:FLT3:IT D cells lines, we harvested 1 mg/mL of the cell lysates and allowed it to bind peptide **27** with or without the presence of peptide **1** before photocrosslinking. In order to avoid unwanted bias, cross over pulldown experiment was included whereby the peptide **1** incubated with light extract (competitive) which should give inverted ratio for specific binders (Figure 3.32). The eluates were then run on SDS PAGE before LC-MS/MS detection. For better retrieval of high confidence interaction partners by quantitative filtering, a cut of value of $P<0.0001$ was implemented in the forward and reverse screen. The log SILAC ratio of proteins identified with at least two unique peptides in each mass spectrometry run is plotted as the forward pull-down (x axis) against the reverse labeling pull-down (y axis). Specific interaction partners show inverse ratios between forward and reverse experiments and is grouped into the upper left quadrant.[128]

Our method allows us to pull down approximately 400 proteins from complex cell lysates and successfully shown that STAT5s is one of the significant binders to peptide **27** in BaF3:FLT3/ITD cells. As expected, we also detected enrichment of other members in STAT

family such as STAT1 and STAT3 due to high structural homology. In addition, scatter 2D plot of peptide **27** pull-down also indicates that STAT5a is plotted in the upper left quandrant (Figure 3.33).. Among 400 identified proteins before filtering, the known interaction partner for the STAT5A has the higher SILAC ratio in the forward but small in the cross-over experiment (Figure 3.33c).

As shown in Figure 3.34, the presence of compound **10** (50 μM) is able to competitively disrupt the binding and photocrosslikning event of peptide **27** in complex BaF3:FLT3/ITD cell lysates. Higher amount of STAT5 were detected in the eluent when only peptide 27 is added and photocrosslinking event was taken place. Skipping the photocrossliking event, lesser amount of STAT5 protein is detected in the eluent. Comparably, the amount of STAT5 presence in the eluent reduced drastically with the presence of compound **10** thus indicating competitive displacement event. The quantitatitve LC-MS/MS data was tabulated and plotted as bar graph to illustrate STAT5 yield in the eluent with or without the presence of **10**. Here, we have successfully validate that **10** is able to interfere the photocrossliking event of peptide **27** indicating specific interaction of **10** and STAT5 (Figure 3.34).
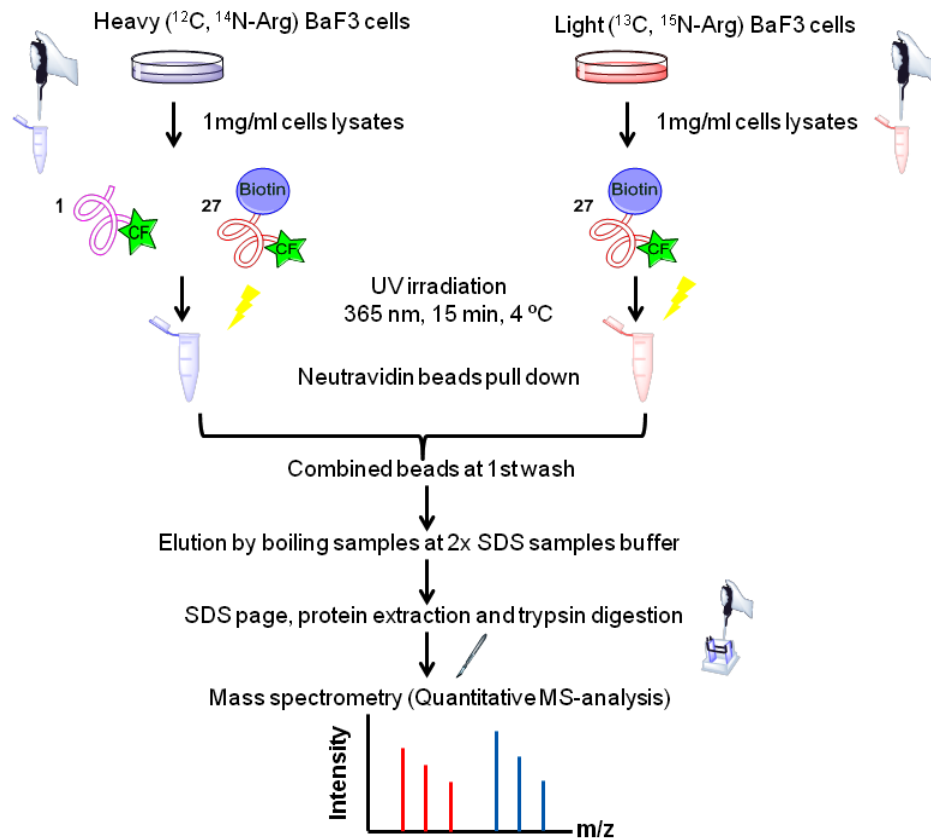
Figure 3.32: Schematic representation of SILAC labeling and proteome analysis. Cells are split and cultured in heavy or light medium containing different amino acid isotopes. Dual labelled peptide, **27** were incubated and photocrosslinked with/without the presence of fluorescence peptide ,**1**.The cells are collected and their proteins are purified for further mass spectrometric analysis. The protein levels in the two samples are compared by quantifying the heavy and light peptides, because isotopic labeling will affect their migration times.

a

Light Heavy Heavy Light

Peptide 27   -   +   *   +   -   *

M   1   2   3   4   5   6   7   8   9   10

kDa

IN SUP IN SUP REL IN SUP IN SUP REL

75 →

48 →

35 →

25 →

Coomasie Blue Staining

[Peptide 27]= 50 µM
[Peptide 1]=200 nM
UV photocrosslinking =15 min, 4ºC

b

M   5   10
     REL   REL

kDa

75 →

48 →

35 →

25 →

Streptavidin -HRP

c

Log (ratio L/H)
forward

100

Pcx

HIST1H2BC

DSP

JUP

STA5A

RAN

UBA52

ACON

10

1

0.1

0.01

0.001   0.01   0.1   1   10

Log (ratio H/L)
Reverse
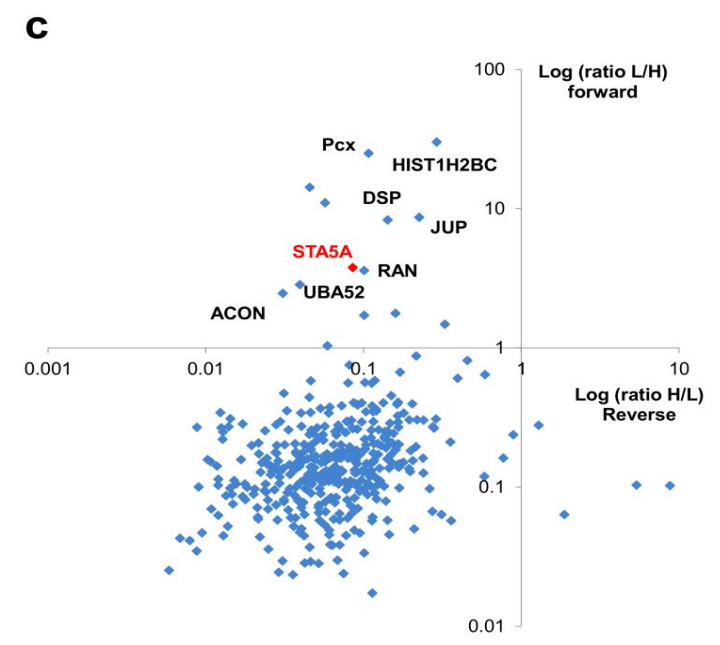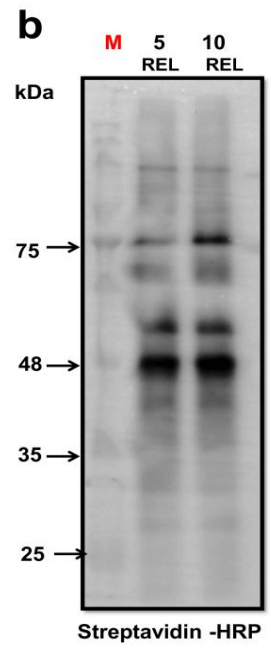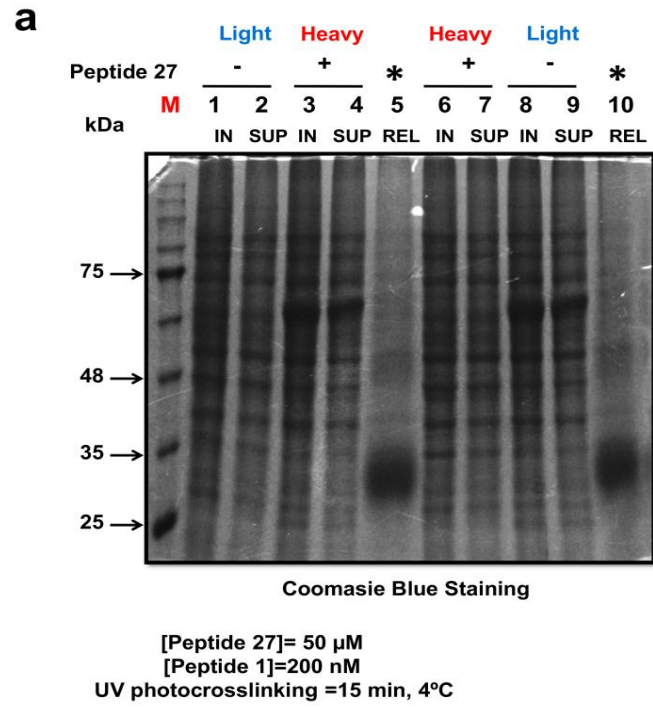
Figure 3.33: (a) Identify specific interacting partners of peptide 27 in BaF3/FLT3:ITD cells. BaF3/ FLT3:ITD cells were maintained in "heavy" medium, while control cell were grown in "light" medium. Whole cell lysates extracted from each cell pool were incubated with peptide 27 in the presence or absence of peptide 1 for 1 hr before subjected to photocrosslinking at 365 nM for 15 min in cold room (4ºC). Lysates were then pool and mixed 1:1 based on the total protein mass and pull-downed using neutravidin beads. Immunoprecipitated protein were then separated by SDS-PAGE separation, in gel trypsin digestion, and LC-MS/MS analysis. (b) Identification of photocrosslinked protein by neutravidin beads in pre or mixed cell lysates (1:1) by immunoblotting. (c) Scatter 2D plot of for peptide 27 pull-down results. The log SILAC ratio of proteins identified with at least two unique peptides in each mass spectrometry run is plotted as the forward pull-down (x axis) against the reverse labeling pull-down (y axis). Specific interaction partners show inverse ratios between forward and reverse experiments, grouping them into the upper left quadrant. Among 400 identified proteins before filtering, the known interaction partner for the STAT5A is represented by a red bullet, having the higher SILAC ratio in the forward but small in the cross-over experiment.
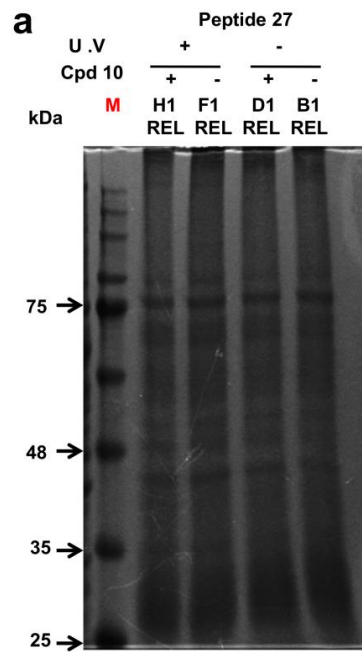
a

Peptide 27

U.V	+		-	
Cpd 10	+	-	+	-
kDa M	H1 REL	F1 REL	D1 REL	B1 REL

75 →
48 →
35 →
25 →

Coomasie Blue Staining

[Peptide 27]= 50 μM
[compound 10]= 50 μM
UV photocrosslinking =15 min, 4ºC

b

Peptide 27

U.V	+		-	
Cpd 10	+	-	+	-
kDa	H1 REL	F1 REL	D1 REL	B1 REL

75 →
48 →
35 →

Streptavidin -HRP

c

(i) +Peptide 27

STAT5

-U.V (LFQ intensity F1)
+ U.V (LFQ intensity H1)

(ii) +Peptide 27

STAT5

+ compound 10 (LFQ intensity B1)
Control (LFQ intensity D1)
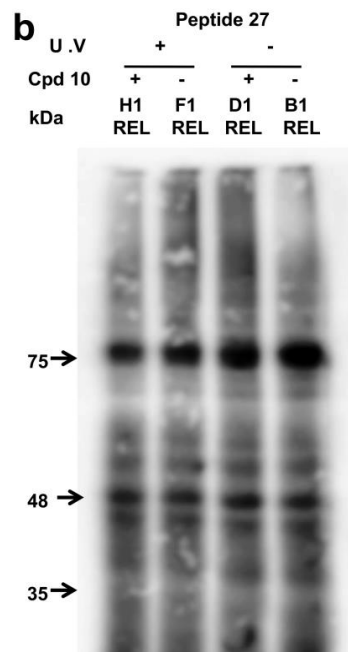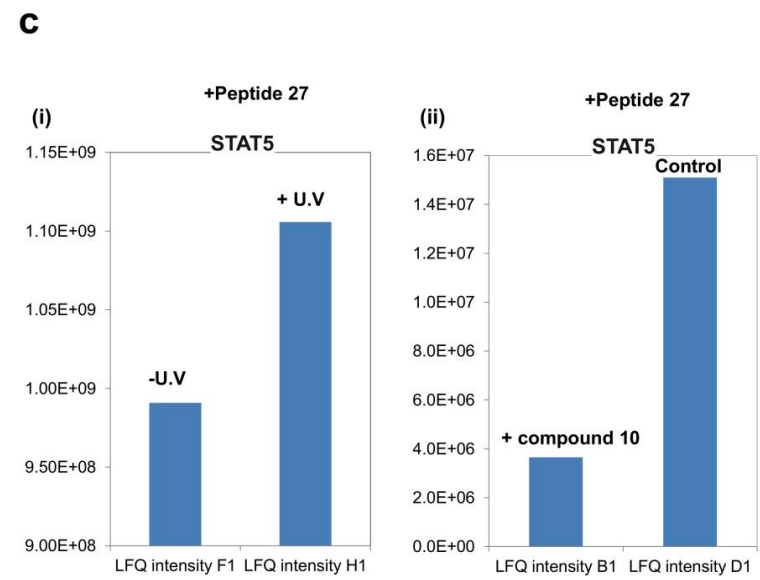
Figure 3.34: Compound **10** affect the photo-crosslinking event of peptide **27** by competitive displacement in BaF3/FLT3-ITD cell lysates. (a-b) Coomasie blue staining and western blotting studies of neutravidin beads pull down eluent upon competitive displacement of peptide **27**. I LC-MS/MS analysis of neutravidin pull down eluent in the presence of peptide **27**. (i) Higher amount of STAT5 were found in the eluent when peptide **27** were incubated and photo-crosslinked with BaF3/FLT3-ITD cell lysates. (ii) Lesser amount of STAT5 were eluted when BaF3/FLT3-ITD cell lysates in the presence of compound 10 which interfere the binding of peptide **27** by competitive displacement. Compound **10** was able to interfere the photo-crosslinking event of peptide **27** indicating specific interaction of **10** with STAT5.
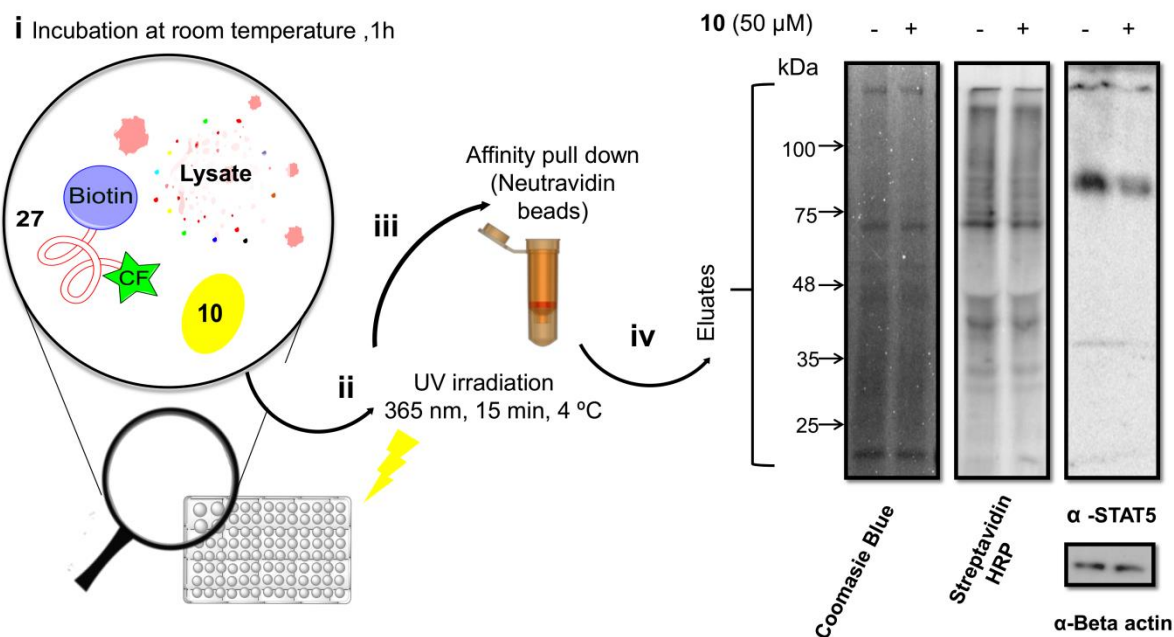
Figure 3.35: Binding of **10** to STAT5 in BaF3/FLT3-ITD cell lysate was determined by photocrosslinking. (**i**) The dual-labeled (carboxyfluorescein and biotin) peptide probe 27 binds to STAT5 with submicromolar affinity and photocrosslinked (**ii**) with target proteins by activating the 4-phosphoncarbonyl residue that acts as a photoactive phosphotyrosine mimetic. (**iii**) Crosslinked proteins can be isolated by biotin pull-down using Neutravidine beads. (**iv**) Displacement of **27** (100 μM) by compound **10** (50 μM) in BaF3/FLT3-ITD cell lysates (1mg/mL) resulted in significantly reduced photo-crosslinking of **27** and STAT5 as demonstrated in the Western blotting using STAT5 antibodies (right lane), whereas other biotinylated proteins were not reduced (middle lane).

The specific interaction of inhibitor **10** with STAT5 was further challenged by interfering with the photo-crosslinking of STAT5b-SH2 and the dual-labeled STAT5-binding peptide 5-CF-K(biotin)GpcFLSLPPW-NH$_2$ **27** (CF= carboxyfluorescein, pcF= phosphono-carboxy-phenylalanine). Peptide **27** was demonstrated to photo-crosslink STAT5b after being exposed to UV irradiation at 365 nm and **10** suppressed the photo-crosslinking in a

concentration-dependent manner (Figure 3.29). When peptide **27** was incubated with BaF3/FLT3-ITD cell lysate, irradiated for 15 min at 4 ℃ and subjected to pulldown using avidin beads, compound **10** repressed STAT5-crosslinking by displacing peptide **27** competitively in the complex lysate (Figure 3.35).

3.6   Functional evaluation of STAT5 inhibitors in living cells and animals.

The biological activity of inhibitors was studied in a cellular disease model using the murine pro-B-cell line BaF3 stably transfected with the internal tandem duplication (ITD) mutation of the human FLT3 receptor (FLT3-ITD).[133] In these cells STAT5 is constitutively phosphorylated without cytokine activation. As the FLT3-ITD mutation is found in 35 % of AML patients it can be considered as a relevant model for this disease. [134]

At first, STAT5 phosphorylation at tyrosine residues (Tyr694/Tyr699) was investigated. 5-Aryl-substituted derivatives like **11-13** could not be tested in cells as they precipitated in buffer. Next, compound **10**, **16** and **18** was assessed for whole cell potency against BaF3/FLT3-ITD (mouse FLT3-ITD) cell lines, MV-4;11 (human FLT3-ITD), K562 (human Bcr-Abl) and respectively. Cell viability was assessed following treatment at various concentrations of inhibitor using Alamar-Blue cell viability assay (48 h). As compared to **10**, *IC$_{50}$* values for **16** were 2−3-fold higher in potency, with activities ranging from 20-30 μM. Encouragingly, **16** displayed the potent activity in STAT5 driven cell lines. We next evaluated **16**-mediated inhibition of STAT5 phosphorylation levels. BaF3/FLT3-ITD cells were treated with serial concentration of **16** (ranging from 25-200 μM) for 6 h, the cells were harvested, and the levels of phosphorylated STAT5 (Y694) were determined via immunoblotting (Figure 3.36a). The strongest inhibition was observed for **16** with >50% reduction of STAT5 phosphorylation at 25 μM (Figure 3.36b) with no change in the total STAT5 concentration. These findings indicate that the **16** exerts selective and potent

inhibitory effect towards dimerization of STAT5 but do not affect the total content expression

of STAT5 protein which is extremely crucial to avoid off-target effect.
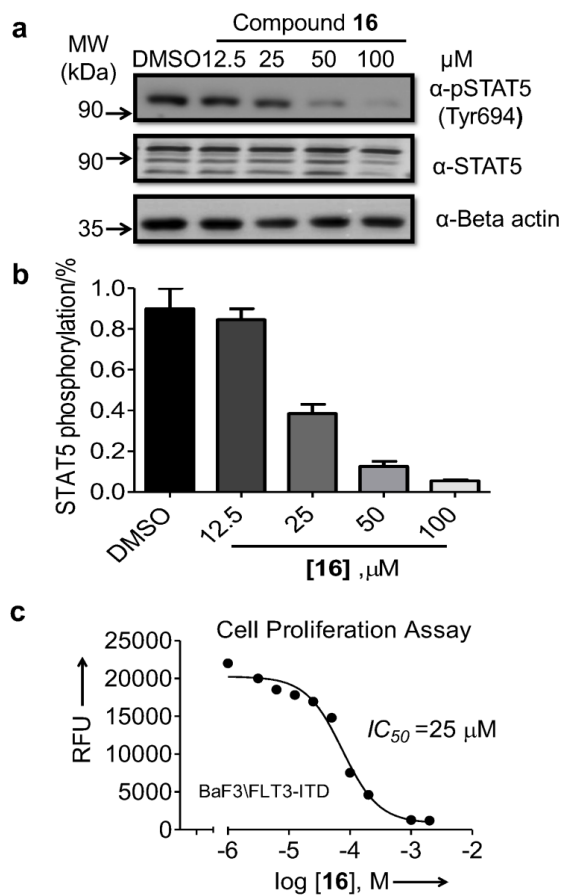
Figure 3.36: STAT5 phosphorylation was reduced upon compound **16** treatment. (a) **16** blocks tyrosine phosphorylation of STAT5 in a dose dependent manner as shown by Western blot analysis in BaF3/FLT3-ITD cells after 6 h treatment. (b) Relative STAT5 phosphorylation levels were plotted as after quantification using Image J[130] software. Experiments were repeated twice; errors bars represent SD. Immunoblotting for beta-actin was used as a control for uniform protein loading.
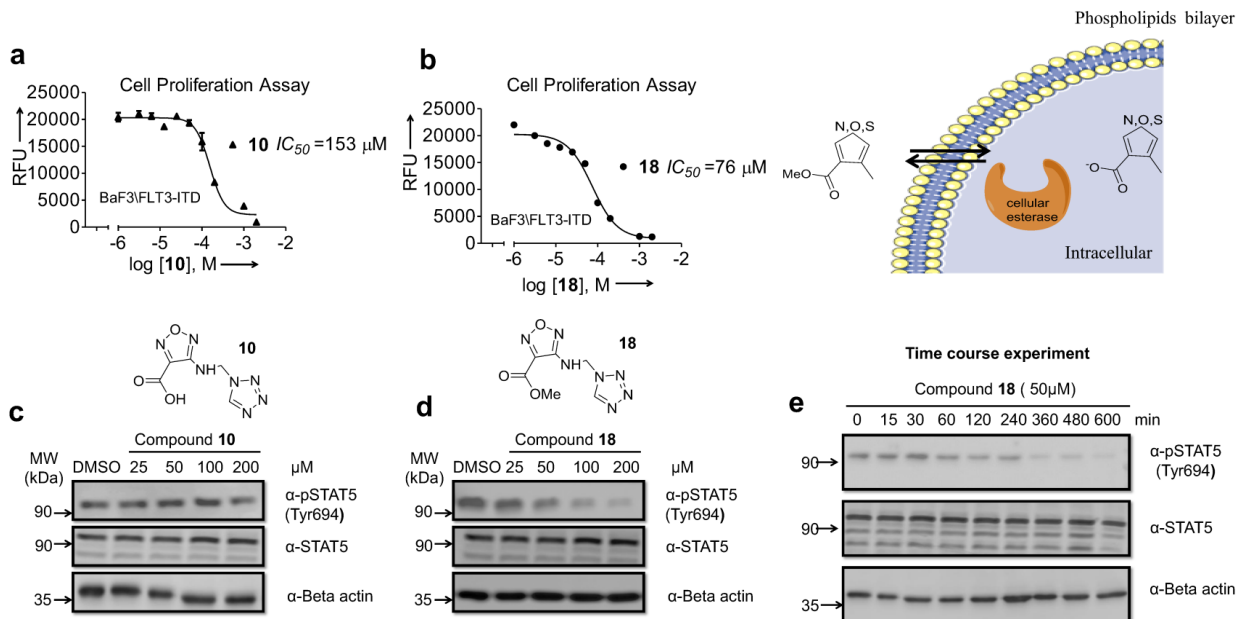
Figure 3.37: Methyl ester (compound **18**) acts as a prodrug and potentially cleaved by cellular esterase to liberate the active compound (compound **10**). (a-b) Compound **18** is 2x more potent than compound **10** in inhibiting the proliferation of BaF3/FLT3-ITD cell after 48 h as determined by the Alamar Blue assay. (c-d) Compound **18** decreases tyrosine phosphorylation of STAT5 in a dose dependent manner leading to inhibition of cell proliferation in BaF3/FLT3-ITD cells; on the other hand, the phosphorylation of STAT5 was mildly inhibited by **10** only with at concentration >100 μM. (e) Compound **18** reduced STAT5 phosphorylation steadily in a time course experiment served as a potential STAT5 prodrug inhibitor

In contrast, the phosphorylation of STAT5 was inhibited by **10** only with an IC_{50} value of >100 μM (Figure 3.37c). We suspected that the low cellular activity of **10** was hampered by low cellular uptake due to its high polarity. This suspicion was substantiated by the higher activity of ester derivative **18**, which might act as prodrug being activated by intracellular esterases.[56,71,135] A time course experiment indeed showed that compound **18** reduced STAT5 phosphorylation steadily over 10 h (Figure 3.37e). Both compounds **16** and **18** had no effect on the overall expression of endogenous STAT5 and STAT3 (Figure 3.37c-d and 3.38a-b). To further determine the selectivity of **16** for STAT5, we tested for off-target kinase activity, a possible alternative target for an effector of STAT5 phosphorylation. **16** and **18** showed negligible effects against FLT3 kinase, an upstream STAT5 activating kinase as well as homologous STAT3. These data suggest that inhibition of pSTAT5 is due to interaction with STAT5′s SH2 domain and not through inhibition of upstream kinases (Figure 3.38). These in vitro functional assays also proven the selectivity and specificity of compound **16** in binding to STAT5b which requires three dimensional conformation that can interact effectively with STAT5b-SH2 domain.
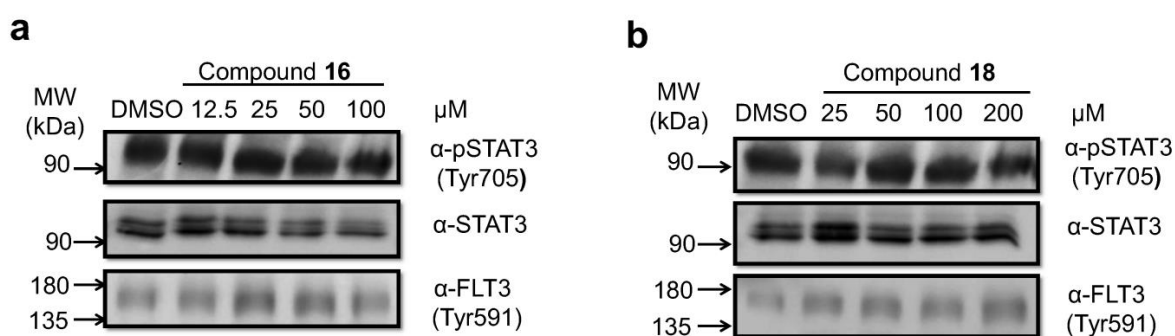
Figure 3.38: Compound **16** (a) and **18** (b) specifically inhibit phosphorylation of STAT5 but exhibit no affect on phosphorylation and endogenous expression of STAT3.

To further investigate selectivity of compound **16** and **18**, MDA-MB-231 breast cancer cells which harbor high pSTAT3 and negligible pSTAT5 activity, were assessed for differential pSTAT inhibition by 50 μM (Figure 3.39). Encouragingly, pSTAT3 was not inhibited at doses corresponding to pSTAT5 inhibition within the leukemic cell line and total STAT3 were also not affected. It was shown that both compounds exhibit negligible cytotoxicity in MDA-MB-231 than in the high pSTAT5 leukemic cell line.[58] This suggest that compound **16** target STAT5 selectivity without interfering with other crucial proteins *in cellulo* and could be a potential STAT5 inhibitor for targeted anti-cancer therapy.
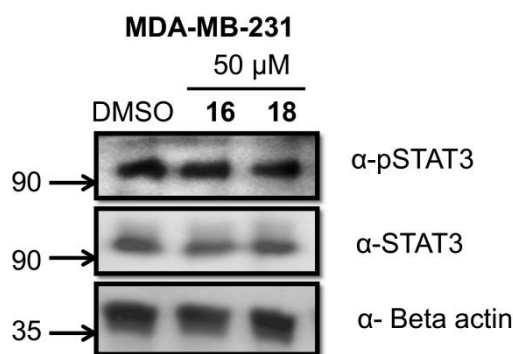
Figure 3.39: Compounds **16** and **18** show no effect on pSTAT3 in MDA-MB-231 cells, which rely heavily on pSTAT3 but not pSTAT5 activity for cell proliferation.

Encouraged by the ability of **16** to significantly block STAT5 DNA-binding, we next investigated whether **16** could antagonize STAT5-driven transcriptional activity in living cells. BaF3/FLT3-ITD cells transfected with a dual firefly/Renilla luciferase system were treated with **16** for 6 h and the activity of the STAT5-transcribed luciferase reporter gene was found to reduce significantly in a dose-dependent manner (Figure 3.40b). The results revealed that **16** attenuated STAT5b-directed transcription in a dose-dependent fashion, with an IC_{50} value of *ca.* 50 μM. By attenuating STAT5 dimerization, **16** blocked the ability of pSTAT to activate the luciferase reporter construct[136,137], thus effectively blocks subsequent

events associated with STAT5 activity including nuclear translocation and transcriptional activity. These results also indicate that **16** could inhibit STAT5b-directed transcription in living cells, and is consistent with its effects on the STAT5-DNA interaction as described above.

. Inhibition of the endogenous transcription of STAT5 target genes by **16** and **18** was studied, too. BaF3/FLT3-ITD cells were treated with inhibitors for 6 h, mRNA was harvested and analyzed by quantitative RT-PCR. Transcription and protein expression of three target genes of STAT5, Pim1 kinase, Bcl-xl, and Cis, which play essential roles in cell cycle progression and survival, was found to be strongly reduced (Figure 3.40c).The effect of STAT5 inhibitors **10**, **16**, and **18** on the proliferation of cancer cells carrying the common FLT3-ITD mutation after 48 h was quantified by the Alamar Blue assay (Figure 3.36c, Figure 3.27a-b). All three compounds showed a clear dose-dependent inhibition of cell proliferation.

For comparison, the compounds were tested with four non-STAT5-dependent cell lines (HT-29, COS-7, HeLa and MDA-MB-231) and the cytotoxicity was negligible at up to 500 μM (Figure 3.41). This experiment ensures minimal off-target effect and determines the therapeutic window of **16.** Most encouragingly, the compounds also showed no effects on STAT3 phosphorylation and on endogenous STAT3 expression (Figure 3.39).[58]

The percentage of necrotic vs. apoptotic cells death after treatment with **16** was studied by flow cytometry staining with a fluorescent annexin-V conjugate and with propidium iodide (PI), likewise reduced STAT5 phosphorylation was studied using a fluorophor-conjugated anti-pSTAT5 antibody (PE-Cy7 Mouse anti-STAT5, pY694, Figure 3.40a).

Downstream of STAT5 namely Pim1 kinase, Bcl-xl, and Cyclin D1 were further assessed for modulation of the STAT5 transcriptional targets at protein level upon treatment with **16** using immunoblotting (Figure3.42). We reasoned that **16** and **18** should decrease

gene expression and induce apoptosis by 24 h. BaF3/ FLT3-ITD were dosed with **16** and **18** at the same serial concentrations (12.5-200) μM respectively for selective STAT5 inhibition. At 6 h, we observed dose-dependent decreases in the protein expression of downstream targets which correlates with the gene expression pattern evaluated in the RT-PCR experiment (Figure 3.40c).
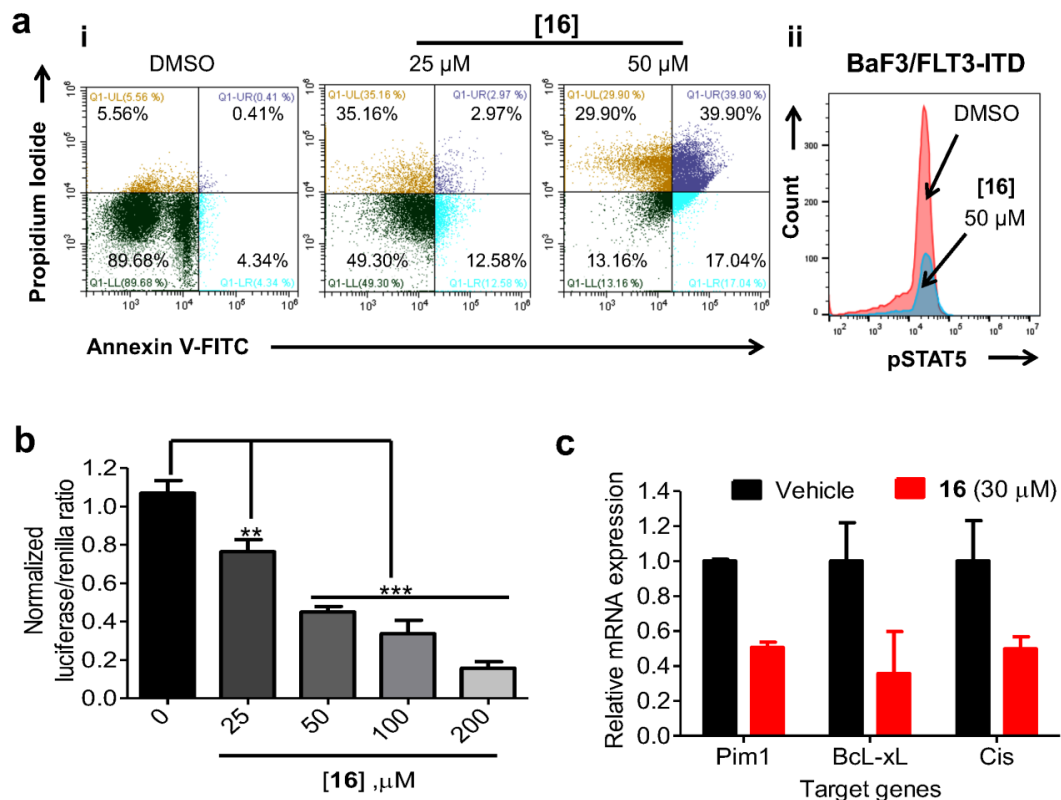
Figure 3.40: Activity and functional effects of STAT5 inhibitor **16** in STAT5-dependent cells. (a) (i) BaF3/FLT3-ITD cells were treated with compound **16** after which annexin V/propidium iodide staining and flow cytometry were performed; (**ii**) Intracellular levels of phosphorylated STAT5 were evaluated by flow cytometry after 6 h exposure of cells to compound **16** for 50 μM. (b) Compound **16** inhibits transcriptional activity of STAT5 in BaF3/FLT3-ITD cells as measured by normalized Fluc/Rluc ratio in dual luciferase reporter

assay. (c) Expression of downstream targets of STAT5 Pim 1, BcL-xL and Cis was reduced after 18 h of treatment with compound **16**. Gene expression was quantified by quantitative PCR.
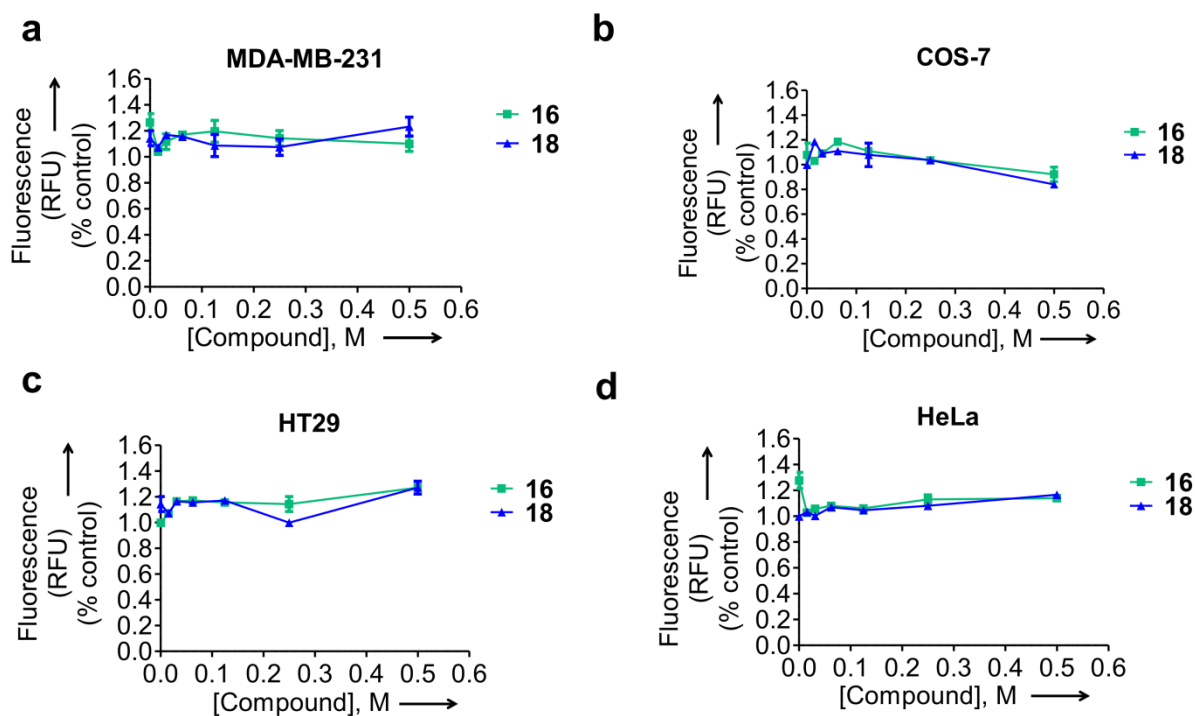
Figure 3.41: (a-d) Compounds **16** and **18** show no cytotoxicity in STAT5-independent cancer cell lines MDA-MB-231 (human breast cancer), monkey fibroblasts (COS-7), HT29 (human colon adenocarcinoma) and HeLa (human cervix carcinoma).
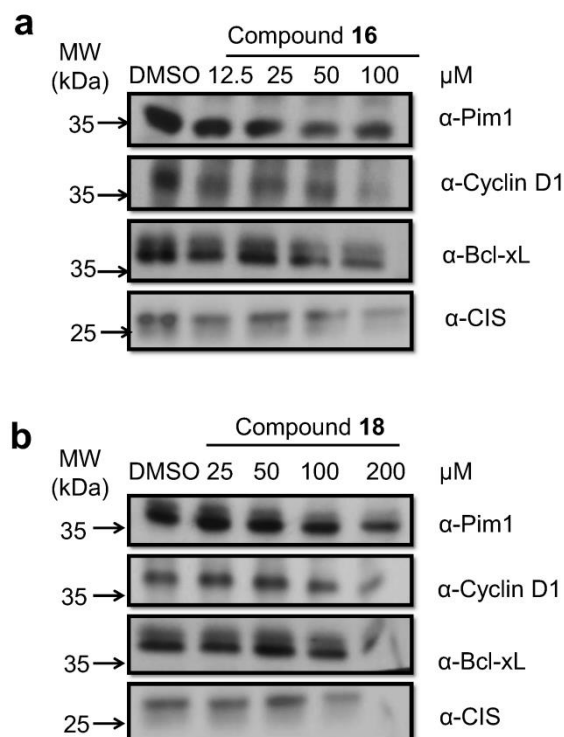
Figure 3.42: Cellular treatment with **16** (a) and **18** (b) impair the expression of its downstream target genes.

Target specificity of compound **16** to STAT5 in living cells was evaluated using isothermal dose-response fingerprints (ITDRF), a variation of CETSA[127,138,139] experiments. BaF3/FLT3-ITD cells were treated with **16** at concentrations between 0 to 100 μM for 6 h. All samples were heated for 3 min to 60 °C, the denaturation temperature based on the T_m curves in the CETSA experiment (Figure 3.25), lyzed and immunoblotted with STAT5a/b antibodies. The amount of STAT5 protein found in the blot was plotted against logarithmic concentration of the inhibitor, indicating the in-cell occupancy (OC_{50}) of STAT5a/b of 63 and 28 μM, respectively, correlating well with the inhibition of target phosphorylation and cell proliferation (Figure 3.43). [109]
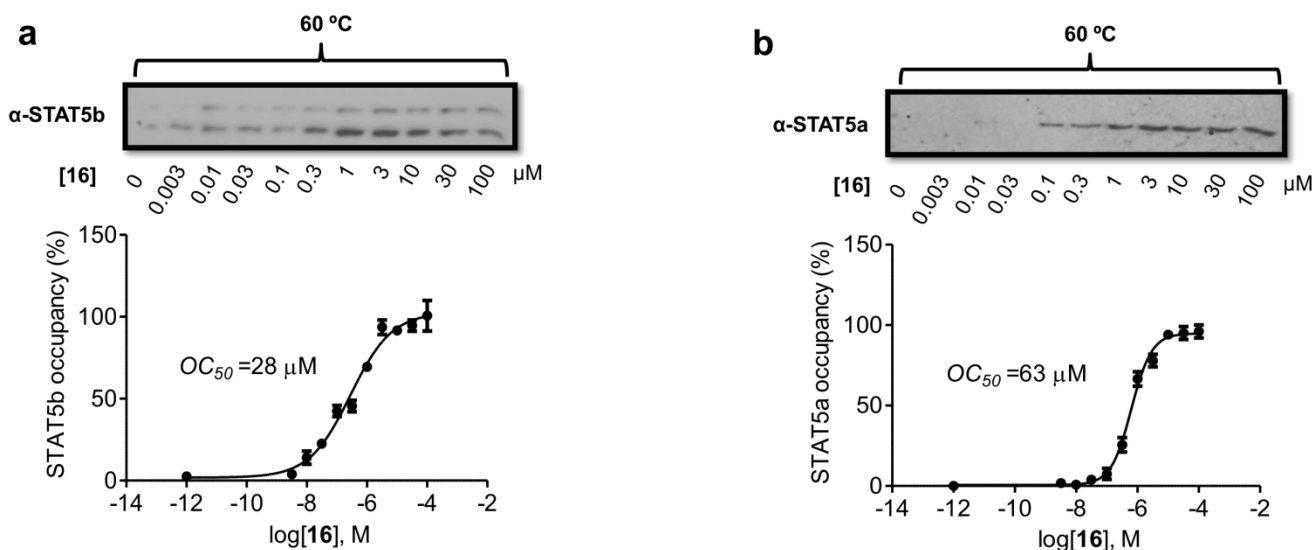
Figure 3.43: (a-b) In cell occupancy of STAT5a and STAT5b by compound **16** in BaF3/FLT3-ITD, determined using ITDRF. ITDRF of compound **16** on STAT5a and STAT5b denaturization at 60 ℃ for 3 min based on raw data from Western blotting chemiluminescence readings. CETSA, cellular thermal shift assay; ITDRF, isothermal dose-response fingerprint; $OC_{50,}$ the concentration at which 50% of the STAT5 in the cell was occupied by inhibitor.

We further evaluated **16** in K562 cell to determine STAT5 phosphoreduction and the therapeutic window. The pSTAT5 expression was examined using flow cytometry after staining cells with a fluorophore-conjugated anti-pSTAT antibody (Phosflow™ PE-Cy™7 mouse anti-Stat5 (pY694) upon treatment with **16**; whereas cell cycle effect was determined using propidium iodide (PI) and annexin V staining. As shown in Figure 3.44a, K562 cells treated with compound **16** show an increase in both necrotic and apoptotic cells compared to the untreated control group. Most encouragingly, there existed promising inhibition potency in cell viability and pSTAT5 inhibition at 50 μM Intracellular levels of phosphorylated STAT5 (pSTAT5) were evaluated by flow cytometry after 6 h exposure of cells to compound

16 at a serial concentration **16** (Figure 3.44). At the same concentration, **16** is able to induce almost 50% apoptotic rate in K562 cell population. Phospho-flow[140] evaluates the intracellular levels of phosphorylated STAT5 (pSTAT5) after 6 h exposure of cells to compound **16** at a serial concentration. The median fluorescence value of K562 stained with anti-pSTAT5 after 6 h exposure to compound **16** at 100 μM has successfully reduced 80% of pSTAT5 activity thus revealed inhibitory activities on pSTAT5 in both CML and AML cell lines.

To obtain insight into the consequences of STAT5 inhibition in MV-411 cells (human FLT-ITD$^+$ AML). We then treated MV-411 cells with compound **16** after which annexin V/propidium iodide staining and flow cytometry were performed. Undoubtedly, compound **16** inhibits the proliferation of K562 cells after 48 h as shown in the Alamar Blue assay.[58]   Nevertheless, compound **16** blocks tyrosine phosphorylation of STAT5 in a dose dependent manner as shown by Western blot analysis (Figure 3.45c) in MV-411 cells after 6 h treatment. Interestingly, **16**, led to a significant increase in apoptosis in a dose-dependent manner in similar pattern as other STAT5 driven cell lines (Figure 3.45). Compound **16** portrays high potential in targeting STAT5 protein selectively in leukemic cell lines.

In summary, we have identified the first binding inhibitor of STAT5 protein via protein induced Mannich ligation. Moreover, lead compound **16** has been shown to potently and selectively disrupt STAT5-phosphopeptide interactions as compared to STAT3. With no off-target kinase activity, **16** was shown to suppress pSTAT5 thereafter reduce leukemic cell viability.
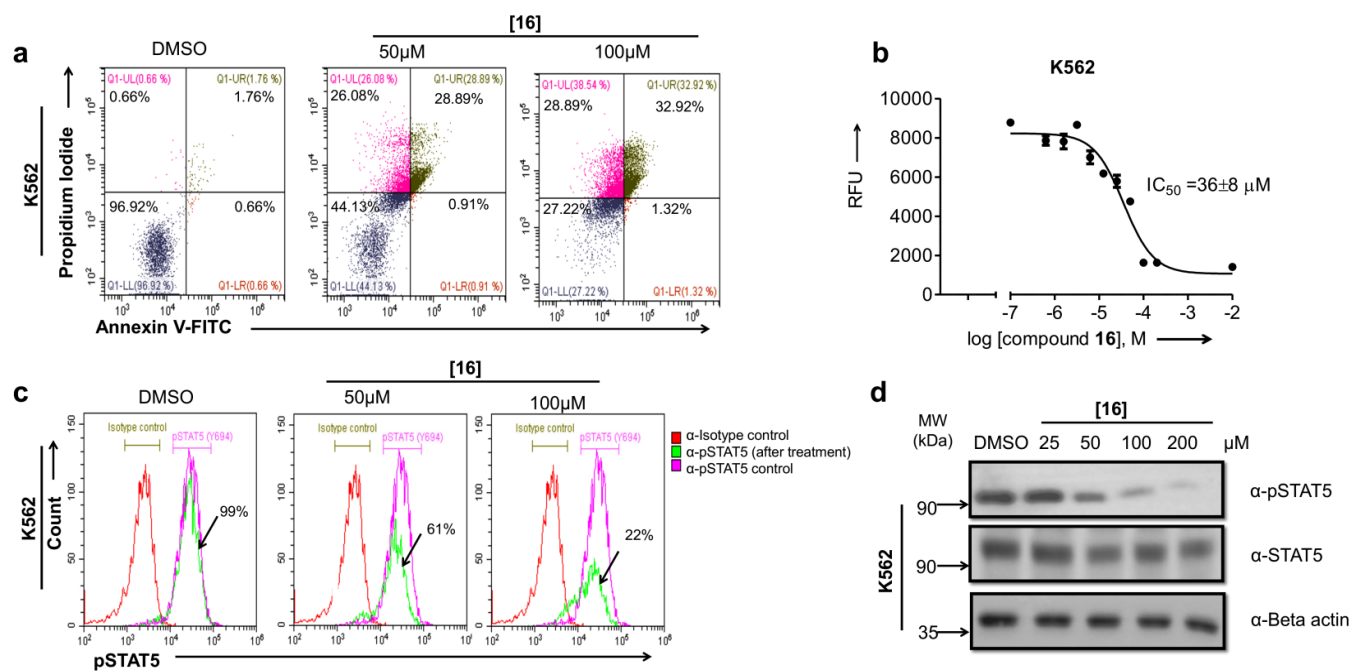
Figure 3.44: Inhibitory effects of STAT5 inhibitor **16** in K562 cells, human derived chronic myeloid leukemia (CML) cell lines**.** (a) K562 cells were treated with compound **16** after which annexin V/propidium iodide staining and flow cytometry were performed. (b) Compound **16** inhibits the proliferation of K562 cells after 48 h as determined by the Alamar Blue assay. (c) Intracellular levels of phosphorylated STAT5 (pSTAT5) were evaluated by flow cytometry after 6 h exposure of cells to compound **16** at a serial concentration. (d) Compound **16** blocks tyrosine phosphorylation of STAT5 in a dose dependent manner as shown by Western blot analysis in K562 cells after 6 h treatment. Experiments were repeated twice and immunoblotting for beta-actin was used as a control for uniform protein loading.
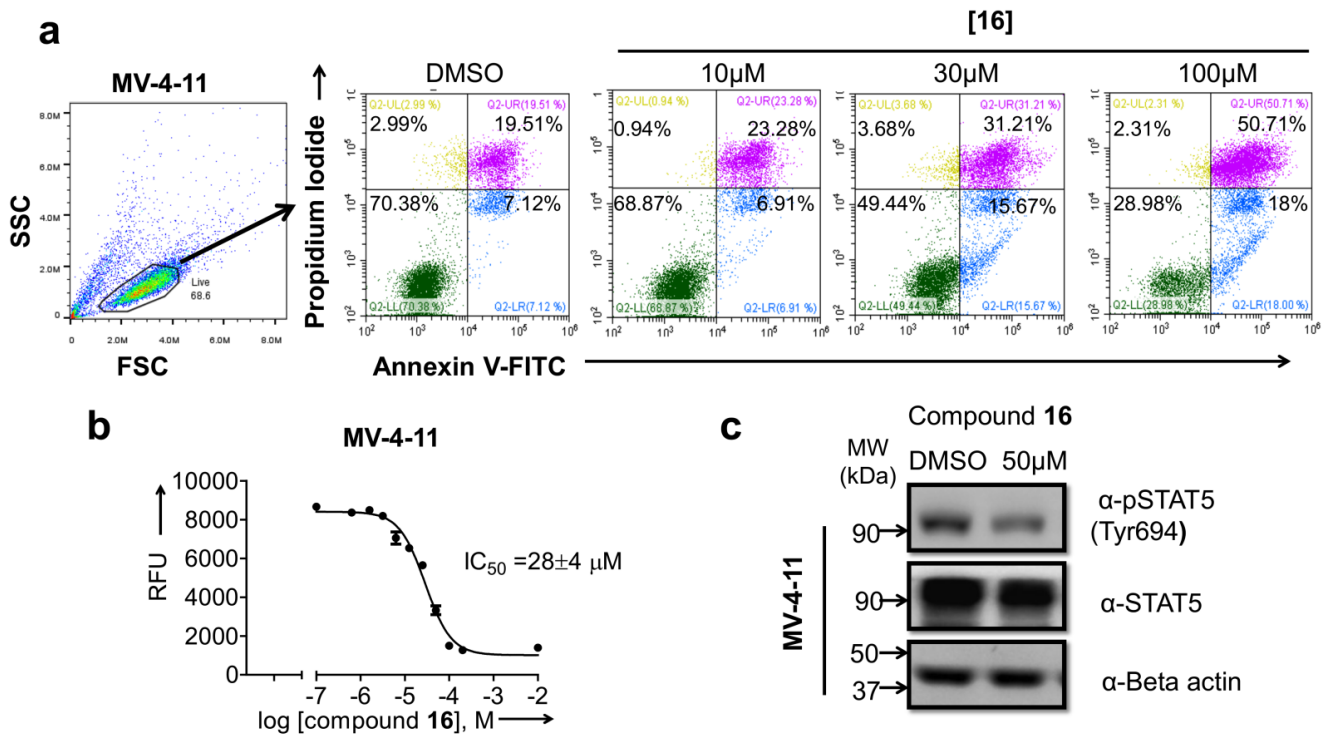
Figure 3.45: Inhibitory effects of STAT5 inhibitor 16 in MV-411 cells. (a) MV-411 cells were treated with compound **16** after which annexin V/propidium iodide staining and flow cytometry were performed. (b) Compound **16** inhibits the proliferation of K562 cells after 48 h as determined by the Alamar Blue assay. (c) Compound **16** blocks tyrosine phosphorylation of STAT5 in a dose dependent manner as shown by Western blot analysis in MV-411 cells after 6 h treatment. Experiments were repeated twice and immunoblotting for beta-actin was used as a control for uniform protein loading.
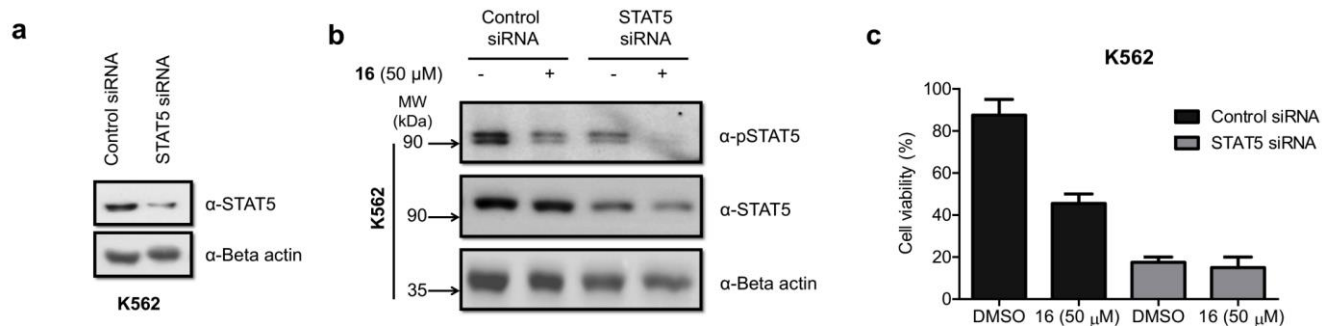
Figure 3.46: Stat5a/b knockdown in K562 cells indicate that cellular effect are primarily due to loss of Stat5a/b activity and not to off-target effects of compound **16**. (a) K562 cells were transfected with control siRNA (control siRNA-A, sc-37007, Santa Cruz, CA) or siRNA directed against STAT5 (sc-29495, Santa Cruz Biotechnology, Santa Cruz, CA) as indicated. Protein knockdown was confirmed by western blotting using antibodies against STAT5. β-Actin served as loading control. (b) Western blot analyses of STAT5 protein in K562 cells treated with compound **16** and/or STAT5 siRNA. (**c**) The effect of compound **16** on K562 cell viability was tested after genetic knockdown of STAT5. Cells were first transfected with STAT5 siRNA or control siRNA and incubated for 24 h before treated with compound **16** (50 μM) or DMSO for 48 h. Viable cells was distinguished using an ATP-dependent bioluminescence assay (CellTiter-Glo, Promega).

3.7   STAT5 knockdown elucidates target specificity of compound 16.

Previous study has shown that overexpression of constitutively active STAT5 can rescue leukemic cells from cell death induced by a specific STAT5 inhibitor. We have instead used the genetic knockdown with siRNA to deplete endogenously expressed STAT5 and to verify thereby the selectivity of our inhibitors toward STAT5.To test out the hypothesis whether the reduction in K562 cell viability was mainly due to STAT5 inhibition by **16**, we assessed the effect of STAT5 knockdown on K562 cell viability. Indeed, genetic knockdown of STAT5 by STAT5-siRNA in the STAT5-driven leukemic cell line K562 depleted STAT5 expression in comparison to control siRNA, which had no effect (Figure 3.46a). As expected, compound **16** did not affect STAT5 expression, neither in the case of STAT5-siRNA nor in that of control siRNA treatment (Figure 3.46b-c). Cell viability was reduced by >50% when K562 cells were treated with inhibitor **16** and control siRNA, while there was no effect on viability with only control siRNA (Figure 3.46a). On the contrary, STAT5-siRNA reduced viability by ca. 80% without any additional effect of compound 16. These results strongly suggest that the effect of compound **16** on cell viability is exerted by inhibition of STAT5 and not by additional off-target effects.[110]

3.8   Drug combination studies using Chou-Talalay method.

Drug combination studies are widely applied in cancer and auto-immunodeficiency diseases (AIDS). The main objectives of drug combination are to achieve synergistic therapeutic effect in order to reduce dose and toxicity and also delay the development of drug resistance.

Synergism created between different therapeutic drugs minimizes toxicity as well as side effect as lower drug concentration could be administered to achieve similar therapeutic effect.

The Chou-Talalay method for drug combination is based on the median-effect equation and also encompasses general equation including the Michaelis- Menten, Hill, Henderson-Hasselbalch, and Scatchard equations which have been widely applied in biochemistry and biophysics. Chou and his professor, Talalay introduced a scientific term "combination index (CI) to quantitatively defined synergism (CI <1), additive effect (CI=1) and antagonism (CI>1) in drug combinations. This theory was further applied to provides algorithms for automated computer simulations for both synergism and antagonism at respective dose level and can be illustrated as CI plot and isobologram, respectively.[141]

A few points are worthwhile to take note while carrying out synergistic studies in vitro. Firstly, dose range and dose density has to be determined several data points above IC_{50} and several below IC_{50} as this increase the accuracy of the assay. Secondly, constant-ratio drug combinations are a pre-requisite for generating Fa-CI plot (Chou-Talalay plot), Fa-DRI plot (dose-reduction index plot) and the class isobologram. In non-constant ratio design, no "computer simulated" CI plot will be generated and rather substitute with a conservative, normalized isobologram.[142]

3.9   Combination studies of Peroxygenin and Temozolomide in both B and T cells.

Molecular mechanism of conventional chemotherapeutic drugs is often associated with oxidative DNA damage giving rise to cell death executed by apoptosis and necrosis. Inevitably, compounds that induce oxidative DNA stress will trigger DNA damage response, eventually lead to tumor cell death. Here, we apply an in house substance, Peroxygenin that give rise to reactive oxygen species (ROS) which may lead to oxidative DNA damage and cytotoxic activity in cancer cells.[143,144] On the other hand, Temozolomide (TMZ) is a gold

standard in glioblastoma treatment and acts as an oral alkylating agent since 1987. Surprisingly, molecular mechanism of TMZ involved DNA interference forming cytotoxic methylguanine and methyladenine which are cytotoxic.[145] In addition, these mismatched lethal base pairs result in DNA breakage inducing cell cycle arrest at G2/M phase causing apoptosis and necrosis. On the downside, TMZ is treated at high dose (up to 400 µM) in glioblastoma patient and leads to undesirable side effect, thus it is worth to carry out drug combination studies to seek possible synergism with peroxygenin.
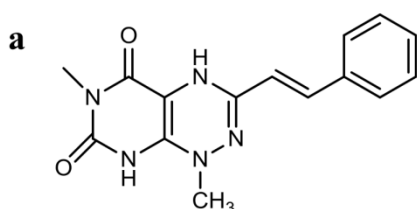
Molecular Weight: 297.32

Peroxygenin
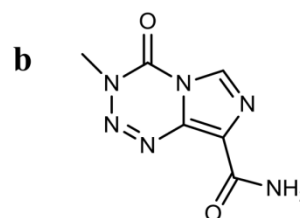
Molecular Weight: 194.15

Temozolomide

Figure 3.47: Chemical structures of Peroxygenin and Temozolomide.

We carried out the drug combination studies in two different namely BaF3/FLT3: ITD and Jurkat T cell. Treatment with TMZ alone in both cell lines required high working concentration ranging from 400-800 µM). The combination of Peroxygenine (IC_{50} = 0.5 µM) and TMZ reduced the IC_{50} from 300 µM to 113 µM in Jurkat T cell whereas in BaF3 FLT3: ITD cells the IC_{50} reduced from 725 to 478 µM (Figure 3.48-3.51). However, this drug combination does not confidently demonstrate synergistic effect in Chou-Talalay combination index (CI). At certain drug combination ratio, antagonism effects were observed in both cell lines.

3.10 Synergistic effect of 16 and PKC412 on STAT5 inhibition in leukemic cell lines.

The synergistic effect of STAT5 inhibitor **16** with the staurosporine-derived FLT3-inhibitor PKC412 was investigated.[146,147] STAT5 is a transcription factor that critically contributing to the transforming effects of FLT3-ITD and previous studies have shown that FLT3 ligand and mutated FLT3 (internal tandem duplication) enhance STAT5 overactivation. PKC412 is a staurosporine-derived, potent inhibitor of the kinase domain of the receptor tyrosine kinase FLT3, which is responsible for the phosphorylation and over-activation of STAT5 leading to cellular hyperproliferation in those cases of AML carrying the FLT3-ITD mutation. Therefore, the combinatorial targeting of STAT5 and FLT3 with both a STAT5 and an FLT3 inhibitor should be a valuable strategy for AML treatment in these cells. To test this hypothesis, we investigated the functional synergism of the two inhibitors PKC412 and compound **16** acting on the two targets, FLT3 and STAT5, within the same signal transduction pathway. Therefore, combination treatment of leukemic cells with two inhibitors targeting the same signal transduction pathway (FLT3-ITD-STAT5 signaling) can be a promising strategy to overcome or prevent resistance toward kinase inhibitors.

PKC412, a staurosporine-derived potent inhibitor of the kinase FLT3 exhibits therapeutic effect on AML patients bearing the FLT3 mutation. Treatment with PKC412 alone, however, often leads to major drawbacks such as incomplete target inhibition and short-lived responses. Here, we explored the synergistic possibility of targetting the FLT3 and its downstream mediator, STAT5 to deliver drug combinatorial approach for improved treatment efficacy[134,146] and better patient outcomes. MV-411 leukemic cells were treated with concentrations of inhibitors resulting in 20% of cell apoptosis individually as well as in combination. The combination of **16** and PKC412 resulted in a 3-fold increase in annexin-V-staining corresponding to 60% apoptotic cells, in decreased reporter gene expression, and in reduced STAT5 phosphorylation (Figure 3.52b). Our experiments revealed the synergistic

inhibition of STAT5 phosphorylation and the induction of apoptosis at significantly lower doses of the two inhibitors (IC_{20}) when compared to the use of the single substances. (Figure 3.52a) Both compounds impaired synergistically the cell proliferation after 48 h of treatment as demonstrated by a Chou-Talalay[141] combination index (CI) plot (Figure 3.52c). For example, the IC_{50} of compound **16** reduced 3-fold in the presence of 1.25 nM (IC_{10}) of PKC412. (Figure 3.52c)
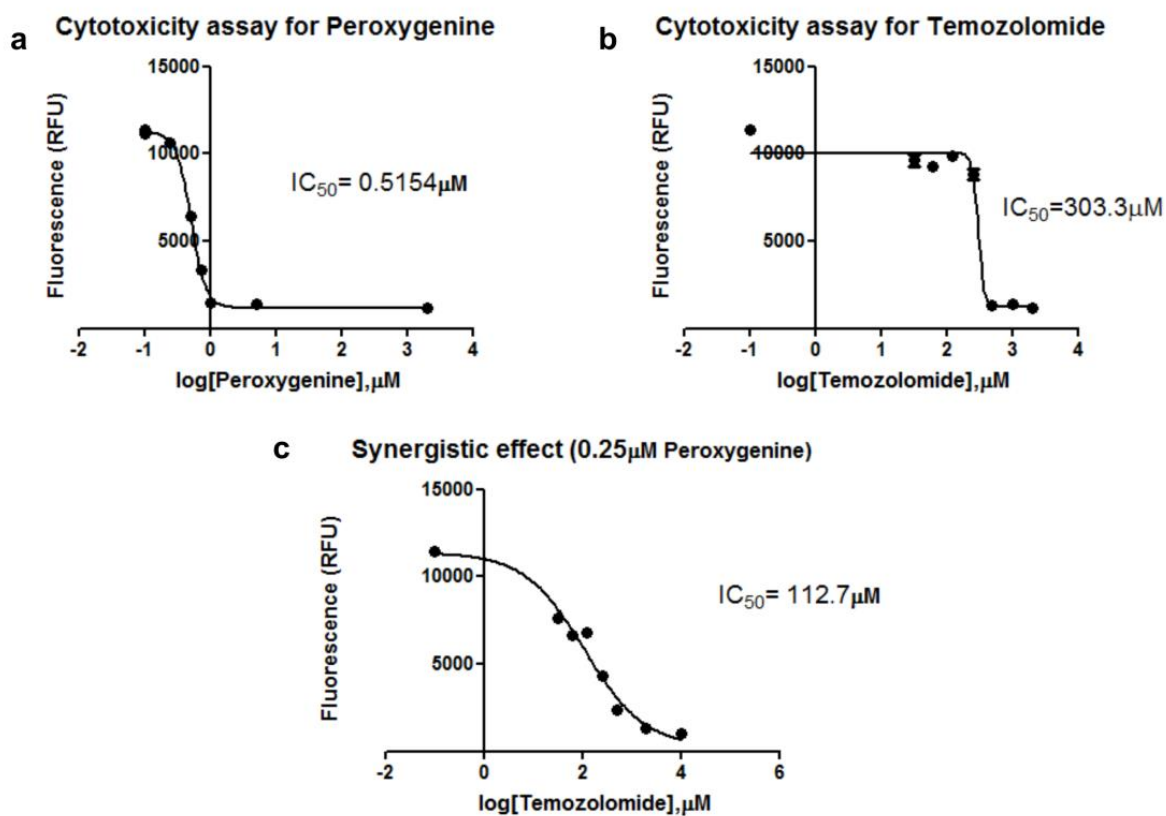
Figure 3.48: Synergistic effect of drug combination using Peroxygenine and Temozolomide in Jurkat E6.1 cells. Effect of drug treatment using Peroxygenine (a) and Temozolomide (b) alone and in combination (**c**) on Jurkat E6.1 cell viability as shown by Alamar blue assays.
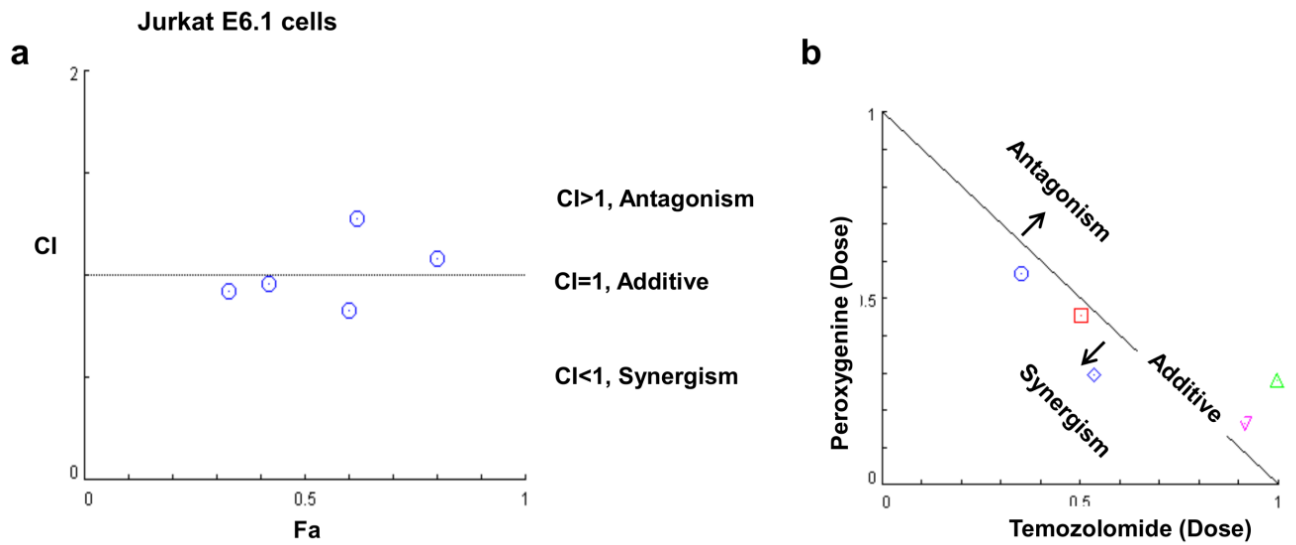
Figure 3.49: Combination index (*CI*) plot showing the synergistic effect of Peroxygenine and Temozolomide in Jurkat E6.1 cells. (a) *CI* values were generated using CalcuSyn software (Conservion, Ferguson, MO) and plotted as a function of fractional growth inhibition (*Fa*) where $Fa = (A_{570} \text{ control} - A_{570} \text{ treated})/A_{570}\text{control}$. *CI* values of < 1, $=1$, and >1 indicate synergism, additivity and antagonism, respectively (b) Analysis of the synergistic effect of the combination of Peroxigenine and Temozolomide in Jurkat E6.1 cells The calculated EC_{90} values for the combination were plotted as the fractional concentration (*F_c*) of Peroxygenine and Temozolomide on the x and y axes.

BaF3/FLT3:ITD

a Cytotoxicity assay for Peroxygenine

$IC_{50} = 0.4463\mu M$

Fluorescence (RFU)

log[Temozolomide], μM
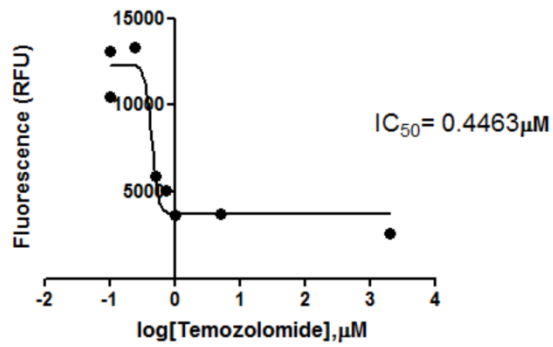
b Cytotoxicity assay for Temozolomide

$IC_{50} = 725.2\mu M$

Fluorescence (RFU)

log[Temozolomide], μM

c Synergistic effect (0.25μM Peroxygenine)

$IC_{50} = 478.0\mu M$

Fluorescence (RFU)
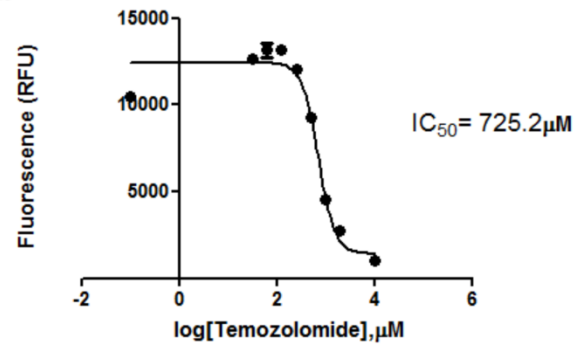
log[Temozolomide], μM
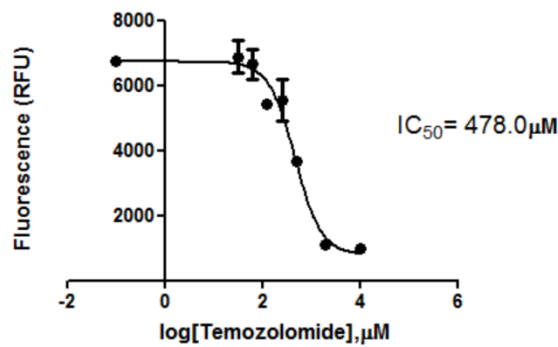
Figure 3.50: Synergistic effect of drug combination using Peroxigenine and Temozolomide in BaF3/FLT3-ITD cells. Effect of drug treatment using Peroxygenine (a) and Temozolomide (b) alone and in combination (c) on BaF3/FLT3-ITD cell viability as shown by Alamar blue assays.
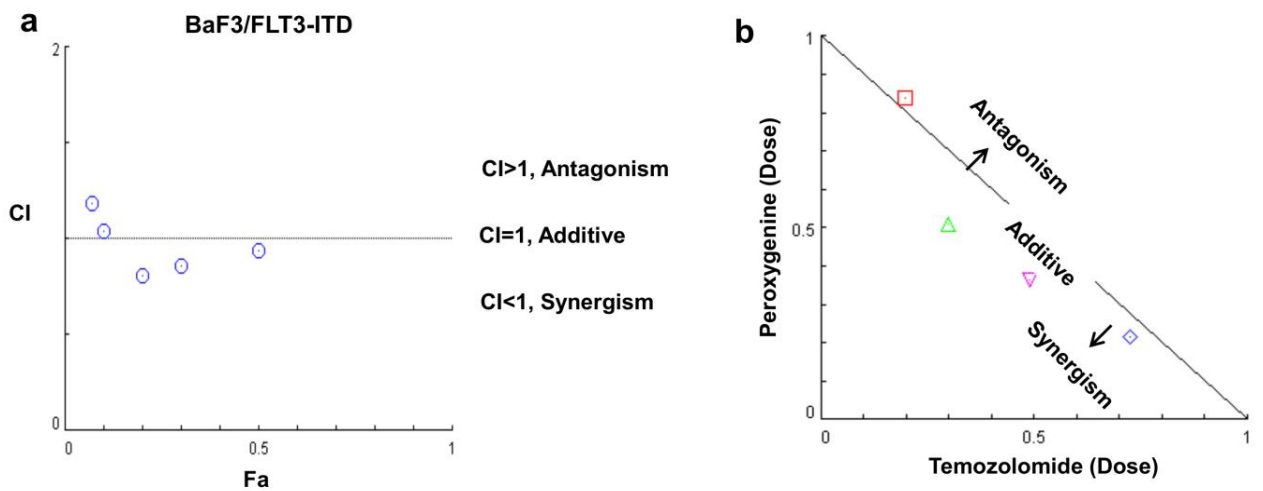
Figure 3.51: Combination index (*CI*) plot showing the synergistic effect of Peroxygenine and Temozolomide in BaF3/FLT3-ITD cells. (a) *CI* values were generated using CalcuSyn software (Conservion, Ferguson, MO) and plotted as a function of fractional growth inhibition (*Fa*) where $Fa = (A_{570}$ control $- A_{570}$ treated$)/A_{570}$control. *CI* values of < 1, $=1$, and >1 indicate synergism, additivity and antagonism, respectively (b) Analysis of the synergistic effect of the combination of Peroxygenine and Temozolomide in BaF3/FLT3-ITD cells. The calculated EC_{90} values for the combination were plotted as the fractional concentration (*F_c*) of Peroxygenine and Temozolomide on the x and y axes.
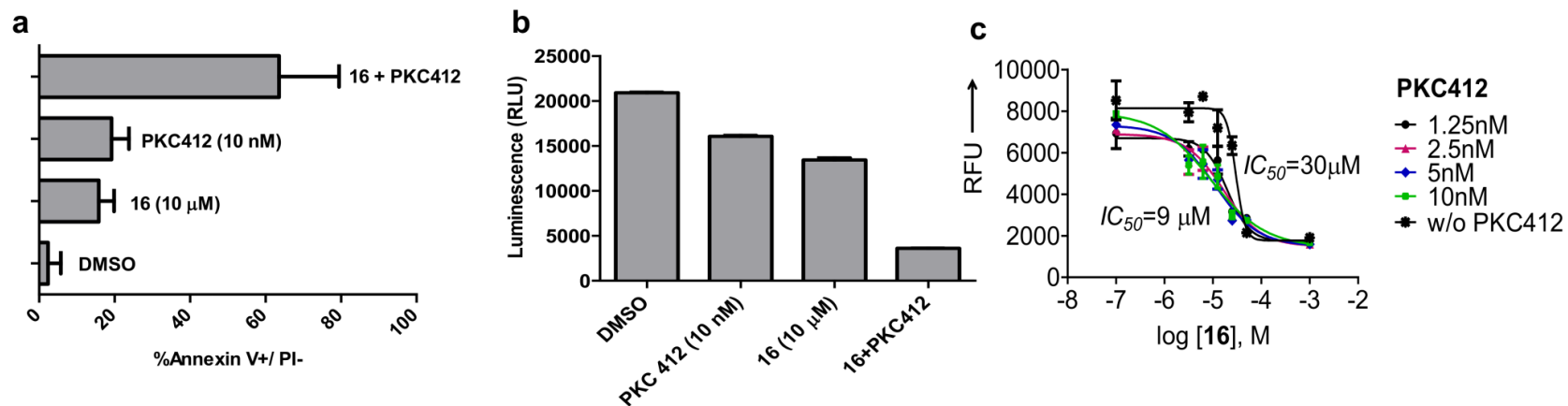
Figure 3.52: Synergy of STAT5 inhibitor **16** with kinase inhibitor midostaurin (PKC412) in MV-411 cells; dose-finding study and activity in a murine cancer model. (a) MV-411 cells were treated with PKC412 (10 nM) or compound 16 (10 μM) alone or in combination and incubated for 24 h followed by annexin V/ propidium iodide staining and flow cytometry. Apoptosis was quantitated for three independent experiments. (b) Cell viability assays were carried out by treating MV-411 cells with compound 16 (10 μM) and PKC412 (10 nM) alone or in combination. The number of viable cells was distinguished using an ATP-dependent bioluminescence assay (CellTiter-Glo, Promega). (c) Effect of drug combination (**16**and PKC412) on cell viability as shown by Alamar blue assays.
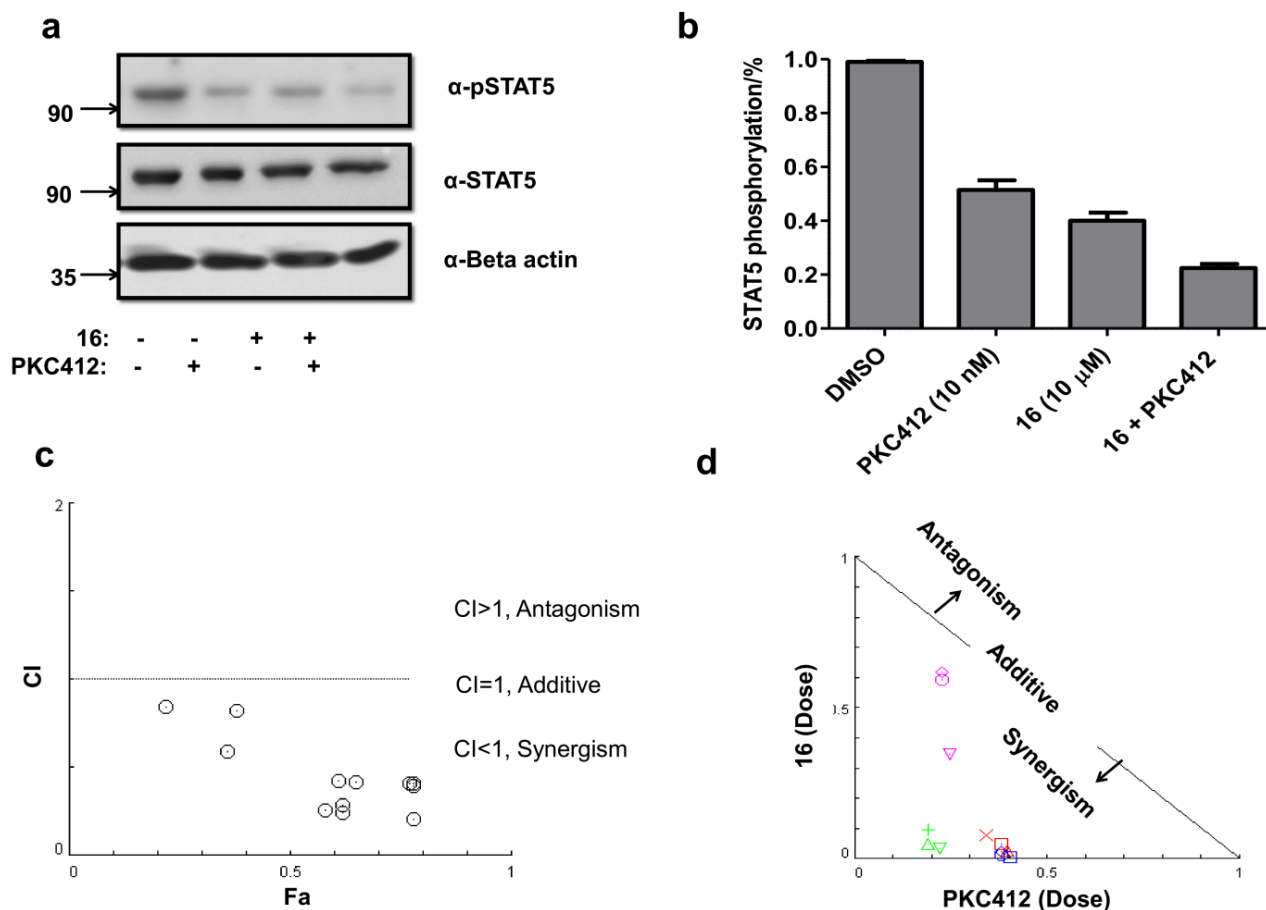
Figure 3.53: (a) MV-4-11 cells were treated with **16** or PKC412 alone or in combination and incubated for 6 h and immunobloted with pSTAT5 to study synergistic effect of both compounds on STAT5 phosphorylation reduction. (b) Relative STAT5 phosphorylation levels were plotted based on the raw data from Western blotting chemiluminescence readings to study the synergistic effect of both compounds on STAT5 phosphorylation reduction. MV-411 cells were treated with compound **16** or PKC412 alone or in combination and incubated for 6 h. (c) Analysis of the synergistic effect of the combination of 16 with PKC412. The calculated EC90 values for the combination were plotted as the fractional concentration (Fc) of 16 and PKC412 on the x and y axes. (d) Combination index (CI) plot showing the synergistic effect of compound **16** and PKC412 in MV-411 cells. CI values were generated using CalcuSyn software (Conservion, Ferguson, MO) and plotted as a function of fractional

growth inhibition (Fa) where Fa = (A_{570} control − A_{570} treated)/A_{570}control. CI values of < 1, =1, and >1 indicate synergism, additivity and antagonism, respectively.
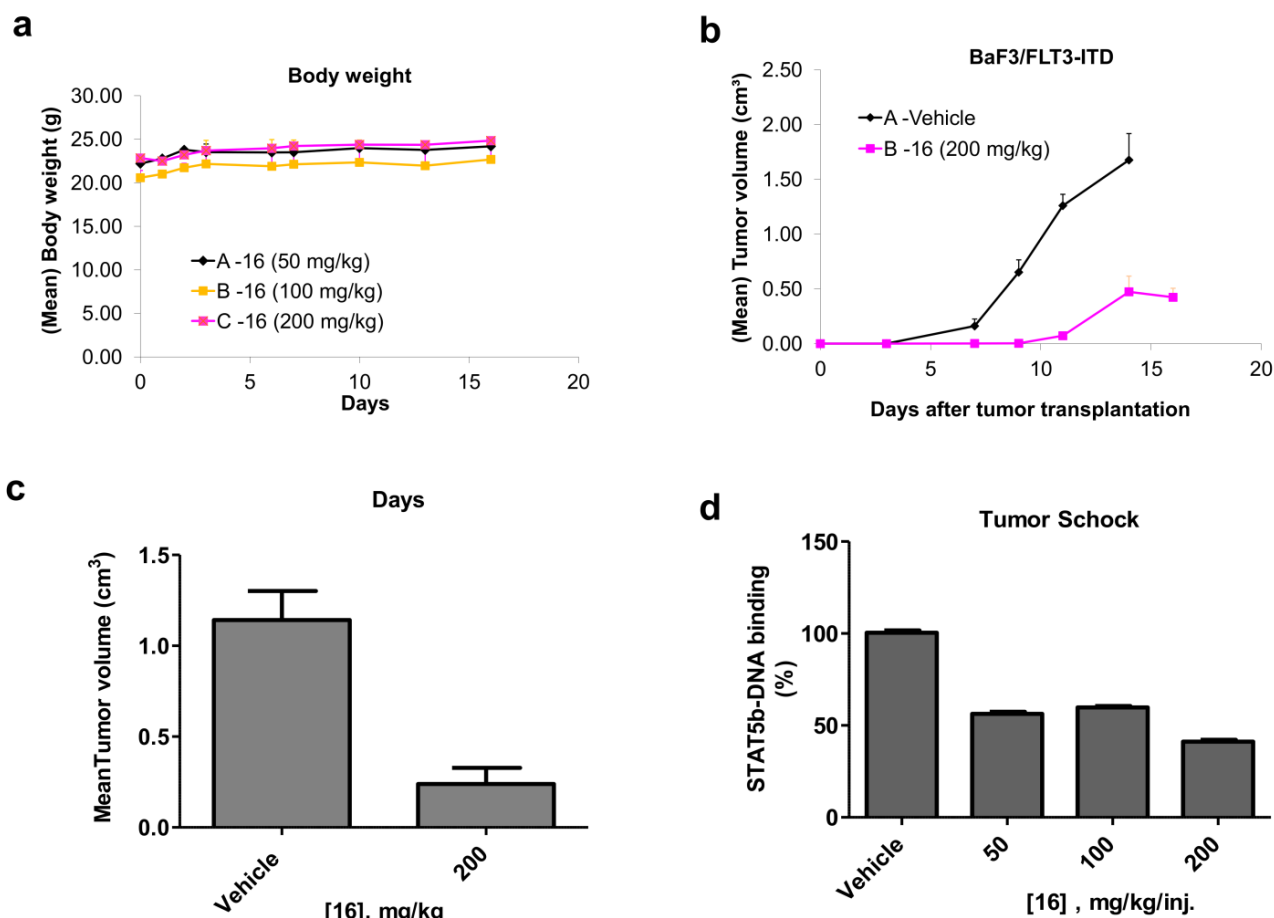
Figure 3.54: Dose-finding study and activity in a murine cancer model. (a) The corresponding body weight changes in non-xenografted mice during compound **16** treatments. (b) Compound **16** significantly inhibits tumor growth in BaF3/FLT3-ITD xenograft tumor model. Time course of tumor growth suppressed by compound **16** (200 mg/kg) in mice bearing BaF3/FLT3-ITD tumor.(c) Significant reduction in tumor volume was observed in compound **16**- treated groups, compared with vehicle treated group. Tumor volume change in BaF3/FLT3-ITD xenografts treated with **16** (200mg/kg) and vehicle respectively. (d) Treated group shows reduction in activated STAT5 and has lower STAT5-DNA binding activity in the nuclear extract from tumor schock compared to non treated vehicle group.

Finally, the inhibitory effect of **16** was examined in a murine xenograft model of leukemia. Treatment of nude mice with **16** was tolerated well and had no significant effect on mice body weight (Figure 4.42a). Nude mice were inoculated subcutaneously with BaF3/FLT3-ITD cells. The control group displayed rapid tumor growth, while tumor growth in the group treated s.c. with compound **16** (200 mg/kg) was delayed and became first apparent on day 11 (Figure 4.42b). Tumor growth in the treated group was reduced to 6% T/C on day 11 and 28% on day 14 proving that compound **16** exhibited anti-tumor efficacy in vivo.

Chapter 4

Discussion

In this contribution, protein-induced Mannich ligations have been discovered and characterized as protein-catalyzed, non-enzymatic reactions following a fundamental mechanism for the formation and identification of protein ligands. The reactions delivered potent, specific and cellularly active inhibitors of the transcription factor STAT5. The starting point, phosphate-mimetic fragment **3** was activated by the protein STAT5b-SH2 enabling three-component reactions with FA and various 1*H*-tetrazoles in aqueous physiological buffer yielding low-micromolar and sub-micromolar inhibitors of the protein-protein-interaction site. The progress of the observed Mannich ligations depended on the pH of the solution and on the presence of the protein. At pH 7.4 the reaction occurred only in the presence of the protein, while at pH 5.0 it was switched to an entirely protein-independent reaction. Protein-induced reactions were analyzed using FP and TS assays; products formed were quantified by HPLC-MS and protein-induced product was saturated at 432 nM (average of 3 independent experiments) with 250 nM protein. Product saturation is typical for protein-dependent reactions and resulted from auto-inhibition by the products formed. The reaction was also inhibited competitively by alternative ligands of the SH2 domain confirming that the phosphotyrosine recognition site constituted the catalytic center.

Remarkably, all initial 1*H*-tetrazole fragments like compound **25** did not bind to the STAT5b-SH2 protein at all ($K_I > 10$ mM) while for example the ligation product of **3**, FA, and **25**, namely 5-tetrazolyl-1-methylamino-furazane-3-carboxylate **10**, displayed super-additive binding with an affinity of 1.4 μM and the enhanced ligand efficiency of 2.23 kJ mol^{-1} per non-hydrogen atom. These findings excluded the mechanism of a protein-templated reaction, which requires the binding of both fragments to the protein template in order to initiate the reaction. Instead, an alternative mechanism of protein-dependent reactions was observed, in which only one of the starting molecules, here fragment **3**, binds to the protein. Molecular modeling suggested that H-bonding by the side chain amide of Asn642 induced the reaction of fragment **3** with FA, that of the intermediary formiminium ion with tetrazoles, and

the high selectivity of the reactions.[117] This hypothesis was challenged by investigating the protein-dependent reaction of **3**, FA, and 1*H*-tetrazole with the phosphotyrosine binding site of STAT3-SH2, which is structurally closely related containing Arg618 and Ser622 but lacks Asn642. Indeed STAT3-SH2 did not catalyze the Mannich ligation reaction and no product was identified in HPLC-MS. In agreement with this result, STAT3, STAT1, and the protein tyrosine phosphatase SHP2, all lacking the Asn-residue in the phosphotyrosine recognition sites, did not bind the STAT5-inhibitors **10** and **16**, although cross-reactivity has been reported for other STAT-inhibitors.[148,149] The importance of Asn642 was further confirmed by the mutant STAT5b N642A, which was generated by site-directed mutagenesis. The mutant protein displayed strongly reduced binding affinity to peptide **1** and to inhibitor **10** and did not catalyze a Mannich ligation reaction as shown for the wild-type protein. In conclusion, the observed protein-dependent reaction constitutes indeed a protein-induced reaction in which the protein catalytically activates the bound fragment **3** by specific binding interactions without templating the reacting fragments priorly.

Specificity of the formed inhibitors for STAT5 was also confirmed in complex cellular systems. Binding of inhibitors **10** and **16** to STAT5a,b in cell lysates was determined by cellular thermal shift experiments (CETSA). This experiment was carried out by incubating cell lysates with **10** and **16** for 1 hr respectively, the compound-lysate mixtures were then aliquoted and heated at temperatures ranging from 43-73 ℃. The melting temperature of STAT5 shown an obvious shift, indicating both compounds exert thermal stabilization on STAT5 protein in complex cell lysates. The high selectivity of the protein-ligand interaction was demonstrated by the fact that inhibitor **10** in cell lysates suppressed photocrosslinking of the biotinylated STAT5 ligand **27** with STAT5 but not with other proteins. In addition, the selectivity of compound **16** in living cells was proven by isothermal dose-response fingerprints (ITDRF). It was found that 50% of the target proteins STAT5a and b were occupied in living cells with **16** at concentrations (OC_{50} values) being in the same range as the

IC_{50} values observed for the inhibition of STAT5 phosphorylation and cell proliferation, indicating that the interaction of **16** with the target STAT5 alone was sufficient to generate and explain the observed biological effects. Likewise, compound **16** was able to block STAT5 transcription and to inhibit cellular proliferation of cancer cells in a mouse model. Another proof for the cellular selectivity of **16** for STAT5 was that the proliferation of all tested cell lines which proliferate independently from STAT5 activation was not inhibited by **16** and these cells showed no sign of toxicity.

Our work demonstrates the growing power of protein-dependent fragment ligations in fragment based drug discovery. Protein-induced multicomponent reactions such as Mannich ligations enlarge the chemical diversity of protein ligands accessible by the method considerably. Protein-induced fragment ligations seem to be especially advantageous for the formation of potent and specific ligands as molecular interactions responsible for binding catalyze the ligation reaction. Considering the omnipresence of formaldehyde in living cells and the versatility of reactions this and other aldehydes can undergo, the mechanism should find broad application on numerous protein targets and many bioactive fragments should be expandable to chemically diverse and potent protein ligands, possibly even in living cells.[149,150] Thus, protein-induced reactions seem to constitute an additional, non-enzymatic mechanism exerted by proteins enabling the molecular evolution of ligands and modulating protein activities and functions.

Chapter 5

Conclusion & Outlook

STAT5 activation is often associated with leukemia initiation and maintenance, qualifying it as a promising therapeutic target for blood cancer treatment and also tackling the rising rate of secondary resistance. Priorly, this thesis explored the therapeutic potential of STAT5 by assembling potent inhibitors via protein-induced Mannich Ligation which provides an additional avenue for protein templated ligand formation. In these studies, STAT5 protein was employed as target protein and served as the template that catalyzes three component reactions of a highly potential phosphate mimetic, **3**, formaldehyde, and 1H-tetrazoles to generate ligands with binding affinity for the protein. The above-mentioned Mannich ligation are proven to be very specifically catalyzed by STAT5 active site and can be carried out in physiological condition; no product was formed and detected when the same reactions were carried out with closely related protein such as STAT3, mutated STAT5$_{N642A}$, SHP2 and PTP1B. Nonetheless, we also include proper control namely bovine serum albumin (BSA) and isolation tag, maltose binding protein (MBP) to test the reaction feasibility. As predicted, no product was detected validating the protein induced Mannich ligation is target selective and specific.

The reaction product, **10** that binds and serves to inhibit STAT5 activity was detected in mass spectrometry, fluorescence polarization assay and thermal shift assay. Molecular modelling and docking was carried out to study structure-activity relationship and the key binding residues involved in protein-ligand binding. Based on the molecular docking results, we deduced residue Asn642 plays an important role in initiating the fragment **3** binding at the STAT5 active site in protein-induced Mannich ligation. To prove our hypothesis, we have prepared the mutant STAT5$_{N642A}$ by site directed mutagenesis and confirmed the sequence of the mutant gene construct. Coherently, the mutant protein shown to bind to compound **16** with reduced affinity (30 μM) while the protein induced Mannich ligation reactions with fragment **3**, formaldehyde and 1H-tetrazol conduced at physiological condition in the presence of STAT5 protein yield no products. These finding support our hypothesis on the functional

relevance of the residue Asn642 in initiating the Mannich ligation reaction via prior binding of fragment **3** and latter the binding of the formed inhibitors.

By studying the binding pocket of STAT5-SH2 domain, we designed compound **16** from ligation product **10** for better cellular permeability thus higher cellular potency. As planned, the poor physiochemical properties of compound 10 is well tackled as compound 16 portrayed 10 fold higher in cellular efficacy. We then proceed to characterize the activities and the properties of both of the leading compounds in regard to the STAT5 inhibition using functional biochemical assays. Firstly, we employed BaF3/FLT3: ITD as cellular model to test out the *in cellulo* efficacy of the compounds in a mimicked acute myeloid leukemia model. Compound **16** reduced STAT5 phosphorylation and disrupts $STAT_2$: DNA binding, significantly affect cell survival and proliferation. Consequently, the expression of STAT5 downstream target was drastically reduced upon STAT5 inhibition by compound 16 as shown in both RT-PCR and luciferase reporter assay experiments.

Furthermore, we also examined the drug selectivity and specificity of both compound **10** and **16** in complex cell lysates by recruiting dual labelled peptide, **27** for photo-cross linking experiment. To our surprise, both compounds competitively displaced peptide **27** leading to lower STAT5 yield in the eluent of Neutravidin pull down assays. This strongly indicates that these compounds selectively bind to STAT5 even in complex cellular environment which further supports and validates our observation in the functional biochemical assay. Nonetheless, we also proved the binding of the inhibitors to STAT5 protein in whole cell lysates using cellular thermal shift assays (CETSA). CETSA indicated that the binding of inhibitors to STAT5 still occur in the lysates, suggesting that there was no significant competition presence for the ligand by other proteins. On the same page, the photo-cross linking of peptide **27** with STAT5 but not other proteins was inhibited by compound **10**.

Besides that, the selectivity of STAT5 inhibitors was investigated in living cells using isothermal dose response finger prints (ITDRF). The cellular occupancy of STAT5a protein (OC_{50} = 25 µM) in cells was comparable and close to the observed IC_{50} of cellular proliferation assay (28 µM), thus indicating our inhibitors are STAT5 specific and no other nonspecific binding is responsible for the observed phenotype. To exclude any off-target effect, we carried out siRNA experiment and the results suggested that the effect of inhibitors on cell viability is solely due to STAT5 inhibition. We also examined the effect of both compounds in cell lines known to be driven by STAT5, including K562 (human CML cell line) and MV-4-11 (human AML cell line) and observed reduction in cell proliferation and increase in apoptotic cells. On the other hand, our inhibitors do not exhibit cytotoxicity towards normal epithelial cell and other types of cancers that are not driven by STAT5.

As we have observed STAT inhibition in animal cell lines with constitutively active STAT5, i.e. BaF3/FLT3: ITD, K562 and MV-411, we conclude that compound **16** inhibits STAT5 not only in mouse model (BaF3/ FLT3: ITD) but also human leukemic cell lines (MV-411 and K562) that are known to be driven by constitutively active STAT5. This positive finding has encouraged us to proceed with treating xenograft mouse model with compound **16**. We have observed slower tumor growth in mice group treated with compound **16** (200mg/kg). Tumor growth in the treated group was reduced to 28% confirming that compound 16 is equally potent in vivo and exhibit desired anti tumor efficacy.

Given that drug combination is an alternative to achieve synergistic therapeutic effect for dose and toxicity reduction as well as minimize drug resistance. We intended to apply combination studies of compound 16 with a known FLT3 inhibitor, PKC412. Briefly, PKC412 is a staurosporine, derived potent inhibitor of receptor tyrosine kinase FLT3, which is responsible for the phosphorylation and over-activation of STAT5 leading to cellular hyperproliferation in those cases of AML carrying FLT3-ITD mutation. We deduced that by combinatorial targeting both STAT3 and its upstream, FLT3 with a STAT5 inhibitor and an

FLT3 inhibitor could be a valuable strategy for AML treatment. We tested out our hypothesis by investigating the functional synergism of the two inhibitors PKC412 and compound 17 acting on the two targets, FLT3 and STAT5 with the same signal transduction pathway. Our findings revealed synergistic inhibition of STAT5 phosphorylation and the induction of apoptosis at significantly lower doses of the two inhibitors (IC_{20}) when compared to the use of the single substances. Current findings provide alternative in applying lower dose of STAT5 specific inhibitor, compound **16** but still able to achieve desired effect in leukemic cell lines. Drug toxicity and resistancy can be avoided as an outcome of synergism.

Our studies have illustrated the development of specific STAT5 inhibitor via protein-induced Mannich ligation. We have also employed different biophysical and biochemical assay to characterize the effect and activities of our inhibitors in vitro using leukemic cellular model as well as in vivo using xenograft mouse model. We have also examined the selectivity and specificity of our inhibitors using photo cross linking experiment and their synergism with receptor tyrosine kinase inhibitor, PKC412 has been well examined. Most interestingly, we have revealed the residues Asn642 plays vital role in initiating the protein templated reaction as well as protein-ligand binding. The importance of the residues Asn642 was then proven using site directed mutagenesis.

Undeniably, the reaction condition of protein induced mannich ligation mimics the physiological conditions in living cells. Experiments have been conducted with increasing concentration of formaldehyde finding that a concentration of 250 μM yielded optimal results of the ligation reactions without affecting the protein and the protein assays. This concentration of formaldehyde is in fact a physiologically relevant concentration, increasing the feasibility of reaction in mammalian cells. This intriguing observation serves as a platform to study the possibility in cellulo assembly of potent ligand.

Chapter 6

Experimental Method

6.1   Fluorescence Polarization assay and screening.

Ca. 17000 compounds and fragments from the ChemBioNet library were tested in a fluorescence polarization (FP) assay to investigate their ability to bind to STAT5b-SH2 domain by displacing the fluorophore-labeled peptide 5-carboxyfluorescein-GY(PO$_3$H$_2$)LSLPPW-NH$_2$ **1**. Purified compounds were tested in the same assay. The peptide purity was >95% and the assays were performed at room temperature. The final concentration of buffer components used was 10 mM HEPES (pH 7.5), 1 mM EDTA, 0.1% Igepal CA-630, 50 mM NaCl, and 5% DMSO and the final concentration of protein used was at 125 nM. The protein was first added to the black 384-well plate (Corning 3676) followed by test compounds and fluorophore-labeled peptide. The plates were centrifuged, and measured using Safire[24] well plate reader (Tecan, Crailsheim, Germany) after 15 min incubation at room temperature. For testing secondary site binding of primary hit fragments, the same assay was conducted in the presence of 4-formylphenyl phosphate **2** as described earlier. For specificity analysis, FP assay was conducted with 100 nM GST-tagged, full length human STAT3 protein (SignalChem, Richmond, BC, Canada) and 10 nM fluorophore-labeled peptides (5-carboxyfluorescein-GY (PO$_3$H$_2$) LPQTV-NH$_2$). The assay buffer contains 50 mM NaCl, 10 mM HEPES (pH 7.5), 1 mM EDTA, 0.01% Triton-X100 and 2 mM dithiothreitol). The test compounds were serially diluted and incubated with STAT3 protein at room temperature for 1 h followed by 10 nM of fluorophore-labeled peptide. The mixture was centrifuged and incubated for 30 min at room temperature before FP was recorded using the MTP reader. For analysis of the data GraphPad Prism 5[129] was used. Ligand efficiencies (LE) were calculated using the equation LE = -ΔGº/HA with ΔGº being the standard free energy of binding in kJM$^-$^{1} and HA the number of heavy, non-hydrogen atoms.

6.2   Detection of protein-induced ligand formation via FP assay.

All FP assays were conducted in a total volume of 20 μl in 50mM of MOPS buffer (pH 7.4) at room temperature. For investigating the tolerance of the assay for FA, serial dilutions of

FA (concentration range: 0–1mM) were prepared and incubated with 250 nM of MBP-STAT5b in buffer. For the protein-induced reaction, 250 nM of MBP-STAT5b protein were added to a mixture of 250 μM of 3 and one heteraryl nucleophile per microtiter plate well with increasing concentration of FA up to the concentration of 250 μM. Reaction mixtures were incubated for 12 h with mild shaking. Plates were centrifuged and 10 nM of FP probe 1 were added and incubated for 1 h with mild shaking before measurement with Safire[24] well plate reader (Tecan, Crailsheim, Germany).

6.3   Detection of ligand formation via mass spectrometry

Extracted ion chromatography was performed with reaction mixtures containing 250 nM of MBP-STAT5b protein, 250 μM (IC_{20}) 4-amino-furazane-3-carboxylic acid 3, equimolar amount (250 μM) of one heteraryl nucleophile and FA with a total volume of 100 μl. The reaction mixtures were vortexed to mix thoroughly and incubated overnight at room temperature and was analyzed using a HPLC/QTOF-MS instrument by Agilent, consisting of an Infinity 1290 UHPLC coupled to a 6550 iFunnel QTOF. After 12 h each sample was analyzed in triplicate by injecting (10 μl) into the LC/MS instrument and the ligation products were identified by their molecular weights and by comparison of the retention times of synthetic reference. Calibration curve for hit compounds 9, 10 and 16 is given in Appendix Figure 10. Eluents were mixtures of water and acetonitrile (with 0.1% formic acid). Injection volume was set to 10 μL. Samples were eluted using gradient elution of started off with 97:3 (water/acetonitrile) for 1 min followed by 95:5 to 5:95 over 5 min. Flow rate was set to 0.3 ml/min. The QTOF is equipped with an electrospray ionisation-source used with the following parameters: negative ion mode, fragmentor voltage 175 V, capillary voltage 4000 V, nozzle voltage 1000 V, gas temperature 200 ºC, gas flow 14 l/min, stealth gas temperature 350 ºC, stealth gas flow 11 1/min. The reference masses 121.050873 m/z and 922.009798 m/z were used for reference ion correction. The mass range was set to 100-1000 and a scan rate of

1 spectrum/s was chosen. Due to the low complexity of sample matrix, the instrument was run in full-scan mode (ms-only) with sufficient selectivity and sensitivity. In order to have a clear separation and lower interference from the buffer salts, HPLC-flow from 1.3 to 5 min was directed to the mass detector. Data processing and integration were performed using the MassHunter software by Agilent Technologies with mass window set to 10 ppm. All control experiments were run consecutively and carried out as described below.

Lane 1: Blank reaction, negative control

For a negative control, 4-amino-furazane-3-carboxylic acid **3** (250 µM, IC_{20}), equimolar amounts (250 µM) of a hetaryl nucleophile, e.g. 5-benzyl-1H-tetrazol **26**, and formaldehyde were incubated for 24 h at room temperature in MOPS buffer (50 mM) at pH 7.4 in the absence of the protein template (MBP-STAT5b-SH2). The reaction mixture was analyzed using the method described above.

Lane 2: Protein-induced ligation

4-Amino-furazane-3-carboxylic acid **3** (250 µM, IC_{20}) and equimolar amounts (250 µM) of a hetaryl nucleophile, e.g. 5-benzyl-1H-tetrazol **26** or and formaldehyde were incubated for 24h at room temperature in MOPS buffer (50 mM) at pH 7.4 in the presence of the protein template (MBP-STAT5b-SH2). The reaction mixture was analyzed using the method described above.

Lane 3 and **4**: **Protein-induced reaction in the presence of high affinity FP probe 1**

Ligations were carried out after pre-incubating MBP-STAT5b-SH2 in MOPS buffer (50 mM) at pH 7.4 with 100 nM and 300 nM of **1**, respectively, for 1 h at room temperature followed by the addition of 4-amino-furazane-3-carboxylic acid **3** (250 µM), an equimolar amount (250 µM) of a 1H-tetrazole, and of FA in total assay volume of 100 µl. The reaction mixture was incubated for 24 h at room temperature and was analyzed using method as described above.

Lane 5 and **6: Protein-induced ligation in the presence of competitive inhibitor 10**

Ligations were carried out by pre-incubating MBP-STAT5b (final concentration 250 nM) with 1 and 5 µM of **10** for 1 h at room temperature followed by addition of 250 µM (IC_{20}) 4-amino-furazane-3-carboxylic acid **3**, equimolar amounts (250 µM) of one hetaryl nucleophile and FA. The reaction mixtures were incubated for 24 h at room temperature and was analyzed using method as described above.

Lane 7: Protein-induced Mannich ligation experiments with maltose binding protein (MBP) in place of MBP-STAT5-SH2 protein

Ligations were carried out by mixing 1 µM (in excess) of MBP protein, 250 µM (IC_{20}) 4-amino-furazane-3-carboxylic acid **3**, equimolar amount (250 µM) of one heteraryl nucleophile and FA The reaction mixtures were incubated for 24 h at room temperature and was analyzed using method as described below.

6.4   Detection of protein-induced ligand formation via TSA.

The possibility of using TSA48 assay to determine protein-induced ligand formation. The compatibility of FA with the TSA[109,118] was investigated using MBP-STAT5b-SH2 protein (500 nM) mixed with increasing concentrations of FA up to the concentration of 250 µM and incubated at room temperature with mild shaking in a sealed 384 PCR plate. To determine the formation of ligand via a protein-induced reaction, MBP-STAT5b-SH2 protein 500 nM was added to 250 µM (*IC20*) 4-aminofurazane-3-carboxylic acid 3, equimolar amount (250 µM) of one heterarylnucleophile per PCR plate well with increasing concentration of FA up to the concentration of 250 µM. Reaction mixtures were incubated for 12 h with mild shaking at room temperature, respectively. After 12 h, the plates were centrifuged and 1 µl of 400X Sypro Orange solution (Thermo Scientific) was added, resulting in a total assay volume of 20 µl, with a final protein concentration of 475 nM. The PCR plates were again sealed with optical seal, shaken for 15 min, and centrifuged. Thermal scanning (20–95 °C at 1 °C min−1) was performed using a real-time PCR setup LightCycler (Roche Diagnostics, Mannheim,

Germany) and fluorescence intensity was measured after every 0.3 s. Curve fitting, melting temperature calculation,and report generation on the raw data were performed using GraphPad Prism 5[129] software.

6.5   Molecular modelling and docking

6.5.1   Homology modelling of STAT5B

Template was adopted from the C-terminal region (Trp589 to Ser680, 92 amino acids) of crystal structure, 1Y1U[64]. The alignment was taken from Lin et al. Seven side chains were mutated to turn the SH2-domain of mouse STAT5A to human STAT5B using Sybyl8.1. The side chain conformation of Arg618 from the template structure of 1Y1U was manually adjusted so that it may interact in a bidentate coordination with the acidic group of the substrate like observed in other SH2 domains (e.g. 1BKM or 1O46).

6.5.2   Preparation of STAT5 conformations

The software AutoDockTools was used to convert homology modeled STAT5 and ligands to PDBQT from the PDB files. Polar hydrogens were assigned and Gasteiger charges were added and finally structures were saved in the PDBQT file format for docking.

6.5.3   Molecular docking

6.5.3.1 Sybyl 8.1 (Surflex-Dock)

In order to rationalize the binding of the synthesized compounds in the active site of HuSTAT5B model, docking calculations were performed using Surflex-Dock interfaced within Sybyl8.1. The surflex-dock scoring function was used to score the docking interaction. The surflex-dock score considers several factors related to ligand-receptor

interaction, hydrophobicity, polarity, repulsiveness, entropy, and solvation. The docking parameters included ligand flexibility and rigid protein structure, and all other parameters were set to their default values. The resulting compounds were minimized using the *Powell* module with the standard *Tripos* force field within the pocket while the receptor was fixed.

6.5.3.2 AutoDock Vina docking

The *AutoGrid* and *AutoDock* Vina[122] procedures were used to conduct the grid point energy calculations of the receptor and the binding pose scoring of the ligands, respectively. The binding conformations of the ligands were optimized using the Lamarckian Genetic Algorithm (LGA), where the initial population size for each ligand was set to 2 500 000 and the grid was set at 30x 30x 30 Å, centered around the phosphotyrosines binding site in the SH2 domain of STAT5. The exhaustiveness was set to 100 for a better global minimum search.

6.5.3.3 BINding ANAlyzer

Docking conformation with minimum $E_{FreeBind}$ was loaded into BINANA for descriptors calculations. BINANA[124] is a python implemented algorithm that assist in characterizing binding of inhibitor-receptor complex. Receptor and ligand files were prepared by MGLTools[123] 1.5.6 in PDBQT format. BINANA descriptors consist of (i) close contacts, (ii) electrostatic interactions; (iii) hydrophobic contacts, (iv) hydrogen bonds, (v) salt bridges and (vi) π interactions.

6.6 Biochemical Assays

6.6.1 Expression of MBP-STAT5b protein

Expression of the truncated version of STAT5b (aa 136-703) cloned into a modified pQE70, with N-terminal MBP-tag and C-terminal His-tag was conducted on autoinduction medium (overnight express / Novagen). Cells were grown to an optical density (O.D.) of 0.3 at 37 °C, then the temperature was reduced to 20 °C for further 48 h of expression. Comparable soluble expression levels were obtained with Rosetta2 (DE3) and BL21 (DE3) pLysS (both Novagen). The protein was purified by Ni-chelating chromatography followed by gel filtration (Superdex 200 / 10 mM HEPES pH 7.8, 100 mM NaCl, 1 mM EDTA, 1 mM DTT, 10% glycerol). A yield of 15 mg MBP-STAT5b-His per liter of culture was obtained and aliquots (200 µl of 3.2 mg/ml) were quick-frozen and stored at –80 °C, ready for use.

6.6.2   Thermal shift assays

Thermal shift assays were performed with fragments **3**, **25**, and **26** as described previously[118] in 96-well PCR plates (catalog no: HSL9901 Bio-Rad Laboratories, Richmond, CA). Assays were carried out using 500 nM of MBP-STAT5b protein mixed with serial concentration of fragments in the presence of 20x Sypro Orange (Thermo Scientific). Assay buffer contains 300 mM HEPES, pH 7.4, 175 mM NaCl and 1% DMSO. The PCR plates were sealed with optical seal, shaken for 15 min, and centrifuged. Thermal scanning (20 to 95°C at 1°C/min) was performed using a real-time PCR setup (Light Cycler, Roche Diagnostics, Mannheim, Germany and fluorescence intensity was measured after every 0.3 s. Curve fitting, melting temperature calculation and report generation on the raw data were performed using GraphPad Prism 5[129] software.

6.6.3   Activity measurement of SHP-2 using a DiFMUP assay.

An enzyme assay using (DiFMUP) as a substrate was employed for the determination of SHP-2[151] activity. Test compounds were dissolved in dimethyl sulfoxide (DMSO) at a

concentration of 100 mM and the assay was carried out at a final DMSO concentration < 1 %. The phosphatase reactions were performed at room temperature in 384-well black plate, clear flat bottom, low flange, non-binding surface (Corning, Cat# 3766) using a final volume of 20 µL and the DiFMUP assay buffer contained a final concentration of 50 mM MOPS (pH = 6.5), 200 mM NaCl, 0.03 % Tween-20, 1 mM DTT (freshly added prior to each measurement) and 2.5 nM SHP-2 (final concentration). SHP-2 and tested compound in buffer solution were incubated for 30 min at r.t. The reaction was started by adding DiFMUP (Invitrogen, cat# D6567, 10 µM, correspond to the experimentally determined K_M values of the enzymes) and the measurements were performed on microplate reader (infinite M1000 Pro, Tecan) using excitation and emission wavelengths of 360 nm and 460 nm. Measurements were performed in triplicate and the IC_{50} values were calculated with GraphPad Prism 5[129]. Determinated IC_{50} values were converted into the corresponding K_I values applying the Cheng Prusoff equation $K_I = IC_{50} / (1 + [S]/K_M)$.

6.6.4 Photo-crosslinking and competitive displacement of 27 with recombinant MBP-STAT5 SH2 protein.

Peptide probe **27** (100 µM) was incubated with 200 µL of recombinant MBP-STAT5 SH2 protein in the binding buffer (50 mM HEPES, pH 7.5, 200 mM NaCl, 2 mM $MgCl_2$, 0.1% tween-20, 20% glycerol, 2 mM PMSF, Roche Complete EDTA-free protease inhibitor cocktail) for 1 h at 4 °C. The samples were then irradiated at 365 nM using a UV transilluminator for 15 min at 4 °C. For competitive displacement studies, non fluorescent; phosphotyrosines containing control peptide (0-100 µM) was added together with peptide probe **27** and incubated with recombinant MBP-STAT5 SH2 protein for 1 h at 4 °C prior to UV photo-crosslinking for 15 min at 4 °C. SDS sample buffer (final concentration 1x) were added to the buffer and boiled before running on SDS PAGE followed by western blotting.

6.6.5 Neutravidin pull-down

A total amount of 1mg/mL of heavy and light cell lysates were added with 100 μM of peptide **27** and allowed to incubate for 1 h at 4 ℃. The samples were then irradiated at 365 nM using a UV transilluminator for 15 min at 4 ℃. For competitive displacement studies, non fluorescent; phosphotyrosines containing control peptide (0-100 μM) or compound **10** was added together with peptide probe **27** and incubated with for 1 h at 4 ℃ prior to UV photo-crosslinking for 15 min at 4 ℃. Then, 10 mg of Neutravidin agarose beads (Thermoscientific), which trapped biotinylated proteins was added to the cell lysates and mxed well at 4 ℃ overnight. Next, neutravidin beads were extensively washed for five times with 1X PBS before boiling with 1x SDS-PAGE sample loading buffer (Sigma) for 5 min. The eluate was subjected to Western blot and the cytosolic β-acin serves as the loading control for the total cell lysates.[132]

6.6.6 LC-MS/MS Data Acquisition and Data Analysis.

In-solution digestion and MS analysis was performed. Peptides were desalted on Stage Tips and analyzed using LTQ-Orbitrap XL (Thermo Electron). Peptides were separated on a C18-reversed-phase column packed with Reprosil and directly mounted on the electrospray ion source on an LTQ-Orbitrap XL. We used a 140-min gradient from 2% to 60% acetonitrile in 0.5% acetic acid at a flow of 200 nL/min. The raw files were processed with MaxQuant (version 1.0.11.5) and searched with the Mascot search engine (MatrixScience) against a IPIhuman v3.37 protein database concatenated with a decoy of the reversed sequences. Carbamidomethylation was set as fixed modification while methionine oxidation and protein Nacetylation were considered as variable modifications.The search was performed with an initial mass tolerance of 7 ppm mass accuracy for the precursor ion and 0.5 Da for the MS/MS spectra. Search results were processed with MaxQuant filtered with a false discovery rate of 0.01. Before statistical analysis, known contaminants and reverse hits were removed. Only

proteins identified with at least 2 unique peptides and 2 quantitation events were considered for analysis. Appendix tables 5 contain all proteins identified with $p < 0.05$ in forward or cross-over experiments.[128,132]

6. 7   Cellular Assays

6.7.1   Nuclear and cytoplasmic extracts preparation

Nuclear extracts and cytoplasmic extracts were prepared from BaF3/FLT3-ITD cells using the Nuclear Extraction kit (Active Motif, Carlsbad, CA, USA) according to the manufacturer's protocol.

6.7.2   Whole cell lysate preparation

BaF3/FLT3-ITD cells were grown in suspension at 37 ℃ in a humidified atmosphere with 5% CO_2 in RPMI medium containing 10% dialyzed FBS. After harvesting, cell pellets were washed twice with PBS and frozen with liquid N_2. To prepare whole cell lysates, the cell pellets were resuspended in a hypotonic buffer (10 mM HEPES, pH 7.5, 2 mM $MgCl_2$, 0.1% tween-20, 20% glycerol, 2 mM PMSF, and Roche Complete EDTA-free protease inhibitors) and incubated for 10 min at 4 ℃. The suspension was centrifuged at 16000 xg for 15 min at 4 ℃ and the supernatant was kept for use later. The pellets were resuspended in a high-salt buffer (50 mM HEPES, pH 7.5, 420 mM NaCl, 2 mM $MgCl_2$, 0.1% tween-20, 20% glycerol, 2 mM PMSF, and Roche Complete EDTA-free protease inhibitors) and incubated for 30 min at 4 ℃ . The suspension was then centrifuged at 16000 xg for 15 min at 4 ℃ and the supernatant was combined with the soluble fraction in hypotonic buffer to give the whole cell lysates.

6.7.3 SILAC BaF3/FLT3: ITD cell extract.

BaF3/FLT3:ITD cells were SILAC-labelled in RPMI 1640 medium containing 10% FBS and L-Glutamine supplemented with 84mg/mL $^{13}C_6$, $^{15}N_4$ L-arginine and $^{13}C_6$,$^{15}N_2$ L-Lysine (SIGMA ALRICH) or the corresponding non labelled (light) amino acids, respectively. Five consecutive batches of cells were independently harvested, and cell extracts were prepared as described below (6.7.2 whole cell lysate preparation).

6.7.4 Cellular Thermal Shift Assay (CETSA)

Cellular thermal shift assays[127] were performed to monitor the target engagement of **10** and **16** for STAT5a and STAT5b protein in BaF3/FLT3-ITD cells. Briefly, cell lysate from a total of 2×10^6 BaF3/FLT3-ITD cells was collected, diluted in PBS and separated in identical aliquots. Lysates were divided into 45 μL in each of PCR tubes and heated individually at different temperatures with Thermocycler (Biometra, Göttingen, Germany). The heated lysates were centrifuged and the supernatants were analyzed by SDS-PAGE followed by immunoblotting analysis by probing with anti-STAT5a (C-6) sc271542 and STAT5b (G-2) sc-1656 (Santa Cruz Biotechnology) antibody, respectively.

6.7.5 Isothermal dose response fingerprint experiments (ITDRF [139])

BaF3/FLT3-ITD cells were grown in suspension at 37 ℃ in a humidified atmosphere with 5% CO_2 in RPMI medium containing 10% dialyzed FBS. Approximately 2×10^6 cells were collected, washed with PBS buffer and replaced with fresh RPMI with 10% FBS. Cells were then separated in identical aliquots before treated with compound **16** at a final concentration between 0 and 100 μM (0.1% DMSO) and incubated under standard tissue culture conditions for 6 h. Cells were re-suspended in PBS supplemented with Complete EDTA-free protease inhibitors (Roche), aliquots (100 μl) containing equal cell numbers in PCR tubes were prepared. Tubes were incubated at approximately the T_m of the proteins of interest as

determined by CETSA melting curve experiments, 60 °C (T_m for actin) for 3 min, followed by room temperature for 3 min. The tubes were centrifuged (300 g, 3 min, 4 °C). The supernatant was removed and cells suspended in lysis buffer (100 mM HEPES, 300 mM NaCl, 2% NP-40 and 10 mM EDTA, pH 7.4), supplemented with protease inhibitors. The tubes were incubated at 4 °C for 1 h, with vortexing every 20 min. Samples were centrifuged for 30 min at 16,000 x g at 4 °C to pellet cell debris and precipitated proteins. The supernatants were analyzed by SDS-PAGE followed by immunoblotting analysis by probing with anti-STAT5a (C-6) sc271542 and STAT5b (G-2) sc-1656 (Santa Cruz Biotechnology) antibody, respectively.

6.7.6 Western blot analysis and immunoprecipitation

Cells were seeded at 0.5×10^6 and allowed to grow overnight followed by 6 h incubation with test compounds (0.1% DMSO) before protein extraction with M-PER^{TM} Mammalian Protein Extraction Reagent (Pierce) containing 1% (vol/vol) complete protease inhibitor cocktail (Roche Molecular Biochemicals) and 1% (vol/vol) phosphate inhibitor cocktail (Sigma). For Western blotting, 15 µg of protein from each sample were then separated on a 10% SDS-PAGE and transferred to a PVDF membrane. The blots were blocked with TBST buffer (20 mM Tris-HCl [pH 7.4], 140 mM sodium chloride, and 0.05% Tween 20) containing 5% BSA at room temperature for 1 h, washed 3 times in TBST buffer, and incubated with primary antibody overnight at 4°C. The membranes were then incubated with HRP-conjugated secondary antibody at room temperature for 1 h. The reaction products were detected using Syngene Pxi4 imager and quantified by Image J[130].

6.7.7 STAT5 luciferase reporter assay

BaF3/FLT3-ITD cells (5×10^6 cells in 0.3 ml) were co-transfected with a ratio of 10:1 pGL-STAT5 and pRL-TK as a transfection efficiency control in Opti-MEM medium via electroporation. (ECM 830 electroporator, BTX Instruments, Holliston, MA). The transfected

cells were then seeded in a 24-well plate and treated with serial dilution of compounds for 6 h. The cells were collected 48 h after transfection, and the luciferase activities in the cell lysates were determined using the dual luciferase reporter assay system (Promega, WI, USA). Each transfection was performed in triplicate and repeated twice.

6.7.8 RNA isolation and real-time PCR

RNA was harvested using NucleoSpin RNA kit (Macherey-Nagel). cDNA was generated using the SuperScript™ II Reverse Transcriptase (Thermo Scientific) and Real-Time quantitative RT-PCR was performed using Transcriptor High Fidelity cDNA Synthesis and Light-Cycler 480 SYBR Green I Master Kits on a Light-Cycler 480 Real-Time PCR System according to instructions given by the manufacturer (Roche). Data were evaluated using the Light-Cycler 480 software (1.5). Quantitative reverse transcription polymerase chain reaction (RT-PCR) was performed using primers as described. Data are expressed as mean fold change ± SE of 3 replicates and S9 expression was used as an internal control. The sequences of the oligo-primers used are shown in Appendix Table 1.

6.7.9 Transient transfection of STAT5 siRNA

Transient transfection for knockdown of endogenous STAT5 proteins was prepared by using STAT5 siRNA (STAT5 siRNA (h), sc-29495) from Santa Cruz Biotechnology (Santa Cruz, CA) and Control siRNA (control siRNA-A, sc-37007) was used a negative control. Cell were transfected with STAT5 siRNA using siRNA transfection reagent (sc-29528, Santa Cruz, CA) according to the manufacturer's instructions. Selective silencing of STAT5 was confirmed by western blot analysis. To assay the effect of STAT5 knockdown on cell viability, cells were first transfected with STAT5 siRNA or control siRNA and incubated for 24 h before treated with compound **16** (50 μM) or DMSO for 48 h. Viable cells was distinguished using an ATP-dependent bioluminescence assay (CellTiter-Glo, Promega).

6.7.10 Cell proliferation assay

The effect of compounds on cell lines was evaluated by In Vitro Toxicology Assay Kit, Resazurin based with indicator dye Alamar Blue (Sigma). Adherent and suspension cells were plated at 5×10^3 per well and 1×10^4 per well respectively in triplicate in 96-well plates and incubated in medium containing 10% FBS. For adherent cells, the complete medium was replaced after 24 h and incubated with test medium containing vehicle control or serial concentration of compounds for 48 h at 37 °C. The remaining unused wells in the periphery of microtiter well plate were added with PBS to avoid evaporation effects. Alamar Blue was then added, and all plates were incubated at 37 °C, and a colorimetric change was measured according to the manufacturer's protocol.

6.7.11 Phospho-specific flow cytometry of intracellular protein

BaF3/ FLT3-ITD or K562 cells were seeded at 0.2×10^6 cells/ml per well in 6-well plates overnight and incubated with serial concentration of tested compounds for 6 h. A total amount of 10^6 cells were collected and washed twice in 1xPBS and resuspended in 100 μl cytofix/cytoperm solution (BD Biosciences) at 4 °C. After 20 min, cells were washed twice with BD Perm/Wash buffer solution and incubated with 20 μl of specific fluorochrome (PE) conjugated monoclonal antibody anti-p-STAT5 (Phosflow™ PE-Cy™7 mouse anti-Stat5 (pY694) (BD Biosciences) at 4 °C. After 30 min, the cells were washed twice and analyzed by flow cytometry. For isotype control, the cells were incubated with 2 μL of PE conjugated rat anti-mouse IgG1 monoclonal antibody (BD Biosciences) at 4 °C for 30 min and washed twice in before being analyzed on a FACScan Flow Cytometer (Becton-Dickinson, San Jose, CA). Data interpretation was done using the Flowjo software[152] (Treestar, Inc., San Carlos, CA).

6.7.12 Cell viability assay

The effect of compounds on cell viability was evaluated using Cell Titer-Glo Luminescent Cell Viability assay kit (Promega). Cells were plated at 5×10^3 per well and 1×10^4 per well respectively in triplicate in white-walled, clear-bottom 96-well plates (3903, Corning Costar) and incubated in medium containing 10% FBS overnight. Cells were treated with or without compounds at 37 ℃ for 48 h before carrying out the viability assay. The number of viable cells was measured using the CellTiter-Glo ATP-dependent luminescent assay (Promega, Madison, WI) following the manufacturer instruction. Luminescence reading was measured using Tecan Infinite M1000 plate reader (Tecan, Männedorf, Switzerland). The graphically represented values are means ± s.d. for three independent samples.

6.7.13 Cell apoptosis analysis

Cell apoptosis was determined using Annexin V staining. BaF3/FLT3-ITD or K562 suspension cells were plated at 0.2×10^6 per well in 6-well plates and incubated with serial concentration of tested compounds for 48 h. Cells were washed twice in ice-cold PBS resuspended in 1x binding buffer (10 mM Hepes (pH 7.4), 140 mM NaCl and 2.5 mM $CaCl_2$) to a final concentration of 1×10^6 cells/ml. Subsequently, FITC Annexin V solution (5 μl) was added to 100 μl of the cell suspension. The mixture was incubated for 30 min at room temperature and washed in 1x Binding Buffer and again resuspended in 200 μl of 1x Binding buffer. Propidium iodide staining solution (5 μl, Sigma) was added shortly before analysis on a FACScan Flow Cytometer (Becton-Dickinson, San Jose, CA). Data interpretation was done using the Flowjo software (Treestar, Inc., San Carlos, CA).

6.7.14 Electrophoretic mobility shift assay (EMSA)

Gel shift assay was conducted using a double-stranded, biotin-labeled oligonucleotide probe containing the consensus binding site for STAT5 (sense strand, 5′AGATTTCTAGGAATTCAATCC -3′), using the Gelshift Chemiluminescent EMSA kit (Active Motif) according to the manufacturer's protocol. Protein-DNA complexes were resolved on a nondenaturing polyacrylamide gel, transferred to a positively charged nylon membrane, and cross-linked to a membrane using the UV-light cross-linker. After blocking, the membrane was incubated with blocking buffer containing streptavidin conjugated to HRP. After washing, protein-DNA complexes were detected using a chemi-luminescent substrate (Active Motif)[126,138] .

6.7.15 Quantitative evaluation and inhibition of DNA-binding of activated STATs by ELISA

STAT1, STAT3 and STAT5a and b activity were determined in nuclear protein extracts (20 μg) by the TransAM STATs family kits from Active Motif (Carlsbad, CA). All assays were performed following the manufactory instruction after the nuclear protein extraction.

6.7.16 Statistical analysis

Statistical calculations were performed using GraphPad Prism 5[129] software and reported as mean $\pm$ SEM. Experiments were performed in triplicates and/or repeated at least three times unless indicated otherwise. Two-tailed Student's t-tests and one-way ANOVA were used to identify statistically significant data. p-values are considered as follows: * $p\text{-value} < 0.05$; ** $p\text{-value} < 0.01$; and *** $p\text{-value} < 0.001$. Synergy in cell viability assays was determined by plotting isobolograms and calculating the combination index (CI) using CalcuSyn software (Calcusyn software, Biosoft, San Diego, CA, USA) (Conservion, Ferguson, MO) using the

Chou–Talalay[141] method to ascertain if the effects of drug combinations were synergistic (CI < 1), additive (CI = 1), or antagonistic (CI > 1).

6.7.17 Animal experiments

NSG mice (NOD/Shi-scid/IL-2Rγnull) from obtained from The Jackson Laboratory aged 6 weeks with an average body weight of 22 grams. Studies were conducted at EPO GmbH, Berlin, in accordance with the United Kingdom Coordinating Committee on Cancer Research Regulations for the Welfare of Animals and in accordance with the German Animal Protection Law approved by the local responsible authorities, Berlin, Germany. BaF3/FLT3-ITD cells were injected into mice subcutanously (106 cells per mouse). Inoculated and control mice (6 in each group) were treated for 16 d once daily s.c. with either the vehicle (10% (v/v) DMSO / 0.25% Tween 80) or compound 16 (200 mg kg-1) dissolved in vehicle, starting shortly after tumor cell inoculation. Former studies had shown that this concentration of test compound is well tolerated by the mice. Tumor volumes and body weights were recorded daily and expressed as mean ± standard deviation.

6.8 Chemical Synthesis (This part is carried out by Dr. Eric Nawrotzky and Thomas Rudolf)

General synthetic methods

Method A: To a solution of 4-amino-furazan-3-carboxylic acid or methylester (1.0 mmol) and tetrazole (1.2 mmol) in 2.7 mL of acetonitrile (hipersolv chromanorm) and 0.3 mL of acetic acid, formaldehyde (37 % solution in water, 2.0 mmol) was added and this reaction mixture was stirred at r.t. for 16 h. Afterwards the mixture was lyophilizated and residue was purified by flash column chromatograph.

Method B: A solution of 4-amino-furazan-3-carboxylic acid (1.2 mmol), tetrazole (1.0 mmol), and formaldehyde (37 % aqueous solution, 10.0 mmol) in 2.7 mL of acetonitrile and 0.3 mL of concentrated hydrochloric acid was stirred in a sealed microwave reaction vial at 105 °C in a microwave reactor for 5 h. After cooling the reaction, solids were filtrated off, washed with a small amount of water and dried under reduced pressure. The residue was purified by flash column chromatography.

Method C:
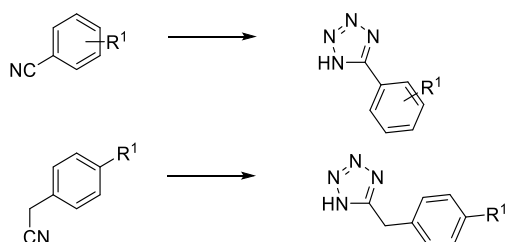
A suspension of the nitrile component (1.0 mmol), NaN$_3$ (2 mmol), and NH$_4$Cl (1.1 mmol) in DMF (5 mL) was stirred in a sealed microwave reaction vial at 140 °C in a microwave reactor for 1 h. After the mixture was evaporated in vacuum, the residue was poured into water and acidified with concentrated HCl to pH = 2 and cooled to 5 °C. Then the precipitate was filtrated off, washed with cold water, and dried under reduced pressure to give the desired compounds.

5-CF-GY*LSLPPW-NH$_2$ [1]

Synthesized as described previously.

4-Formylphenyl-dihydrogen-phosphate [2]
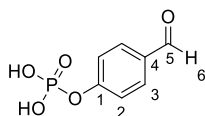
Diethylchlorophosphate (1.18 mL, 8.19 mmol, 1 eq.) was added dropwise to a cooled (0°C) solution of 4-hydroxybenzaldehyde (1.0 g, 8.19 mmol, 1 eq.) and triethylamine (1.36 mL,

9.83 mmol, 1.2 eq.) in dry DCM (5 mL) under inert atmosphere. The reaction mixture was warmed to room temperature and stirred furthermore for 3 h. Afterwards the organic phase was extracted with 1 M HCl, saturated NaHCO$_3$, dried over sodium sulfate and after filtration the filtrate was evaporated in vacuum.

The protected phosphate (0.5 g, 1.94 mmol, 1 eq.) and trimethylsilylbromide (0.51 mL, 3.88 mmol, 2 eq.) was stirred in MeCN (5 mL) at room temperature for 6 h. Subsequently the reaction mixture was quenched with 10 mL of H$_2$O/MeOH (1:10), Amberlite® IR120 in protonated form (4 g) was added and the mixture was stirred at room temperature for 12 h. After filtration and purification by flash column chromatography the product was obtained as white solid (0.254 g, 1.26 mmol, 64 %).

^{1}H-NMR (500 MHz, DMSO-d_6): δ = 9.94 (s, 1H, H-6), 7.92 (d, J = 8.3 Hz, 2H, H-3), 7.37 (d, J = 8.3 Hz, 2H, H-2) ppm. **^{13}C-NMR** (101 MHz, DMSO-d_6): δ = 192.32 (C-5), 156.36 (C-1), 132.23 (C-4), 132.09(C-3), 120.94 (C-2) ppm. **^{31}P-NMR** (162 MHz, DMSO-d_6):δ = 21.3 (m, 1P, P) ppm. **HRMS:** (ESI): C$_7$H$_7$O$_5$P [M], 202.0031 Da. calcd m/z 200.9953 [M-H]$^-$, found m/z 200.9893 [M-H]$^-$.

4-Amino-1,2,5-oxadiazole-3-carboxylic acid [3]
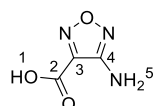
To a stirred suspension of ethyl cyanoacetate (28.3 g, 0.25 mol, 1 eq.) and sodium nitrite (17.3 g, 0.25 mol, 1.0 eq.) in a mixture of EtOH (17 mL) and water (200 mL) was added dropwise 85% H$_3$PO$_4$ (10 mL) at 10-15 °C and stirred for 12 h. Afterwards the reaction mixture was treated with NaOH (4×10 g, 1 mol, 4 eq.) and KOH (2×14 g, 0.5 mol, 2.0 eq.). To the resulting solution NH$_2$OH·HCl (69.5 g, 1.0 mol, 4.0 eq.) was slowly added at room temperature and heated upto 95 °C, stirred for 2 h, cooled to ambient temperature and quenched with conc. HCl to pH 1. Precipitation occurred on cooling to 0 °C for 12 h and the precipitate was collected by filtration and dried. The filtrate was extracted with diethyl ether

(3×30 mL). The combined organic extracts were evaporated under reduced pressure. The residue was combined with the precipitate and recrystallized from hot water to givecompound **1** (21.3 g, 0.165 mol, 66 %) as white solid.

^{1}H-NMR (300 MHz, DMSO-d_6): δ = 9.69 (br s, 1H, H-1), 6.24 (s, 2H, H-5) ppm. **^{13}C-NMR** (75 MHz, DMSO-d_6): δ = 162.5 (C-2), 157.1 (C-3), 144.9 (C-4) ppm. **HRMS:** (ESI): $C_3H_3N_3O_3$ [M], 129.0174 Da. calcd m/z 128.0096 [M-H]⁻, found m/z 128.0106 [M-H]⁻.

4-Amino-1,2,5-oxadiazole-3-carboxylic acid methylester [X1]
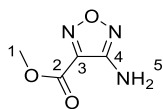
To a solution of 4-amino-1,2,5-oxadiazole-3-carboxylic acid **3** (2 g, 15.5 mmol, 1.0 eq.) in MeOH (20mL) was added dropwise a catalytic amount of conc. H_2SO_4 and heated up to 60 °C and stirred for 3 h. Afterwards the reaction mixturewas evaporated in vacuum, the residue was dissolved in DCM (50 mL), washed with water, saturated solution of NaOH and Brine. Subsequently the mixtures was evaporated and recrystallized from hot CHCl₃to give compound **2** (2.11 g, 14.73 mmol, 95 %) as white solid.

^{1}H-NMR (300 MHz, DMSO-d_6): δ = 6.24 (s, 2H, H-5), 3,76 (s, 3H, H-1) ppm. **^{13}C-NMR** (75 MHz, DMSO-d_6): δ = 159.4 (C-2), 156.5 (C-3), 139.9 (C-4), 53.5 (C-1) ppm. **HRMS:**(ESI): $C_4H_5N_3O_3$ [M], 143.0331 Da. calcd m/z 166.0229 [M+Na]⁺, 181.9968 [M+K]⁺, found m/z 166.0253 [M+Na]⁺, 181.9977 [M+K]⁺.

4-Acetamido-1,2,5-oxadiazole-3-carboxylic acid [4]
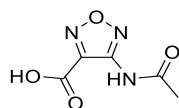
Commercial available at Sigma-Aldrich (#CDS002372)

Methyl 4-(2-bromoacetamido)-1,2,5-oxadiazole-3-carboxylate [X2]
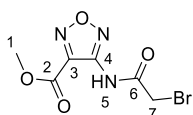
To a solution of 4-amino-1,2,5-oxadiazole-3-carboxylic acid methylester **X1** (143 mg, 1 mmol, 1 eq.) and 4-DMAP (369.3 mg, 1.0 mmol, 1.0 eq.) in dried DCM (15 mL) 2-bromoacetyl bromide (242.2 mg, 1.2 mmol, 1.2 eq.) was slowly added under inert atmosphere. The reaction mixture was stirred at 0 °C for 2 h, evaporated in vacuum and was purified by flash column chromatography to give the product (339.7 mg, 0.92 mmol) in 92 % yield as a white solid.

^{1}H NMR (300 MHz, CDCl$_3$): δ = 9.92 (s, 1H, H-5), 4.13 (s, 2H, H-7), 4.11 (s, 3H, H-1) ppm.

^{13}C-NMR (75 MHz, CDCl$_3$): δ = 160.02 (C-6), 159.85 (C-2), 153.56 (C-3), 138.71 (C-4), 54.06 (C-1), 28.01 (C-7) ppm. **HRMS:** C$_6$H$_6$BrN$_3$O$_4$ [M], 262.9542 Da. calcd m/z 285.9439 [M+Na]$^+$, found m/z 285.9289 [M+Na]$^+$.

Methyl 4-(2-(*1H*-tetrazol-1-yl)acetamido)-1,2,5-oxadiazole-3-carboxylate [X3]
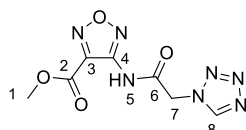
To a solution of Methyl 4-(2-bromoacetamido)-1,2,5-oxadiazole-3-carboxylate **X2** (264.2 mg, 1.5 mmol, 1.0 eq.) and *1H*-tetrazol (9.1 mL (0.45M solution), 1.65 mmol, 1.1 eq.) in acetonitrile (5 mL) was added Et$_3$N (0.15 mL, 1.5 mmol, 1.0 eq.) and stirred at 90 °C for 5 h. After the mixture was evaporated in vacuum, the residue was dissolved in DCM (20 mL) and washed with H$_2$O (5 mL). The organic phase was dried over Na$_2$SO$_4$ and after filtration the filtrate was evaporated in vacuum. The residue was purified by flash column chromatography to give the product (229.1 mg, 0.65 mmol) in 43 % yield as a white solid.

^{1}H NMR (300 MHz, CD$_3$CN): δ = 9.41 (s, 1H, H-5), 8.72 (s, 1H, H-8), 5.79 (s, 2H, H-7), 4.00 (s, 3H, H-1) ppm. **^{13}C-NMR** (75 MHz, CD$_3$CN): δ = 163.78 (C-6), 159.67 (C-2), 154.51

(C-3), 150.25 (C-8), 142.29 (C-4), 56.11 (C-1), 54.50 (C-7) ppm. **HRMS:** (ESI): C$_7$H$_7$N$_7$O$_4$ [M], 253.0560 Da. calcd *m/z* 276.0457 [M+Na]$^+$, found *m/z* 276.0451 [M+Na]$^+$.

4-(2-(1*H*-tetrazol-1-yl)acetamido)-1,2,5-oxadiazole-3-carboxylic acid [5]
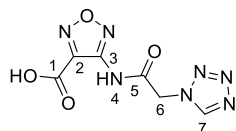
To a stirred solution of Methyl 4-(2-(*1H*-tetrazol-1-yl)acetamido)-1,2,5-oxadiazole-3-carboxylate **X3** (50.0 mg, 0.2 mmol, 1.0 eq.) in THF (1.0 mL) was added 0.1 M LiOH (0.1 mL) and Water (0.4 mL) and the reaction mixture was stirred at r.t. for 30 min. Afterwards the reaction mixture was neutralized with Amberlite$^®$ IR-120 hydrogen form, filtrated and washed with H$_2$O/THF (2.0 mL, 1:1 (*v/v*)). The mixture was evaporated to give compound **5** (43.9 mg, 0.18 mmol, 92 %) as white solid.

^{1}H NMR (300 MHz, CD$_3$CN): δ = 9.31 (s, 1H, H-4), 8.82 (s, 1H, H-7), 5.43 (s, 2H, H-6) ppm.

^{13}C-NMR (75 MHz, CD$_3$CN): δ = 164.28 (C-5), 160.61 (C-1), 155.11 (C-2), 151.3 (C-7), 142.89 (C-3), 54.62 (C-6) ppm. **HRMS:** (ESI): C$_6$H$_5$N$_7$O$_4$ [M], 239.0403 Da. calcd *m/z* 262.0301[M+Na]$^+$, found *m/z* 262.0296 [M+Na]$^+$.

4-((*1H*-1,2,3-Triazol-1-yl)methylamino)-1,2,5-oxadiazole-3-carboxylic acid [6]
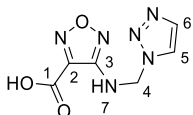
Prepared according to general procedure Method A using 4-amino-1,2,5-oxadiazole-3-carboxylic acid **3** (129 mg, 1 mmol, 1.0 eq.), *1H*-1,2,3-triazolezole (103.6, 1.5 mmol, 1.5 eq.) and formaldehyde (0.2 mL, 2.0 mmol, 2.0 eq.) to give the product (165.9 mg, 0.79 mmol) in 79 % yield as a white solid.

^{1}H NMR (300 MHz, DMSO-d_6): δ = 8.16 (m, 1H, H-6), 7.81 (t, J = 7.0 Hz, 1H, H-7), 7.71 (m, 1H, H-5), 5.82 (d, J = 6.9 Hz, 2H, H-7) ppm. **^{13}C-NMR** (75 MHz, DMSO-d_6): δ = 160.1 (C-1), 155.4 (C-2), 140.2 (C-3), 133.2 (C-6), 124.6 (C-5), 57.8 (C-4) ppm. **HRMS:** (ESI): $C_6H_6N_6O_3$ [M], 210.1530 Da. calcd m/z 209.1450 [M-H]⁻, found m/z 209.0470 [M-H]⁻.

4-((*1H*-Benzo[d][1,2,3]triazol-1-yl)methylamino)-1,2,5-oxadiazole-3-carboxylic acid [7]
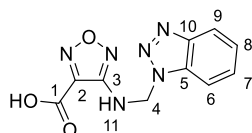
Prepared according to general procedure Method A using 4-amino-1,2,5-oxadiazole-3-carboxylic acid **3** (129 mg, 1.0 mmol, 1.0 eq.), *1H*-benzotriazole (179 mg, 1.5 mmol, 1.5 eq.) and formaldehyde (0.2 mL, 2.0 mmol, 2.0 eq.) to give the product (93.8 mg, 0.36 mmol) in 36 % yield as a white solid.

^{1}H NMR (300 MHz, DMSO-d_6): δ = 8.09 (d, J = 8.4 Hz, 1H, H-9), 8.05 (t,J = 7.0 Hz 1H, H-11), 8.03 (d, J = 8.3 Hz 1H, H-6), 7.57 (t, J = 7.6 Hz, 1H, H-8), 7.39 (t, J = 7.5 Hz, 1H, H-7), 6.17 (d, J = 6.9 Hz, 2H, H-4) ppm. **^{13}C-NMR** (75 MHz, DMSO-d_6): δ = 160.2 (C-1), 156.1 (C-2), 145.8 (C-10), 143.5 (C-3), 132.9 (C-5), 127.9 (C-8), 124.6 (C-7), 119.6(C-9), 111.9(C-6), 57.2(C-4) ppm. **HRMS:** (ESI): $C_{10}H_8N_6O_3$ [M], 260.0658 Da. calcd m/z 259.0580 [M-H]⁻, found m/z 259.0590 [M-H]⁻.

4-((*1H*-Pyrazol-1-yl)methylamino)-1,2,5-oxadiazole-3-carboxylic acid [8]
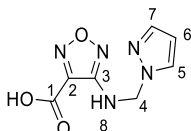
Prepared according to general procedure Method A using 4-amino-1,2,5-oxadiazole-3-carboxylic acid **3** (129 mg, 1.0 mmol, 1.0 eq.), *1H*-pyrazole (102.1, 1.5 mmol, 1,5 eq.) and formaldehyde (0.2 mL, 2.0 mmol, 2.0 eq.) to give the product (198.8 mg, 0.95 mmol) in 95 % yield as a white solid.

¹H NMR (300 MHz, DMSO-d_6): δ = 7.82 (d, *J* = 2.2 Hz, 1H, H-7), 7.61 (t, *J* = 6.9 Hz, 1H, H-8), 7.45 (d, *J* = 2.1 Hz, 1H, H-5), 6.23 (t, *J* = 2.1 Hz, 1H, H-6), 5.52 (d, *J* = 6.8 Hz, 3H, H-4) ppm. **¹³C-NMR** (75 MHz, DMSO-d_6): δ = 159.7 (C-1), 155.6 (C-2), 139.1 (C-3), 130.1 (C-7), 129.5 (C-5), 105.3 (C-6), 59.2 (C-4) ppm. **HRMS:** (ESI): $C_7H_7N_5O_3$ [M], 209.0549 Da. calcd *m/z* 208.0471 [M-H]⁻, found *m/z* 208.0465 [M-H]⁻.

4-((*1H*-1,2,4-Triazol-1-yl)methylamino)-1,2,5-oxadiazole-3-carboxylic acid [9]
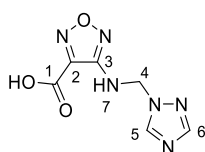
Prepared according to general procedure Method A using 4-amino-1,2,5-oxadiazole-3-carboxylic acid **3** (129 mg, 1.0 mmol, 1.0 eq.), *1H*-1,2,4-triazolezole (103.6, 1.5 mmol, 1.5 eq.) and formaldehyde (0.2 mL, 2.0 mmol, 2.0 eq.) to give the product (138.7 mg, 0.66 mmol) in 66 % yield as a white solid.

¹H NMR (300 MHz, DMSO-d_6): δ = 8.59 (s, 1H, H-6), 7.97 (s, 1H, H-5), 7.69 (t, *J* = 6.9 Hz, 1H, H-7), 5.61 (d, *J* = 6.8 Hz, 2H, H-4) ppm. **¹³C-NMR** (75 MHz, DMSO-d_6): δ = 159.6 (C-1), 155.3 (C-2), 151.5 (C-3), 144.5 (C-5), 140.2 (C-6), 57.3 (C-4) ppm. **HRMS:** (ESI): $C_6H_6N_6O_3$ [M], 210.1530 Da. calcd *m/z* 209.1450 [M-H]⁻, found *m/z* 209.0459 [M-H]⁻.

4-((*1H*-Tetrazol-1-yl)-methylamino)-1,2,5-oxadiazole-3-carboxylic acid [10]
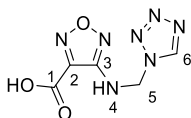
Prepared according to general procedure Method A using 4-amino-1,2,5-oxadiazole-3-carboxylic acid **3** (129 mg, 1.0 mmol, 1.0 eq.), *1H*-tetrazol (3.3 mL (0.45M solution), 1.5 mmol, 1.5 eq.) and formaldehyde (0.2 mL, 2.0 mmol, 2.0 eq.) to give the product (184.8 mg, 0.88 mmol) in 88 % yield as a white solid.

¹H NMR (300 MHz, DMSO-d_6):δ = 9.43 (s, 1H, H-6), 7.90 (t, J = 6.9 Hz, 1H, H-4), 5.91 (d, J = 6.9 Hz, 2H, H-5) ppm. **¹³C-NMR** (75 MHz, DMSO-d_6): δ = 160.2 (C-1), 155.8 (C-2), 144.6 (C-3), 140.7 (C-6), 57.2 (C-5) ppm. **HRMS:**(ESI): $C_5H_5N_7O_3$ [M], 211.0454 Da. calcd m/z 210.0376 [M-H]⁻, found m/z 210.0397 [M-H]⁻. **Anal:** calcd for $C_5H_5N_7O_3$: C, 28.44; H, 2.39; N, 46.44; found C, 28.12; H, 2.26; N, 46.82.

4-((5-Phenyl-*1H*-tetrazol-1-yl)methylamino)-1,2,5-oxadiazole-3-carboxylic acid [11]
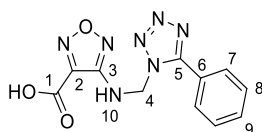
Prepared according to general procedure Method A using 4-amino-1,2,5-oxadiazole-3-carboxylic acid **3** (129 mg, 1.0 mmol, 1.0 eq.), 5-phenyl-*1H*-tetrazole (219 mg, 1.5 mmol, 1.5 eq.) and formaldehyde (0.2 mL, 2.0 mmol, 2.0 eq.) to give the product (252.6 mg, 0.88 mmol) in 88 % yield as a white solid.

¹H NMR (300 MHz, DMSO-d_6): δ = 8.10 (t, J = 7.0 Hz, 1H, H-10), 8.04 (d, J = 7.8 Hz, 2H, H-7), 7.58 – 7.52 (m, 3H, H-8, H-9), 6.14 (d, J = 7.0 Hz, 2H, H-4) ppm. **¹³C-NMR** (75 MHz, DMSO-d_6): δ = 164.7 (C-5), 160.2 (C-1), 155.8 (C-2), 140.7 (C-3), 131.2 (C-6), 129.9 (C-7), 127.4 (C-9), 126.9 (C-8), 62.1 (C-4) ppm. **HRMS:** (ESI): $C_{11}H_9N_7O_3$ [M], 287.2390 Da. calcd m/z 286.2310 [M-H]⁻, found m/z 286.2110 [M-H]⁻.

4-((5-(3-(Trifluoromethyl)phenyl)-*1H*-tetrazol-1-yl)methylamino)-1,2,5-oxadiazole-3-carboxylic acid [12]
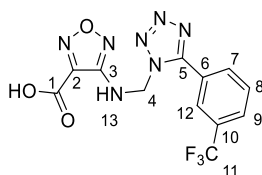
Prepared according to general procedure Method A using 4-amino-1,2,5-oxadiazole-3-carboxylic acid **3** (83.9 mg, 0.7 mmol, 1.3 eq.), 5-(4-(trifluoromethyl)phenyl)-*1H*-tetrazole (147.2 mg, 0.5 mmol, 1.0 eq.) and formaldehyde (0.1 mL, 2.0 mmol, 2.0 eq.) to give the product (159.9 mg, 0.45 mmol) in 90 % yield as a white solid. **^{1}H NMR** (300 MHz, CDCl$_3$): δ = 8.40 (s, 1H, H-12), 8.32 (d, *J* = 7.8 Hz, 1H, H-7), 7.72 (d, *J* = 7.9 Hz, 1H, H-9), 7.60 (t, *J* = 7.8 Hz, 1H, H-8), 6.88 (t, *J* = 7.5 Hz, 1H, H-13), 6.20 (d, *J* = 7.6 Hz, 2H, H-4) ppm. **^{13}C-NMR** (75 MHz, CDCl$_3$): δ = 163.6 (C-5), 160.90 (C-1), 155.20 (C-2), 138.94 (C-3), 131.68(C-10), 130.16 (C-7), 129.47 (C-8), 127.83 (C-6), 127.06 (C-9), 125.54 (C-11), 123.87 (C-12), 60.72 (C-4) ppm. **HRMS:** (ESI): C$_{12}$H$_8$F$_3$N$_7$O$_3$ [M], 355.0641 Da. calcd *m/z* 394.0278 [M+K]$^+$, found *m/z* 394.0263[M+K]$^+$.

4-((5-(3-Fluorophenyl)-*1H*-tetrazol-1-yl)methylamino)-1,2,5-oxadiazole-3-carboxylic acid [13]
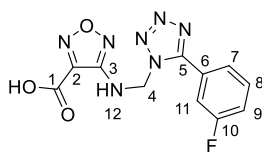
Prepared according to general procedure Method B using 4-amino-1,2,5-oxadiazole-3-carboxylic acid **3** (167.7 mg, 0.7 mmol, 1.3 eq.), 5-(3-fluorophenyl)-*1H*-tetrazole (164.2 mg, 1.0 mmol, 1.0 eq.) and formaldehyde (0.15 mL, 2.0 mmol, 2.0 eq.) to give the product (250.3 mg, 0.82 mmol) in 82 % yield as a white solid.

^{1}H NMR (300 MHz, CDCl$_3$): δ = 7.94 (d, *J* = 7.8 Hz, 1H, H-7), 7.84 (dd, *J* = 9.5, 2.2 Hz, 1H, H-11), 7.46 (ddd, *J* = 8.3, 7.8, 5.8 Hz, 1H, H-8), 7.17 (t, *J* = 8.4 Hz, 1H, H-9), 6.85 (t, *J* = 7.6 Hz, 1H, H-12), 6.20 (d, *J* = 7.6 Hz, 2H, H-4) ppm. **^{13}C-NMR**(75 MHz, DMSO-*d$_6$*): δ = 163.72 (C-5), 159.56 (C-1), 155.83 (C-2), 140.95 (C-3), 134.28 (C-6), 131.65 (C-10), 129.16 (C-8), 123.72 (C-7), 121.85 (C-11), 118.93 (C-9), 61.85 (C-4) ppm. **HRMS:** (ESI): C$_{11}$H$_8$FN$_7$O$_3$ [M], 305.0673 Da. calcd *m/z* 304.0594 [M-H]$^-$, found *m/z* 304.0641 [M-H]$^-$.

4-((5-(3-(Trifluoromethoxy)phenyl)-1*H*-tetrazol-1-yl)methylamino)-1,2,5-oxadiazole-3-carboxylic acid [14]
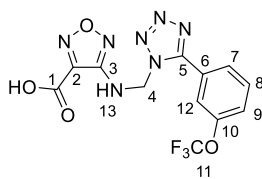
Prepared according to general procedure Method B using 4-amino-1,2,5-oxadiazole-3-carboxylic acid **3** (83.9 mg, 0.7 mmol, 1.3 eq.), 3-(1H-tetrazol-5-yl)phenyl hypofluorite (115.1 mg, 1.0 mmol, 1.0 eq.) and formaldehyde (0.1 mL, 2.0 mmol, 2.0 eq.) to give the product (252.4 mg, 0.82 mmol) in 68 % yield as a white solid.

^{1}H NMR (300 MHz, CDCl$_3$): δ = 8.09 (d, *J* = 8.0 Hz, 1H, H-7), 8.00 (s, 1H, H-12), 7.52 (dd, *J* = 7.8 Hz, 1H, H-8), 7.32 (d, *J* = 8.0 Hz, 1H, H-9), 6.85 (t, *J* = 7.6 Hz, 1H, H-13), 6.20 (d, *J* = 7.6 Hz, 2H, H-4) ppm. **^{13}C-NMR** (75 MHz, DMSO-*d$_6$*): δ = 163.20 (C-5), 159.82 (C-1), 155.54 (C-2), 149.11 (C-10), 140.82 (C-3), 132.03 (C-8), 129.21 (C-6), 126.32 (C-7), 125.76 (C-9), 123.44 (C-11), 118.73 (C-12), 62.04 (C-4) ppm. **HRMS:** (ESI): C$_{12}$H$_8$F$_3$N$_7$O$_4$ [M], 371.2362 Da. calcd *m/z* 370.2282 [M-H]$^-$, found *m/z* 370.0547 [M-H]$^-$.

4-((5-(4-Fluorophenyl)-*1H*-tetrazol-1-yl)methylamino)-1,2,5-oxadiazole-3-carboxylic acid [15]
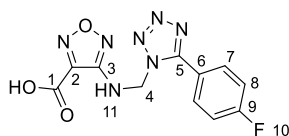
Prepared according to general procedure Method B using 4-amino-1,2,5-oxadiazole-3-carboxylic acid **3** (167.7 mg, 0.7 mmol, 1.3 eq.), 5-(4-fluorophenyl)-1H-tetrazole (164.2 mg, 1.0 mmol, 1.0 eq.) and formaldehyde (0.15 mL, 2.0 mmol, 2.0 eq.) to give the product (213.7 mg, 0.7 mmol) in 70 % yield as a white solid. **^{1}H NMR** (300 MHz, CDCl$_3$): δ = 8.14 (dd, *J* = 8.7, 5.5 Hz, 2H, H-7), 7.17 (t, *J* = 8.7 Hz, 2H, H-8), 6.81 (t, *J* = 7.6 Hz, 1H, H-11),

6.19 (d, J = 7.6 Hz, 2H, H-4) ppm. ^{13}**C-NMR** (75 MHz, DMSO-d_6): δ = 163.68 (C-5), 159.83 (C-1), 155.56 (C-2), 140.61 (C-3), 134.08 (C-6), 129.85 (C-7), 129.16 (C-8), 123.72 (C-9), 116.85 (C-10), 61.85 (C-4) ppm. **HRMS:** (ESI): $C_{11}H_8FN_7O_3$ [M], 305.0673 Da. calcd m/z 304.0594 [M-H]$^-$, found m/z 304.0618 [M-H]$^-$.

4-((5-Benzyl-*1H*-tetrazol-1-yl)methylamino)-1,2,5-oxadiazole-3-carboxylic acid [16]
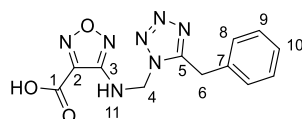
Prepared according to general procedure Method B using 4-amino-1,2,5-oxadiazole-3-carboxylic acid **3** (80.2 mg, 0.62 mmol, 1.2 eq.), 5-benzyl-1H-tetrazole (100.0 mg, 0.52 mmol, 1.0 eq.) and formaldehyde (0.47 mL, 5.2 mmol, 10.0 eq.) to give the product (81.3 mg, 0.27 mmol) in 52 % yield as a off white solid.

^{1}**H NMR** (500 MHz, DMSO-d_6): δ = 7.9 (t, J = 6.6 Hz, 2H, H-11), 7.27 (d, J = 7.0 Hz, H-8), 7.25 - 7.22 (m, 3H, H-9, H-10), 5.89 (d, J = 6.6 Hz, 2H, H-4), 4.48 (s, 2H, H-6) ppm. ^{13}**C-NMR** (126 MHz, DMSO-d_6): δ = 159.99 (C-1), 155.42 (C-2), 154.9 (C-5), 140.28 (C-3), 135.65 (C-7), 129.17 (C-8), 128.93 (C-9), 127.34 (C-10), 56.36 (C-4), 28.57 (C-6) ppm. **HRMS:** (ESI): $C_{12}H_{11}N_7O_3$ [M], 301.0923 Da. calcd m/z 300.0845 [M-H]$^-$, found m/z 300.0805 [M-H]$^-$. **Anal:** calcd for $C_{12}H_{11}N_7O_3$: C, 47.84; H, 3.68; N, 32.55; found C, 48.11; H, 3.81; N, 32.18.

4-((5-([1,1'-Biphenyl]-4-yl)-1*H*-tetrazol-1-yl)methylamino)-1,2,5-oxadiazole-3-carboxylic acid [17]
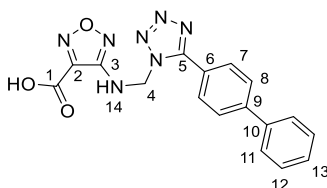
Prepared according to general procedure Method A using 4-amino-1,2,5-oxadiazole-3-carboxylic acid **3** (143 mg, 1.0 mmol, 1.0 eq.), 5-([1,1'-biphenyl]-4-yl)-*1H*-tetrazole (266 mg, 1.2 mmol, 1.2 eq.) and formaldehyde (0.1 mL, 2.0 mmol, 2 eq.) to give the product (221.5mg, 0.61 mmol) in 61 % yield as a white solid.

^{1}H NMR (300 MHz, CDCl$_3$): δ = 8.14 (d, *J* = 8.2 Hz, 2H, H-7), 8.11 (t, *J* = 7.0 Hz, 1H, H-14), 7.86 (d, *J* = 8.4 Hz, 2H, H-8), 7.74 (d, *J* = 7.2 Hz, 2H, H-11), 7.50 (t, *J* = 7.6 Hz, 2H, H-12), 7.41 (t, *J* = 7.2 Hz, 1H, H-13), 6.17 (d, *J* = 7.0 Hz, 2H, H-4) ppm. **^{13}C-NMR** (75 MHz, CDCl$_3$): δ = 164.41 (C-5), 160.09 (C-1), 155.78 (C-2), 142.59 (C-9), 140.69 (C-10), 139.58 (C-3), 129.54 (C-12), 128.52 (C-13), 127.95 (C-6), 127.45 (C-7), 127.20 (C-8), 126.27 (C-11), 62.03 (C-4) ppm. **HRMS:** (ESI): C$_{17}$H$_{13}$N$_7$O$_3$ [M], 363.1080 Da. calcd *m/z* 386.0978 [M+Na]$^+$, found *m/z* 386.0920 [M+Na]$^+$.

Methyl 4-(((*1H*-tetrazol-1-yl)methylamino)-1,2,5-oxadiazole-3-carboxylate [18]
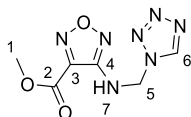
Prepared according to general procedure Method A using 4-amino-1,2,5-oxadiazole-3-carboxylic acid methylester **X1** (143 mg, 1.0 mmol, 1.0 eq.), *1H*-tetrazol (3.3 mL (0.45M solution), 1.5 mmol, 1.5 eq.) and formaldehyde (0.2 mL, 2.0 mmol, 2.0 eq.) to give the product (184.8 mg, 0.88 mmol) in 88 % yield as a white solid.

^{1}H NMR (300 MHz, DMSO-d_6): δ = 9.44 (s, 1H, H-6), 8.01 (t, J = 6.9 Hz, 1H, H-7), 5.92 (d, J = 6.9 Hz, 2H, H-5) ppm. **^{13}C-NMR** (75 MHz, DMSO-d_6): δ = 159.5 (C-2), 155.6 (C-3), 144.6 (C-4), 126.2 (C-6), 53.9 (C-5), 53.8 (C-1) ppm. **HRMS:** (ESI): $C_6H_7N_7O_3$ [M], 225.0610 Da. calcd m/z 248.0508 [M+Na]$^+$, found m/z 248.0510 [M+Na]$^+$.

1-Bromoethyl-acetate [X4]
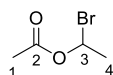
To a stirred solution of acetylbromide (0.85 mL, 11.35 mmol, 3.0 eq.) and cat. amount of zinc(II) chloride (5 mg) in dry DCM (2.5 mL) was added paraldehyde (0.51 mL, 3.78 mmol, 1 eq.) under inert atmosphere and the reaction stirred for 45 min at 0 °C. The reaction mixture was quenched with water and the organic phase was washed two times with water. After evaporation of methylene chloride the product was obtained as colourless oil (467.8 mg, 2.82 mmol) in 75 %.

^{1}H NMR (400 MHz, DMSO-d_6): δ = 6.67 (q, J = 5.9 Hz, 1H, H-3), 2.09 (s, 3H, H-1)), 1.97 (d, J = 5.9 Hz, 3H, H-4) ppm. **^{13}C-NMR** (101 MHz, DMSO-d_6): δ = 168.45 (C-2), 71.76 (C-3), 26.82 (C-1), 21.06 (C-4) ppm. **HRMS:** (ESI): $C_4H_7BrO_2$ [M], 165.9629 Da. calcd m/z 166.9708 [M+H]$^+$, found m/z 166.9688 [M+H]$^+$.

1-Acetoxyethyl 4-((1H-tetrazol-1-yl)methylamino)-1,2,5-oxadiazole-3-carboxylate [19]
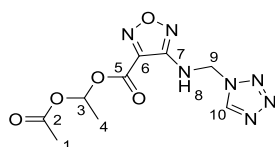
To a stirred solution of 4-((*1H*-tetrazol-1-yl)methylamino)-1,2,5-oxadiazole-3-carboxylic acid **16** (100 mg, 0.47 mmol, 1.0 eq.) and DIPEA (0.16 mL, 0.94 mmol, 2 eq.) in DMF (2 mL) was

added 1-bromoethyl-acetate **X4** (156 mg, 0.94 mmol, 2 eq.) and the reaction was stirred for 18 h at room temperature. The reaction mixture was evaporated in vacuum and purified by flash column chromatography to give the product (63.7 mg, 0.21 mmol) in 45 % yield as a brownish oil.

^{1}H NMR (500 MHz, DMSO-d_6): δ = 9.44 (s, 1H, H-10), 8.02 (t, J = 6.9 Hz, 1H, H-8), 7.04 (q, J = 5.5 Hz, 1H, H-3), 5.93 (d, J = 6.9 Hz, 2H, H-9), 2.09 (s, 3H, H-1), 1.57 (d, J = 5.5 Hz, 3H, H-4) ppm. **^{13}C-NMR** (126 MHz, DMSO-d_6): δ = 169.03 (C-5), 156.90 (C-2), 155.76 (C-7), 144.48 (C-6), 139.22 (C-10), 89.85 (C-3), 56.97 (C-9), 20.98 (C-4), 20.75 (C-1) ppm. **HRMS:** (ESI): $C_9H_{11}N_7O_5$ [M], 297.0822 Da. calcd m/z 320.0719 [M+Na]$^+$, 336.0459 [M+K]$^+$, found m/z 320.0730 [M+Na]$^+$, 336.0470 [M+K]$^+$.

4-((5-(3-(Benzyloxy)phenyl)-1H-tetrazol-1-yl)methylamino)-1,2,5-oxadiazole-3-carboxylic acid [20]
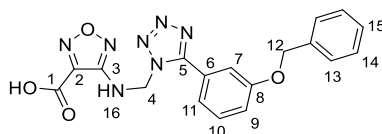
Prepared according to general procedure Method A using 4-amino-1,2,5-oxadiazole-3-carboxylic acid **3** (143 mg, 1.0 mmol, 1.0 eq.), 5-(3-benzyloxyphenyl)-*1H*-tetrazole (302 mg, 1.2 mmol, 1.2 eq.) and formaldehyde (0.1 mL, 2.0 mmol, 2 eq.) to give the product (204.24mg, 0.52 mmol) in 52 % yield as a white solid.

^{1}H NMR (300 MHz, CDCl$_3$): δ = 8.12 (t, J = 7.0 Hz, 1H, H-16), 7.67 – 7.62 (m, 2H, H-9, H-10), 7.49 (m, 1H, H-11), 7.48 (m, 2H, H-14), 7.40 (m, 2H, H-13), 7.34 (s, 1H, H-7), 7.19 (d, J = 8.4 Hz, 1H, H-15), 6.15 (d, J = 7.1 Hz, 2H, H-4), 5.20 (s, 2H, H-12) ppm. **^{13}C-NMR** (75 MHz, CDCl$_3$): δ = 164.47 (C-5), 160.06 (C-1), 159.27 (C-2), 155.78 (C-8), 137.27 (C-3), 131.06 (C-10), 128.93 (C-14), 128.58 (C-15), 128.35 (C-6), 128.23 (C-11), 128.15 (C-13),

119.41 (C-9), 117.83 (C-7), 69.82 (C-12), 58.60 (C-4) ppm. **HRMS:** (ESI): $C_{18}H_{15}N_7O_4$ [M], 393.1186 Da. calcd *m/z* 392.1107 [M-H]⁻, found 392.1025 [M-H]⁻.

Methyl 4-((5-phenyl-*1H*-tetrazol-1-yl)methylamino)-1,2,5-oxadiazole-3-carboxylate [21]
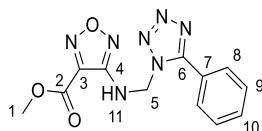
Prepared according to general procedure Method A using 4-amino-1,2,5-oxadiazole-3-carboxylic acid methylester **X1** (143 mg, 1.0 mmol, 1.0 eq.), 5-phenyl-*1H*-tetrazole (219 mg, 1.5 mmol, 1.5 eq.) and formaldehyde (0.2 mL, 2.0 mmol, 2 eq.) to give the product (183.7 mg, 0.61 mmol) in 61 % yield as a white solid.

¹H NMR (300 MHz, CDCl₃): δ = 8.13 (dd, *J* = 6.7, 2.9 Hz, 2H, H-9), 7.49 (m, 1H, H-10), 7.47 (d, *J* = 2.7 Hz, 2H, H-8), 6.69 (t, *J* = 7.5 Hz, 1H, H-11), 6.19 (d, *J* = 7.5 Hz, 2H, H-5), 4.03 (s, 3H, H-1) ppm. **¹³C-NMR** (75 MHz, CDCl₃): δ = 165.7 (C-6), 159.9 (C-2), 155.2 (C-3), 137.9 (C-4) 130.6 (C-10), 128.9 (C-9), 126.9 (C-8), 126.9 (C-7), 60.4 (C-1), 53.6 (C-5) ppm. **HRMS:** (ESI): $C_{12}H_{11}N_7O_3$ [M], 301.2660 Da. calcd *m/z* 324.2558 [M+Na]⁺, 340.3643 [M+K]⁺, found *m/z* 324.3816 [M+Na]⁺, 340.0548 [M+K]⁺.

Methyl   4-((5-(3-hydroxyphenyl)-*1H*-tetrazol-1-yl)methylamino)-1,2,5-oxadiazole-3-carboxylate [22]
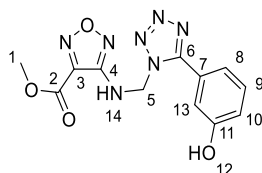
Prepared according to general procedure Method A using 4-amino-1,2,5-oxadiazole-3-carboxylic acid methylester **X1**   (72.6 mg, 0.5 mmol, 1.0 eq.), 3-(*1H*-tetrazol-5-yl)phenol (97.3 mg, 0.6 mmol, 1.2 eq.) and formaldehyde (0.1 mL, 1.0 mmol, 2.0 eq.) to give the product (236.2 mg, 0.64 mmol) in 64 % yield as a white solid.

¹H NMR (300 MHz, DMSO-d_6): δ = 9.82 (s, 1H, H-12), 8.18 (t, J = 6.9 Hz, 1H, H-14), 7.48 (m, 1H, H-10), 7.46 (s, 1H, H-13), 7.34 (t, J = 7.8 Hz, 1H, H-9), 6.91 (d, J = 8.1 Hz, 1H, H-8), 6.13 (d, J = 6.9 Hz, 2H, H-5), 3.94 (s, 3H, H-1). **¹³C-NMR** (75 MHz, DMSO-d_6): δ = 164.79 (C-6), 158.81 (C-2), 158.6 (C-11), 155.61 (C-3), 140.03 (C-4), 131.05 (C-7), 128.44 (C-9), 118.25 (C-8), 117.61 (C-13), 113.47 (C-10), 61.93 (C-1), 53.81 (C-5). **HRMS:** (ESI): $C_{12}H_{11}N_7O_4$ [M], 317.0873 Da. calcd m/z 340.0770 [M+Na]⁺, found m/z 340.0782 [M+Na]⁺

Methyl 4-((5-(3-(fluoroxy)phenyl)-1H-tetrazol-1-yl)methylamino)-1,2,5-oxadiazole-3-carboxylate [23]
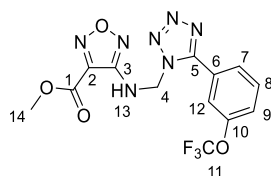
Prepared according to general procedure Method B using 4-amino-1,2,5-oxadiazole-3-carboxylic acid methylester (83.9 mg, 0.7 mmol, 1.3 eq.), 3-(1H-tetrazol-5-yl)phenyl hypofluorite (115.1 mg, 1.0 mmol, 1.0 eq.) and formaldehyde (0.1 mL, 2.0 mmol, 2.0 eq.) to give the product (252.4 mg, 0.82 mmol) in 68 % yield as a yellowish solid.

¹H NMR (300 MHz, CDCl₃): δ = 8.22 (t, J = 7.8 Hz, 1H, H-8), 8.08 (d, J = 7.8 Hz, 1H, H-7), 7.91 (s, 1H, H-12), 7.72 (t, J = 7.5 Hz, 1H, H-13), 7.56 (d, J = 7.8 Hz, 1H), 6.17 (d, J = 7.3 Hz, 2H, H-4), 3.94 (s, 3H, H-14) ppm. **¹³C-NMR** (75 MHz, DMSO-d_6): δ = ¹³C NMR (126 MHz, DMSO-D_6) δ 163.49 (C-5), 158.80 (C-1), 155.58 (C-2), 149.41 (C-10), 140.03 (C-3), 132.34 (C-8), 129.45 (C-6), 126.03 (C-7), 123.75 (C-9), 122.39 (C-11), 118.98 (C-12), 62.23 (C-4), 53.80 (C-14) ppm. **HRMS:** (ESI): $C_{13}H_{10}F_3N_7O_4$ [M], 385.2632 Da. calcd m/z 408.2530 [M+Na]⁺, 424.3615 [M+K]⁺, found m/z 408.0624 [M+Na]⁺, 424.0362 [M+K]⁺.

Methyl 4-((5-(3-hydroxyphenyl)-*1H*-tetrazol-1-yl)methylamino)-1,2,5-oxadiazole-3-carboxylate [24]
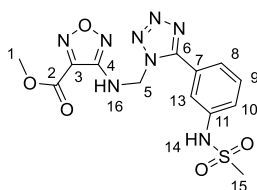
Prepared according to general procedure Method A using 4-amino-1,2,5-oxadiazole-3-carboxylic acid methylester **X1** (72.6 mg, 0.5 mmol, 1.0 eq.), 3-(*1H*-tetrazol-5-yl)phenol (97.3 mg, 0.6 mmol, 1.2 eq.) and formaldehyde (0.1 mL, 1.0 mmol, 2.0 eq.) to give the product (236.2 mg, 0.64 mmol) in 64 % yield as a white solid.

^{1}H NMR (300 MHz, CD$_3$CN): δ = 7.98 (s, 1H, H-13), 7.89 (d, J = 7.6 Hz, 1, H-8), 7.70 (s, 1H, H-14), 7.51 (t, J = 7.9 Hz, 1H, H-9), 7.38 (d, J = 7.7 Hz, 1H, H-10), 7.09 (t, J = 7.3 Hz, 1H, H-16), 6.14 (d, J = 7.3 Hz, 2H, H-5), 3.98 (s, 3H, H-1), 2.97 (s, 3H, H-15) ppm. **^{13}C-NMR** (75 MHz, CD$_3$CN): δ = 165.48 (C-6), 160.10 (C-2), 156.44 (C-3), 140.38 (C-11), 139.80 (C-4), 131.41 (C-9), 129.58 (C-7), 123.76 (C-10), 123.18 (C-8), 119.10 (C-13), 61.98 (C-7), 54.13 (C-8), 39.78 (C-15) ppm. **HRMS:** (ESI): C$_{13}$H$_{14}$N$_8$O$_5$S [M], 394.0808 Da. calcd *m/z* 417.0706 [M+Na]$^+$, found *m/z* 417.0676 [M+Na]$^+$.

1*H*-Tetrazol [25]

Commercial available at Sigma-Aldrich (#88185), lyophilization of 0.45 M solution give 1*H*-tetrazol as white solid.

5-Benzyl-1*H*-tetrazole [26]
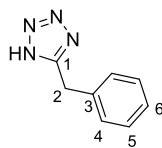
Prepared according to general procedure Method C using phenylacetonitrile (1.15 mL, 10.0 mmol, 1.0 eq.), NaN_3 (1.3 g, 20.0 mmol, 2.0 eq.), and NH_4Cl (535 mg, 10.0 mmol, 1.0 eq.) to give the product **26** (1039.7 mg, 0.64 mmol) in 65 % yield as an off white solid.

^{1}H NMR (500 MHz, DMSO-d_6): δ = 7.39 - 7.29 (m, 2H, H-5), 7.33 - 7.27 (m, 2H, H-4), 7.26 - 7.22 (m, 1H, H6), 4.29 (s, 2H, H-2). ppm. **^{13}C-NMR** (126 MHz, DMSO-d_6): δ = 145.09 (C-1), 138.20 (C-3), 129.28 (C-5), 129.21 (C-4), 127.57 (C-6), 33.87 (C-2) ppm. **HRMS:** (ESI): $C_8H_8N_4$ [M], 160.0749 Da. calcd *m/z* 183.0647 [M+Na]$^+$, found *m/z* 183.0651 [M+Na]$^+$.

5-CF -K(biotin)GpcFLSLPPW-NH$_2$ [27] (synthesized by Dr. Stefan Wagner)

The dual labelled peptide was synthesized according to previously published work. The photoactive building blocks sodium-(*N*-fluorenyl-9-methyloxycarbonyl-4-(*O*-benzyl-sodiumphosphonocarbonyl))-phenylalanine and was furnished after multistep. For evaluations of affinity experiments utilizing avidin-biotin analysis *N*-Fluorenyl-9-methoxycarbonyl-N^6-(biotin)-lysine was synthesized. Coupling of *N*-Fmoc-protected amino acids and consequent basic deprotection that followed the photoactive building block were performed under modified protocols described in literature.[153] Acylation with 5,6-carboxyfluorescein, NH-$_4$HCO$_3$ buffered HPLC purification and ion-exchange towards the sodium salt furnished peptide **27** in 12 % yield.

HRMS (ESI-TOF, [m/z]): calculated: [M+H$^+$] $^+$: 1733.6757; found [M+H$^+$]$^+$:1733.69

Appendix
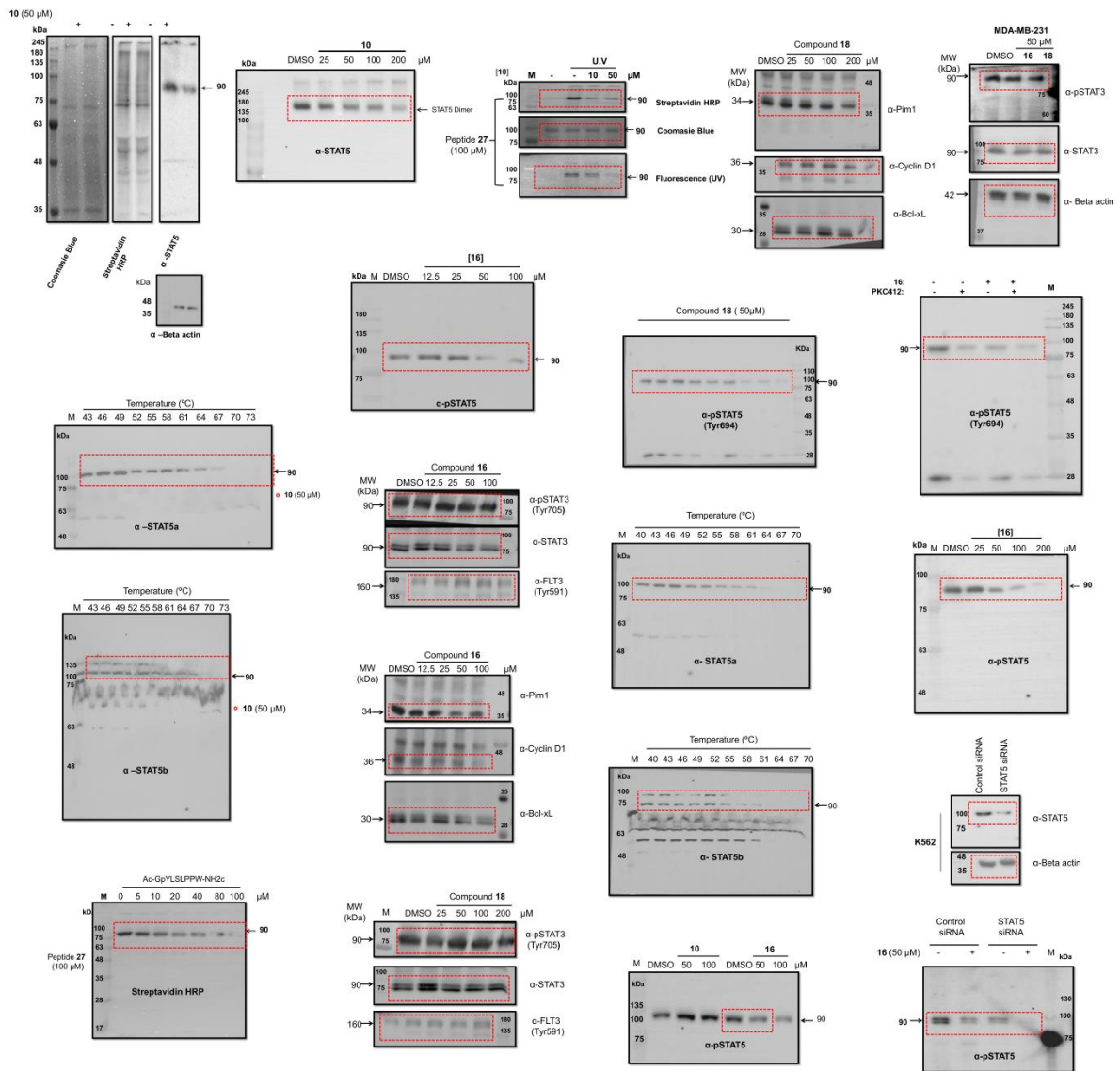
Appendix Figure 1: Uncropped pictures of western blots from the corresponding cropped western blots shown in the result section. Molecular weight markers are indicated.
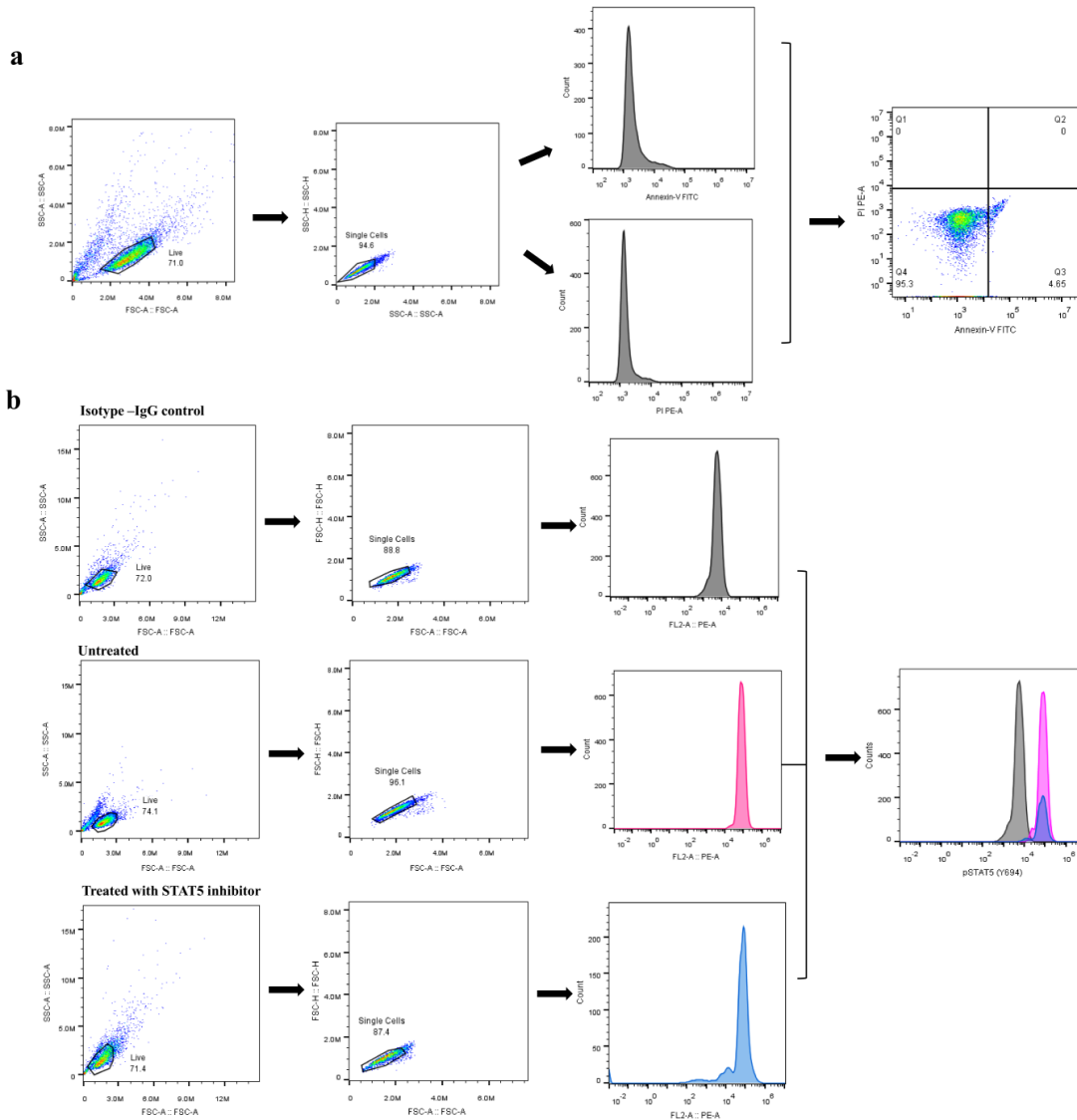
Appendix Figure 2: Gating strategies used for flow cytometry stainings**.** a, Gating strategy used for flow cytometry staining to determine apoptosis using fluorescein isothiocyanate (FITC)-conjugated annexin-V and dual stainied with phycoerythrin (PE)-conjugated propidium iodide to exclude necrotic cells. Debris were excluded using a forward scatter area (FSC-A) versus side scatter area (SSC-A) gate. Single cells (singlets) were then selected on a FSC-A versus FSC-W plot to exclude signaling data from doublets. b, Phospho-flow cytometry gating strategy used for the analysis of STAT5 phosphorylation using PE Mouse Anti-Stat5 (pY694) and PE conjugated rat anti-mouse IgG monoclonal antibody as isotype control.
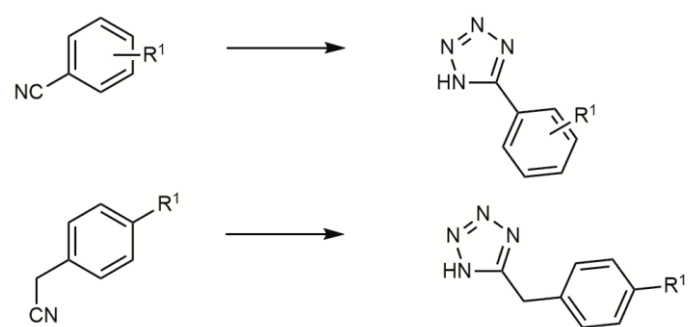
Appendix Figure 3: Reaction scheme for the synthesis of tetrazole derivatives.
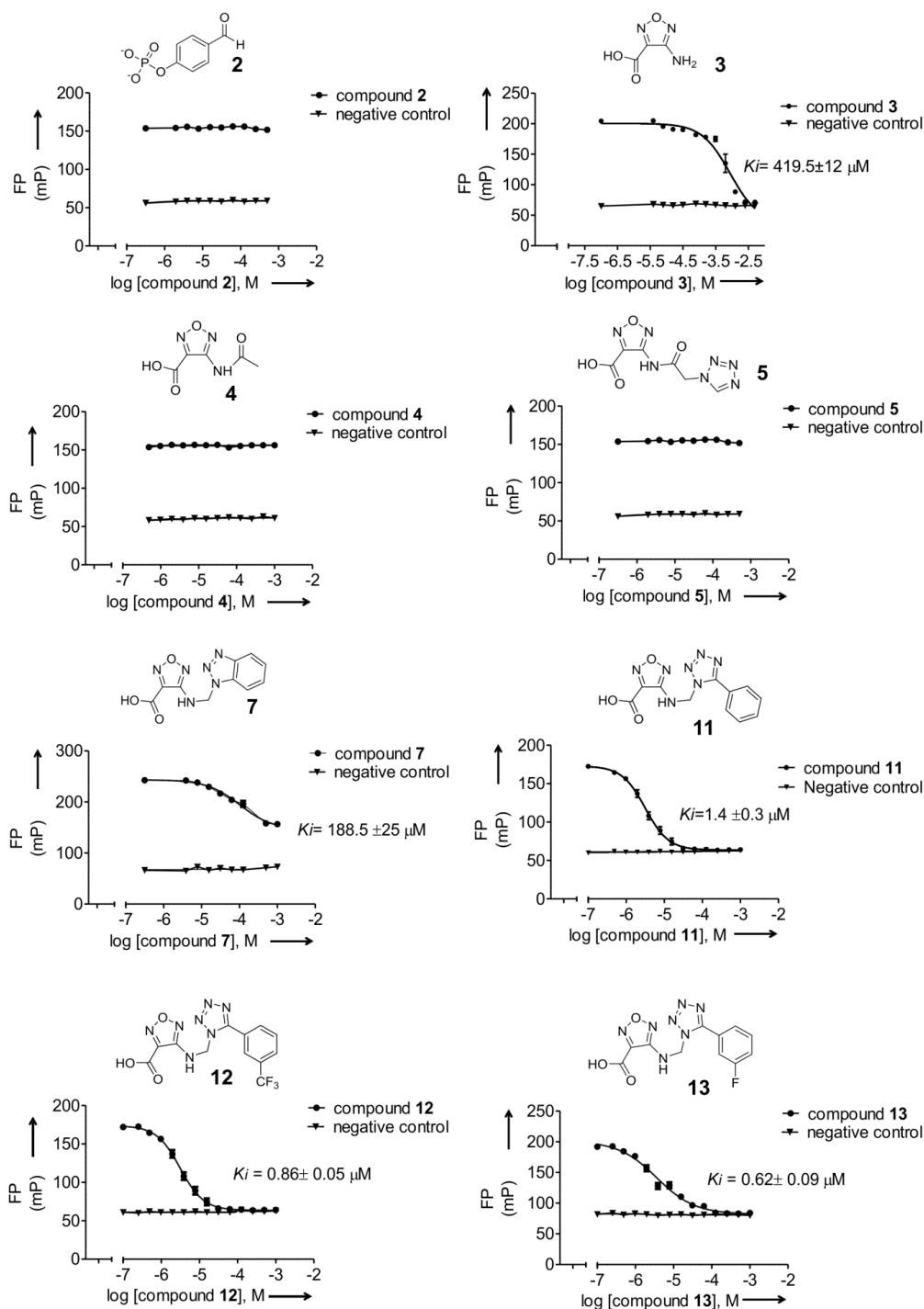
Appendix Figure 4: Fluorescence polarization binding assays of STAT5 inhibitors. Dose-response fluorescence polarization (FP) curves for the competitive binding of compounds **2**-**13** refer to Appendix Table 2 to recombinant STAT5-SH2 domain (*n*=3). Error bars denote mean ± SEM.
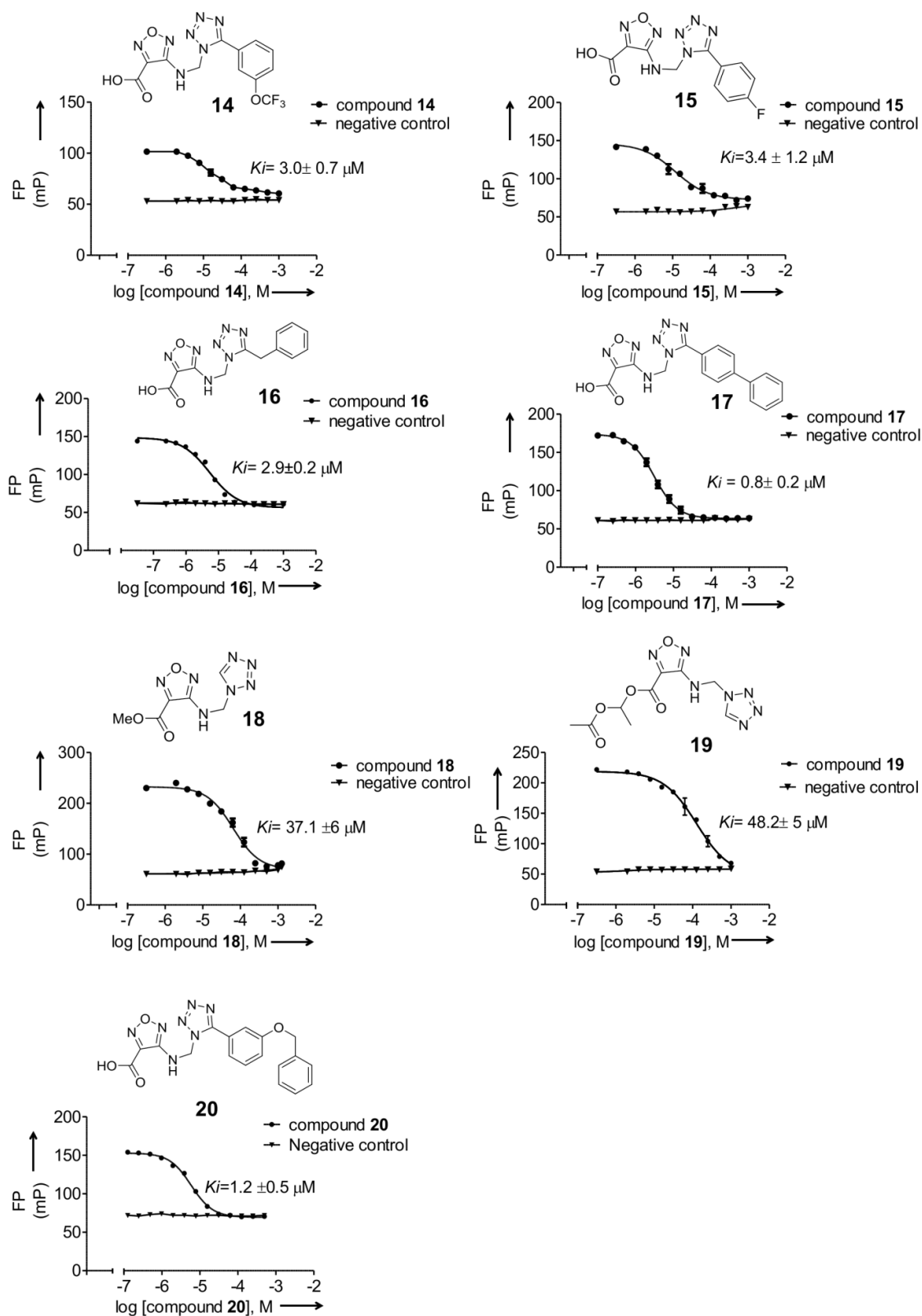
Appendix Figure 5: Dose-response fluorescence polarization (FP) curves for the competitive binding of compounds **14**-**20** refer to Appendix Table 2 to recombinant STAT5-SH2 domain (n=3). Error bars denote mean ± SEM.
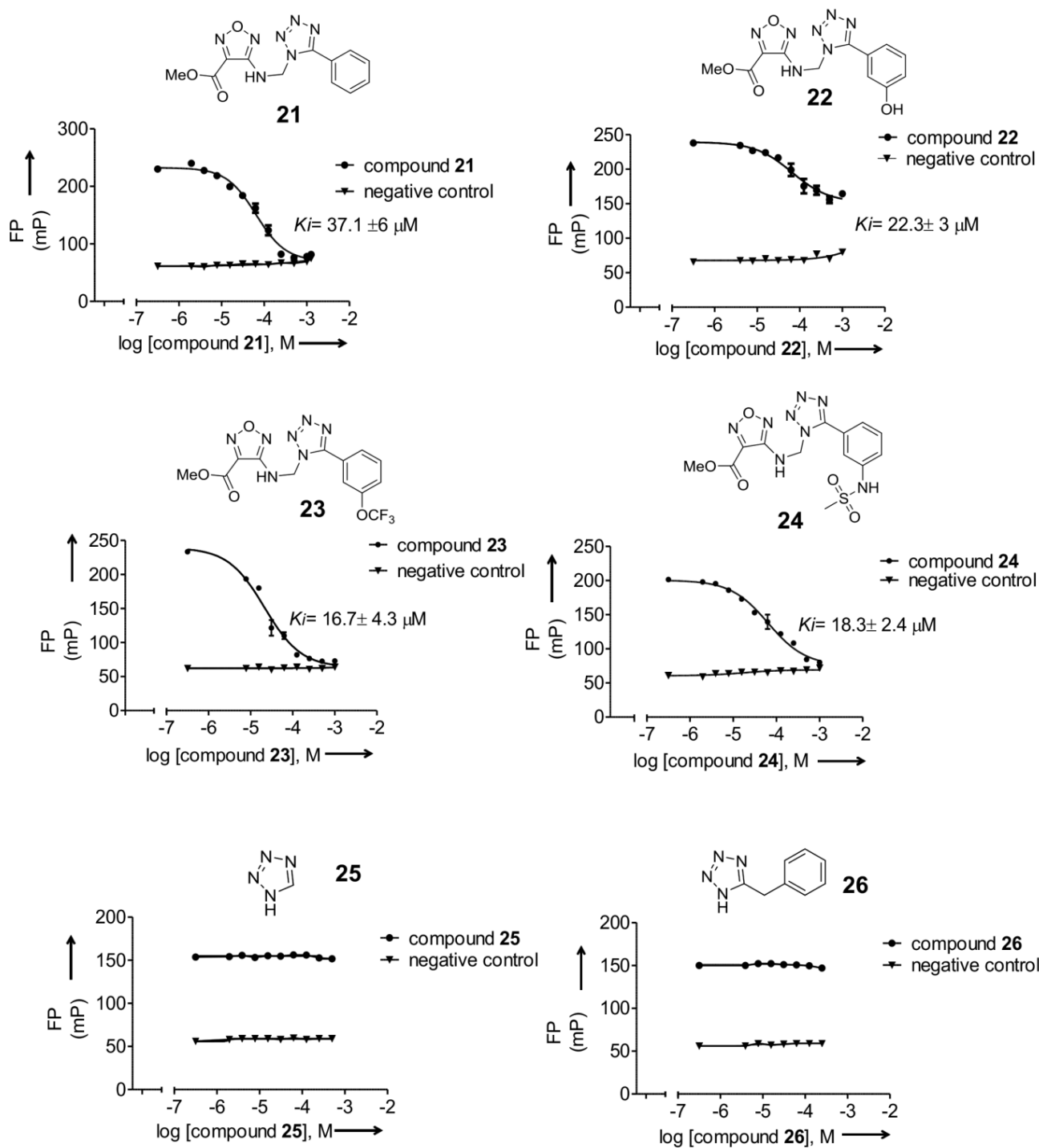
Appendix Figure 6: Dose-response fluorescence polarization (FP) curves for the competitive binding of compounds **21**-**26** refer to (Appendix table 3) to recombinant STAT5-SH2 domain (*n*=3). Error bars denote mean ± SEM.
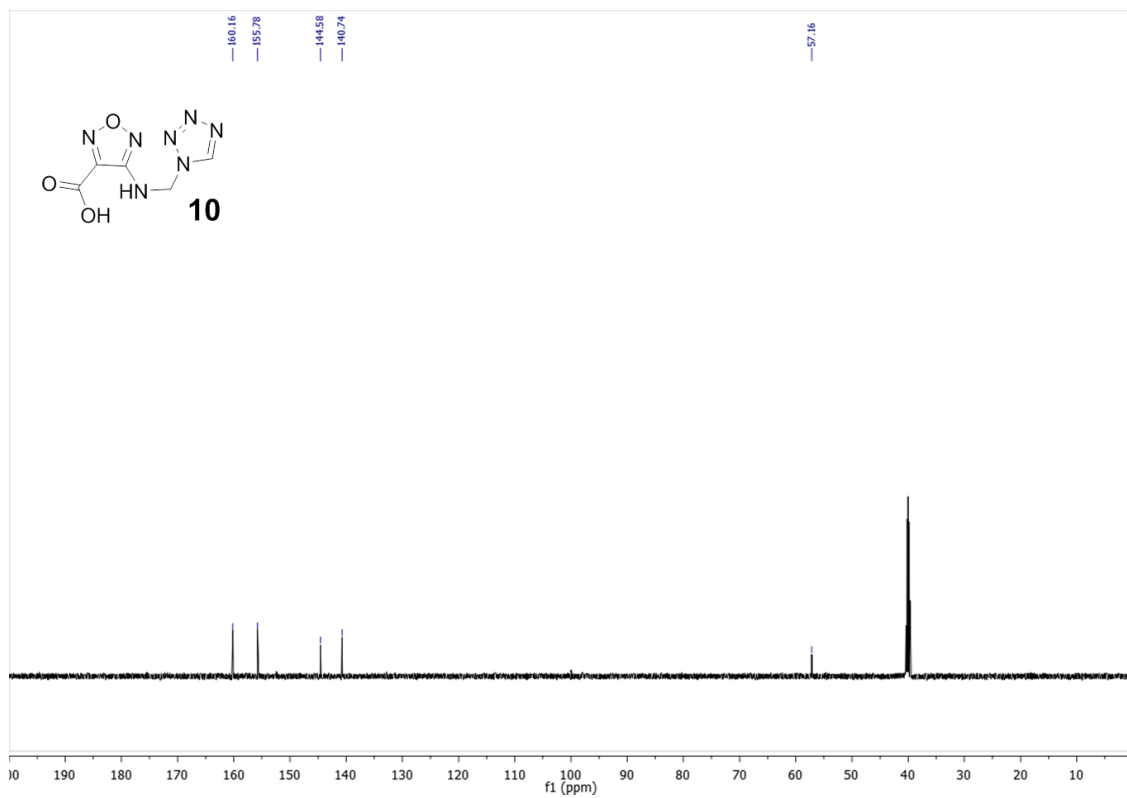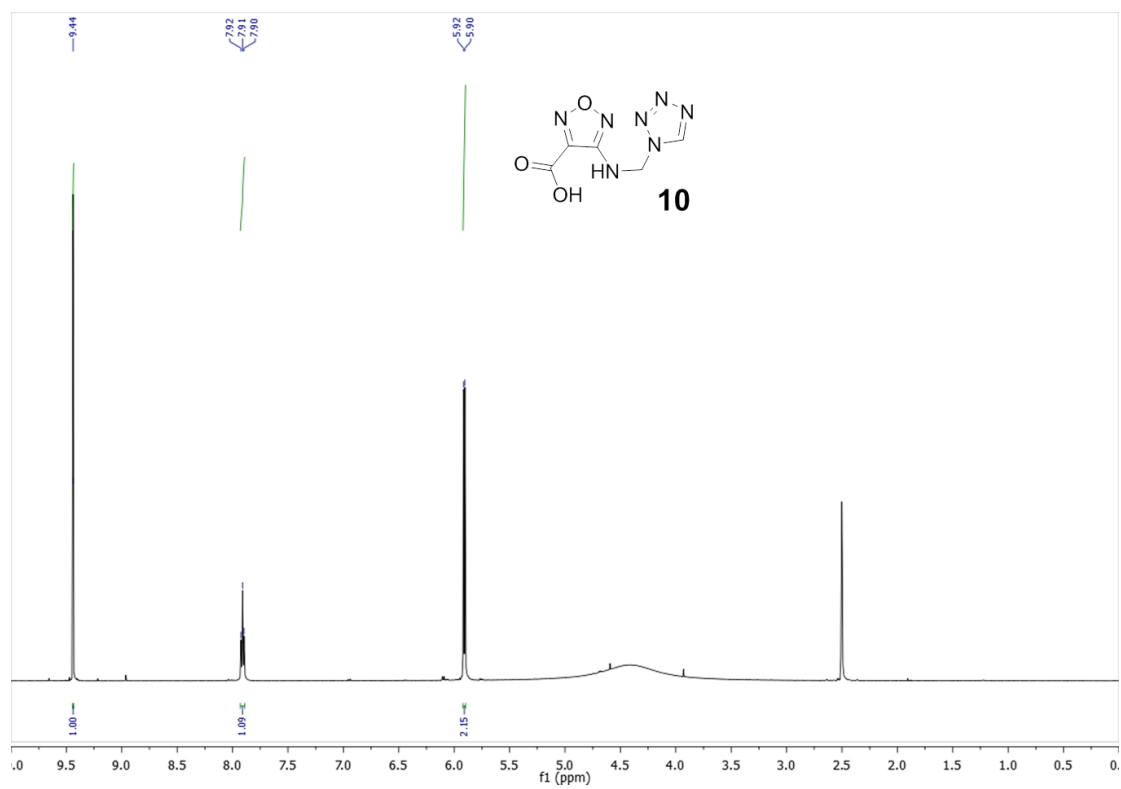
Appendix Figure 7: ^{1}H- and ^{13}C-NMR spectrum of **10**
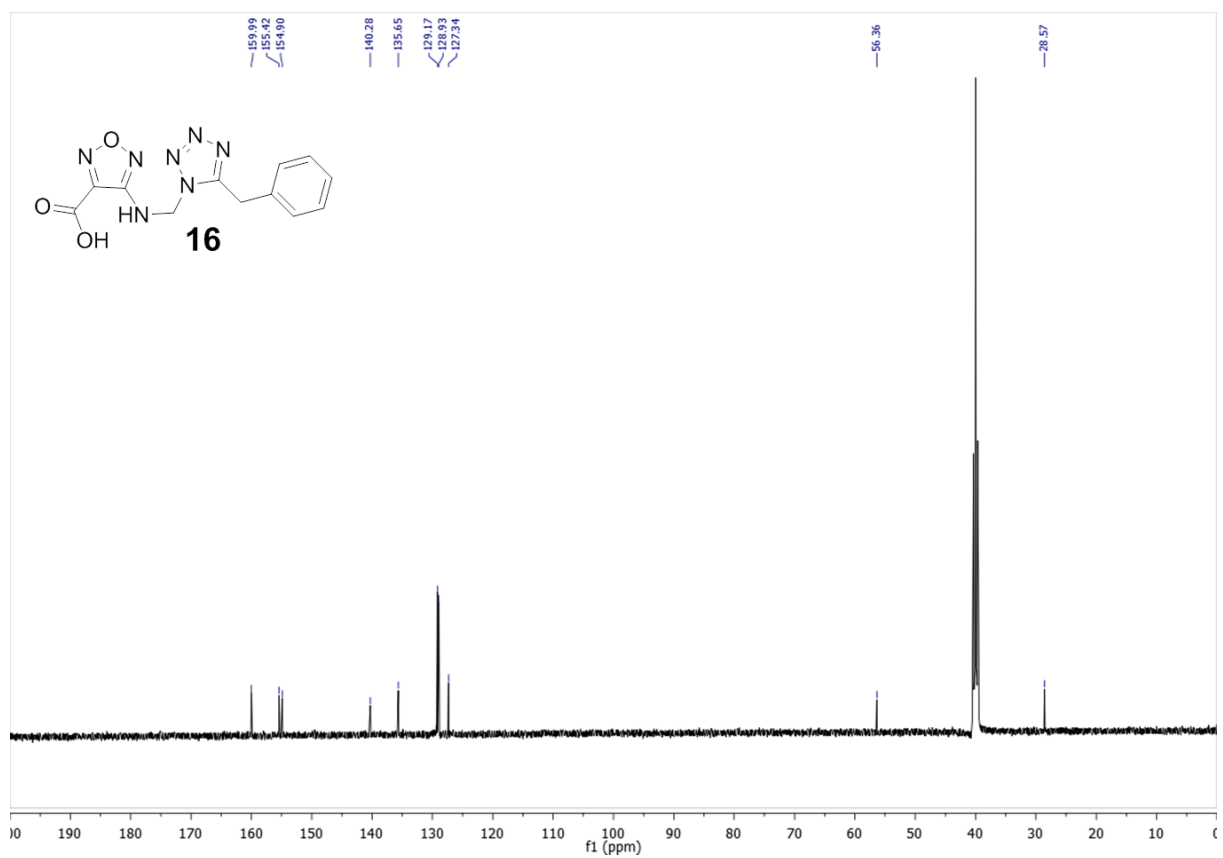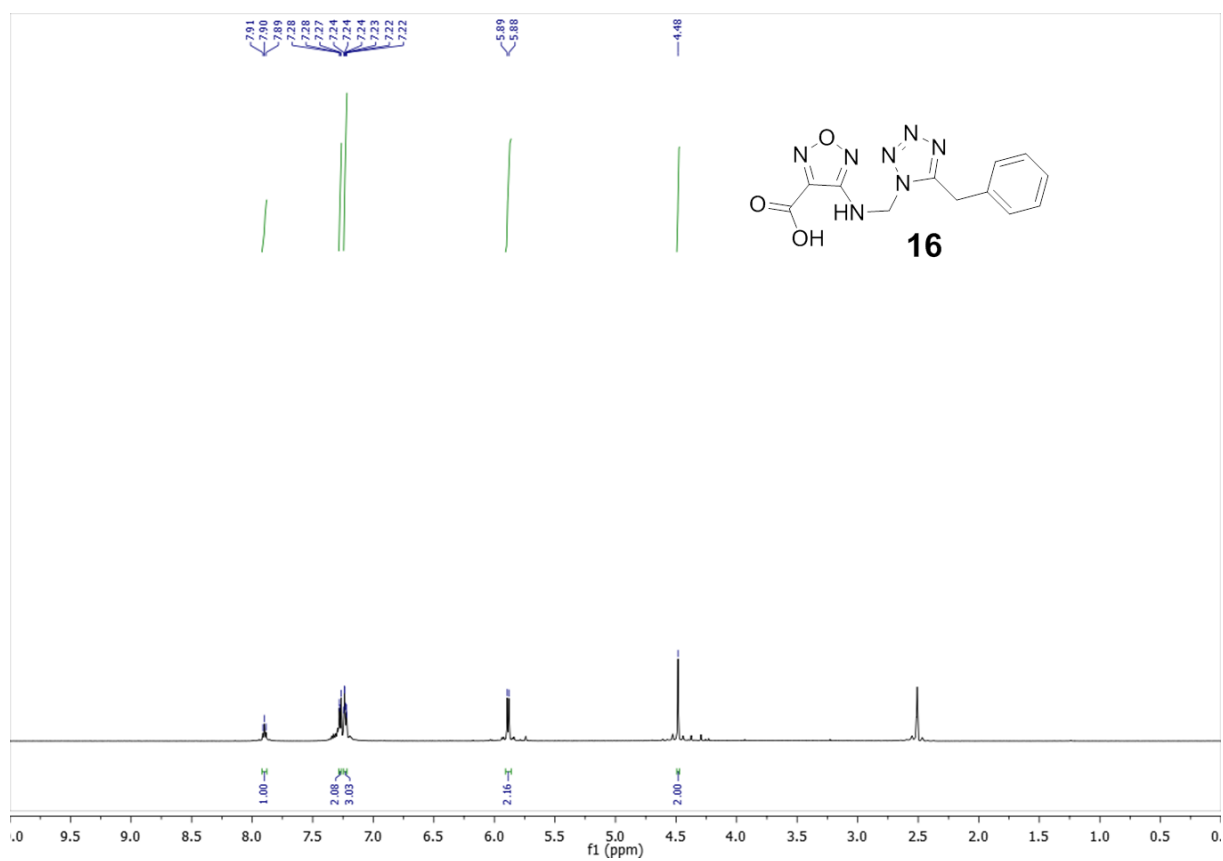
Appendix Figure 8: ^{1}H- and ^{13}C-NMR spectrum of **16**
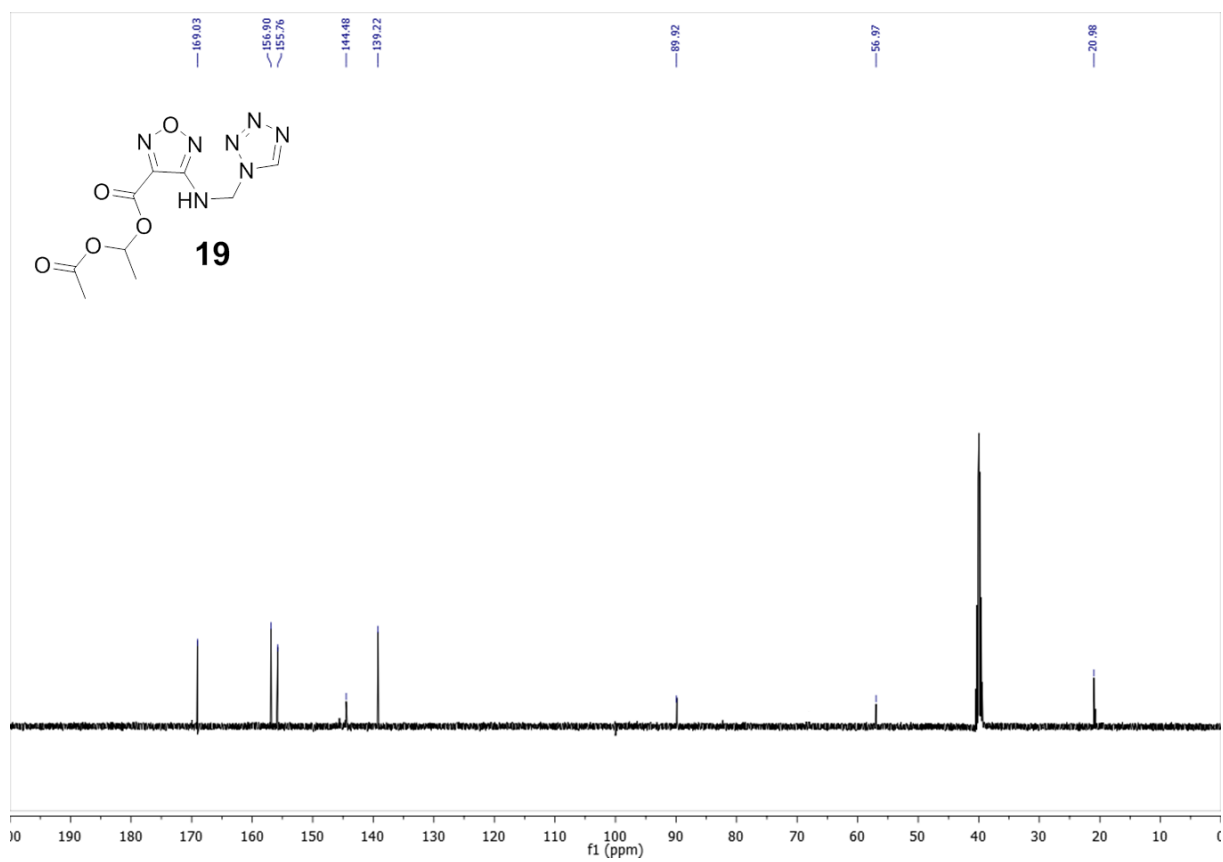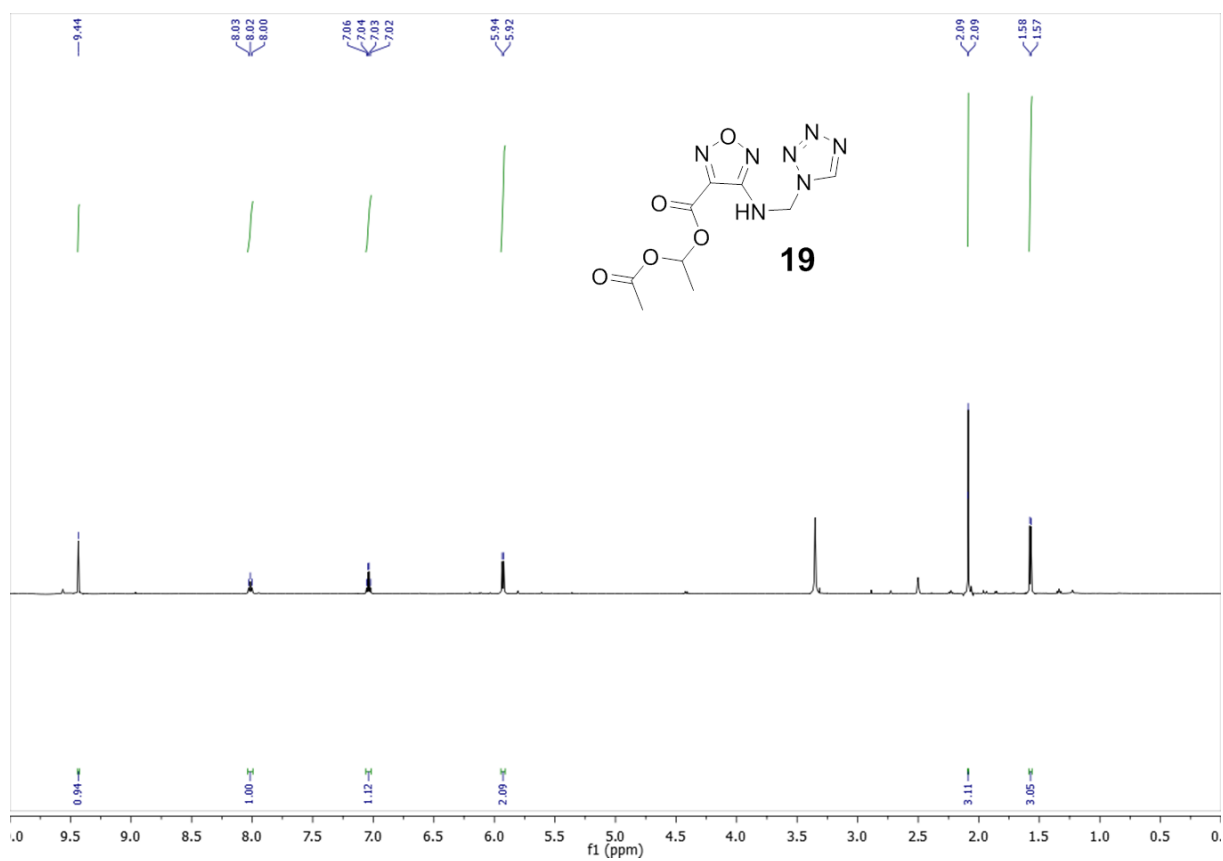
Appendix Figure 9: ^{1}H- and ^{13}C-NMR spectrum of **19**
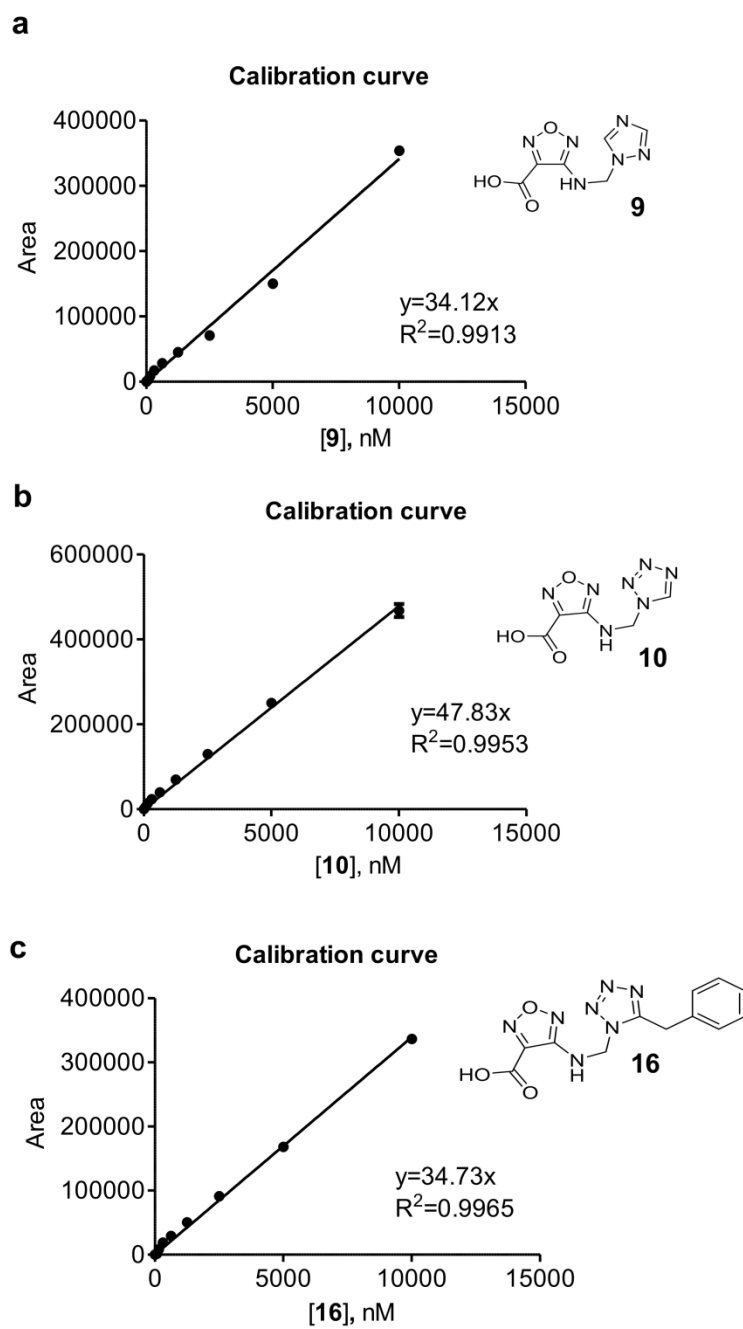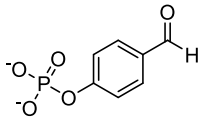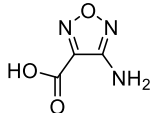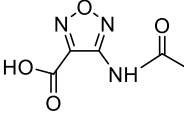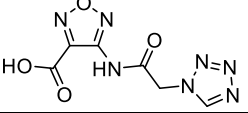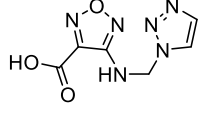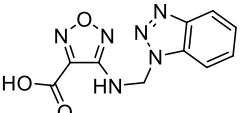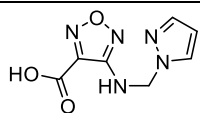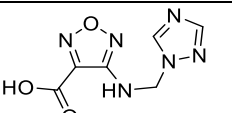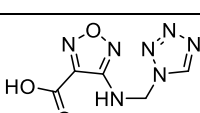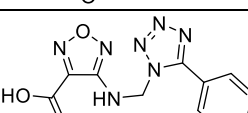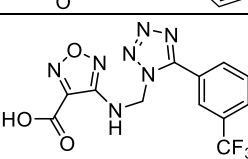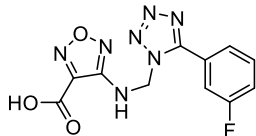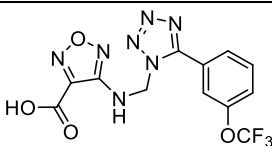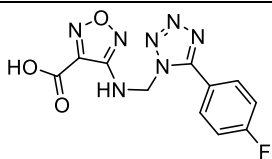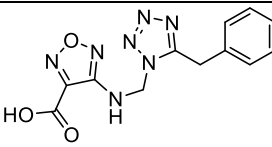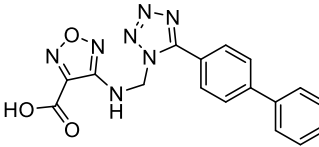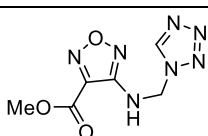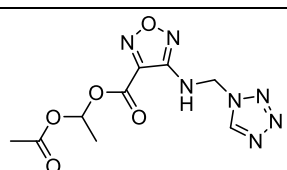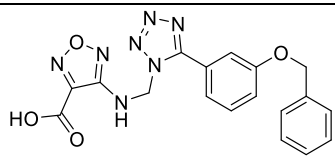
Appendix Figure 10: (a-c) Standard calibration curves of 6 different concentrations of compound **9**, **10** and **16** (*n*=3). Error bars denote mean $\pm$ SEM.

Appendix Table 1: List of primers used in this study.
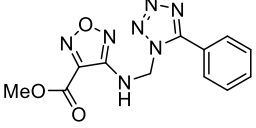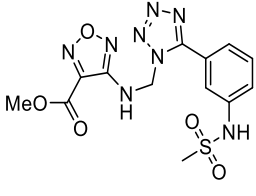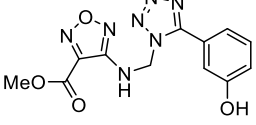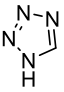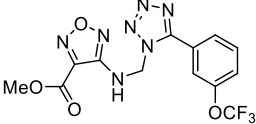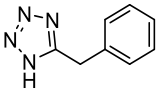
Genes	Forward Primer	Reverse Primer
Pim-1(m)	TCTTCTGGCAGGTGCTG	GGTAGCGAATCCACTCTG
Bcl-xL(m)	ATGGCAGCAGTGAAGCAAGC	ACGATGCGACCCCAGTTTACTC
Cis(m)	CTGGACTCTAACTGCTTGTC	TAGGCAGCACCGAGTCAC
S9(m)	GGGATGTTCACCACCTG	GCAAGATGAAGCTGGATTAC

Appendix Table 2: STAT5 inhibitors and their respective K_I values and ligand efficiencies

Cpd #	Structure	K_I (μM)	LE (kJ M^{-1} NA^{-1})	Cpd #	Structure	K_I (μM)	LE (kJ M^{-1} NA^{-1})
1	5-CF-GY*LSLPPW-NH$_2$	0.055±0.006	0.42	13		0.6±0.09	1.38
2		>2500	n.a.	14		3.0±0.7	1.21
3		419.5±12	2.14	15		3.4±1.2	1.42
4		>2500	n.a.	16		2.9±0.2	1.44
5		> 2500	n.a.	17		0.8±0.2	1.30
6		190.6±24	1.41	18		37.4±1.2	1.58
7		188.5±25	1.12	19		4.6±1.7	1.45
8		121.5±25	1.49	20		1.2±0.5	1.16
9		47.5±8.5	1.64				
10		1.4±0.5	2.23				
11		1.4±0.3	1.59				
12		0.9±0.05	1.38				

Appendix Table 3: Ester derivatives (**21**-**24**) of STAT5 inhibitors**.**

Cpd #	Structure	K_I (µM)	LE (kJ M^{-1} NA^{-1})	Cpd #	Structure	K_I (µM)	LE (kJ M^{-1} NA^{-1})
21		37.1±6	1.15	24		18.3±2.4	1.00
22		22.3±3	1.21	25		>2500	n.a.
23		16.7± 4.3	1.01	26		>2500	n.a.

Conversion of *IC$_{50}$* values into *K$_I$* values was carried out as described and ligand efficiency was calculated using the equation derived.[1]

n.a. = not applicable, NA = number of non-hydrogen

Accession	Description						
sp|Q9JKR6|H sp|Q9JKR6|H 10;5;1	>sp|Q9JKR6|HYOU1_MOUSE Hypoxia up-regulated protein 1 OS=Mus musculus GN=Hyou1 PE=1 SV=1;>tr|F6TRP3|F6TRP3_MOUSE Hypoxia up-regulated protein 1 (Fragment) OS=Mus musculus GN=Hyou1 PE=4 SV=1	8	4	8	4	0.13506	0.17838
sp|Q9EPL8|II sp|Q9EPL8|II 5	>sp|Q9EPL8|IPO7_MOUSE Importin-7 OS=Mus musculus GN=Ipo7 PE=1 SV=2	5	4	5	4	0.13353	0.10069
tr|H3BK84|H tr|H3BK84|H 5;5;2,2	>tr|H3BK84|H3BK84_MOUSE cAMP-dependent protein kinase type II-beta regulatory subunit OS=Mus musculus GN=Prkar2b PE=4 SV=1;>sp|P31324|KAP3_MOUSE cAMP-dependent protein kinase type II-beta regulatory subunit	4	4	4	4	0.12937	1.6952
sp|Q9CZ13|C sp|Q9CZ13|C 7	>sp|Q9CZ13|QCR1_MOUSE Cytochrome b-c1 complex subunit 1, mitochondrial OS=Mus musculus GN=Uqcrc1 PE=1 SV=2	3	6	3	6	0.12748	0.76809
sp|Q9CW03| sp|Q9CW03| 15	>sp|Q9CW03|SMC3_MOUSE Structural maintenance of chromosomes protein 3 OS=Mus musculus GN=Smc3 PE=1 SV=2	14	5	14	5	0.12647	0.12125
sp|P62814|V sp|P62814|V 12;4	>sp|P62814|VATB2_MOUSE V-type proton ATPase subunit B, brain isoform OS=Mus musculus GN=Atp6v1b2 PE=1 SV=1	10	7	10	7	0.1248	5.0067
tr|A2A6U5|A tr|A2A6U5|A 10;10;10;10;1	>tr|A2A6U5|A2A6U5_MOUSE Septin-9 (Fragment) OS=Mus musculus GN=Sept9 PE=4 SV=1;>sp|Q80UG5-2|SEPT9_MOUSE Isoform 2 of Septin-9 OS=Mus musculus GN=Sept9;>tr|A2A6U3|A2A6U3_MOUSE Septin-9 OS=Mus musc	8	9	8	9	0.12372	1.0277
sp|P35486|C sp|P35486|C 7	>sp|P35486|ODPA_MOUSE Pyruvate dehydrogenase E1 component subunit alpha, somatic form, mitochondrial OS=Mus musculus GN=Pdha1 PE=1 SV=1	5	4	5	4	0.12327	2.0154
sp|Q62376|R sp|Q62376|R 5;4	>sp|Q62376|RU17_MOUSE U1 small nuclear ribonucleoprotein 70 kDa OS=Mus musculus GN=Snrnp70 PE=1 SV=2;>sp|Q62376-2|RU17_MOUSE Isoform 2 of U1 small nuclear ribonucleoprotein 70 kDa OS=Mus musculus GN=Snrr	4	3	4	3	0.12238	0.092291
sp|Q7TPR4|A sp|Q7TPR4|A 29;27;4;2	>sp|Q7TPR4|ACTN1_MOUSE Alpha-actinin-1 OS=Mus musculus GN=Actn1 PE=1 SV=1;>tr|A1BN54|A1BN54_MOUSE Alpha actinin 1a OS=Mus musculus GN=Actn1 PE=2 SV=1	25	13	16	8	0.12111	1.152
sp|P62962|P sp|P62962|P 3;1	>sp|P62962|PROF1_MOUSE Profilin-1 OS=Mus musculus GN=Pfn1 PE=1 SV=2	2	3	2	3	0.12048	0.20023
sp|P16125|Li sp|P16125|Li 3;2	>sp|P16125|LDHB_MOUSE L-lactate dehydrogenase B chain OS=Mus musculus GN=Ldhb PE=1 SV=2;>tr|D3Z7F0|D3Z7F0_MOUSE L-lactate dehydrogenase (Fragment) OS=Mus musculus GN=Ldhb PE=3 SV=1	3	1	3	1	0.12007	0.21873
sp|Q8R5C5|/ sp|Q8R5C5|/ 3;2;2	>sp|Q8R5C5|ACTY_MOUSE Beta-centractin OS=Mus musculus GN=Actr1b PE=1 SV=1	3	2	3	2	0.11815	2.9554
sp|Q9EP69|S sp|Q9EP69|S 12	>sp|Q9EP69|SAC1_MOUSE Phosphatidylinositide phosphatase SAC1 OS=Mus musculus GN=Sacm1l PE=2 SV=1	12	7	12	7	0.11795	1.3438
tr|G3UZI2|G tr|G3UZI2|G 13;13;13;13;1	>tr|G3UZI2|G3UZI2_MOUSE Heterogeneous nuclear ribonucleoprotein Q OS=Mus musculus GN=Syncrip PE=4 SV=1;>sp|Q7TMK9-2|HNRPQ_MOUSE Isoform 2 of Heterogeneous nuclear ribonucleoprotein Q OS=Mus musculus GI	13	7	12	6	0.11777	0.10312
sp|Q8BTS4|N sp|Q8BTS4|N 6	>sp|Q8BTS4|NUP54_MOUSE Nuclear pore complex protein Nup54 OS=Mus musculus GN=Nup54 PE=1 SV=1	6	3	6	3	0.11662	1.656
sp|P35585|A sp|P35585|A 13;5;4;4;4	>sp|P35585|AP1M1_MOUSE AP-1 complex subunit mu-1 OS=Mus musculus GN=Ap1m1 PE=1 SV=3	10	6	10	6	0.1165	3.8158
sp|Q99LI7|C! sp|Q99LI7|C! 4	>sp|Q99LI7|CSTF3_MOUSE Cleavage stimulation factor subunit 3 OS=Mus musculus GN=Cstf3 PE=1 SV=1	4	2	4	2	0.1155	0.22749
sp|P61164|A sp|P61164|A 9	>sp|P61164|ACTZ_MOUSE Alpha-centractin OS=Mus musculus GN=Actr1a PE=2 SV=1	7	6	4	4	0.11541	3.7717
sp|P23116|E sp|P23116|E 22	>sp|P23116|EIF3A_MOUSE Eukaryotic translation initiation factor 3 subunit A OS=Mus musculus GN=Eif3a PE=1 SV=5	19	12	19	12	0.11527	0.18847
sp|Q8BH59|(sp|Q8BH59|(12;3	>sp|Q8BH59|CMC1_MOUSE Calcium-binding mitochondrial carrier protein Aralar1 OS=Mus musculus GN=Slc25a12 PE=1 SV=1	8	8	5	8	0.11498	0.86275
sp|Q9D0F9|F sp|Q9D0F9|F 17;14	>sp|Q9D0F9|PGM1_MOUSE Phosphoglucomutase-1 OS=Mus musculus GN=Pgm1 PE=1 SV=4;>tr|A2CEK3|A2CEK3_MOUSE Phosphoglucomutase-2 OS=Mus musculus GN=Pgm2 PE=1 SV=1	11	11	11	11	0.11417	0.12104
tr|H3BKM0|I tr|H3BKM0|I 18;18;18;18;3	>tr|H3BKM0|H3BKM0_MOUSE AP-2 complex subunit beta OS=Mus musculus GN=Ap2b1 PE=4 SV=1;>sp|Q9DBG3|AP2B1_MOUSE AP-2 complex subunit beta OS=Mus musculus GN=Ap2b1 PE=1 SV=1;>tr|H3BIY9|H3BIY9_MOUSE	17	4	7	0	0.114	3.2447
sp|P16546-2 sp|P16546-2 45;45;45;45;4	>sp|P16546-2|SPTN1_MOUSE Isoform 2 of Spectrin alpha chain, non-erythrocytic 1 OS=Mus musculus GN=Sptan1;>tr|A3KGU5|A3KGU5_MOUSE Spectrin alpha chain, non-erythrocytic 1 OS=Mus musculus GN=Sptan1 PE=1 SV=1;	33	25	33	25	0.1138	0.12378
sp|P26638|S' sp|P26638|S' 11;11;9;5	>sp|P26638|SYSC_MOUSE Serine--tRNA ligase, cytoplasmic OS=Mus musculus GN=Sars PE=2 SV=3;>tr|Q8C483|Q8C483_MOUSE Serine--tRNA ligase, cytoplasmic OS=Mus musculus GN=Sars PE=2 SV=1;>tr|A2AFS0|A2AFS0_MOU	9	9	9	9	0.11341	5.0646
tr|G3XA10|G tr|G3XA10|G 14;14	>tr|G3XA10|G3XA10_MOUSE Heterogeneous nuclear ribonucleoprotein U, isoform CRA_b OS=Mus musculus GN=Hnrnpu PE=1 SV=1;>sp|Q8VEK3|HNRPU_MOUSE Heterogeneous nuclear ribonucleoprotein U OS=Mus musculus (	14	8	14	8	0.11327	0.25363
tr|S4R1W1|S tr|S4R1W1|S 7;7;6;6;4;2;1;	>tr|S4R1W1|S4R1W1_MOUSE Glyceraldehyde-3-phosphate dehydrogenase OS=Mus musculus GN=Gm3839 PE=3 SV=1;>sp|P16858|G3P_MOUSE Glyceraldehyde-3-phosphate dehydrogenase OS=Mus musculus GN=Gapdh PE=1 S	5	6	1	2	0.11266	2.5866
sp|P06240|Li sp|P06240|Li 11;11;1;1;1;1;	>sp|P06240|LCK_MOUSE Proto-oncogene tyrosine-protein kinase LCK OS=Mus musculus GN=Lck PE=1 SV=4;>tr|E9Q696|E9Q696_MOUSE Proto-oncogene tyrosine-protein kinase LCK OS=Mus musculus GN=Lck PE=4 SV=1	10	6	10	6	0.11207	2.2918
sp|Q92SI1|A sp|Q92SI1|A 10;8;4;3;3	>sp|Q92SI1|ATAD3_MOUSE ATPase family AAA domain-containing protein 3 OS=Mus musculus GN=Atad3 PE=1 SV=1;>sp|Q92SI1-2|ATAD3_MOUSE Isoform 2 of ATPase family AAA domain-containing protein 3 OS=Mus muscu	7	6	7	6	0.11179	0.09032
sp|Q9EPU0-2 sp|Q9EPU0-2 18;18	>sp|Q9EPU0-2|RENT1_MOUSE Isoform 2 of Regulator of nonsense transcripts 1 OS=Mus musculus GN=Upf1;>sp|Q9EPU0|RENT1_MOUSE Regulator of nonsense transcripts 1 OS=Mus musculus GN=Upf1 PE=1 SV=2	18	4	18	4	0.11157	0.17819
sp|Q9JHU4|C sp|Q9JHU4|C 70;4	>sp|Q9JHU4|DYHC1_MOUSE Cytoplasmic dynein 1 heavy chain 1 OS=Mus musculus GN=Dync1h1 PE=1 SV=2	68	5	68	5	0.11014	0.23873
sp|Q9D7N9| sp|Q9D7N9| 5	>sp|Q9D7N9|APMAP_MOUSE Adipocyte plasma membrane-associated protein OS=Mus musculus GN=Apmap PE=1 SV=1	4	4	4	4	0.10987	2.7483
sp|Q61768|K sp|Q61768|K 15;10;6;4	>sp|Q61768|KINH_MOUSE Kinesin-1 heavy chain OS=Mus musculus GN=Kif5b PE=1 SV=3;>tr|E9QAK5|E9QAK5_MOUSE Kinesin-1 heavy chain (Fragment) OS=Mus musculus GN=Kif5b PE=3 SV=1	15	3	15	3	0.10902	0.50531
tr|G5E8R3|G tr|G5E8R3|G 4;4;4	>tr|G5E8R3|G5E8R3_MOUSE Pyruvate carboxylase OS=Mus musculus GN=Pcx PE=1 SV=1;>sp|Q05920|PYC_MOUSE Pyruvate carboxylase, mitochondrial OS=Mus musculus GN=Pc PE=1 SV=1;>tr|E9QPD7|E9QPD7_MOUSE Pyruva	3	1	3	1	0.1078	0.1489
sp|O55029|C sp|O55029|C 17	>sp|O55029|COPB2_MOUSE Coatomer subunit beta OS=Mus musculus GN=Copb2 PE=2 SV=2	17	3	17	3	0.10691	0.918
tr|E9PXV7|E! tr|E9PXV7|E! 9;9;8;8;8	>tr|E9PXV7|E9PXV7_MOUSE Protein diaphanous homolog 1 OS=Mus musculus GN=Diap1 PE=1 SV=1;>sp|O08808|DIAP1_MOUSE Protein diaphanous homolog 1 OS=Mus musculus GN=Diap1 PE=1 SV=1;>tr|Q6NS79|Q6NS79_M	7	5	7	5	0.10598	0.21519
sp|O70194|E sp|O70194|E 10	>sp|O70194|EIF3D_MOUSE Eukaryotic translation initiation factor 3 subunit D OS=Mus musculus GN=Eif3d PE=1 SV=2	7	4	7	4	0.10453	0.13862
sp|Q501J6|D sp|Q501J6|D 17;17;12	>sp|Q501J6|DDX17_MOUSE Probable ATP-dependent RNA helicase DDX17 OS=Mus musculus GN=Ddx17 PE=1 SV=1;>tr|Q3U741|Q3U741_MOUSE DEAD (Asp-Glu-Ala-Asp) box polypeptide 17, isoform CRA_a OS=Mus musculus G	16	10	12	8	0.10385	0.22448
sp|Q8CI94|P sp|Q8CI94|P 13;4	>sp|Q8CI94|PYGB_MOUSE Glycogen phosphorylase, brain form OS=Mus musculus GN=Pygb PE=1 SV=3	13	3	10	2	0.10373	1.2929
sp|P68372|T sp|P68372|T 7;1	>sp|P68372|TBB4B_MOUSE Tubulin beta-4B chain OS=Mus musculus GN=Tubb4b PE=1 SV=1	6	7	1	1	0.10244	2.4452
sp|Q8BHJ5|T sp|Q8BHJ5|T 5;2	>sp|Q8BHJ5|TBL1R_MOUSE F-box-like/WD repeat-containing protein TBL1XR1 OS=Mus musculus GN=Tbl1xr1 PE=1 SV=1	5	2	5	2	0.10217	6.6732
sp|Q76MZ3| sp|Q76MZ3| 12;3	>sp|Q76MZ3|2AAA_MOUSE Serine/threonine-protein phosphatase 2A 65 kDa regulatory subunit A alpha isoform OS=Mus musculus GN=Ppp2r1a PE=1 SV=3	12	6	11	6	0.10185	4.0088
sp|Q62095|C sp|Q62095|C 8;8;7	>sp|Q62095|DDX3Y_MOUSE ATP-dependent RNA helicase DDX3Y OS=Mus musculus GN=Ddx3y PE=1 SV=2;>sp|Q62167|DDX3X_MOUSE ATP-dependent RNA helicase DDX3X OS=Mus musculus GN=Ddx3x PE=1 SV=3;>sp|P16381	7	2	7	2	0.10103	4.5744
sp|P12382|P sp|P12382|P 11	>sp|P12382|PFKAL_MOUSE ATP-dependent 6-phosphofructokinase, liver type OS=Mus musculus GN=Pfkl PE=1 SV=4	4	11	3	10	0.10099	0.19892
sp|G5E866|G sp|G5E866|G 22;22	>sp|G5E866|G5E866_MOUSE Splicing factor 3B subunit 1 OS=Mus musculus GN=Sf3b1 PE=1 SV=1;>sp|Q99NB9|SF3B1_MOUSE Splicing factor 3B subunit 1 OS=Mus musculus GN=Sf3b1 PE=1 SV=1	21	9	21	9	0.10097	0.12034
sp|P62827|R sp|P62827|R 6;5;2	>sp|P62827|RAN_MOUSE GTP-binding nuclear protein Ran OS=Mus musculus GN=Ran PE=1 SV=3;>tr|Q14AA6|Q14AA6_MOUSE MCG49183 OS=Mus musculus GN=1700009N14Rik PE=2 SV=1	4	5	4	5	0.10087	1.2177
sp|Q6P5F9|X sp|Q6P5F9|X 16;3;1	>sp|Q6P5F9|XPO1_MOUSE Exportin-1 OS=Mus musculus GN=Xpo1 PE=1 SV=3	15	6	15	6	0.10042	1.6436
sp|Q62261-2 sp|Q62261-2 50;50;6;2;2;2	>sp|Q62261-2|SPTB2_MOUSE Isoform 2 of Spectrin beta chain, non-erythrocytic 1 OS=Mus musculus GN=Sptbn1;>sp|Q62261|SPTB2_MOUSE Spectrin beta chain, non-erythrocytic 1 OS=Mus musculus GN=Sptbn1 PE=1 SV=2	45	21	45	21	0.099606	0.21417
sp|P14211|C sp|P14211|C 20	>sp|P14211|CALR_MOUSE Calreticulin OS=Mus musculus GN=Calr PE=1 SV=1	15	16	15	16	0.099289	1.1836
sp|Q91V12-2 sp|Q91V12-2 6;6;6;6;5	>sp|Q91V12-2|BACH_MOUSE Isoform A of Cytosolic acyl coenzyme A thioester hydrolase OS=Mus musculus GN=Acot7;>sp|Q91V12-4|BACH_MOUSE Isoform D of Cytosolic acyl coenzyme A thioester hydrolase OS=Mus musculu	5	6	5	6	0.09748	2.6786
tr|Q05DV1|C tr|Q05DV1|C 9;9;4;3;1	>tr|Q05DV1|Q05DV1_MOUSE NADPH--cytochrome P450 reductase OS=Mus musculus GN=Por PE=2 SV=1;>sp|P37040|NCPR_MOUSE NADPH--cytochrome P450 reductase OS=Mus musculus GN=Por PE=1 SV=2	6	6	6	6	0.097427	6.6091
tr|Q3TWV4| tr|Q3TWV4| 11;11	>tr|Q3TWV4|Q3TWV4_MOUSE AP-2 complex subunit mu OS=Mus musculus GN=Ap2m1 PE=2 SV=1;>sp|P84091|AP2M1_MOUSE AP-2 complex subunit mu OS=Mus musculus GN=Ap2m1 PE=1 SV=1	11	5	11	5	0.096909	0.75557
sp|Q9WUA2| sp|Q9WUA2| 8;3;1	>sp|Q9WUA2|SYFB_MOUSE Phenylalanine--tRNA ligase beta subunit OS=Mus musculus GN=Farsb PE=2 SV=2	7	5	4	4	0.095049	0.071678
sp|Q8VDN2| sp|Q8VDN2| 12;2;2;2;2;2;1	>sp|Q8VDN2|AT1A1_MOUSE Sodium/potassium-transporting ATPase subunit alpha-1 OS=Mus musculus GN=Atp1a1 PE=1 SV=1	12	9	5	3	0.094862	0.31689
sp|P57780|A sp|P57780|A 16;6;5;3;1;1	>sp|P57780|ACTN4_MOUSE Alpha-actinin-4 OS=Mus musculus GN=Actn4 PE=1 SV=1;>tr|E9Q2W9|E9Q2W9_MOUSE Alpha-actinin-4 (Fragment) OS=Mus musculus GN=Actn4 PE=4 SV=1	13	7	12	7	0.094465	2.0346
sp|Q60676|F sp|Q60676|F 9;7	>sp|Q60676|PPP5_MOUSE Serine/threonine-protein phosphatase 5 OS=Mus musculus GN=Ppp5c PE=1 SV=3;>tr|F7BX26|F7BX26_MOUSE Serine/threonine-protein phosphatase (Fragment) OS=Mus musculus GN=Ppp5c PE=3 SV	8	8	8	8	0.094372	6.2842
sp|Q91VD9|I sp|Q91VD9|I 9	>sp|Q91VD9|NDUS1_MOUSE NADH-ubiquinone oxidoreductase 75 kDa subunit, mitochondrial OS=Mus musculus GN=Ndufs1 PE=1 SV=2	5	7	5	7	0.092129	0.18146
sp|Q91WQ3| sp|Q91WQ3| 20;20;3	>sp|Q91WQ3|SYYC_MOUSE Tyrosine--tRNA ligase, cytoplasmic OS=Mus musculus GN=Yars PE=2 SV=3;>tr|A2A7S7|A2A7S7_MOUSE Tyrosine--tRNA ligase OS=Mus musculus GN=Yars PE=3 SV=1	13	12	13	12	0.091939	1.6423
sp|Q5XJY5|C sp|Q5XJY5|C 14	>sp|Q5XJY5|COPD_MOUSE Coatomer subunit delta OS=Mus musculus GN=Arcn1 PE=2 SV=1	11	10	11	10	0.091387	5.8546
sp|Q99KV1|[sp|Q99KV1|[9	>sp|Q99KV1|DJB11_MOUSE DnaJ homolog subfamily B member 11 OS=Mus musculus GN=Dnajb11 PE=1 SV=1	7	2	7	2	0.091155	2.489
sp|Q9Z2N8|/ sp|Q9Z2N8|/ 5;3	>sp|Q9Z2N8|ACL6A_MOUSE Actin-like protein 6A OS=Mus musculus GN=Actl6a PE=1 SV=2;>tr|D3YVN1|D3YVN1_MOUSE Actin-like protein 6A (Fragment) OS=Mus musculus GN=Actl6a PE=3 SV=1	3	3	3	3	0.091116	3.2396
sp|Q9DCH4|I sp|Q9DCH4|I 10	>sp|Q9DCH4|EIF3F_MOUSE Eukaryotic translation initiation factor 3 subunit F OS=Mus musculus GN=Eif3f PE=1 SV=2	8	7	8	7	0.090523	3.4285
sp|P05064|A sp|P05064|A 17;17;15;13;1	>sp|P05064|ALDOA_MOUSE Fructose-bisphosphate aldolase A OS=Mus musculus GN=Aldoa PE=1 SV=2;>tr|A6ZI44|A6ZI44_MOUSE Fructose-bisphosphate aldolase OS=Mus musculus GN=Aldoa PE=2 SV=1;>tr|D3YWI1|D3YWI1_	8	17	8	16	0.090458	0.099334
sp|Q6A4J8-3 sp|Q6A4J8-3 12;12;12;12;1	>sp|Q6A4J8-3|UBP7_MOUSE Isoform 3 of Ubiquitin carboxyl-terminal hydrolase 7 OS=Mus musculus GN=Usp7;>tr|F8VPX1|F8VPX1_MOUSE Ubiquitin carboxyl-terminal hydrolase 7 OS=Mus musculus GN=Usp7 PE=1 SV=1;>sp|Q6A	11	2	11	2	0.089543	0.21634
sp|P27773|P sp|P27773|P 29;4	>sp|P27773|PDIA3_MOUSE Protein disulfide-isomerase A3 OS=Mus musculus GN=Pdia3 PE=1 SV=2	11	28	11	28	0.088498	3.8117
sp|Q9Z110-2 sp|Q9Z110-2 16;16;4;2;1	>sp|Q9Z110-2|P5CS_MOUSE Isoform Short of Delta-1-pyrroline-5-carboxylate synthase OS=Mus musculus GN=Aldh18a1;>sp|Q9Z110|P5CS_MOUSE Delta-1-pyrroline-5-carboxylate synthase OS=Mus musculus GN=Aldh18a1 PE=1	7	16	7	16	0.087961	4.427
sp|O9OUR6| sp|O9OUR6| 14	>sp|Q9QUR6|PPCE_MOUSE Prolyl endopeptidase OS=Mus musculus GN=Prep PE=2 SV=1	12	6	12	6	0.08784	4.6177

Accession	Description						
tr|Q3TL72|Q	>tr|Q3TL72|Q3TL72_MOUSE NEDD8-activating enzyme E1 catalytic subunit OS=Mus musculus GN=Uba3 PE=2 SV=1;>sp|Q8C878|UBA3_MOUSE NEDD8-activating enzyme E1 catalytic subunit OS=Mus musculus GN=Uba3 PE=1 SV	8	5	8	5	0.085839	3.3205
sp|P42230|S	**>sp|P42230|STA5A_MOUSE Signal transducer and activator of transcription 5A OS=Mus musculus GN=Stat5a PE=1 SV=1;>tr|B2C3G8|B2C3G8_MOUSE Signal transducer and activator of transcription OS=Mus musculus GN=Stat5a**	**8**	**6**	**1**	**1**	**0.085487**	**2.5527**
tr|A2A4A6|A	>tr|A2A4A6|A2A4A6_MOUSE Phosphoinositide phospholipase C OS=Mus musculus GN=Plcg1 PE=1 SV=1;>sp|Q62077|PLCG1_MOUSE 1-phosphatidylinositol 4,5-bisphosphate phosphodiesterase gamma-1 OS=Mus musculus GN=	14	10	14	10	0.085335	0.09536
sp|P63005|LI	>sp|P63005|LIS1_MOUSE Platelet-activating factor acetylhydrolase IB subunit alpha OS=Mus musculus GN=Pafah1b1 PE=1 SV=2;>sp|P63005-2|LIS1_MOUSE Isoform 2 of Platelet-activating factor acetylhydrolase IB subunit alpha	7	5	7	5	0.084773	2.5441
sp|Q8R326-2|	>sp|Q8R326-2|PSPC1_MOUSE Isoform 2 of Paraspeckle component 1 OS=Mus musculus GN=Pspc;>sp|Q8R326|PSPC1_MOUSE Paraspeckle component 1 OS=Mus musculus GN=Pspc1 PE=1 SV=1	7	4	7	4	0.084743	5.4367
sp|Q62318|T	>sp|Q62318|TIF1B_MOUSE Transcription intermediary factor 1-beta OS=Mus musculus GN=Trim28 PE=1 SV=3;>sp|Q62318-2|TIF1B_MOUSE Isoform 2 of Transcription intermediary factor 1-beta OS=Mus musculus GN=Trim28	14	4	14	4	0.084629	1.7714
tr|A0A087WI	>tr|A0A087WPL5|A0A087WPL5_MOUSE ATP-dependent RNA helicase A OS=Mus musculus GN=Dhx9 PE=1 SV=1;>tr|E9QNN1|E9QNN1_MOUSE ATP-dependent RNA helicase A OS=Mus musculus GN=Dhx9 PE=1 SV=1;>O7013	12	6	12	6	0.083734	0.2856
sp|P10852|4	>sp|P10852|4F2_MOUSE 4F2 cell-surface antigen heavy chain OS=Mus musculus GN=Slc3a2 PE=1 SV=1;>sp|P10852-2|4F2_MOUSE Isoform 2 of 4F2 cell-surface antigen heavy chain OS=Mus musculus GN=Slc3a2	2	11	2	11	0.08284	0.11344
sp|Q9D8U8|	>sp|Q9D8U8|SNX5_MOUSE Sorting nexin-5 OS=Mus musculus GN=Snx5 PE=1 SV=1	9	9	9	9	0.082627	2.7063
tr|Z4YKV1|Z	>tr|Z4YKV1|Z4YKV1_MOUSE Guanine nucleotide-binding protein G(s) subunit alpha isoforms short OS=Mus musculus GN=Gnas PE=4 SV=1;>sp|P63094-2|GNAS2_MOUSE Isoform Gnas-2 of Guanine nucleotide-binding protein G(	9	5	8	4	0.081753	2.7793
sp|Q9WVK4|	>sp|Q9WVK4|EHD1_MOUSE EH domain-containing protein 1 OS=Mus musculus GN=Ehd1 PE=1 SV=1;>sp|Q9QXY6|EHD3_MOUSE EH domain-containing protein 3 OS=Mus musculus GN=Ehd3 PE=1 SV=2	13	5	12	4	0.081373	0.061364
sp|Q6P5E4|L	>sp|Q6P5E4|UGGG1_MOUSE UDP-glucose:glycoprotein glucosyltransferase 1 OS=Mus musculus GN=Uggt1 PE=1 SV=4	8	4	8	4	0.080025	0.079792
tr|Q8VHM5|	>tr|Q8VHM5|Q8VHM5_MOUSE Heterogeneous nuclear ribonucleoprotein R OS=Mus musculus GN=Hnrnpr PE=1 SV=1;>tr|F7B5B5|F7B5B5_MOUSE Protein Hnrnpr OS=Mus musculus GN=Hnrnpr PE=1 SV=1;>tr|A2AW41|A2AW4	10	5	10	5	0.079965	0.27926
sp|P28656|N	>sp|P28656|NP1L1_MOUSE Nucleosome assembly protein 1-like 1 OS=Mus musculus GN=Nap1l1 PE=1 SV=2;>tr|E9PW66|E9PW66_MOUSE Nucleosome assembly protein 1-like 1 OS=Mus musculus GN=Nap1l1 PE=1 SV=1	4	4	4	4	0.079778	1.642
sp|P61222|A	>sp|P61222|ABCE1_MOUSE ATP-binding cassette sub-family E member 1 OS=Mus musculus GN=Abce1 PE=2 SV=1	15	10	15	10	0.079319	0.31061
sp|Q8CG48|S	>sp|Q8CG48|SMC2_MOUSE Structural maintenance of chromosomes protein 2 OS=Mus musculus GN=Smc2 PE=1 SV=1	10	3	10	3	0.079301	0.071703
sp|Q60967|F	>sp|Q60967|PAPS1_MOUSE Bifunctional 3'-phosphoadenosine 5'-phosphosulfate synthase 1 OS=Mus musculus GN=Papss1 PE=1 SV=1	11	4	11	4	0.078688	0.10693
sp|O09106|H	>sp|O09106|HDAC1_MOUSE Histone deacetylase 1 OS=Mus musculus GN=Hdac1 PE=1 SV=1;>tr|D3YYI8|D3YYI8_MOUSE Histone deacetylase OS=Mus musculus GN=Gm10093 PE=3 SV=1	9	7	5	3	0.078181	0.11883
sp|Q9CZ30|C	>sp|Q9CZ30|OLA1_MOUSE Obg-like ATPase 1 OS=Mus musculus GN=Ola1 PE=1 SV=1;>sp|Q9CZ30-2|OLA1_MOUSE Isoform 2 of Obg-like ATPase 1 OS=Mus musculus GN=Ola1;>tr|B1AYJ9|B1AYJ9_MOUSE Obg-like ATPase 1 OS=	5	3	5	3	0.077866	2.5504
sp|Q8QZY1|E	>sp|Q8QZY1|EIF3L_MOUSE Eukaryotic translation initiation factor 3 subunit L OS=Mus musculus GN=Eif3l PE=1 SV=1	17	10	17	10	0.077624	0.32919
sp|P61202|C	>sp|P61202|CSN2_MOUSE COP9 signalosome complex subunit 2 OS=Mus musculus GN=Cops2 PE=1 SV=1;>sp|P61202-2|CSN2_MOUSE Isoform 2 of COP9 signalosome complex subunit 2 OS=Mus musculus GN=Cops2;>tr|A2AQE	12	9	12	9	0.077542	1.894
sp|Q91VC3|I	>sp|Q91VC3|IF4A3_MOUSE Eukaryotic initiation factor 4A-III OS=Mus musculus GN=Eif4a3 PE=2 SV=3;>tr|A2AFK7|A2AFK7_MOUSE Eukaryotic initiation factor 4A-III (Fragment) OS=Mus musculus GN=Eif4a3 PE=3 SV=1;>tr|E9PV	13	10	13	10	0.077017	2.9792
sp|P48722-2|	>sp|P48722-2|HS74L_MOUSE Isoform 2 of Heat shock 70 kDa protein 4L OS=Mus musculus GN=Hspa4l;>sp|P48722|HS74L_MOUSE Heat shock 70 kDa protein 4L OS=Mus musculus GN=Hspa4l PE=1 SV=2;>tr|E0CY23|E0CY23_MO	6	2	6	2	0.076216	0.94495
sp|P19324|S	>sp|P19324|SERPH_MOUSE Serpin H1 OS=Mus musculus GN=Serpinh1 PE=1 SV=3	4	6	4	6	0.074734	2.6602
tr|A0A087WI	>tr|A0A087WR97|A0A087WR97_MOUSE TAR DNA-binding protein 43 (Fragment) OS=Mus musculus GN=Tardbp PE=4 SV=1;>sp|Q921F2|TADBP_MOUSE TAR DNA-binding protein 43 (Fragment) OS=Mus musculus GN=Tardbp PE=1 SV=1;>tr	6	6	6	6	0.073518	2.2821
sp|Q8BK67|F	>sp|Q8BK67|RCC2_MOUSE Protein RCC2 OS=Mus musculus GN=Rcc2 PE=1 SV=1	10	9	10	9	0.07325	0.57737
sp|P29341|P	>sp|P29341|PABP1_MOUSE Polyadenylate-binding protein 1 OS=Mus musculus GN=Pabpc1 PE=1 SV=2;>tr|Q9D4E6|Q9D4E6_MOUSE Protein Pabpc6 OS=Mus musculus GN=Pabpc6 PE=2 SV=1	13	13	11	10	0.072743	0.65595
sp|P14206|R	>sp|P14206|RSSA_MOUSE 40S ribosomal protein SA OS=Mus musculus GN=Rpsa PE=1 SV=4	5	5	5	5	0.072629	2.1428
sp|Q9Z2X1-2	>sp|Q9Z2X1-2|HNRPF_MOUSE Isoform 2 of Heterogeneous nuclear ribonucleoprotein F OS=Mus musculus GN=Hnrnpf;>sp|Q9Z2X1|HNRPF_MOUSE Heterogeneous nuclear ribonucleoprotein F OS=Mus musculus GN=Hnrnpf PE=	3	4	3	4	0.072574	2.6155
sp|P50580|P	>sp|P50580|PA2G4_MOUSE Proliferation-associated protein 2G4 OS=Mus musculus GN=Pa2g4 PE=1 SV=3;>tr|D3YVH7|D3YVH7_MOUSE Proliferation-associated protein 2G4 (Fragment) OS=Mus musculus GN=Pa2g4 PE=1 SV=1	14	11	14	11	0.072029	1.6173
sp|Q91W50|	>sp|Q91W50|CSDE1_MOUSE Cold shock domain-containing protein E1 OS=Mus musculus GN=Csde1 PE=2 SV=1	14	4	14	4	0.071884	0.14159
sp|Q8VEM8|	>sp|Q8VEM8|MPCP_MOUSE Phosphate carrier protein, mitochondrial OS=Mus musculus GN=Slc25a3 PE=1 SV=1;>tr|G5E902|G5E902_MOUSE MCG10343, isoform CRA_b OS=Mus musculus GN=Slc25a3 PE=1 SV=1	5	3	5	3	0.070666	0.094289
sp|P62196|P	>sp|P62196|PRS8_MOUSE 26S protease regulatory subunit 8 OS=Mus musculus GN=Psmc5 PE=1 SV=1;>tr|Q8K1K2|Q8K1K2_MOUSE 26S protease regulatory subunit 8 OS=Mus musculus GN=Psmc5 PE=2 SV=1	15	12	15	12	0.070641	1.8772
tr|E9QAI5|E	>tr|E9QAI5|E9QAI5_MOUSE CAD protein OS=Mus musculus GN=Cad PE=3 SV=1;>sp|B2RQC6|PYR1_MOUSE CAD protein OS=Mus musculus GN=Cad PE=2 SV=1;>sp|B2RQC6-2|PYR1_MOUSE Isoform 2 of CAD protein OS=Mus mu	31	5	31	5	0.070564	0.17007
sp|Q61081|C	>sp|Q61081|CDC37_MOUSE Hsp90 co-chaperone Cdc37 OS=Mus musculus GN=Cdc37 PE=2 SV=1	3	3	3	3	0.070545	0.5865
sp|O88342|V	>sp|O88342|WDR1_MOUSE WD repeat-containing protein 1 OS=Mus musculus GN=Wdr1 PE=2 SV=3	16	18	16	18	0.07044	0.15464
sp|Q6P4T2|L	>sp|Q6P4T2|U520_MOUSE U5 small nuclear ribonucleoprotein 200 kDa helicase OS=Mus musculus GN=Snrnp200 PE=1 SV=1	28	7	28	7	0.070426	0.12476
sp|P17183|E	>sp|P17183|ENOG_MOUSE Gamma-enolase OS=Mus musculus GN=Eno2 PE=1 SV=2;>tr|D3Z6E4|D3Z6E4_MOUSE Enolase OS=Mus musculus GN=Eno2 PE=3 SV=1	7	5	7	5	0.069879	2.4873
sp|Q8VDP4|	>sp|Q8VDP4|CCAR2_MOUSE Cell cycle and apoptosis regulator protein 2 OS=Mus musculus GN=Ccar2 PE=1 SV=2	6	4	6	4	0.069501	0.25318
sp|O35737|F	>sp|O35737|HNRH1_MOUSE Heterogeneous nuclear ribonucleoprotein H OS=Mus musculus GN=Hnrnph1 PE=1 SV=3;>tr|Q8C2Q7|Q8C2Q7_MOUSE Heterogeneous nuclear ribonucleoprotein H OS=Mus musculus GN=Hnrnph1 P	7	6	2	1	0.069123	1.6499
sp|O08553|L	>sp|O08553|DPYL2_MOUSE Dihydropyrimidinase-related protein 2 OS=Mus musculus GN=Dpysl2 PE=1 SV=2	15	13	15	13	0.068599	0.49884
sp|Q9D8W5|	>sp|Q9D8W5|PSD12_MOUSE 26S proteasome non-ATPase regulatory subunit 12 OS=Mus musculus GN=Psmd12 PE=1 SV=4;>tr|B1AT36|B1AT36_MOUSE 26S proteasome non-ATPase regulatory subunit 12 OS=Mus musculus GN	7	8	7	8	0.068406	1.6752
sp|P70168|I	>sp|P70168|IMB1_MOUSE Importin subunit beta-1 OS=Mus musculus GN=Kpnb1 PE=1 SV=2	15	9	15	9	0.068388	0.94467
sp|P27659|R	>sp|P27659|RL3_MOUSE 60S ribosomal protein L3 OS=Mus musculus GN=Rpl3 PE=1 SV=3	13	8	13	8	0.067458	1.6645
sp|Q00612|C	>sp|Q00612|G6PD1_MOUSE Glucose-6-phosphate 1-dehydrogenase X OS=Mus musculus GN=G6pdx PE=1 SV=3;>tr|A3KG36|A3KG36_MOUSE Glucose-6-phosphate 1-dehydrogenase (Fragment) OS=Mus musculus GN=G6pdx PE=	12	13	12	13	0.067422	0.66659
sp|P49717|M	>sp|P49717|MCM4_MOUSE DNA replication licensing factor MCM4 OS=Mus musculus GN=Mcm4 PE=1 SV=1	14	8	14	8	0.067311	0.18577
sp|Q3U0V1|I	>sp|Q3U0V1|FUBP2_MOUSE Far upstream element-binding protein 2 OS=Mus musculus GN=Khsrp PE=1 SV=1	5	5	5	5	0.067084	3.8948
sp|Q99L45|II	>sp|Q99L45|IF2B_MOUSE Eukaryotic translation initiation factor 2 subunit 2 OS=Mus musculus GN=Eif2s2 PE=1 SV=1	5	5	5	5	0.066398	2.2877
tr|Q3TUE1|C	>tr|Q3TUE1|Q3TUE1_MOUSE Far upstream element-binding protein 1 OS=Mus musculus GN=Fubp1 PE=2 SV=1;>sp|Q91WJ8|FUBP1_MOUSE Far upstream element-binding protein 1 OS=Mus musculus GN=Fubp1 PE=1 SV=1;>sp	12	3	11	3	0.066051	0.2685
sp|O35685|N	>sp|O35685|NUDC_MOUSE Nuclear migration protein nudC OS=Mus musculus GN=Nudc PE=1 SV=1	13	8	13	8	0.065804	0.81592
tr|B1AU25|B	>tr|B1AU25|B1AU25_MOUSE Apoptosis-inducing factor 1, mitochondrial OS=Mus musculus GN=Aifm1 PE=1 SV=1;>sp|Q9Z0X1|AIFM1_MOUSE Apoptosis-inducing factor 1, mitochondrial OS=Mus musculus GN=Aifm1 PE=1 SV=1	9	8	9	8	0.065457	0.15737
tr|B7FAV1|B	>tr|B7FAV1|B7FAV1_MOUSE Filamin, alpha (Fragment) OS=Mus musculus GN=Flna PE=1 SV=1;>tr|B7FAU9|B7FAU9_MOUSE Filamin, alpha OS=Mus musculus GN=Flna PE=1 SV=1;>sp|Q8BTM8|FLNA_MOUSE Filamin-A OS=Mus m	46	13	43	12	0.065305	0.33011
sp|Q8R1B4|E	>sp|Q8R1B4|EIF3C_MOUSE Eukaryotic translation initiation factor 3 subunit C OS=Mus musculus GN=Eif3c PE=1 SV=1	14	10	14	10	0.0653	1.1621
sp|P54823|D	>sp|P54823|DDX6_MOUSE Probable ATP-dependent RNA helicase DDX6 OS=Mus musculus GN=Ddx6 PE=1 SV=1	10	4	10	4	0.064996	1.3401
sp|P16627|H	>sp|P16627|HS71L_MOUSE Heat shock 70 kDa protein 1-like OS=Mus musculus GN=Hspa1l PE=1 SV=1	3	2	3	2	0.064753	4.9132
sp|P14685|P	>sp|P14685|PSMD3_MOUSE 26S proteasome non-ATPase regulatory subunit 3 OS=Mus musculus GN=Psmd3 PE=1 SV=3	18	15	18	15	0.064738	0.2514
sp|Q8C1B7-3|	>sp|Q8C1B7-3|SEP11_MOUSE Isoform 3 of Septin-11 OS=Mus musculus GN=Sept11;>sp|Q8C1B7-2|SEP11_MOUSE Isoform 2 of Septin-11 OS=Mus musculus GN=Sept11;>sp|Q8C1B7|SEP11_MOUSE Septin-11 OS=Mus musculus	14	9	5	3	0.064166	1.571
sp|Q68FD5|C	>sp|Q68FD5|CLH1_MOUSE Clathrin heavy chain 1 OS=Mus musculus GN=Cltc PE=1 SV=3;>tr|Q5SXR6|Q5SXR6_MOUSE Clathrin heavy chain OS=Mus musculus GN=Cltc PE=1 SV=1	35	24	35	24	0.063551	0.1041
sp|P50396|G	>sp|P50396|GDIA_MOUSE Rab GDP dissociation inhibitor alpha OS=Mus musculus GN=Gdi1 PE=1 SV=3	8	9	8	9	0.062431	1.3849
sp|O35841|A	>sp|O35841|API5_MOUSE Apoptosis inhibitor 5 OS=Mus musculus GN=Api5 PE=2 SV=2	8	10	8	10	0.062427	1.4901
tr|Q7M739|C	>tr|Q7M739|Q7M739_MOUSE Nuclear pore complex-associated intranuclear coiled-coil protein TPR OS=Mus musculus GN=Tpr PE=1 SV=1;>sp|F6ZDS4|TPR_MOUSE Nucleoprotein TPR OS=Mus musculus GN=Tpr PE=1 SV=1	19	5	19	5	0.062403	0.051167

Protein IDs / Fasta headers	Razor + unique peptides A	Razor + unique peptides B	Razor + unique peptides C	Razor + unique peptides D	Razor + unique peptides E	Unique peptides A	Unique peptides B	Unique peptides C	Unique peptides D	Unique peptides E	Sequence coverage A [%]	Sequence coverage B [%]	Sequence coverage C [%]	Sequence coverage D [%]	Sequence coverage E [%]	Intensity	Intensity A	Intensity B	Intensity C	Intensity D
sp|P42232|S >sp|P42232|STA5B_MOUSE Signal transducer and activator of transcri	**11**	**12**	**10**	**12**	**13**	**2**	**2**	**2**	**2**	**2**	**16.8**	**18.3**	**14.4**	**18.3**	**21.1**	**106300000**	**14294000**	**15145000**	**25826000**	**19576000**
5|MBP-STAT >5|MBP-STAT5b|MBP-STAT5b	1	2	2	2	3	1	2	2	2	2	7.4	9.5	7.9	9.5	13.3	125100000	623890	2462100	6411800	21674000
sp|Q921M3| >sp|Q921M3|SF3B3_MOUSE Splicing factor 3B subunit 3 OS=Mus muscu	21	26	26	25	26	21	26	26	25	26	22.5	28.1	28.1	27.3	28.1	764770000	51903000	97136000	262900000	144930000
sp|P46172|R >sp|P46172|RS3_BUCAK 30S ribosomal protein S3 (Fragment) OS=Buchr	2	2	1	1	1	2	2	1	1	1	9.8	9.8	3.9	3.9	3.9	10188000	3302100	3796400	995340	1133900
sp|Q2LAP6|T >sp|Q2LAP6|TES_RAT Testin OS=Rattus norvegicus GN=Tes PE=2 SV=1;>	2	2	2	2	2	2	2	2	2	2	6.2	6.2	6.2	6.2	6.2	6179100	759810	921410	2068300	1026300
sp|Q3YWU2| >sp|Q3YWU2|RL2_SHISS 50S ribosomal protein L2 OS=Shigella sonnei (s	3	2	2	2	3	3	2	2	2	3	15.8	12.1	12.1	12.1	15.8	49262000	11024000	9670600	11074000	8378800
sp|A1L1K3|A >sp|A1L1K3|APC5_RAT Anaphase-promoting complex subunit 5 OS=Ratt	3	3	2	2	2	3	3	2	2	2	6.1	6.1	3.4	6.1	3.4	9351500	2072800	1630600	1893400	2718000
sp|A4UMC6| >sp|A4UMC6|TFP11_MONDO Tuftelin-interacting protein 11 OS=Monoc	2	2	2	2	2	2	2	2	2	2	3.2	3.2	3.2	3.2	3.2	8762300	1272800	1053300	2717800	1673700
sp|Q9XSU7|F >sp|Q9XSU7|RL27_CANFA 60S ribosomal protein L27 OS=Canis familiari	4	4	4	4	4	4	4	4	4	4	30.9	30.9	30.9	30.9	30.9	79625000	10951000	10408000	22959000	17647000
sp|Q5R924|F >sp|Q5R924|RS20_PONAB 40S ribosomal protein S20 OS=Pongo abelii (	2	2	2	2	2	2	2	2	2	2	12.6	12.6	12.6	12.6	12.6	36985000	5640500	5267700	13035000	7027100
sp|A2A432|C >sp|A2A432|CUL4B_MOUSE Cullin-4B OS=Mus musculus GN=Cul4b PE=:	17	16	17	17	18	13	12	13	13	14	22.6	19.9	21.9	22.6	23.2	136130000	23779000	12590000	35255000	26284000
sp|A2A6Q5|C >sp|A2A6Q5|CDC27_MOUSE Cell division cycle protein 27 homolog OS=	1	1	1	1	2	1	1	1	1	2	1.8	1.8	1.8	1.8	6.3	7124200	712380	817770	1872200	1592600
sp|Q96SU4|(>sp|Q96SU4|OSBL9_HUMAN Oxysterol-binding protein-related protein	2	2	2	2	2	2	2	2	2	2	2.9	2.9	2.9	2.9	2.9	12558000	2436300	1674100	3402500	1933900
sp|A2ADY9|I >sp|A2ADY9|DDI2_MOUSE Protein DDI1 homolog 2 OS=Mus musculus C	2	2	1	2	2	2	2	1	2	2	8.3	8.3	4.8	8.3	8.3	9563200	1758400	1647600	1162000	2214200
sp|A2AGT5|C >sp|A2AGT5|CKAP5_MOUSE Cytoskeleton-associated protein 5 OS=Mus	6	7	7	7	7	6	7	7	7	7	3.8	4.3	4.3	4.3	4.3	44494000	6146800	5576500	14777000	7252100
sp|A2AN08|l >sp|A2AN08|UBR4_MOUSE E3 ubiquitin-protein ligase UBR4 OS=Mus m	4	4	6	5	5	4	4	6	5	5	1.4	1.2	1.9	1.7	1.7	21995000	1998700	1548700	9706800	4279400
sp|A2AWA9| >sp|A2AWA9|RBGP1_MOUSE Rab GTPase-activating protein 1 OS=Mus	2	2	3	3	3	2	2	3	3	3	2.4	3.1	4	4	4	11529000	696710	814800	3212400	2482600
sp|Q9ES70|N >sp|Q9ES70|NEK6_MOUSE Serine/threonine-protein kinase Nek6 OS=M	2	3	3	3	3	2	2	3	3	3	12.5	15	15	15	15	10626000	1373800	1235100	3736800	2318200
sp|A2BE28|L >sp|A2BE28|LAS1L_MOUSE Protein LAS1 homolog OS=Mus musculus GI	7	7	7	7	5	7	7	7	7	5	14.6	14.6	14.6	14.6	10.8	35399000	4113000	3552800	12412000	7146600
sp|A2BH40| >sp|A2BH40|ARI1A_MOUSE AT-rich interactive domain-containing prote	2	2	2	2	2	2	2	2	2	2	1.4	1.4	1.4	1.4	1.4	7023800	1085000	950640	1951300	1240700
sp|Q66RN5|I >sp|Q66RN5|EF1A1_FELCA Elongation factor 1-alpha 1 OS=Felis catus G	25	23	25	26	26	2	1	1	2	1	59.5	51.9	53.7	60	53.7	6487900000	971480000	668360000	2189600000	1223900000
sp|Q71U34|I >sp|Q71U34|HSP7C_SAGOE Heat shock cognate 71 kDa protein OS=Sag	33	32	31	31	31	13	12	11	12	12	55.4	51.9	48.6	54.3	53.3	5377700000	1485600000	888430000	1201500000	941860000
sp|A2RSY6|T >sp|A2RSY6|TRM1L_MOUSE TRM1-like protein OS=Mus musculus GN=T	3	2	4	4	4	3	2	4	4	4	7.7	4.7	11	11	11	23596000	1956200	1703400	7832700	4933200
sp|Q8R574|k >sp|Q8R574|KPRB_MOUSE Phosphoribosyl pyrophosphate synthetase-ass	2	2	2	2	2	2	2	2	2	2	11.4	11.4	11.4	11.4	11.4	8881100	1350200	1229700	2407800	1629200
sp|Q5R8U3|>sp|Q5R8U3|SEP11_PONAB Septin-11 OS=Pongo abelii GN=SEPT11 PE=:	3	2	3	3	2	3	2	3	3	2	11.5	6.8	11.5	11.5	6.8	27269000	4831400	3246400	9059400	5086300
sp|Q9Z1K5|A >sp|Q9Z1K5|ARI1_MOUSE Protein ariadne-1 homolog OS=Mus musculu	3	3	3	3	2	3	3	3	3	2	9.4	9.4	9.4	9.4	4.5	27673000	4072900	2804500	11417000	5458000
sp|A3KGB4|1 >sp|A3KGB4|TBC8B_MOUSE TBC1 domain family member 8B OS=Mus n	2	2	3	3	3	2	2	3	3	3	2.3	3.8	4.8	4.8	4.8	6466500	671720	230420	1966500	1687700
sp|Q6VN20|l >sp|Q6VN20|RBP10_HUMAN Ran-binding protein 10 OS=Homo sapiens	3	3	3	3	3	3	3	3	3	3	5.6	5.6	5.6	5.6	5.6	18666000	3777400	2776000	5392700	3614000
sp|Q689Z5|S >sp|Q689Z5|SBNO1_MOUSE Protein strawberry notch homolog 1 OS=N	1	2	6	2	2	1	2	6	2	2	1.4	2.4	8.4	2.1	2.4	15930000	268450	798880	12244000	867640
sp|Q5R6T6|V >sp|Q5R6T6|WDR91_PONAB WD repeat-containing protein 91 OS=Pon	3	3	3	4	4	3	3	3	4	4	5.1	5.1	5.1	6.6	6.6	17501000	2141500	1969000	4405600	3988300
sp|O08810|U >sp|O08810|U5S1_MOUSE 116 kDa U5 small nuclear ribonucleoprotein	29	27	29	30	29	29	27	29	30	29	40.9	36.5	41.4	41.5	40.3	550890000	60206000	51135000	195320000	106790000
sp|A4FUD6|E >sp|A4FUD6|ELMO2_BOVIN Engulfment and cell motility protein 2 OS=E	2	2	2	2	2	2	2	2	2	2	7.1	7.1	7.1	7.1	7.1	5942800	804750	666240	2143900	1321800
sp|Q5RC34|N >sp|Q5RC34|ML12A_PONAB Myosin regulatory light chain 12A OS=Pon	2	3	2	3	3	2	3	2	3	3	17.5	28.1	17.5	28.1	28.1	27797000	3207100	3323600	7746200	6555500
sp|Q5ZJK4|S >sp|Q5ZJK4|STK4_CHICK Serine/threonine-protein kinase 4 OS=Gallus g:	1	0	0	1	1	1	0	0	1	1	2.7	0	0	2.3	2.7	2248100	583990	0	0	1176500
sp|A5EX85|E >sp|A5EX85|EFG_DICNV Elongation factor G OS=Dichelobacter nodosus	2	1	2	1	1	2	1	2	1	1	3.3	3.3	2	3.3	2	8729500	2649700	1960200	1395300	1404600
sp|P46664|P >sp|P46664|PURA2_MOUSE Adenylosuccinate synthetase isozyme 2 OS	4	4	4	4	4	4	4	4	4	4	10.1	10.1	10.1	10.1	10.1	65243000	9550200	7997900	18731000	14754000
sp|P49312|R >sp|P49312|ROA1_MOUSE Heterogeneous nuclear ribonucleoprotein A	8	8	8	7	8	8	8	8	7	8	28.1	28.1	28.1	27.8	28.1	153940000	24924000	25750000	43336000	24039000
sp|Q5R546|/ >sp|Q5R546|ATPA_PONAB ATP synthase subunit alpha, mitochondrial O	5	5	4	5	3	5	5	4	5	3	13.2	13.2	11.4	13.2	7.4	36214000	6435500	4941500	10856000	8861000
sp|O00303|E >sp|O00303|EIF3F_HUMAN Eukaryotic translation initiation factor 3 sul	6	5	6	6	6	6	5	6	6	6	21.8	18.5	21.8	21.8	21.8	81199000	11514000	9716300	26602000	14318000
sp|Q5R4I9|D >sp|Q5R4I9|DDX5_PONAB Probable ATP-dependent RNA helicase DDX5	7	8	9	7	10	1	1	1	1	1	23	23	23.1	23	25.1	170240000	14899000	16571000	54256000	32732000
sp|P84586|H >sp|P84586|HNRPG_RAT Heterogeneous nuclear ribonucleoprotein G O	2	2	2	2	2	2	2	2	2	2	7.7	7.7	7.7	7.7	7.7	14397000	1967500	1915900	5620700	3520800
sp|Q8IXH7|N >sp|Q8IXH7|NELFD_HUMAN Negative elongation factor C/D OS=Homo	2	2	1	2	1	2	2	1	2	1	4.9	4.9	2.2	4.9	2.2	5298200	800410	935830	968810	1700400
sp|P20280|R >sp|P20280|RL21_RAT 60S ribosomal protein L21 OS=Rattus norvegicus	5	5	5	5	4	5	5	5	5	4	31.9	31.9	31.9	31.9	30	115120000	19754000	13232000	42353000	13061000
sp|Q5TJE9|R >sp|Q5TJE9|RS18_CANFA 40S ribosomal protein S18 OS=Canis familiaris	11	11	11	12	12	11	11	11	12	12	46.7	46.7	46.7	52	52	276860000	31672000	35358000	87745000	68168000
sp|Q6IQE5|A >sp|Q6IQE5|ASNA_DANRE ATPase asna1 OS=Danio rerio GN=asna1 PE=:	4	4	4	3	3	4	4	4	3	3	19.4	19.4	19.4	13.2	13.2	52782000	9051400	7422100	14705000	10117000
sp|Q5EB96|S >sp|Q5EB96|SEPT1_RAT Septin-1 OS=Rattus norvegicus GN=Sept1 PE=2	2	3	3	3	3	2	3	3	3	3	7.4	10.4	10.4	10.4	10.4	13994000	1136700	1577600	4672400	3245300
sp|Q6ZQ08|C >sp|Q6ZQ08|CNOT1_MOUSE CCR4-NOT transcription complex subunit :	2	2	3	2	3	2	2	3	2	3	0.9	0.9	1.3	0.9	1.3	7438900	924680	548460	3087200	1118600
sp|Q5RT64|R >sp|Q5RT64|RS7_FELCA 40S ribosomal protein S7 OS=Felis catus GN=RP	5	5	5	5	5	5	5	5	5	5	25.8	25.8	25.8	25.8	25.8	172090000	23230000	17003000	46851000	44837000
sp|B5FZY7|IF >sp|B5FZY7|IF4A3_TAEGU Eukaryotic initiation factor 4A-III OS=Taeniop	4	6	6	5	4	3	5	5	4	3	15.6	23.4	19.5	20.2	15.1	34187000	4077300	3819900	13442000	6469300
sp|Q6ZWN5| >sp|Q6ZWN5|RS9_MOUSE 40S ribosomal protein S9 OS=Mus musculus	4	5	5	5	4	4	5	5	5	4	14.9	20.1	20.1	20.1	20.1	246870000	29815000	26795000	88074000	52323000
sp|Q4GWZ2| >sp|Q4GWZ2|RSSA_PIG 40S ribosomal protein SA OS=Sus scrofa GN=RP!	12	12	12	13	13	11	11	11	11	11	39.7	39.7	39.7	49.5	49.5	769170000	101480000	92669000	237290000	158520000
sp|Q7ZXV3|A >sp|Q7ZXV3|ARP2B_XENLA Actin-related protein 2-B OS=Xenopus laevis	4	4	5	5	5	4	4	5	5	5	16	16	19.8	19.8	20.3	91385000	12911000	10761000	32850000	17993000
sp|Q9BT78|C >sp|Q9BT78|CSN4_HUMAN COP9 signalosome complex subunit 4 OS=H	3	4	4	2	3	3	4	4	2	3	12.3	16.5	16.5	7.4	12.3	20035000	2553200	2950800	8140300	3079100
sp|Q8CIG8|A >sp|Q8CIG8|ANM5_MOUSE Protein arginine N-methyltransferase 5 OS=	2	2	2	2	2	2	2	2	2	2	3	3	3	3	3	11188000	2445500	1503200	2964100	2031700
sp|A7Z019|SI >sp|A7Z019|SMCA4_BOVIN Transcription activator BRG1 OS=Bos taurus	3	4	4	5	3	3	4	4	5	3	2.9	3.9	3.9	4.5	2.9	21329000	2506100	1197600	6891100	5517700
sp|Q14677|E >sp|Q14677|EPN4_HUMAN Clathrin interactor 1 OS=Homo sapiens GN=	11	10	9	9	11	2	2	2	2	2	22.9	19.7	16.8	20	19.7	76654000	19374000	12804000	18034000	12758000
sp|Q6Y1R6|C >sp|Q6Y1R6|DPS_PROVU DNA protection during starvation protein OS=	2	2	1	1	1	2	2	1	1	1	22.2	22.2	11.4	11.4	10.8	5464800	1836600	1453700	917990	1027400
sp|Q9Y3I0|C\ >sp|Q9Y3I0|CV028_HUMAN Probable UPF0027 protein C22orf28 OS=Homo	6	10	8	10	9	6	10	8	10	9	20.2	28.9	19	28.9	25	90578000	9238000	11404000	18537000	22724000
sp|Q6ZWV3| >sp|Q6ZWV3|RL10_MOUSE 60S ribosomal protein L10 OS=Mus muscul	5	5	4	5	5	5	5	4	5	5	29.9	29.9	24.3	29.9	29.9	189570000	26771000	27596000	45978000	47977000
sp|Q5RDW4| >sp|Q5RDW4|EM55_PONAB 55 kDa erythrocyte membrane protein OS=	4	4	3	4	3	4	4	3	4	3	15	15	9	15	9	34600000	5813800	4767000	4982800	8988800
sp|Q6YKA4|I >sp|Q6YKA4|HMGB1_CANFA High mobility group protein B1 OS=Canis f:	3	4	4	4	4	3	4	4	4	4	24.2	21.4	27.4	25.6	25.6	39174000	6546400	6129400	11000000	8758400
sp|Q8CGP6|I >sp|Q8CGP6|H2A1H_MOUSE Histone H2A type 1-H OS=Mus musculus G	3	2	3	3	3	2	2	3	3	3	30.5	23.4	30.5	30.5	30.5	125590000	21386000	4958200	38368000	36616000
sp|Q9WVJ2|I >sp|Q9WVJ2|PSD13_MOUSE 26S proteasome non-ATPase regulatory su	9	7	9	9	9	9	7	9	9	9	29.5	22.1	29.5	29.5	29.5	60690000	9292600	5242100	20161000	11178000
sp|B2KI97|Tl >sp|B2KI97|THOC2_RHIFE THO complex subunit 2 OS=Rhinolophus ferr	2	2	2	2	2	2	2	2	2	2	1.8	1.8	1.8	1.8	1.8	8671700	1052000	744020	2770200	1560500
sp|Q5D44|I >sp|Q5D44|IF2P_MOUSE Eukaryotic translation initiation factor 5B OS=	12	12	13	11	8	12	12	13	11	8	15.6	16.4	18.3	15.7	12.4	208640000	38847000	30647000	71577000	46729000
sp|Q91YE7|R >sp|Q91YE7|RBM5_MOUSE RNA-binding protein 5 OS=Mus musculus GI	2	1	1	2	2	1	1	1	2	2	5	1.7	1.7	5	5	11839000	1631600	537820	1018000	4113900
sp|Q9D0K2|S >sp|Q9D0K2|SCOT1_MOUSE Succinyl-CoA:3-ketoacid-coenzyme A trans	3	4	4	4	4	3	4	4	4	4	10	10	10	10	10	18580000	1856400	2415800	6422800	4598700
sp|B2RRE7|C >sp|B2RRE7|OTUD4_MOUSE OTU domain-containing protein 4 OS=Mus	1	1	2	1	1	1	1	2	1	1	1.1	1.1	2.5	1.1	2.5	4450300	326840	462920	1944600	616940
sp|B2RUP2|L >sp|B2RUP2|UN13D_MOUSE Protein unc-13 homolog D OS=Mus muscu	5	3	5	3	4	5	3	5	3	4	7.1	4.5	7.1	4.5	5.8	18372000	2253900	1538000	6168700	3345100
sp|B2RXC1|C >sp|B2RXC1|CD041_MOUSE Putative UPF0636 protein C4orf41 homolog OS=Mu	2	2	2	1	3	2	2	2	1	3	2	2	2	0.8	3.7	6261600	600830	577670	1573900	635610
sp|B2RXR6|A >sp|B2RXR6|ANR44_MOUSE Serine/threonine-protein phosphatase 6 re	6	6	6	6	5	6	6	6	6	5	6.7	6.7	6.7	6.7	5.7	23886000	3050900	2700000	8032400	4039500

sp|Q9JKF1|IC sp|Q9JKF1|IC	26	>sp|Q9JKF1|IQGA1_MOUSE Ras GTPase-activating-like protein IQGAP1 OS=Mus musculus GN=Iqgap1 PE=1 SV=2	24	11	23	11	0.058114	0.076771
sp|P09411|P sp|P09411|P 26;20		>sp|P09411|PGK1_MOUSE Phosphoglycerate kinase 1 OS=Mus musculus GN=Pgk1 PE=1 SV=4;>tr|S4R2M7|S4R2M7_MOUSE Phosphoglycerate kinase OS=Mus musculus GN=Pgk1 PE=1 SV=1	25	19	17	11	0.057522	1.1267
sp|P56480|A sp|P56480|A	26	>sp|P56480|ATPB_MOUSE ATP synthase subunit beta, mitochondrial OS=Mus musculus GN=Atp5b PE=1 SV=2	21	23	21	23	0.057078	1.2592
sp|P07356|A sp|P07356|A 6;5;5;3		>sp|P07356|ANXA2_MOUSE Annexin A2 OS=Mus musculus GN=Anxa2 PE=1 SV=2;>tr|B0V2N7|B0V2N7_MOUSE Annexin (Fragment) OS=Mus musculus GN=Anxa2 PE=1 SV=1;>tr|B0V2N5|B0V2N5_MOUSE Annexin (Fragment) OS=	4	3	4	3	0.057076	0.30118
sp|Q8BMJ2|: sp|Q8BMJ2|:	12	>sp|Q8BMJ2|SYLC_MOUSE Leucine--tRNA ligase, cytoplasmic OS=Mus musculus GN=Lars PE=1 SV=2	10	5	10	5	0.057026	0.081705
sp|Q8R180|E sp|Q8R180|E	10	>sp|Q8R180|ERO1A_MOUSE ERO1-like protein alpha OS=Mus musculus GN=Ero1l PE=1 SV=2	6	7	6	6	0.056933	0.23143
sp|Q8BY71|F sp|Q8BY71|F 5;5		>sp|Q8BY71|HAT1_MOUSE Histone acetyltransferase type B catalytic subunit OS=Mus musculus GN=Hat1 PE=1 SV=1;>tr|A2ATU9|A2ATU9_MOUSE Histone acetyltransferase type B catalytic subunit OS=Mus musculus GN=Hat1 F	5	2	5	2	0.05685	2.1991
sp|Q9D8E6|F sp|Q9D8E6|F	13	>sp|Q9D8E6|RL4_MOUSE 60S ribosomal protein L4 OS=Mus musculus GN=Rpl4 PE=1 SV=3	8	9	8	9	0.056409	0.80416
sp|Q9QYI3|C sp|Q9QYI3|C 15;8;5		>sp|Q9QYI3|DNJC7_MOUSE DnaJ homolog subfamily C member 7 OS=Mus musculus GN=Dnajc7 PE=1 SV=2;>tr|F7BTP8|F7BTP8_MOUSE DnaJ homolog subfamily C member 7 (Fragment) OS=Mus musculus GN=Dnajc7 PE=4 SV=1	13	10	13	10	0.055712	3.6388
sp|Q99LF4|R sp|Q99LF4|R	15	>sp|Q99LF4|RTCB_MOUSE tRNA-splicing ligase RtcB homolog OS=Mus musculus GN=Rtcb PE=2 SV=1	12	7	12	7	0.055707	1.6886
sp|O08749|C sp|O08749|C	12	>sp|O08749|DLDH_MOUSE Dihydrolipoyl dehydrogenase, mitochondrial OS=Mus musculus GN=Dld PE=1 SV=2	4	11	4	11	0.055431	2.475
sp|Q99MR6-: sp|Q99MR6-: 11;11;11;11		>sp|Q99MR6-3|SRRT_MOUSE Isoform C of Serrate RNA effector molecule homolog OS=Mus musculus GN=Srrt;>sp|Q99MR6-4|SRRT_MOUSE Isoform D of Serrate RNA effector molecule homolog OS=Mus musculus GN=Srrt;>sp|	11	2	11	2	0.055317	1.2842
sp|P97310|N sp|P97310|N	15	>sp|P97310|MCM2_MOUSE DNA replication licensing factor MCM2 OS=Mus musculus GN=Mcm2 PE=1 SV=3	14	7	14	7	0.054431	0.04463
sp|P05201|A sp|P05201|A 6;2		>sp|P05201|AATC_MOUSE Aspartate aminotransferase, cytoplasmic OS=Mus musculus GN=Got1 PE=1 SV=3	6	5	6	5	0.054066	1.5951
sp|Q8CIE6|C sp|Q8CIE6|C 24;24;2		>sp|Q8CIE6|COPA_MOUSE Coatomer subunit alpha OS=Mus musculus GN=Copa PE=1 SV=2;>tr|F8WHL2|F8WHL2_MOUSE Coatomer subunit alpha OS=Mus musculus GN=Copa PE=1 SV=1	24	8	24	8	0.053982	0.10847
sp|P49718|N 14;14		>sp|P49718|MCM5_MOUSE DNA replication licensing factor MCM5 OS=Mus musculus GN=Mcm5 PE=2 SV=1;>tr|Q52KC3|Q52KC3_MOUSE DNA replication licensing factor MCM5 OS=Mus musculus GN=Mcm5 PE=2 SV=1	11	5	11	5	0.053574	0.14352
sp|Q9CZW5| sp|Q9CZW5|	9	>sp|Q9CZW5|TOM70_MOUSE Mitochondrial import receptor subunit TOM70 OS=Mus musculus GN=Tomm70a PE=1 SV=2	8	5	8	5	0.053422	2.8352
tr|A2ACG7|A tr|A2ACG7|A 12;12		>tr|A2ACG7|A2ACG7_MOUSE Dolichyl-diphosphooligosaccharide--protein glycosyltransferase subunit 2 OS=Mus musculus GN=Rpn2 PE=4 SV=1;>sp|Q9DBG6|RPN2_MOUSE Dolichyl-diphosphooligosaccharide--protein glycosyltra	10	6	10	6	0.053088	0.073934
sp|Q3UM45| sp|Q3UM45| 6;3		>sp|Q3UM45|PP1R7_MOUSE Protein phosphatase 1 regulatory subunit 7 OS=Mus musculus GN=Ppp1r7 PE=1 SV=2;>tr|A0A087WRA7|A0A087WRA7_MOUSE Protein phosphatase 1 regulatory subunit 7 (Fragment) OS=Mus musc	6	3	6	3	0.052731	1.5368
sp|Q80X90|F sp|Q80X90|F	24	>sp|Q80X90|FLNB_MOUSE Filamin-B OS=Mus musculus GN=Flnb PE=1 SV=3	24	3	22	3	0.052708	0.16831
sp|P26443|D sp|P26443|D 23;5		>sp|P26443|DHE3_MOUSE Glutamate dehydrogenase 1, mitochondrial OS=Mus musculus GN=Glud1 PE=1 SV=1	15	20	15	20	0.052075	1.2795
sp|P08003|P sp|P08003|P	22	>sp|P08003|PDIA4_MOUSE Protein disulfide-isomerase A4 OS=Mus musculus GN=Pdia4 PE=1 SV=3	10	18	10	18	0.052046	1.3794
sp|Q8CGC7|: sp|Q8CGC7|:	16	>sp|Q8CGC7|SYEP_MOUSE Bifunctional glutamate/proline--tRNA ligase OS=Mus musculus GN=Eprs PE=1 SV=4	12	10	12	10	0.051999	0.069001
sp|Q3TXS7|F sp|Q3TXS7|F 19;2		>sp|Q3TXS7|PSMD1_MOUSE 26S proteasome non-ATPase regulatory subunit 1 OS=Mus musculus GN=Psmd1 PE=1 SV=1	19	5	19	5	0.051931	0.50945
sp|P42208|Si 9;8;6;6;5;4;		>sp|P42208|SEPT2_MOUSE Septin-2 OS=Mus musculus GN=Sept2 PE=1 SV=2;>tr|E9Q3V6|E9Q3V6_MOUSE Septin-2 OS=Mus musculus GN=Sept2 PE=1 SV=1;>tr|F6WYM0|F6WYM0_MOUSE Septin-2 (Fragment) OS=Mus muscult	8	6	8	6	0.050954	1.4894
sp|Q9ERK4|> sp|Q9ERK4|> 19;18;13;8;1		>sp|Q9ERK4|XPO2_MOUSE Exportin-2 OS=Mus musculus GN=Cse1l PE=2 SV=1;>tr|E9Q1T9|E9Q1T9_MOUSE Exportin-2 OS=Mus musculus GN=Cse1l PE=4 SV=1;>tr|F6ZEW4|F6ZEW4_MOUSE Exportin-2 (Fragment) OS=Mus musc	18	8	18	8	0.05084	0.46349
sp|P47856-2 sp|P47856-2 16;16;2;1;1		>sp|P47856-2|GFPT1_MOUSE Isoform 2 of Glutamine--fructose-6-phosphate aminotransferase [isomerizing] 1 OS=Mus musculus GN=Gfpt1;>sp|P47856|GFPT1_MOUSE Glutamine--fructose-6-phosphate aminotransferase [isome	15	10	15	10	0.049877	0.33068
sp|Q9D0I9|S sp|Q9D0I9|S	15	>sp|Q9D0I9|SYRC_MOUSE Arginine--tRNA ligase, cytoplasmic OS=Mus musculus GN=Rars PE=2 SV=2	12	9	12	9	0.049721	0.081592
sp|Q62465|\ sp|Q62465|\	4	>sp|Q62465|VAT1_MOUSE Synaptic vesicle membrane protein VAT-1 homolog OS=Mus musculus GN=Vat1 PE=1 SV=3	3	3	3	3	0.049515	0.94596
sp|P25206|N sp|P25206|N	17	>sp|P25206|MCM3_MOUSE DNA replication licensing factor MCM3 OS=Mus musculus GN=Mcm3 PE=1 SV=1	16	7	16	7	0.048894	1.0213
tr|E9PYI8|E9 tr|E9PYI8|E9 9;9		>tr|E9PYI8|E9PYI8_MOUSE Ubiquitin carboxyl-terminal hydrolase OS=Mus musculus GN=Usp14 PE=1 SV=1;>sp|Q9JMA1|UBP14_MOUSE Ubiquitin carboxyl-terminal hydrolase 14 OS=Mus musculus GN=Usp14 PE=1 SV=3	7	5	7	5	0.048752	0.084276
tr|B1AU76|B tr|B1AU76|B 6;6;6;5		>tr|B1AU76|B1AU76_MOUSE Nuclear autoantigenic sperm protein OS=Mus musculus GN=Nasp PE=4 SV=1;>tr|B1AU75|B1AU75_MOUSE Nuclear autoantigenic sperm protein OS=Mus musculus GN=Nasp PE=1 SV=1;>sp|Q99MD	4	4	4	4	0.048594	1.0131
sp|Q8BP47|: sp|Q8BP47|:	8	>sp|Q8BP47|SYNC_MOUSE Asparagine--tRNA ligase, cytoplasmic OS=Mus musculus GN=Nars PE=1 SV=2	4	5	4	5	0.047918	0.33956
sp|Q3U1J4|C sp|Q3U1J4|C	28	>sp|Q3U1J4|DDB1_MOUSE DNA damage-binding protein 1 OS=Mus musculus GN=Ddb1 PE=1 SV=2	26	9	26	9	0.047812	0.067481
sp|Q64514-2 sp|Q64514-2 11;10;5;3;2;1		>sp|Q64514-2|TPP2_MOUSE Isoform Short of Tripeptidyl-peptidase 2 OS=Mus musculus GN=Tpp2;>sp|Q64514|TPP2_MOUSE Tripeptidyl-peptidase 2 OS=Mus musculus GN=Tpp2 PE=1 SV=3	7	5	7	5	0.04714f	0.04701
sp|Q9CZU6|(sp|Q9CZU6|(7;4		>sp|Q9CZU6|CISY_MOUSE Citrate synthase, mitochondrial OS=Mus musculus GN=Cs PE=1 SV=1;>tr|Q80X68|Q80X68_MOUSE Citrate synthase OS=Mus musculus GN=Csl PE=1 SV=1	7	6	7	6	0.047128	1.0409
sp|Q8VDM4| 20;11		>sp|Q8VDM4|PSMD2_MOUSE 26S proteasome non-ATPase regulatory subunit 2 OS=Mus musculus GN=Psmd2 PE=1 SV=1;>tr|J3KMQ2|J3KMQ2_MOUSE Uncharacterized protein OS=Mus musculus GN=Gm5422 PE=4 SV=1	18	4	18	4	0.046759	0.29153
tr|Q3UJQ9|C tr|Q3UJQ9|C 11;11		>tr|Q3UJQ9|Q3UJQ9_MOUSE Succinyl-CoA:3-ketoacid-coenzyme A transferase OS=Mus musculus GN=Oxct1 PE=1 SV=1;>sp|Q9D0K2|SCOT1_MOUSE Succinyl-CoA:3-ketoacid coenzyme A transferase 1, mitochondrial OS=Mus mu	4	10	4	10	0.04655	1.1111
sp|Q8JZQ9|E sp|Q8JZQ9|E	15	>sp|Q8JZQ9|EIF3B_MOUSE Eukaryotic translation initiation factor 3 subunit B OS=Mus musculus GN=Eif3b PE=1 SV=1	14	5	14	5	0.046486	0.51806
sp|Q99MN1| 14;14		>sp|Q99MN1|SYK_MOUSE Lysine--tRNA ligase OS=Mus musculus GN=Kars PE=1 SV=1;>tr|Q8R2P8|Q8R2P8_MOUSE Lysine--tRNA ligase OS=Mus musculus GN=Kars PE=1 SV=1	6	10	6	10	0.046381	0.058249
sp|Q8BFZ3|A sp|Q8BFZ3|A	3	>sp|Q8BFZ3|ACTBL_MOUSE Beta-actin-like protein 2 OS=Mus musculus GN=Actbl2 PE=1 SV=1	2	3	2	3	0.046302	0.08964
sp|P63037|D sp|P63037|D 7;4;2;2		>sp|P63037|DNJA1_MOUSE DnaJ homolog subfamily A member 1 OS=Mus musculus GN=Dnaja1 PE=1 SV=1;>tr|B1AXY1|B1AXY1_MOUSE DnaJ homolog subfamily A member 1 (Fragment) OS=Mus musculus GN=Dnaja1 PE=4 SV=	7	2	7	2	0.046259	1.7894
sp|Q8BKC5| 14;13;1		>sp|Q8BKC5|IPO5_MOUSE Importin-5 OS=Mus musculus GN=Ipo5 PE=1 SV=3;>sp|Q8BKC5-2|IPO5_MOUSE Isoform 2 of Importin-5 OS=Mus musculus GN=Ipo5	13	7	13	7	0.046216	0.42677
sp|Q8R016|E sp|Q8R016|E 9;7;3;1;1		>sp|Q8R016|BLMH_MOUSE Bleomycin hydrolase OS=Mus musculus GN=Blmh PE=1 SV=1;>tr|E9PY26|E9PY26_MOUSE Bleomycin hydrolase (Fragment) OS=Mus musculus GN=Blmh PE=4 SV=1	5	7	5	7	0.046206	0.70779
sp|Q8BT60|C sp|Q8BT60|C 6;1;1;1;1;1;		>sp|Q8BT60|CPNE3_MOUSE Copine-3 OS=Mus musculus GN=Cpne3 PE=2 SV=2	6	4	4	3	0.046142	0.5567
tr|Q8C872|Q tr|Q8C872|Q 5;5		>tr|Q8C872|Q8C872_MOUSE Transferrin receptor protein 1 OS=Mus musculus GN=Tfrc PE=1 SV=1;>sp|Q62351|TFR1_MOUSE Transferrin receptor protein 1 OS=Mus musculus GN=Tfrc PE=1 SV=1	3	3	3	3	0.046049	4.1427
<mark>sp|Q6ZWN5| sp|Q6ZWN5| 4;3;3;1</mark>		<mark>>sp|Q6ZWN5|RS9_MOUSE 40S ribosomal protein S9 OS=Mus musculus GN=Rps9 PE=1 SV=3;>tr|F7CJS8|F7CJS8_MOUSE 40S ribosomal protein S9 (Fragment) OS=Mus musculus GN=Rps9 PE=1 SV=1;>tr|D3YWH9|D3YWH9_MOUS</mark>	<mark>3</mark>	<mark>1</mark>	<mark>3</mark>	<mark>1</mark>	<mark>0.0456</mark>	<mark>0.051274</mark>
sp|Q8K2B3|S sp|Q8K2B3|S	17	>sp|Q8K2B3|SDHA_MOUSE Succinate dehydrogenase [ubiquinone] flavoprotein subunit, mitochondrial OS=Mus musculus GN=Sdha PE=1 SV=1	9	14	9	14	0.045573	0.048159
sp|P61979-3 sp|P61979-3 15;15;14;14;1		>sp|P61979-3|HNRPK_MOUSE Isoform 3 of Heterogeneous nuclear ribonucleoprotein K OS=Mus musculus GN=Hnrnpk;>tr|B2M1R6|B2M1R6_MOUSE Heterogeneous nuclear ribonucleoprotein K OS=Mus musculus GN=Hnrnpk F	15	11	15	11	0.045364	0.19305
sp|Q8BWY3| sp|Q8BWY3|	11	>sp|Q8BWY3|ERF1_MOUSE Eukaryotic peptide chain release factor subunit 1 OS=Mus musculus GN=Etf1 SV=4	9	5	9	5	0.045354	1.1107
tr|E9QS9I9|E5 tr|E9QS9I9|E5 7;7;5;1		>tr|E9QS9I9|E9QS9I9_MOUSE 26S proteasome non-ATPase regulatory subunit 13 OS=Mus musculus GN=Psmd13 PE=4 SV=1;>sp|Q9WVJ2|PSD13_MOUSE 26S proteasome non-ATPase regulatory subunit 13 OS=Mus musculus GN=F	6	4	6	4	0.044999	0.87756
sp|Q9Z1D1|E sp|Q9Z1D1|E	6	>sp|Q9Z1D1|EIF3G_MOUSE Eukaryotic translation initiation factor 3 subunit G OS=Mus musculus GN=Eif3g PE=1 SV=2	6	3	6	3	0.044605	0.26334
sp|P62334|P sp|P62334|P	16	>sp|P62334|PRS10_MOUSE 26S protease regulatory subunit 10B OS=Mus musculus GN=Psmc6 PE=1 SV=1	15	7	15	7	0.044063	0.8418
sp|Q9Z0N1| sp|Q9Z0N1| 13;8		>sp|Q9Z0N1|IF2G_MOUSE Eukaryotic translation initiation factor 2 subunit 3, X-linked OS=Mus musculus GN=Eif2s3x PE=1 SV=2;>tr|A2AAW9|A2AAW9_MOUSE Eukaryotic translation initiation factor 2 subunit 3, X-linked OS=Mu	12	10	2	2	0.042743	1.0203
sp|Q02053|L sp|Q02053|L	18	>sp|Q02053|UBA1_MOUSE Ubiquitin-like modifier-activating enzyme 1 OS=Mus musculus GN=Uba1 PE=1 SV=1	17	7	12	6	0.042395	0.16697
sp|Q99LD4|C sp|Q99LD4|C 7;7;7;6;6		>sp|Q99LD4|CSN1_MOUSE COP9 signalosome complex subunit 1 OS=Mus musculus GN=Gps1 PE=1 SV=1;>tr|Q3MIA8|Q3MIA8_MOUSE COP9 signalosome complex subunit 1 OS=Mus musculus GN=Gps1 PE=1 SV=1;>tr|G3UXW9	4	5	4	5	0.042272	2.761
sp|O88544|C sp|O88544|C 12;11;10;9		>sp|O88544|CSN4_MOUSE COP9 signalosome complex subunit 4 OS=Mus musculus GN=Cops4 PE=1 SV=1;>tr|F6QTS1|F6QTS1_MOUSE COP9 signalosome complex subunit 4 (Fragment) OS=Mus musculus GN=Cops4 PE=4 SV=1;>	11	3	11	3	0.042156	1.3777
sp|Q3THK7|(sp|Q3THK7|(	17	>sp|Q3THK7|GUAA_MOUSE GMP synthase [glutamine-hydrolyzing] OS=Mus musculus GN=Gmps PE=1 SV=1	16	5	16	5	0.042037	0.13979
sp|P22892|A sp|P22892|A 13;13		>sp|P22892|AP1G1_MOUSE AP-1 complex subunit gamma-1 OS=Mus musculus GN=Ap1g1 PE=1 SV=3;>tr|Q8CBB7|Q8CBB7_MOUSE AP-1 complex subunit gamma-1 OS=Mus musculus GN=Ap1g1 PE=2 SV=1	13	2	13	2	0.042001	2.8879
sp|Q922D8|C sp|Q922D8|C	13	>sp|Q922D8|C1TC_MOUSE C-1-tetrahydrofolate synthase, cytoplasmic OS=Mus musculus GN=Mthfd1 PE=1 SV=4	12	7	12	7	0.041573	0.57667
sp|Q91ZJ5-2 sp|Q91ZJ5-2 11;11		>sp|Q91ZJ5-2|UGPA_MOUSE Isoform 2 of UTP--glucose-1-phosphate uridylyltransferase OS=Mus musculus GN=Ugp2;>sp|Q91ZJ5|UGPA_MOUSE UTP--glucose-1-phosphate uridylyltransferase OS=Mus musculus GN=Ugp2 PE=2 S	10	6	10	6	0.041396	0.93157
sp|Q8BG32| sp|Q8BG32| 17;7;5;5;5;5;5		>sp|Q8BG32|PSD11_MOUSE 26S proteasome non-ATPase regulatory subunit 11 OS=Mus musculus GN=Psmd11 PE=1 SV=3	17	9	17	9	0.041119	0.56619
sp|P07901|H sp|P07901|H 32;3;3		>sp|P07901|HS90A_MOUSE Heat shock protein HSP 90-alpha OS=Mus musculus GN=Hsp90aa1 PE=1 SV=4	26	28	24	25	0.040435	0.081797
sp|P97311|N sp|P97311|N 21;20;1		>sp|P97311|MCM6_MOUSE DNA replication licensing factor MCM6 OS=Mus musculus GN=Mcm6 PE=1 SV=1;>tr|Q3ULG5|Q3ULG5_MOUSE DNA replication licensing factor MCM6 OS=Mus musculus GN=Mcm6 PE=1 SV=1	20	8	20	8	0.040412	0.68915
sp|Q91YQ5|I sp|Q91YQ5|I	22	>sp|Q91YQ5|RPN1_MOUSE Dolichyl-diphosphooligosaccharide--protein glycosyltransferase subunit 1 OS=Mus musculus GN=Rpn1 PE=1 SV=1	15	17	15	17	0.040376	0.1113

ID	Description	C1	C2	C3	C4	Val1	Val2
tr|Q3V117|C tr|Q3V117|C 29;28;10	>tr|Q3V117|Q3V117_MOUSE ATP-citrate synthase OS=Mus musculus GN=Acly PE=1 SV=1;>sp|Q91V92|ACLY_MOUSE ATP-citrate synthase OS=Mus musculus GN=Acly PE=1 SV=1	28	11	28	11	0.03796	0.51526
tr|D3YVN7|D tr|D3YVN7|D 14;14;12	>tr|D3YVN7|D3YVN7_MOUSE Elongation factor Tu OS=Mus musculus GN=Gm9755 PE=3 SV=1;>sp|Q8BFR5|EFTU_MOUSE Elongation factor Tu, mitochondrial OS=Mus musculus GN=Tufm PE=1 SV=1;>sp|Q8BFR5-2|EFTU_MOUSE	13	11	13	11	0.037419	1.4475
tr|S4R1M0|S tr|S4R1M0|S 7;7;7;7;7	>tr|S4R1M0|S4R1M0_MOUSE Receptor-type tyrosine-protein phosphatase C OS=Mus musculus GN=Ptprc PE=1 SV=1;>sp|P06800-3|PTPRC_MOUSE Isoform 3 of Receptor-type tyrosine-protein phosphatase C OS=Mus musculus G	7	2	7	2	0.037396	0.087011
sp|P26043|R sp|P26043|R 9;6	>sp|P26043|RADI_MOUSE Radixin OS=Mus musculus GN=Rdx PE=1 SV=3;>tr|Q7TSG6|Q7TSG6_MOUSE Radixin OS=Mus musculus GN=Rdx PE=1 SV=1	4	9	4	9	0.037315	0.076912
sp|Q99KP6|F sp|Q99KP6|F 9;9;8	>sp|Q99KP6|PRP19_MOUSE Pre-mRNA-processing factor 19 OS=Mus musculus GN=Prpf19 PE=1 SV=1;>sp|Q99KP6-2|PRP19_MOUSE Isoform 2 of Pre-mRNA-processing factor 19 OS=Mus musculus GN=Prpf19;>sp|Q99KP6-3|PR	6	6	6	6	0.037178	0.19609
sp|Q99KE1|N sp|Q99KE1|N 13;1	>sp|Q99KE1|MAOM_MOUSE NAD-dependent malic enzyme, mitochondrial OS=Mus musculus GN=Me2 PE=2 SV=1	7	11	7	11	0.037063	1.8396
sp|Q61191|F sp|Q61191|F 4;4	>sp|Q61191|HCFC1_MOUSE Host cell factor 1 OS=Mus musculus GN=Hcfc1 PE=1 SV=2;>tr|B1AUX2|B1AUX2_MOUSE Host cell factor 1 OS=Mus musculus GN=Hcfc1 PE=1 SV=1	3	3	3	3	0.036842	1.6114
sp|Q9JLJ2|AI sp|Q9JLJ2|AI 6;6	>sp|Q9JLJ2|AL9A1_MOUSE 4-trimethylaminobutyraldehyde dehydrogenase OS=Mus musculus GN=Aldh9a1 PE=1 SV=1;>tr|Q3U367|Q3U367_MOUSE 4-trimethylaminobutyraldehyde dehydrogenase OS=Mus musculus GN=Aldh9	3	5	3	5	0.036453	1.1364
sp|Q9D0R2|S sp|Q9D0R2|S 20;2	>sp|Q9D0R2|SYTC_MOUSE Threonine--tRNA ligase, cytoplasmic OS=Mus musculus GN=Tars PE=1 SV=2	12	17	12	17	0.036165	1.8073
sp|Q61699-2 sp|Q61699-2 10;10;10;2;2	>sp|Q61699-2|HS105_MOUSE Isoform HSP105-beta of Heat shock protein 105 kDa OS=Mus musculus GN=Hsph1;>tr|E9Q0U7|E9Q0U7_MOUSE Heat shock protein 105 kDa OS=Mus musculus GN=Hsph1 PE=1 SV=1;>sp|Q61699|F	9	4	9	4	0.036067	0.64025
sp|Q61696|F sp|Q61696|F 10;10	>sp|Q61696|HS71A_MOUSE Heat shock 70 kDa protein 1A OS=Mus musculus GN=Hspa1a PE=1 SV=2;>sp|P17879|HS71B_MOUSE Heat shock 70 kDa protein 1B OS=Mus musculus GN=Hspa1b PE=1 SV=3	8	10	5	7	0.035679	0.23096
sp|Q921M3| sp|Q921M3| 26;25	>sp|Q921M3|SF3B3_MOUSE Splicing factor 3B subunit 3 OS=Mus musculus GN=Sf3b3 PE=1 SV=3	22	13	22	13	0.034636	0.0284
tr|Q8CB58|C tr|Q8CB58|C 8;8;8;6;5;3;2;	>tr|Q8CB58|Q8CB58_MOUSE MCG13402, isoform CRA_d OS=Mus musculus GN=Ptbp1 PE=1 SV=1;>tr|Q8BGJ5|Q8BGJ5_MOUSE MCG13402, isoform CRA_a OS=Mus musculus GN=Ptbp1 PE=1 SV=1;>tr|Q922I7|Q922I7_MOUSE M	5	7	5	7	0.034204	2.1912
sp|O89053|C sp|O89053|C 11;9;5;3;3	>sp|O89053|COR1A_MOUSE Coronin-1A OS=Mus musculus GN=Coro1a PE=1 SV=5;>tr|G3UYK8|G3UYK8_MOUSE Coronin OS=Mus musculus GN=Coro1a PE=3 SV=1	6	9	6	9	0.03412	2.272
sp|Q11136|F sp|Q11136|F 5;1	>sp|Q11136|PEPD_MOUSE Xaa-Pro dipeptidase OS=Mus musculus GN=Pepd PE=2 SV=3	3	5	3	5	0.034007	2.2645
sp|P60122|R sp|P60122|R 18;5;1	>sp|P60122|RUVB1_MOUSE RuvB-like 1 OS=Mus musculus GN=Ruvbl1 PE=1 SV=1	15	16	15	16	0.033464	0.79878
sp|P11499|H sp|P11499|H 58;14;10;8;8	>sp|P11499|HS90B_MOUSE Heat shock protein HSP 90-beta OS=Mus musculus GN=Hsp90ab1 PE=1 SV=3	53	54	33	35	0.033355	0.078963
tr|Q8C605|C tr|Q8C605|C 13;13;10;3;1	>tr|Q8C605|Q8C605_MOUSE 6-phosphofructokinase OS=Mus musculus GN=Pfkp PE=1 SV=1;>sp|Q9WUA3|PFKAP_MOUSE ATP-dependent 6-phosphofructokinase, platelet type OS=Mus musculus GN=Pfkp PE=1 SV=1;>sp|Q9WL	7	11	6	10	0.032967	0.064934
sp|P13439|U sp|P13439|U 6	>sp|P13439|UMPS_MOUSE Uridine 5-monophosphate synthase OS=Mus musculus GN=Umps PE=2 SV=3	4	4	4	4	0.032686	0.80043
sp|Q99K48|N sp|Q99K48|N 12;6;1	>sp|Q99K48|NONO_MOUSE Non-POU domain-containing octamer-binding protein OS=Mus musculus GN=Nono PE=1 SV=3;>sp|Q99K48-2|NONO_MOUSE Isoform 2 of Non-POU domain-containing octamer-binding protein OS=M	10	7	9	6	0.031646	0.87679
sp|P61161|A sp|P61161|A 10	>sp|P61161|ARP2_MOUSE Actin-related protein 2 OS=Mus musculus GN=Actr2 PE=1 SV=1	10	7	10	7	0.031269	0.67628
sp|Q8R146-2 sp|Q8R146-2 7;7	>sp|Q8R146-2|APEH_MOUSE Isoform 2 of Acylamino-acid-releasing enzyme OS=Mus musculus GN=Apeh;>sp|Q8R146|APEH_MOUSE Acylamino-acid-releasing enzyme OS=Mus musculus GN=Apeh PE=2 SV=3	6	6	6	6	0.031262	0.74919
sp|Q60864|S sp|Q60864|S 30	>sp|Q60864|STIP1_MOUSE Stress-induced-phosphoprotein 1 OS=Mus musculus GN=Stip1 PE=1 SV=1	22	24	22	24	0.031256	0.093303
sp|Q8BGQ7| sp|Q8BGQ7|	>sp|Q8BGQ7|SYAC_MOUSE Alanine--tRNA ligase, cytoplasmic OS=Mus musculus GN=Aars PE=1 SV=1	10	7	10	7	0.030953	0.18382
sp|Q99KI0|A sp|Q99KI0|A 17	>sp|Q99KI0|ACON_MOUSE Aconitate hydratase, mitochondrial OS=Mus musculus GN=Aco2 PE=1 SV=1	10	14	10	14	0.030795	0.071606
sp|P26040|E sp|P26040|E 16	>sp|P26040|EZRI_MOUSE Ezrin OS=Mus musculus GN=Ezr PE=1 SV=3	7	16	7	16	0.03067	1.3962
tr|F8WJK8|F tr|F8WJK8|F 6;6;2;1	>tr|F8WJK8|F8WJK8_MOUSE Hsc70-interacting protein OS=Mus musculus GN=St13 PE=1 SV=1;>sp|Q99L47|F10A1_MOUSE Hsc70-interacting protein OS=Mus musculus GN=St13 PE=1 SV=1	4	6	4	6	0.029664	0.72643
sp|P42209|S sp|P42209|S 8;7;3	>sp|P42209|SEPT1_MOUSE Septin-1 OS=Mus musculus GN=Sept1 PE=2 SV=2;>tr|D3Z3V3|D3Z3V3_MOUSE Septin-1 OS=Mus musculus GN=Sept1 PE=3 SV=1	8	3	8	3	0.029662	0.031638
sp|P62192|P sp|P62192|P 16	>sp|P62192|PRS4_MOUSE 26S protease regulatory subunit 4 OS=Mus musculus GN=Psmc1 PE=1 SV=1	16	9	16	9	0.029374	1.1028
sp|P63038|C sp|P63038|C 47;10;5	>sp|P63038|CH60_MOUSE 60 kDa heat shock protein, mitochondrial OS=Mus musculus GN=Hspd1 PE=1 SV=1	33	42	19	26	0.029358	0.18906
sp|P08113|E sp|P08113|E 44;26	>sp|P08113|ENPL_MOUSE Endoplasmin OS=Mus musculus GN=Hsp90b1 PE=1 SV=2;>tr|F7C312|F7C312_MOUSE Endoplasmin (Fragment) OS=Mus musculus GN=Hsp90b1 PE=1 SV=1	39	29	39	29	0.029027	0.79377
sp|P10126|E sp|P10126|E 21;15;15;12	>sp|P10126|EF1A1_MOUSE Elongation factor 1-alpha 1 OS=Mus musculus GN=Eef1a1 PE=1 SV=3;>tr|D3Z3I8|D3Z3I8_MOUSE Elongation factor 1-alpha 1 (Fragment) OS=Mus musculus GN=Eef1a1 PE=1 SV=1;>tr|D3YZ68|D3YZ68	17	19	17	19	0.028853	0.87606
sp|P52480|K sp|P52480|K 46	>sp|P52480|KPYM_MOUSE Pyruvate kinase PKM OS=Mus musculus GN=Pkm PE=1 SV=4	26	44	2	4	0.028837	0.16639
sp|P35564|C sp|P35564|C 17	>sp|P35564|CALX_MOUSE Calnexin OS=Mus musculus GN=Canx PE=1 SV=1	9	13	9	13	0.02848	0.071836
sp|Q9R1T4-2 sp|Q9R1T4-2 2;2;2;2	>sp|Q9R1T4-2|SEPT6_MOUSE Isoform I of Septin-6 OS=Mus musculus GN=Sept6;>sp|Q9R1T4-3|SEPT6_MOUSE Isoform V of Septin-6 OS=Mus musculus GN=Sept6;>sp|Q9R1T4|SEPT6_MOUSE Septin-6 OS=Mus musculus GN=Sep	2	2	2	2	0.028202	0.67317
sp|Q9CZD3|S sp|Q9CZD3|S 14	>sp|Q9CZD3|SYG_MOUSE Glycine--tRNA ligase OS=Mus musculus GN=Gars PE=1 SV=1	9	12	9	12	0.028079	0.72246
sp|Q922B2|S sp|Q922B2|S 17;2	>sp|Q922B2|SYDC_MOUSE Aspartate--tRNA ligase, cytoplasmic OS=Mus musculus GN=Dars PE=2 SV=2	12	13	12	13	0.027965	0.70259
sp|O54734|C sp|O54734|C 16	>sp|O54734|OST48_MOUSE Dolichyl-diphosphooligosaccharide--protein glycosyltransferase 48 kDa subunit OS=Mus musculus GN=Ddost PE=1 SV=2	13	11	13	11	0.027935	1.0806
tr|A2AIW9|A tr|A2AIW9|A 6;6	>tr|A2AIW9|A2AIW9_MOUSE Mitochondrial-processing peptidase subunit alpha OS=Mus musculus GN=Pmpca PE=1 SV=1;>sp|Q9DC61|MPPA_MOUSE Mitochondrial-processing peptidase subunit alpha OS=Mus musculus GN=Pt	6	3	6	3	0.027749	0.67955
tr|G3UVV4|C tr|G3UVV4|C 9;9;9;9;9;2;2;	>tr|G3UVV4|G3UVV4_MOUSE Hexokinase 1, isoform CRA_f OS=Mus musculus GN=Hk1 PE=3 SV=1;>sp|P17710-3|HXK1_MOUSE Isoform HK1 of Hexokinase-1 OS=Mus musculus GN=Hk1;>sp|P17710-4|HXK1_MOUSE Isoform HK1	7	5	5	3	0.027646	0.82552
sp|Q8VIJ6|SF sp|Q8VIJ6|SF 10	>sp|Q8VIJ6|SFPQ_MOUSE Splicing factor, proline- and glutamine-rich OS=Mus musculus GN=Sfpq PE=1 SV=1	10	3	10	3	0.02729	0.87759
sp|Q8C7X2-2 sp|Q8C7X2-2 11;10;10;2	>sp|Q8C7X2-2|EMC1_MOUSE Isoform 2 of ER membrane protein complex subunit 1 OS=Mus musculus GN=Emc1;>tr|Z4YJW0|Z4YJW0_MOUSE ER membrane protein complex subunit 1 OS=Mus musculus GN=Emc1 PE=4 SV=1;>s	10	4	10	4	0.026311	0.10817
sp|Q99KQ4|I sp|Q99KQ4|I 7	>sp|Q99KQ4|NAMPT_MOUSE Nicotinamide phosphoribosyltransferase OS=Mus musculus GN=Nampt PE=1 SV=1	6	4	6	4	0.025923	0.28105
sp|P20152|V sp|P20152|V 31;5;5;5;5;5;5	>sp|P20152|VIME_MOUSE Vimentin OS=Mus musculus GN=Vim PE=1 SV=3	25	23	23	22	0.025835	0.67998
sp|Q9CWJ9|I sp|Q9CWJ9|I	>sp|Q9CWJ9|PUR9_MOUSE Bifunctional purine biosynthesis protein PURH OS=Mus musculus GN=Atic PE=1 SV=2	5	9	5	9	0.024968	0.1015
sp|P20029|G sp|P20029|G 41	>sp|P20029|GRP78_MOUSE 78 kDa glucose-regulated protein OS=Mus musculus GN=Hspa5 PE=1 SV=3	32	37	30	35	0.024848	0.069147
sp|Q8C3J5|D sp|Q8C3J5|D 19;18;12;4	>sp|Q8C3J5|DOCK2_MOUSE Dedicator of cytokinesis protein 2 OS=Mus musculus GN=Dock2 PE=1 SV=3;>tr|Q5SRI3|Q5SRI3_MOUSE Dedicator of cytokinesis protein 2 OS=Mus musculus GN=Dock2 PE=4 SV=2;>tr|D6RGU3|D6RG	19	2	19	2	0.024791	0.052884
sp|Q78ZA7|N sp|Q78ZA7|N 6	>sp|Q78ZA7|NP1L4_MOUSE Nucleosome assembly protein 1-like 4 OS=Mus musculus GN=Nap1l4 PE=1 SV=1	6	4	4	2	0.024522	0.5533
sp|Q9DCL9|F sp|Q9DCL9|F 10;1;1	>sp|Q9DCL9|PUR6_MOUSE Multifunctional protein ADE2 OS=Mus musculus GN=Paics PE=1 SV=4	9	10	9	10	0.024461	0.44539
sp|Q9D8N0|I sp|Q9D8N0|I 18	>sp|Q9D8N0|EF1G_MOUSE Elongation factor 1-gamma OS=Mus musculus GN=Eef1g PE=1 SV=3	11	14	11	14	0.024093	0.080967
sp|Q9Z1N5|I sp|Q9Z1N5|I 16;6	>sp|Q9Z1N5|DX39B_MOUSE Spliceosome RNA helicase Ddx39b OS=Mus musculus GN=Ddx39b PE=1 SV=1	15	14	8	8	0.023954	0.56751
sp|Q9CPY7-2 sp|Q9CPY7-2 9;9	>sp|Q9CPY7-2|AMPL_MOUSE Isoform 2 of Cytosol aminopeptidase OS=Mus musculus GN=Lap3;>sp|Q9CPY7|AMPL_MOUSE Cytosol aminopeptidase OS=Mus musculus GN=Lap3 PE=1 SV=3	6	6	6	6	0.023774	0.59422
sp|P10630|IF sp|P10630|IF 10;10;8;9	>sp|P10630|IF4A2_MOUSE Eukaryotic initiation factor 4A-II OS=Mus musculus GN=Eif4a2 PE=2 SV=2;>sp|P10630-2|IF4A2_MOUSE Isoform 2 of Eukaryotic initiation factor 4A-II OS=Mus musculus GN=Eif4a2;>tr|Q8BTU6|Q8BTU	7	8	7	8	0.023587	0.77256
sp|P24547|IN sp|P24547|IN 16;1;1;1;1	>sp|P24547|IMDH2_MOUSE Inosine-5-monophosphate dehydrogenase 2 OS=Mus musculus GN=Impdh2 PE=1 SV=2	10	14	10	14	0.022689	1.5108
sp|P47791-2| sp|P47791-2| 8;8	>sp|P47791-2|GSHR_MOUSE Isoform Cytoplasmic of Glutathione reductase, mitochondrial OS=Mus musculus GN=Gsr;>sp|P47791|GSHR_MOUSE Glutathione reductase, mitochondrial OS=Mus musculus GN=Gsr PE=1 SV=3	5	8	5	8	0.022257	0.50517
sp|Q9EQH3| sp|Q9EQH3| 15	>sp|Q9EQH3|VPS35_MOUSE Vacuolar protein sorting-associated protein 35 OS=Mus musculus GN=Vps35 PE=1 SV=1	10	9	10	9	0.022024	0.058463
sp|P60843|IF sp|P60843|IF 23	>sp|P60843|IF4A1_MOUSE Eukaryotic initiation factor 4A-I OS=Mus musculus GN=Eif4a1 PE=1 SV=1	20	20	10	12	0.021727	0.70972
sp|P54071|IC sp|P54071|IC 13;5	>sp|P54071|IDHP_MOUSE Isocitrate dehydrogenase [NADP], mitochondrial OS=Mus musculus GN=Idh2 PE=1 SV=3	13	7	12	6	0.021613	0.59798
sp|Q7TSV4|F sp|Q7TSV4|F 13	>sp|Q7TSV4|PGM2_MOUSE Phosphoglucomutase-2 OS=Mus musculus GN=Pgm2 PE=1 SV=1	11	10	11	10	0.02152	0.67623
sp|P09041|P sp|P09041|P 2	>sp|P09041|PGK2_MOUSE Phosphoglycerate kinase 2 OS=Mus musculus GN=Pgk2 PE=1 SV=4	2	1	2	1	0.021361	0.42144
sp|P09103|P sp|P09103|P 26;7	>sp|P09103|PDIA1_MOUSE Protein disulfide-isomerase OS=Mus musculus GN=P4hb PE=1 SV=2	11	25	11	25	0.021225	1.2402
sp|Q9CXY6|I sp|Q9CXY6|I 16	>sp|Q9CXY6|ILF2_MOUSE Interleukin enhancer-binding factor 2 OS=Mus musculus GN=Ilf2 PE=1 SV=1	16	6	16	6	0.020447	0.53017
sp|Q6P1F6|2 sp|Q6P1F6|2 12	>sp|Q6P1F6|2ABA_MOUSE Serine/threonine-protein phosphatase 2A 55 kDa regulatory subunit B alpha isoform OS=Mus musculus GN=Ppp2r2a PE=1 SV=1	12	6	7	4	0.020093	0.49204
sp|P97384|A sp|P97384|A 6;3	>sp|P97384|ANX11_MOUSE Annexin A11 OS=Mus musculus GN=Anxa11 PE=1 SV=2;>tr|D3Z7U0|D3Z7U0_MOUSE Annexin OS=Mus musculus GN=Anxa11 PE=3 SV=1	3	4	3	4	0.019547	0.49109

ID	Accession	No.	Description					Ratio 1	Ratio 2
sp|Q01853|T	sp|Q01853|T	33	>sp|Q01853|TERA_MOUSE Transitional endoplasmic reticulum ATPase OS=Mus musculus GN=Vcp PE=1 SV=4	29	20	29	20	0.014321	0.41428
sp|P62960|Y	sp|P62960|Y	11;5	>sp|P62960|YBOX1_MOUSE Nuclease-sensitive element-binding protein 1 OS=Mus musculus GN=Ybx1 PE=1 SV=3	11	6	5	1	0.014259	0.37666
sp|P68368|T	sp|P68368|T	21;5;5;2;2	>sp|P68368|TBA4A_MOUSE Tubulin alpha-4A chain OS=Mus musculus GN=Tuba4a PE=1 SV=1	19	19	1	2	0.013979	0.18435
sp|Q8BHN3|	sp|Q8BHN3|	15;15;11	>sp|Q8BHN3|GANAB_MOUSE Neutral alpha-glucosidase AB OS=Mus musculus GN=Ganab PE=1 SV=1;>sp|Q8BHN3-2|GANAB Isoform 2 of Neutral alpha-glucosidase AB OS=Mus musculus GN=Ganab;>sp|Q8BHN3-3|GAI	15	6	15	6	0.013791	0.41182
sp|Q9JMH6-2	sp|Q9JMH6-2	5;5	>sp|Q9JMH6-2|TRXR1_MOUSE Isoform 2 of Thioredoxin reductase 1, cytoplasmic OS=Mus musculus GN=Txnrd1;>sp|Q9JMH6|TRXR1_MOUSE Thioredoxin reductase 1, cytoplasmic OS=Mus musculus GN=Txnrd1 PE=1 SV=3	4	5	4	5	0.013451	0.84537
sp|P58252|E	sp|P58252|E	35	>sp|P58252|EF2_MOUSE Elongation factor 2 OS=Mus musculus GN=Eef2 PE=1 SV=2	31	24	30	23	0.012937	0.41043
sp|P46061|R	sp|P46061|R	3	>sp|P46061|RAGP1_MOUSE Ran GTPase-activating protein 1 OS=Mus musculus GN=Rangap1 PE=1 SV=2	3	1	3	1	0.012854	0.97582
sp|P63017|H	sp|P63017|H	36;35;9;9;8	>sp|P63017|HSP7C_MOUSE Heat shock cognate 71 kDa protein OS=Mus musculus GN=Hspa8 PE=1 SV=1;>tr|Q504P4|Q504P4_MOUSE Heat shock cognate 71 kDa protein OS=Mus musculus GN=Hspa8 PE=1 SV=1	34	30	30	25	0.0128	0.085981
sp|O08848|R	sp|O08848|R	6	>sp|O08848|RO60_MOUSE 60 kDa SS-A/Ro ribonucleoprotein OS=Mus musculus GN=Trove2 PE=1 SV=1	5	4	5	4	0.012554	0.80189
sp|P80317|T	sp|P80317|T	20;19;5;3	>sp|P80317|TCPZ_MOUSE T-complex protein 1 subunit zeta OS=Mus musculus GN=Cct6a PE=1 SV=3;>tr|E9QPA6|E9QPA6_MOUSE T-complex protein 1 subunit zeta OS=Mus musculus GN=Cct6a PE=1 SV=1	15	18	15	18	0.012376	0.68021
sp|P80313|T	sp|P80313|T	25	>sp|P80313|TCPH_MOUSE T-complex protein 1 subunit eta OS=Mus musculus GN=Cct7 PE=1 SV=1	21	20	21	20	0.012018	0.76995
sp|P03958|A	sp|P03958|A	7	>sp|P03958|ADA_MOUSE Adenosine deaminase OS=Mus musculus GN=Ada PE=1 SV=3	7	6	7	6	0.012003	0.19347
sp|P09405|N	sp|P09405|N	20	>sp|P09405|NUCL_MOUSE Nucleolin OS=Mus musculus GN=Ncl PE=1 SV=2	14	15	14	15	0.011983	0.32885
sp|P80315|T	sp|P80315|T	19;16;3	>sp|P80315|TCPD_MOUSE T-complex protein 1 subunit delta OS=Mus musculus GN=Cct4 PE=1 SV=3;>tr|G5E839|G5E839_MOUSE T-complex protein 1 subunit delta OS=Mus musculus GN=Cct4 PE=1 SV=1	15	15	15	15	0.011788	0.76996
sp|P80318|T	sp|P80318|T	26;23;9;3	>sp|P80318|TCPG_MOUSE T-complex protein 1 subunit gamma OS=Mus musculus GN=Cct3 PE=1 SV=1;>tr|Q3U0I3|Q3U0I3_MOUSE T-complex protein 1 subunit gamma OS=Mus musculus GN=Cct3 PE=2 SV=1	19	23	2	2	0.010849	0.028847
sp|P99024|T	sp|P99024|T	26;5;5;3	>sp|P99024|TBB5_MOUSE Tubulin beta-5 chain OS=Mus musculus GN=Tubb5 PE=1 SV=1	25	24	6	6	0.010735	0.15753
tr|A2AFJ1|A2	tr|A2AFJ1|A2	11;11;10;5;3	>tr|A2AFJ1|A2AFJ1_MOUSE Histone-binding protein RBBP7 OS=Mus musculus GN=Rbbp7 PE=1 SV=1;>sp|Q60973|RBBP7_MOUSE Histone-binding protein RBBP7 OS=Mus musculus GN=Rbbp7 PE=1 SV=1;>tr|A2AFI9|A2AFI9_MO	8	9	5	3	0.010275	0.25813
sp|P40142|T	sp|P40142|T	23;1	>sp|P40142|TKT_MOUSE Transketolase OS=Mus musculus GN=Tkt PE=1 SV=1	12	20	12	20	0.0094717	0.0083171
sp|P80314|T	sp|P80314|T	29	>sp|P80314|TCPB_MOUSE T-complex protein 1 subunit beta OS=Mus musculus GN=Cct2 PE=1 SV=4	20	24	20	24	0.0090213	0.56494
sp|P42932|T	sp|P42932|T	31;30;16;3;3;	>sp|P42932|TCPQ_MOUSE T-complex protein 1 subunit theta OS=Mus musculus GN=Cct8 PE=1 SV=3;>tr|H3BL49|H3BL49_MOUSE T-complex protein 1 subunit theta OS=Mus musculus GN=Cct8 PE=1 SV=1;>tr|H3BJB6|H3BJB6_M	24	28	24	28	0.0087983	0.52381
sp|Q61316|F	sp|Q61316|F	26;26	>sp|Q61316|HSP74_MOUSE Heat shock 70 kDa protein 4 OS=Mus musculus GN=Hspa4 PE=1 SV=1;>tr|Q3U2G2|Q3U2G2_MOUSE Heat shock 70 kDa protein 4 OS=Mus musculus GN=Hspa4 PE=1 SV=1	22	21	19	18	0.0087767	0.24501
sp|P26041|N	sp|P26041|N	49	>sp|P26041|MOES_MOUSE Moesin OS=Mus musculus GN=Msn PE=1 SV=3	41	43	28	33	0.0079274	0.015614
tr|F8WIT2|F	tr|F8WIT2|F	23;23	>tr|F8WIT2|F8WIT2_MOUSE Annexin OS=Mus musculus GN=Anxa6 PE=1 SV=1;>sp|P14824|ANXA6_MOUSE Annexin A6 OS=Mus musculus GN=Anxa6 PE=1 SV=3	14	20	14	20	0.0068682	0.01261
sp|Q61233|P	sp|Q61233|P	25;3;3;3	>sp|Q61233|PLSL_MOUSE Plastin-2 OS=Mus musculus GN=Lcp1 PE=1 SV=4	17	22	12	18	0.0058547	0.02048
sp|Q3UV17|I	sp|Q3UV17|I	2	>sp|Q3UV17|K22O_MOUSE Keratin, type II cytoskeletal 2 oral OS=Mus musculus GN=Krt76 PE=2 SV=1	2	2	2	2	0.0057514	0.14536

* Interaction partner of peptide **27** is highlighted yellow, having the higher SILAC ratio in the forward but small in the cross-over experiment.

Appendix Table 5: Identification of peptide **27** interaction partners in mouse BaF3 cell spiked with MBP-STAT5b followed by Neutravidin pull down in SILAC experiments.

Protein IDs / Fasta headers	Razor + unique peptides A	Razor + unique peptides B	Razor + unique peptides C	Razor + unique peptides D	Razor + unique peptides E	Unique peptides A	Unique peptides B	Unique peptides C	Unique peptides D	Unique peptides E	Sequence coverage A [%]	Sequence coverage B [%]	Sequence coverage C [%]	Sequence coverage D [%]	Sequence coverage E [%]	Intensity	Intensity A	Intensity B	Intensity C	Intensity D
sp|P42232|S >sp|P42232|STA5B_MOUSE Signal transducer and activator of transcri	11	12	10	12	13	2	2	2	2	2	16.8	18.3	14.4	18.3	21.1	106300000	14294000	15145000	25826000	19576000
5|MBP-STAT >5|MBP-STAT5b|MBP-STAT5b	1	2	2	2	3	1	2	2	2	3	7.4	9.5	7.9	9.5	13.3	125100000	623890	2462100	6411800	21674000
sp|Q921M3| >sp|Q921M3|SF3B3_MOUSE Splicing factor 3B subunit 3 OS=Mus muscu	21	26	26	25	26	21	26	26	25	26	22.5	28.1	28.1	27.3	28.1	764770000	51903000	97136000	262900000	144930000
sp|P46172|R >sp|P46172|RS3_BUCAK 30S ribosomal protein S3 (Fragment) OS=Buchr	2	2	1	1	1	2	2	1	1	1	9.8	9.8	3.9	3.9	3.9	10188000	3302100	3796400	995340	1133900
sp|Q2LAP6|T >sp|Q2LAP6|TES_RAT Testin OS=Rattus norvegicus GN=Tes PE=2 SV=1;>	2	2	2	2	2	2	2	2	2	2	6.2	6.2	6.2	6.2	6.2	6179100	759810	921410	2068300	1026300
sp|Q3YWU2| >sp|Q3YWU2|RL2_SHISS 50S ribosomal protein L2 OS=Shigella sonnei (s	3	2	2	2	3	3	2	2	2	3	15.8	12.1	12.1	12.1	15.8	49262000	11024000	9670600	11074000	8378800
sp|A1L1K3|A >sp|A1L1K3|APC5_RAT Anaphase-promoting complex subunit 5 OS=Ratt	3	3	2	3	2	3	3	2	3	2	6.1	6.1	3.4	6.1	3.4	9351500	2072800	1630600	1893400	2718000
sp|A4UMC6| >sp|A4UMC6|TFP11_MONDO Tuftelin-interacting protein 11 OS=Monod	2	2	2	2	2	2	2	2	2	2	3.2	3.2	3.2	3.2	3.2	8762300	1272800	1053300	2717800	1673700
sp|Q9XSU7|F >sp|Q9XSU7|RL27_CANFA 60S ribosomal protein L27 OS=Canis familiari	4	4	4	4	4	4	4	4	4	4	30.9	30.9	30.9	30.9	30.9	79625000	10951000	10408000	22959000	17647000
sp|Q5R924|F >sp|Q5R924|RS20_PONAB 40S ribosomal protein S20 OS=Pongo abelii C	2	2	2	2	2	2	2	2	2	2	12.6	12.6	12.6	12.6	12.6	36985000	5889400	5267700	13035000	13035000
sp|A2A432|C >sp|A2A432|CUL4B_MOUSE Cullin-4B OS=Mus musculus GN=Cul4b PE=	17	16	17	17	18	13	12	13	13	14	22.6	19.9	21.9	22.6	23.2	136130000	23779000	12590000	35255000	26284000
sp|A2A6Q5| >sp|A2A6Q5|CDC27_MOUSE Cell division cycle protein 27 homolog OS=	1	1	1	1	2	1	1	1	1	2	1.8	1.8	1.8	1.8	6.3	7124200	712380	817770	1872200	1592600
sp|Q96SU4| >sp|Q96SU4|OSBL9_HUMAN Oxysterol-binding protein-related protein	2	2	2	2	2	2	2	2	2	2	2.9	2.9	2.9	2.9	2.9	12558000	2436300	1674100	3402500	1933900
sp|A2ADY9| >sp|A2ADY9|DDI2_MOUSE Protein DDI1 homolog 2 OS=Mus musculus C	2	2	1	2	2	2	2	1	2	2	8.3	8.3	4.8	8.3	8.3	9563200	1758400	1647600	1162000	2214200
sp|A2ADY5| >sp|A2AGT5|CKAP5_MOUSE Cytoskeleton-associated protein 5 OS=Mus	6	7	7	7	7	6	7	7	7	7	3.8	4.3	4.3	4.3	4.3	44494000	6146800	5576500	14777000	7252100
sp|A2AN08|L >sp|A2AN08|UBR4_MOUSE E3 ubiquitin-protein ligase UBR4 OS=Mus m	4	4	6	5	5	4	4	6	5	5	1.4	1.2	1.9	1.7	1.7	21995000	1998700	1548700	9706800	4279400
sp|A2AWA9| >sp|A2AWA9|RBGP1_MOUSE Rab GTPase-activating protein 1 OS=Mus r	2	2	3	3	3	2	2	3	3	3	2.4	3.1	4	4	4	11529000	696710	814800	3212400	2482600
sp|Q9ES70|N >sp|Q9ES70|NEK6_MOUSE Serine/threonine-protein kinase Nek6 OS=M	2	3	3	3	3	2	2	2	2	2	12.5	15	15	15	15	10626000	1373800	1235100	3736800	2318200
sp|A2BE28|L >sp|A2BE28|LAS1L_MOUSE Protein LAS1 homolog OS=Mus musculus Gf	7	7	7	7	5	7	7	7	7	5	14.6	14.6	14.6	14.6	10.8	35399000	4113000	3552800	12412000	7146600
sp|A2BH40|/ >sp|A2BH40|ARI1A_MOUSE AT-rich interactive domain-containing prote	2	2	2	2	2	2	2	2	2	2	1.4	1.4	1.4	1.4	1.4	7023800	1085000	950640	1951300	1240700
sp|Q66RN5|I >sp|Q66RN5|EF1A1_FELCA Elongation factor 1-alpha 1 OS=Felis catus Gi	25	23	25	26	26	2	1	1	2	1	59.5	51.9	53.7	60	53.7	6487900000	971480000	668360000	2189600000	1223900000
sp|Q71U34|I >sp|Q71U34|HSP7C_SAOGE Heat shock cognate 71 kDa protein OS=Sagi	33	32	31	31	31	13	12	11	12	12	55.4	51.9	48.6	54.3	53.3	5377700000	1485600000	888430000	1201500000	941860000
sp|A2RSY6|T >sp|A2RSY6|TRM1L_MOUSE TRM1-like protein OS=Mus musculus GN=T	3	2	4	4	4	3	2	4	4	4	7.7	4.7	11	11	11	23596000	1956200	1703400	7832700	4933200
sp|Q8R574|k >sp|Q8R574|KPRB_MOUSE Phosphoribosyl pyrophosphate synthase-ass	2	2	2	2	2	2	2	2	2	2	11.4	11.4	11.4	11.4	11.4	8881100	1350200	1229700	2407800	1629200
sp|Q5R8U3|! >sp|Q5R8U3|SEP11_PONAB Septin-11 OS=Pongo abelii GN=SEPT11 PE=:	3	2	3	3	2	3	2	3	3	2	11.5	6.8	11.5	11.5	6.8	27269000	4831400	3246400	9059400	5086300
sp|Q9Z1K5|/ >sp|Q9Z1K5|ARI1_MOUSE Protein ariadne-1 homolog OS=Mus musculu	3	3	3	3	2	3	3	3	3	2	9.4	9.4	9.4	9.4	4.5	27673000	4072900	2804500	11417000	5458000
sp|A3KGB4|T >sp|A3KGB4|TBC8B_MOUSE TBC1 domain family member 8B OS=Mus n	2	2	3	3	3	2	2	3	3	3	2.3	3.8	4.8	4.8	4.8	6466500	671720	230420	1966500	1687700
sp|Q6VN20|I >sp|Q6VN20|RBP10_HUMAN Ran-binding protein 10 OS=Homo sapiens	3	3	3	3	3	3	3	3	3	3	5.6	5.6	5.6	5.6	5.6	18666000	3777400	2776000	5392700	3614000
sp|Q689Z5|S >sp|Q689Z5|SBNO1_MOUSE Protein strawberry notch homolog 1 OS=N	1	2	6	2	2	1	2	6	2	2	1.4	2.4	8.4	2.1	2.4	15930000	268450	798880	12244000	867640
sp|Q5R6T6|\ >sp|Q5R6T6|WDR91_PONAB WD repeat-containing protein 91 OS=Pong	3	3	3	4	4	3	3	3	4	4	5.1	5.1	5.1	6.6	6.6	17501000	2141500	1969000	4405600	3988300
sp|O08810|L >sp|O08810|U5S1_MOUSE 116 kDa U5 small nuclear ribonucleoprotein	29	27	29	30	29	29	27	29	30	29	40.9	36.5	41.4	41.5	40.3	550890000	60206000	51135000	195320000	106790000
sp|A4FUD6| >sp|A4FUD6|ELMO2_MOUSE Engulfment and cell motility protein 2 OS=I	2	2	2	2	2	2	2	2	2	2	7.1	7.1	7.1	7.1	7.1	5942800	804750	666240	2143900	1321800
sp|Q5RC34|N >sp|Q5RC34|ML12A_PONAB Myosin regulatory light chain 12A OS=Pong	2	3	2	3	3	2	3	2	3	3	17.5	28.1	17.5	28.1	28.1	27797000	3207100	3323600	7746200	6555500
sp|Q5ZJK4|S >sp|Q5ZJK4|STK4_CHICK Serine/threonine-protein kinase 4 OS=Gallus ga	1	0	0	1	1	1	0	0	1	1	2.7	0	0	2.3	2.7	2248100	583990	0	0	1176500
sp|A5EX85|E >sp|A5EX85|EFG_DICNV Elongation factor G OS=Dichelobacter nodosus	2	2	1	2	1	2	2	1	2	1	3.3	3.3	2	3.3	2	8729500	2649700	1960200	1395300	1404600
sp|P46664|P >sp|P46664|PURA2_MOUSE Adenylosuccinate synthetase isozyme 2 OS	4	4	4	4	4	4	4	4	4	4	10.1	10.1	10.1	10.1	10.1	65243000	9550200	7997900	18731000	14754000
sp|P49312|R >sp|P49312|ROA1_MOUSE Heterogeneous nuclear ribonucleoprotein A	8	8	8	7	8	8	8	8	7	8	28.1	28.1	28.1	27.8	28.1	153940000	24924000	25750000	43336000	24039000
sp|Q5R546|/ >sp|Q5R546|ATPA_PONAB ATP synthase subunit alpha, mitochondrial O	5	5	4	5	3	5	5	4	5	3	13.2	13.2	11.4	13.2	7.4	36214000	6435500	4941500	10856000	8861000
sp|O00303|E >sp|O00303|EIF3F_HUMAN Eukaryotic translation initiation factor 3 sul	6	5	6	6	6	6	5	6	6	6	21.8	18.5	21.8	21.8	21.8	81199000	11514000	9716300	26602000	14318000
sp|Q5R4I9|D >sp|Q5R4I9|DDX5_PONAB Probable ATP-dependent RNA helicase DDX5	7	8	9	7	10	1	1	1	1	1	23	23	23.1	23	25.1	170240000	14899000	16571000	54256000	32732000
sp|P84586|H >sp|P84586|HNRPG_RAT Heterogeneous nuclear ribonucleoprotein G O	2	2	2	2	2	2	2	2	2	2	7.7	7.7	7.7	7.7	7.7	14397000	1967500	1915900	5620700	3520800
sp|Q8IXH7|N >sp|Q8IXH7|NELFD_HUMAN Negative elongation factor C/D OS=Homo :	2	2	1	2	1	2	2	1	2	1	4.9	4.9	2.2	4.9	2.2	5298200	800410	935830	958880	1700400
sp|P20280|R >sp|P20280|RL21_RAT 60S ribosomal protein L21 OS=Rattus norvegicus	5	5	5	5	4	5	5	5	5	4	31.9	31.9	31.9	31.9	30	115120000	19754000	13232000	42353000	13061000
sp|Q5TJE9|R >sp|Q5TJE9|RS18_CANFA 40S ribosomal protein S18 OS=Canis familiaris	11	11	11	12	12	11	11	11	12	12	46.7	46.7	46.7	52	52	276860000	31672000	35358000	87745000	68168000
sp|Q6IQE5|A >sp|Q6IQE5|ASNA_DANRE ATPase asna1 OS=Danio rerio GN=asna1 PE=	4	4	4	3	3	4	4	4	3	3	19.4	19.4	19.4	13.2	13.2	52782000	9051400	7422100	14705000	10117000
sp|Q5EB96|S >sp|Q5EB96|SEPT1_RAT Septin-1 OS=Rattus norvegicus GN=Sept1 PE=2	2	3	3	3	3	2	3	3	3	3	7.4	10.4	10.4	10.4	10.4	13934000	1136700	1577600	4672400	3245300
sp|Q6ZQ08|(>sp|Q6ZQ08|CNOT1_MOUSE CCR4-NOT transcription complex subunit 1	2	2	3	2	3	2	2	3	2	3	0.9	0.9	1.3	0.9	1.3	7438900	924680	548460	3087200	1118600
sp|Q5RT64|F >sp|Q5RT64|RS7_FELCA 40S ribosomal protein S7 OS=Felis catus GN=RP	5	5	5	5	5	5	5	5	5	5	25.8	25.8	25.8	25.8	25.8	172090000	23230000	17003000	46851000	44837000
sp|B5FZY7|IF >sp|B5FZY7|IF4A3_TAEGU Eukaryotic initiation factor 4A-III OS=Taeniop	4	6	6	5	4	3	5	5	4	3	15.6	23.4	19.5	20.2	15.1	34187000	4077300	3819900	13442000	6469300
sp|Q6ZWN5| >sp|Q6ZWN5|RS9_MOUSE 40S ribosomal protein S9 OS=Mus musculus	4	5	5	5	5	4	5	5	5	5	14.9	20.1	20.1	20.1	20.1	246870000	29815000	26795000	88074000	52323000
sp|Q4GWZ2| >sp|Q4GWZ2|RSSA_PIG 40S ribosomal protein SA OS=Sus scrofa GN=RP:	12	12	12	13	13	11	11	11	11	11	39.7	39.7	39.7	49.5	49.5	769170000	101480000	92669000	237290000	158520000
sp|Q7ZXV3|/ >sp|Q7ZXV3|ARP2B_XENLA Actin-related protein 2-B OS=Xenopus laevis	4	4	5	5	5	4	4	5	5	5	16	16	19.8	19.8	20.3	91385000	12911000	10761000	32850000	17993000
sp|Q9BT78|(>sp|Q9BT78|CSN4_HUMAN COP9 signalosome complex subunit 4 OS=H	3	4	4	2	3	3	4	4	2	3	12.3	16.5	16.5	7.4	12.3	20035000	2553200	2950800	8140300	3079100
sp|Q8CIG8|A >sp|Q8CIG8|ANM5_MOUSE Protein arginine N-methyltransferase 5 OS=	2	2	2	2	2	2	2	2	2	2	3	3	3	3	3	11188000	2445500	1503200	2964100	2031700
sp|A7Z019|Si >sp|A7Z019|SMCA4_MOUSE Transcription activator BRG1 OS=Bos taurus	3	4	4	5	3	3	4	4	5	3	2.9	3.9	3.9	4.5	2.9	21329000	2506100	1197600	6891100	5517700
sp|Q14677|E >sp|Q14677|EPN4_HUMAN Clathrin interactor 1 OS=Homo sapiens GN=	11	10	9	9	11	2	2	2	2	2	22.9	19.7	16.8	20	19.7	76654000	19374000	12804000	18034000	12758000
sp|Q6Y1R6|C >sp|Q6Y1R6|DPS_PROVU DNA protection during starvation protein OS=	2	2	1	1	1	2	2	1	1	1	22.2	22.2	11.4	11.4	10.8	5464800	1836600	1453700	91	1027400
sp|Q9Y3I0|C\ >sp|Q9Y3I0|CV002_HUMAN UPF0027 protein C22orf28 OS=Homo sapie	6	10	8	10	9	6	10	8	10	9	20.2	28.9	19	28.9	25	90578000	9238000	11404000	18537000	22724000
sp|Q6ZWV3| >sp|Q6ZWV3|RL10_MOUSE 60S ribosomal protein L10 OS=Mus musculu	5	5	5	5	5	5	5	4	5	5	29.9	29.9	24.3	29.9	29.9	189570000	26771000	27596000	45978000	47977000
sp|Q5RDW4| >sp|Q5RDW4|EM55_PONAB 55 kDa erythrocyte membrane protein OS=	4	4	3	4	3	4	4	3	4	3	15	15	9	15	9	30460000	5813800	4767000	4982800	8988800
sp|Q6YKA4|+ >sp|Q6YKA4|HMGB1_CANFA High mobility group protein B1 OS=Canis fa	3	4	4	4	4	3	4	4	4	4	24.2	21.4	27.4	25.6	25.6	39174000	6546400	6129400	11000000	8758400

Protein																				
sp|Q95NE7|N >sp|Q95NE7|MK14_PANTR Mitogen-activated protein kinase 14 OS=Par	2	2	2	2	2	2	2	2	2	2	12.2	12.2	12.2	12.2	12.2	17279000	1893100	1773700	7024100	2807900
sp|O08528|H >sp|O08528|HXK2_MOUSE Hexokinase-2 OS=Mus musculus GN=Hk2 PE	16	13	17	16	15	15	12	16	15	14	22.9	18.6	22.8	22.8	22.6	213210000	28956000	21226000	70757000	39162000
sp|O08529|C >sp|O08529|CAN2_MOUSE Calpain-2 catalytic subunit OS=Mus muscul	9	9	8	7	6	9	9	8	7	6	18.1	18.1	15.6	13.4	11.1	87333000	20415000	12612000	28240000	16661000
sp|Q80UP3|I >sp|Q80UP3|DGKZ_MOUSE Diacylglycerol kinase zeta OS=Mus muscul	2	2	2	2	2	2	2	2	2	2	3.4	3.4	3.4	3.4	3.4	6519200	558280	698370	2283500	1063500
sp|O08582|C >sp|O08582|GTPB1_MOUSE GTP-binding protein 1 OS=Mus musculus G	12	13	12	14	15	12	13	12	14	15	29.2	31.3	30.8	34.1	38.9	235670000	29033000	26180000	58111000	53523000
sp|O08658|N >sp|O08658|NUP88_RAT Nuclear pore complex protein Nup88 OS=Rattu	4	4	2	4	4	4	4	2	4	4	8	8	2.7	8	8	20809000	3387800	2423100	2724700	5672300
sp|Q3ZC89|A >sp|Q3ZC89|AMPM2_BOVIN Methionine aminopeptidase 2 OS=Bos tau	1	2	1	1	2	1	2	1	1	2	4.8	7.8	4.8	4.8	7.8	7404700	1043200	904740	2105300	1216200
sp|O08709|P >sp|O08709|PRDX6_MOUSE Peroxiredoxin-6 OS=Mus musculus GN=Prd	8	7	7	8	8	8	7	7	8	8	51.3	46	46	51.3	51.3	131260000	19136000	14829000	48371000	17490000
sp|Q6P6R2|D >sp|Q6P6R2|DLDH_RAT Dihydrolipoyl dehydrogenase, mitochondrial OS	0	1	0	1	1	0	1	0	1	1	0	4.9	0	3.7	4.9	1819800	0	633840	0	0
sp|O08784|T >sp|O08784|TCOF_MOUSE Treacle protein OS=Mus musculus GN=Tcof1	16	16	13	13	13	16	16	13	13	13	19.5	19.1	16.9	15.6	16.4	187820000	49390000	38391000	47171000	27490000
sp|O08788|D >sp|O08788|DCTN1_MOUSE Dynactin subunit 1 OS=Mus musculus GN=	1	6	16	11	13	1	6	16	11	13	1.3	6.7	20.8	12.4	14	95442000	359570	2703900	58508000	14744000
sp|O08795|D >sp|O08795|GLU2B_MOUSE Glucosidase 2 subunit beta OS=Mus muscu	5	5	5	6	5	5	5	5	6	5	8.6	8.6	8.6	10.6	8.6	149090000	24709000	19286000	38632000	31771000
sp|O08808|D >sp|O08808|DIAP1_MOUSE Protein diaphanous homolog 1 OS=Mus mu	7	11	21	11	12	7	11	21	11	12	7.3	13.1	23.6	12	14	181440000	3058500	4247000	150140000	12911000
sp|O08856|E >sp|O08856|ELL_MOUSE RNA polymerase II elongation factor ELL OS=N	3	3	3	3	2	3	3	3	3	2	6.1	6.1	6.1	6.1	4.3	7164700	993970	1818200	1595400	1540200
sp|O09131|C >sp|O09131|GSTO1_MOUSE Glutathione S-transferase omega-1 OS=Mu	2	2	2	2	2	2	2	2	2	2	7.9	7.9	7.9	7.9	7.9	16828000	2742700	2502000	4750900	2872600
sp|O09159|N >sp|O09159|MA2B1_MOUSE Lysosomal alpha-mannosidase OS=Mus m	6	7	7	7	7	6	7	7	7	7	8.3	9.4	9.4	9.4	9.4	110770000	17767000	13717000	29700000	21709000
sp|P48508|G >sp|P48508|GSH0_RAT Glutamate--cysteine ligase regulatory subunit OS	3	3	2	2	2	3	3	2	2	2	16.1	16.1	10.6	10.6	10.6	30750000	5515100	3988600	9204300	6454300
sp|Q8BMJ3|I >sp|Q8BMJ3|IF1AX_MOUSE Eukaryotic translation initiation factor 1A, X	2	1	1	1	1	2	1	1	1	1	19.4	11.1	11.1	11.1	11.1	6722000	1641200	1023900	1749600	1117500
sp|O14727|A >sp|O14727|APAF_HUMAN Apoptotic protease-activating factor 1 OS=H	0	0	2	2	2	0	0	2	2	2	0	0	2.3	2.3	2.3	3601200	0		1366900	748740
sp|O14776|T >sp|O14776|TCRG1_HUMAN Transcription elongation regulator 1 OS=H	1	1	2	1	1	1	1	1	2	1	1.1	1.1	1.9	1.1	1.1	6582500	557220	437500	4025500	691100
sp|O15891|T >sp|O15891|TCPA_TETPY T-complex protein 1 subunit alpha OS=Tetrahy	1	2	1	2	1	1	2	1	2	1	5.3	7.1	5.3	7.1	5.3	12833000	286930	4799900	1284400	4399100
sp|O18789|R >sp|O18789|RS2_BOVIN 40S ribosomal protein S2 OS=Bos taurus GN=R	8	7	7	7	8	8	7	7	7	8	32.8	26.3	29	26.3	32.8	436960000	44989000	45775000	156010000	101840000
sp|Q5E9A3|P >sp|Q5E9A3|PCBP1_BOVIN Poly(rC)-binding protein 1 OS=Bos taurus GN	5	4	3	4	4	5	4	3	4	4	30.3	27.2	20.8	23.9	27.8	158690000	24506000	21605000	43247000	34687000
sp|P61980|H >sp|P61980|HNRPK_RAT Heterogeneous nuclear ribonucleoprotein K OS	19	21	19	19	18	3	3	3	3	3	45.1	45.1	44.7	44.7	43	566290000	63767000	58798000	195740000	113560000
sp|Q9Z0E0|N >sp|Q9Z0E0|NCDN_MOUSE Neurochondrin OS=Mus musculus GN=Ncdr	5	6	4	5	5	5	6	4	5	5	9.9	9.9	7.7	9.9	9.9	32724000	4664700	4281400	8363800	8183700
sp|O35114|S >sp|O35114|SCRB2_MOUSE Lysosome membrane protein 2 OS=Mus m	0	1	2	1	1	0	1	2	1	1	0	2.5	7.5	2.5	2.5	7129900	0	528210	3839700	1351300
sp|O55029|C >sp|O55029|COPB2_MOUSE Coatomer subunit beta OS=Mus musculus	23	24	26	25	25	23	24	26	25	25	34.6	37.3	38.6	37.3	37.3	1202400000	147700000	110610000	357190000	249460000
sp|O35218|C >sp|O35218|CPSF2_MOUSE Cleavage and polyadenylation specificity fa	8	8	9	9	9	0	1	1	1	0	17.5	15.6	19.6	17.1	17.8	83200000	8255800	6816000	26044000	21070000
sp|O35226|P >sp|O35226|PSMD4_MOUSE 26S proteasome non-ATPase regulatory su	2	3	2	2	3	2	3	2	2	3	10.1	14.9	8	8	14.9	25621000	1610400	5077100	8417900	4460600
sp|O35242|F >sp|O35242|FAN_MOUSE Protein FAN OS=Mus musculus GN=Nsmaf PE	2	2	2	2	2	2	2	2	2	2	3	3	3	3	3	8294800	1067600	732350	2872900	1634600
sp|O54922|E >sp|O54922|EXOC7_RAT Exocyst complex component 7 OS=Rattus norv	4	5	4	5	3	4	5	4	5	3	10.6	13	10.6	13	8.1	19152000	3546500	3518400	4836700	4961400
sp|Q61206|P >sp|Q61206|PA1B2_MOUSE Platelet-activating factor acetylhydrolase IB	2	2	2	2	2	2	2	2	2	2	12.2	12.2	12.2	12.2	12.2	10973000	1640900	1436900	2670300	2354400
sp|Q5RAZ4|C >sp|Q5RAZ4|DHX15_PONAB Putative pre-mRNA-splicing factor ATP-dep	30	30	30	31	32	26	27	26	27	27	38	35.7	41.5	42.4	49.4	1320400000	191430000	137060000	364550000	288390000
sp|O35295|C >sp|O35295|PURB_MOUSE Transcriptional activator protein Pur-beta O	2	3	3	2	3	2	3	3	2	3	16	21.6	21.6	16	21.6	25120000	2575200	3283400	8071600	5218900
sp|Q09167|S >sp|Q09167|SRSF5_RAT Serine/arginine-rich splicing factor 5 OS=Rattus	1	1	2	2	2	1	1	2	2	2	8.6	8.9	14.1	14.1	14.1	13468000	1277000	560810	4270300	3687900
sp|O35350|C >sp|O35350|CAN1_MOUSE Calpain-1 catalytic subunit OS=Mus muscul	16	18	16	17	15	16	16	18	16	17	26.8	28.5	28.6	28.5	26.9	251880000	35872000	29078000	75793000	60169000
sp|O35382|E >sp|O35382|EXOC4_MOUSE Exocyst complex component 4 OS=Mus mus	14	14	17	14	18	14	14	17	14	18	19.5	21.1	25.5	21.5	26.8	110300000	13970000	11729000	32996000	20594000
sp|P38647|G >sp|P38647|GRP75_MOUSE Stress-70 protein, mitochondrial OS=Mus m	16	15	16	16	11	14	13	14	14	10	29.7	27.7	29.7	29.7	20.9	289390000	77882000	50407000	84084000	59464000
sp|P36412|R >sp|P36412|RB11A_DICDI Ras-related protein Rab-11A OS=Dictyosteliu	1	2	2	2	2	1	2	2	2	2	6.1	10.7	10.7	10.7	10.7	8425500	550610	1378200	3271400	1371200
sp|O35547|A >sp|O35547|ACSL4_RAT Long-chain-fatty-acid--CoA ligase 4 OS=Rattus r	3	4	4	4	4	3	4	4	4	4	7.6	9.9	9.9	9.9	9.9	44206000	4783200	3608400	14078000	9535000
sp|O35601|F >sp|O35601|FYB_MOUSE FYN-binding protein OS=Mus musculus GN=Fy	3	3	3	3	3	3	3	3	3	3	6.7	6.7	6.7	6.7	6.7	15552000	2492900	2770000	4573500	2709000
sp|O35615|F >sp|O35615|FOG1_MOUSE Zinc finger protein ZFPM1 OS=Mus muscul	5	7	7	7	7	5	7	7	7	7	9.2	12.1	12.1	12.1	12.1	36953000	2250800	3932200	15935000	6501100
sp|O35638|G >sp|O35638|STAG2_MOUSE Cohesin subunit SA-2 OS=Mus musculus GN	5	6	9	9	9	5	6	9	9	9	6.2	7.6	13.4	13.4	13.4	111970000	5956600	7956900	39687000	26669000
sp|O35643|A >sp|O35643|AP1B1_MOUSE AP-1 complex subunit beta-1 OS=Mus musc	14	15	17	13	16	14	15	17	13	16	29.2	30.1	31.5	28.8	31.4	510040000	49466000	41766000	172870000	99839000
sp|Q63525|N >sp|Q63525|NUDC_RAT Nuclear migration protein nudC OS=Rattus norv	1	1	2	2	2	1	1	2	2	2	3.3	3.3	7.8	7.8	7.8	12708000	1349800	893850	4097400	3137800
sp|O35691|P >sp|O35691|PININ_MOUSE Pinin OS=Mus musculus GN=Pnn PE=1 SV=4	1	3	3	3	1	1	3	3	3	1	1.5	6.1	6.1	6.5	1.5	9831500	636100	1151400	4137800	3047000
sp|Q9Y223|>sp|Q9Y223|GLCNE_HUMAN Bifunctional UDP-N-acetylglucosamine 2-e	3	3	3	3	2	3	3	3	3	2	6.2	6.2	6.2	6.2	3.7	18317000	4725900	2609500	5386700	3554300
sp|O35841|A >sp|O35841|API5_MOUSE Apoptosis inhibitor 5 OS=Mus musculus GN=	7	7	6	6	6	7	7	6	6	6	17.1	17.1	15.5	15.5	15.5	85648000	15465000	10572000	24987000	18497000
sp|Q6GLM9| >sp|Q6GLM9|CSN5_XENLA COP9 signalosome complex subunit 5 OS=Xe	1	1	0	0	1	1	1	1	0	1	4.2	4.2	0	0	2.1	1012400	441880	570550	0	
sp|O35874|S >sp|O35874|SATT_MOUSE Neutral amino acid transporter A OS=Mus m	2	2	2	2	2	2	2	2	2	2	7.1	7.1	7.1	7.1	7.1	11556000	1713300	1480200	2915700	2934000
sp|O35904|P >sp|O35904|PK3CD_MOUSE Phosphatidylinositol-4,5-bisphosphate 3-ki	2	3	4	3	4	2	3	4	3	4	3.4	6.2	8.5	6.2	8.1	26445000	1786800	1291300	8771200	5818800
sp|Q62419|S >sp|Q62419|SH3G1_MOUSE Endophilin-A2 OS=Mus musculus GN=Sh3g	2	3	3	3	2	2	3	3	3	2	7.1	11.4	9.2	11.4	7.1	15282000	1861100	2380400	4375700	3748600
sp|Q9CZ44|N >sp|Q9CZ44|NSF1C_MOUSE NSFL1 cofactor p47 OS=Mus musculus GN=	4	4	4	3	3	4	4	4	3	3	19.7	19.7	19.7	14.6	14.6	18887000	3384700	2623700	7222900	2963200
sp|O43390|H >sp|O43390|HNRPR_HUMAN Heterogeneous nuclear ribonucleoprotein	6	6	5	5	6	6	6	5	5	6	18	18	16.3	17.1	18	84543000	11532000	9032500	23696000	15614000
sp|Q9WVA3| >sp|Q9WVA3|BUB3_MOUSE Mitotic checkpoint protein BUB3 OS=Mus	5	5	4	5	5	5	5	4	5	5	23.3	23.3	17.2	23.3	23.3	64267000	7039900	5966900	22687000	12194000
sp|O55106|S >sp|O55106|STRN_MOUSE Striatin OS=Mus musculus GN=Strn PE=1 SV	2	2	2	2	2	2	2	2	2	2	5.4	5.4	5.4	5.4	5.4	9531600	1604000	1335900	2406200	1924100
sp|Q9UI12|V >sp|Q9UI12|VATH_HUMAN V-type proton ATPase subunit H OS=Homo s	4	4	4	4	4	4	4	4	4	4	11.6	11.6	11.6	11.6	11.6	35110000	4644600	3612600	12256000	6879800
sp|O54692|Z >sp|O54692|ZW10_MOUSE Centromere/kinetochore protein zw10 hom	3	4	3	4	4	3	4	3	4	4	4.7	8.5	4.7	8.5	8.5	18634000	1720200	1856500	4618600	4495800
sp|O54774|A >sp|O54774|AP3D1_MOUSE AP-3 complex subunit delta-1 OS=Mus mus	9	9	9	10	10	9	9	9	10	10	11.7	11.7	10.8	12.6	12.6	79313000	9366000	8281400	25704000	15131000
sp|O54781|S >sp|O54781|SRPK2_MOUSE Serine/threonine-protein kinase SRPK2 OS=	2	1	2	2	2	2	1	2	2	2	5	3.1	6	5	5	9569200	1133700	702510	3146000	2329500
sp|O54824|I >sp|O54824|IL16_MOUSE Pro-interleukin-16 OS=Mus musculus GN=Il16	5	5	4	5	3	5	5	4	5	3	6.7	6.7	4.5	6.7	3.3	43063000	9027300	6505700	9002600	10936000
sp|O54834|R >sp|O54834|RHG06_MOUSE Rho GTPase-activating protein 6 OS=Mus n	4	4	4	4	4	4	4	4	4	4	6.8	6.8	6.8	6.8	6.8	23120000	2912100	3152500	5500800	4343200
sp|O54916|R >sp|O54916|REPS1_MOUSE RalBP1-associated Eps domain-containing p	6	6	5	6	6	6	6	5	6	6	12.5	12.5	11.2	12.5	12.5	51930000	6338100	5689200	13508000	15065000
sp|Q969G3| >sp|Q969G3|SMCE1_HUMAN SWI/SNF-related matrix-associated actin-	2	1	2	2	2	2	1	2	2	2	6.8	3.6	6.8	6.8	6.8	9046100	1281700	443610	3643400	1775000
sp|O54988|S >sp|O54988|SLK_MOUSE STE20-like serine/threonine-protein kinase OS	11	10	11	10	10	5	4	6	6	6	11.3	10.2	11.1	10.1	10.1	62108000	8714800	7668900	23687000	10452000
sp|O55000|P >sp|O55000|PP1RA_RAT Serine/threonine protein phosphatase 1 regula	6	6	6	6	6	6	6	6	6	6	10.7	10.7	10.7	10.7	10.7	51411000	6620400	5463800	13842000	10633000
sp|O55043|A >sp|O55043|ARHG7_RAT Rho guanine nucleotide exchange factor 7 OS=	5	5	5	6	6	5	5	5	6	6	10.1	10.1	11.3	12.7	12.7	32525000	4519700	3256800	10168000	6663600
sp|O55098|S >sp|O55098|STK10_MOUSE Serine/threonine-protein kinase 10 OS=Mu	9	7	10	8	10	9	7	10	8	10	12.4	8.4	12.4	11.4	12.4	60035000	9666400	6323600	19323000	11054000
sp|Q9WVC0| >sp|Q9WVC0|SEPT7_RAT Septin-7 OS=Rattus norvegicus GN=Sept7 PE=1	10	10	10	9	8	10	10	10	9	8	31.4	29.4	29.4	29.4	25.2	157750000	21566000	18460000	49695000	37083000

Protein	1	2	3	4	5	6	7	8	9	10	11	12	13	14	15	16	17	18	19	20
sp|O70318|E >sp|O70318|E41L2_MOUSE Band 4.1-like protein 2 OS=Mus musculus G	0	0	3	0	1	0	0	3	0	1	0	0	8.1	0	1.6	7496000	0	0	6893500	0
sp|O70400|F >sp|O70400|PDLI1_MOUSE PDZ and LIM domain protein 1 OS=Mus mus	1	2	0	2	1	1	2	0	2	1	4.3	12.8	0	12.8	4.3	8959200	1595900	1912000	0	3405200
sp|O70551|S >sp|O70551|SRPK1_MOUSE Serine/threonine-protein kinase SRPK1 OS=	11	10	10	10	11	10	9	9	9	10	22.4	19.9	20.2	19.9	22.4	204110000	28584000	16987000	56693000	46441000
sp|O70566|C >sp|O70566|DIAP2_MOUSE Protein diaphanous homolog 2 OS=Mus mu	3	2	3	1	2	3	2	3	1	2	3.1	2.2	3.1	1.1	2	12021000	1544700	1289100	4845100	991420
sp|Q91Z67|F >sp|Q91Z67|FNBP2_MOUSE SLIT-ROBO Rho GTPase-activating protein 2	5	4	4	5	6	3	2	2	3	4	6.2	4.9	4.9	6.3	7.6	42373000	4780900	3367300	12337000	8869100
sp|P12815|P >sp|P12815|PDCD6_MOUSE Programmed cell death protein 6 OS=Mus	2	2	2	2	2	2	2	2	2	2	11	11	11	11	11	10610000	1453700	933550	3824600	2111000
sp|Q99NB9|S >sp|Q99NB9|SF3B1_MOUSE Splicing factor 3B subunit 1 OS=Mus muscu	27	24	33	29	31	27	24	33	29	31	27.1	25.5	34.5	30.8	34.4	475620000	37680000	27986000	211170000	87056000
sp|O75643|L >sp|O75643|U520_HUMAN U5 small nuclear ribonucleoprotein 200 kDa	2	1	3	3	3	2	1	3	3	3	0.9	0.5	1.9	1.9	1.9	6704400	552800	264320	2609500	1511300
sp|O88874|C >sp|O88874|CCNK_MOUSE Cyclin-K OS=Mus musculus GN=Ccnk PE=1 S	0	0	2	2	1	0	0	2	2	1	0	0	7.8	7.8	3.4	7170500	0	0	3515400	2713300
sp|Q5RA82|H >sp|Q5RA82|HNRPC_PONAB Heterogeneous nuclear ribonucleoprotein	4	4	3	3	3	4	4	3	3	3	15.7	15.7	10.5	12.1	10.5	29188000	5333800	4477400	7822900	6335100
sp|O88342|V >sp|O88342|WDR1_MOUSE WD repeat-containing protein 1 OS=Mus m	12	11	12	13	12	5	5	5	6	5	30.9	28.2	30.9	35.5	34.3	349890000	49737000	48756000	99777000	69237000
sp|O88351|I >sp|O88351|IKKB_MOUSE Inhibitor of nuclear factor kappa-B kinase sub	7	7	9	9	10	7	7	9	9	10	8.6	9.2	13.2	13.2	15.6	39923000	4386800	4640900	11032000	7865100
sp|O88398|A >sp|O88398|AVIL_MOUSE Advillin OS=Mus musculus GN=Avil PE=1 SV=	25	24	23	25	24	25	24	23	25	24	38.6	34.3	35.3	37	35.3	358330000	45225000	36167000	106330000	76353000
sp|O88487|D >sp|O88487|DC1I2_MOUSE Cytoplasmic dynein 1 intermediate chain 2	7	7	7	7	6	7	7	7	7	6	18	18	18	18	18	97503000	13736000	14419000	27352000	19734000
sp|O88512|A >sp|O88512|AP1G2_MOUSE AP-1 complex subunit gamma-like 2 OS=M	2	3	3	3	3	2	2	2	2	2	5.9	8.3	7.1	7.1	7.1	24849000	2091700	1875900	6173600	5992200
sp|Q6TMG5|N >sp|Q6TMG5|NEMO_RAT NF-kappa-B essential modulator OS=Rattus nc	1	1	2	1	0	1	1	2	1	0	2.7	2.7	7.8	2.7	0	1993500	294320	528250	804400	366560
sp|O88532|Z >sp|O88532|ZFR_MOUSE Zinc finger RNA-binding protein OS=Mus musc	6	6	9	8	7	6	6	9	8	7	8.4	8.4	11.7	10.5	9.4	46252000	3107800	4227300	20472000	9743500
sp|Q2HJ60|R >sp|Q2HJ60|ROA2_BOVIN Heterogeneous nuclear ribonucleoproteins A	11	11	9	10	10	11	11	9	10	10	38.7	38.7	34.9	38.7	38.7	363280000	51981000	49287000	115770000	75224000
sp|O88600|H >sp|O88600|HSP74_RAT Heat shock 70 kDa protein 4 OS=Rattus norveg	3	2	2	2	3	3	2	2	2	3	49.8	50.7	51.4	51.3	50.7	81059000	11830000	4109600	14238000	4758500
sp|O88622|P >sp|O88622|PARG_MOUSE Poly(ADP-ribose) glycohydrolase OS=Mus m	3	3	4	4	4	3	3	3	4	4	4.3	4.3	5.3	5.3	5.3	21325000	2307300	1874900	8202300	2950400
sp|O88656|A >sp|O88656|ARC1B_RAT Actin-related protein 2/3 complex subunit 1B O	6	6	7	6	6	6	6	7	6	6	20.2	19.1	23.9	21.8	19.1	77861000	13253000	9177100	23482000	17939000
sp|Q7L7X3|T >sp|Q7L7X3|TAOK1_HUMAN Serine/threonine-protein kinase TAO1 OS=	2	3	3	3	2	2	3	3	3	2	2.2	3.3	3.3	3.3	2	10999000	558560	1933500	3969200	2678900
sp|O88668|C >sp|O88668|CREG1_MOUSE Protein CREG1 OS=Mus musculus GN=Creg	2	2	2	2	2	2	2	2	2	2	13.2	13.2	13.2	13.2	13.2	6383300	886300	788030	1636300	1745300
sp|Q9Z2F5|C >sp|Q9Z2F5|CTBP1_RAT C-terminal-binding protein 1 OS=Rattus norveg	1	1	2	2	2	1	1	2	2	2	1.9	1.9	3.7	3.7	3.7	6630700	310850	443870	2443300	1766600
sp|O88746|T >sp|O88746|TOM1_MOUSE Target of Myb protein 1 OS=Mus musculus	2	2	2	2	2	2	2	2	2	2	8.3	8.3	8.3	8.3	8.3	13611000	1676400	1922500	4829900	2724500
sp|Q6PF93|P >sp|Q6PF93|PK3C3_MOUSE Phosphatidylinositol 3-kinase catalytic subu	1	3	3	3	3	1	3	3	3	3	1.7	6.5	6.5	6.5	6.5	16684000	398290	1590000	6246500	4133900
sp|O88842|F >sp|O88842|FGD3_MOUSE FYVE, RhoGEF and PH domain-containing pr	2	2	1	2	2	2	2	1	2	2	6.3	6.3	4	6.3	6.3	8941100	1476200	1338300	1832800	2063700
sp|O88844|II >sp|O88844|IDHC_MOUSE Isocitrate dehydrogenase [NADP] cytoplasmi	4	2	4	5	3	4	2	4	5	3	14.5	6	14.7	19.3	9.9	15271000	2337800	968600	4990200	5044500
sp|P14152|N >sp|P14152|MDHC_MOUSE Malate dehydrogenase, cytoplasmic OS=M	5	5	6	6	5	5	3	3	4	4	23.4	21.6	26	26	20.1	100320000	10232000	12185000	30760000	18231000
sp|O89042|D >sp|O89042|DPOLA_RAT DNA polymerase alpha catalytic subunit (Fragr	1	1	2	1	1	1	1	2	1	1	1.3	1.1	2.4	1.3	1.1	6235000	513070	384060	3652100	894730
sp|O89053|C >sp|O89053|COR1A_MOUSE Coronin-1A OS=Mus musculus GN=Coro1a	11	12	12	12	12	11	12	12	12	12	29.5	33.6	33.6	33.6	33.6	460670000	54340000	51845000	152990000	97203000
sp|O89079|C >sp|O89079|COPE_MOUSE Coatomer subunit epsilon OS=Mus musculu	3	3	3	3	3	3	3	3	3	3	14	14	14	14	14	20625000	2726300	2914100	6464800	3790500
sp|O89084|F >sp|O89084|PDE4A_MOUSE cAMP-specific 3,5-cyclic phosphodiesterase	3	3	3	3	4	2	2	2	2	3	7.6	7.6	7.6	7.6	10.9	29185000	2828600	2449300	7744900	6386900
sp|Q5SUF2|L >sp|Q5SUF2|LC7L3_MOUSE Luc7-like protein 3 OS=Mus musculus GN=L	3	3	3	3	3	3	3	3	3	3	10	10	10	10	10	18363000	2713700	2628900	6302500	3625100
sp|Q9EPL8|II >sp|Q9EPL8|IPO7_MOUSE Importin-7 OS=Mus musculus GN=Ipo7 PE=1	17	18	18	17	18	17	18	18	17	18	19.1	21.6	21.6	23.4	23.5	405080000	39980000	42208000	123120000	84334000
sp|O95486|S >sp|O95486|SC24A_HUMAN Protein transport protein Sec24A OS=Hom	1	2	2	1	1	1	1	1	0	0	6.8	8.1	9	6.8	6.8	10711000	522170	1147900	5799900	1594200
sp|Q9Z2N8|A >sp|Q9Z2N8|ACL6A_MOUSE Actin-like protein 6A OS=Mus musculus GN	1	3	3	3	3	1	3	3	3	3	3.3	12.6	12.6	12.6	12.6	9920700	518980	1844900	3814000	2181600
sp|P50398|G >sp|P50398|GDIA_RAT Rab GDP dissociation inhibitor alpha OS=Rattus r	2	2	2	1	2	2	2	2	1	2	14.3	14.3	14.3	11.2	14.3	8547900	782990	954630	2599100	1806800
sp|Q5R9Y4|R >sp|Q5R9Y4|RAB7A_PONAB Ras-related protein Rab-7a OS=Pongo abeli	4	4	4	4	3	4	4	4	4	4	20.8	20.8	20.8	20.8	17.9	33289000	4421100	4308000	12990000	7098000
sp|Q9Z1M9|S >sp|Q9Z1M9|SMC1A_RAT Structural maintenance of chromosomes pro	22	20	33	25	26	7	5	11	7	8	21.4	19.1	32.6	24	24.2	281260000	17948000	13515000	169820000	37417000
sp|O97790|T >sp|O97790|TBCD1_BOVIN TBC1 domain family member 1 (Fragment) C	2	2	2	2	2	2	2	2	2	2	4	4	4	4	4	2719900	247200	201710	856710	691100
sp|Q5R5F0|L >sp|Q5R5F0|LDHA_PONAB L-lactate dehydrogenase A chain OS=Pongo a	0	3	1	1	0	0	1	1	0	0	14.5	25.3	23.8	14.5	20.5	6987800	0	6678500	309350	0
sp|P00375|D >sp|P00375|DYR_MOUSE Dihydrofolate reductase OS=Mus musculus G	2	3	3	3	1	2	3	3	3	1	15	16	16	16	5.3	8759700	860190	1029900	3611600	2435600
sp|P16291|F >sp|P16291|FA9_SHEEP Coagulation factor IX (Fragment) OS=Ovis aries	2	2	2	2	2	2	2	2	2	2	10.6	10.6	10.6	10.6	10.6	7187500	1192500	1146800	1614100	1409600
sp|P01012|C >sp|P01012|OVAL_CHICK Ovalbumin OS=Gallus gallus GN=SERPINB14 P	6	5	5	5	6	6	5	5	5	6	26.2	22	20.2	20.2	26.2	61718000	15552000	9142300	13578000	11520000
sp|P01013|C >sp|P01013|OVALX_CHICK Ovalbumin-related protein X (Fragment) OS=	2	2	2	2	2	2	2	2	2	2	15.1	15.1	15.1	15.1	15.1	5304300	890330	893600	1357300	1081200
sp|Q5RAQ8|| >sp|Q5RAQ8|RS24_PONAB 40S ribosomal protein S24 OS=Pongo abelii	2	2	2	2	2	2	2	2	2	2	20.6	20.6	20.6	20.6	20.6	57796000	5764500	5313700	18438000	16349000
sp|P02578|A >sp|P02578|ACT1_ACACA Actin-1 OS=Acanthamoeba castellanii PE=3 SV	2	2	2	2	2	1	1	1	1	1	36	27.7	36	35.5	36	1982800000	315650000	271490000	613690000	415070000
sp|P02701|A >sp|P02701|AVID_CHICK Avidin OS=Gallus gallus GN=AVD PE=1 SV=3	11	11	10	11	11	11	11	10	11	11	54.6	54.6	54.6	54.6	54.6	4734400000	965950000	1515600000	857440000	644890000
sp|P03336|G >sp|P03336|GAG_MLVAV Gag polyprotein OS=AKV murine leukemia vir	5	5	6	6	6	5	5	6	6	6	10.1	10.1	15.6	15.6	15.6	105320000	14473000	13568000	34774000	21872000
sp|Q920P6|A >sp|Q920P6|ADA_RAT Adenosine deaminase OS=Rattus norvegicus GN	2	2	2	0	1	2	2	2	0	1	13.4	13.4	13.4	0	4.5	8058000	1709000	1240000	0	4178500
sp|P04187|G >sp|P04187|GRAB_MOUSE Granzyme B(G,H) OS=Mus musculus GN=Gzr	5	5	5	5	5	5	5	5	5	5	20.6	20.6	20.6	20.6	20.6	74693000	10062000	7694100	20435000	13754000
sp|P04264|K >sp|P04264|K2C1_HUMAN Keratin, type II cytoskeletal 1 OS=Homo sapi	45	45	45	44	45	2	2	2	2	2	67.4	67.5	67.4	67.4	67.5	5651800000	651960000	1882000000	1406800000	1030700000
sp|P08249|N >sp|P08249|MDHM_MOUSE Malate dehydrogenase, mitochondrial OS=	6	7	5	6	5	6	7	5	6	5	28.1	28.1	19.5	21.6	19.5	41839000	9555700	7476800	9074200	9328400
sp|Q90YQ6|R >sp|Q90YQ6|RS17_ICTPU 40S ribosomal protein S17 OS=Ictalurus punct	6	4	6	5	6	6	4	6	5	6	34.3	31.3	34.3	32.1	34.3	162480000	14216000	19749000	59003000	37944000
sp|P04897|G >sp|P04897|GNAI2_RAT Guanine nucleotide-binding protein G(i) subunit	4	4	4	4	4	3	3	3	3	3	17.2	17.2	17.2	17.2	17.2	58458000	10309000	8739900	16363000	10876000
sp|Q6P069|S >sp|Q6P069|SORCN_MOUSE Sorcin OS=Mus musculus GN=Sri PE=1 SV=	2	3	3	3	2	2	3	3	3	2	10.6	14.6	14.6	14.6	10.6	22502000	3408400	4108000	6687500	4524800
sp|P05064|A >sp|P05064|ALDOA_MOUSE Fructose-bisphosphate aldolase A OS=Mus	20	22	19	22	22	3	4	4	3	4	64.8	58	58	58	65.4	1872700000	300800000	302430000	506180000	378030000
sp|P05132|K >sp|P05132|KAPCA_MOUSE cAMP-dependent protein kinase catalytic su	4	3	4	4	4	3	2	3	3	3	16.2	11.4	16.2	16.2	16.2	31073000	4609400	2868400	9566300	6957100
sp|P05202|K >sp|P05202|AATM_MOUSE Aspartate aminotransferase, mitochondrial	2	2	2	2	1	2	2	2	2	1	6.7	6.7	6.7	6.7	3.3	18860000	3459500	2608000	6580400	4114200
sp|P17252|K >sp|P17252|KPCA_HUMAN Protein kinase C alpha type OS=Homo sapie	6	7	7	5	7	6	7	7	5	7	8.9	11.3	11.3	7.6	11.3	55437000	9286600	7029600	15524000	9768800
sp|P05756|R >sp|P05756|RS13_YEAST 40S ribosomal protein S13 OS=Saccharomyces	2	2	2	2	2	2	2	2	2	2	8.6	8.6	8.6	8.6	8.6	73131000	9510400	8027200	21961000	19516000
sp|Q9CQR2|I >sp|Q9CQR2|RS21_MOUSE 40S ribosomal protein S21 OS=Mus musculu	2	2	2	2	2	2	2	2	2	2	28.9	28.9	28.9	28.9	28.9	16078000	3031500	2607700	5624500	2891000
sp|P06151|L >sp|P06151|LDHA_MOUSE L-lactate dehydrogenase A chain OS=Mus mu	10	9	12	10	11	1	1	1	1	1	35.8	32.5	44.9	35.8	41.9	443740000	61767000	56334000	142840000	91274000
sp|Q5RCH1|C >sp|Q5RCH1|CDK1_PONAB Cell division protein kinase 1 OS=Pongo abel	2	2	2	2	2	1	1	1	1	1	9.1	9.1	9.1	9.1	9.1	13595000	2940600	2511100	2510400	2207500
sp|P06537|G >sp|P06537|GCR_MOUSE Glucocorticoid receptor OS=Mus musculus GN	6	5	7	7	7	6	5	7	7	7	13.7	12.3	13.9	13.9	13.9	35104000	4247700	3685200	11359000	6573500

Protein																				
sp|Q9QY94|(>sp|Q9QY94|GLNA_ACOCA Glutamine synthetase OS=Acomys cahirinus	2	1	2	2	2	2	1	2	2	2	5.6	5.4	5.6	5.6	5.6	15497000	1758100	1530300	5577100	3187100
sp|P47962|R >sp|P47962|RL5_MOUSE 60S ribosomal protein L5 OS=Mus musculus G	14	13	14	14	14	14	13	14	14	14	46.5	46.1	46.5	46.5	46.5	267750000	44011000	42269000	74009000	59512000
sp|Q9GKW3| >sp|Q9GKW3|ALDOC_MACFA Fructose-bisphosphate aldolase C OS=Ma	2	2	2	2	2	2	2	2	2	2	7.1	7.1	7.1	7.1	7.1	316280000	56909000	43326000	90380000	66215000
sp|Q99570|P >sp|Q99570|PI3R4_HUMAN Phosphoinositide 3-kinase regulatory subur	1	2	2	3	3	1	2	2	3	3	1	1.9	1.9	2.9	2.9	8551600	169340	528020	2692700	1956300
sp|Q865C5|L >sp|Q865C5|UBIQ_CAMDR Ubiquitin OS=Camelus dromedarius PE=3 SV	4	3	3	3	3	3	2	2	2	2	55.3	40.8	40.8	40.8	52.6	147020000	29626000	22893000	39620000	33024000
sp|P10107|A >sp|P10107|ANXA1_MOUSE Annexin A1 OS=Mus musculus GN=Anxa1 P	9	11	9	10	10	6	7	6	7	7	25.4	29.5	28.3	29.5	29.5	74438000	10378000	10197000	17801000	18023000
sp|Q6EWQ7| >sp|Q6EWQ7|IF5A1_BOVIN Eukaryotic translation initiation factor 5A-1	2	3	2	4	1	2	3	2	4	1	22.7	23.4	23.4	27.9	7.8	15743000	2041600	2968200	4296100	5679500
sp|Q4KLL0|T >sp|Q4KLL0|TCEA1_RAT Transcription elongation factor A protein 1 OS=	3	3	3	3	3	3	3	3	3	3	11.6	11.6	11.6	11.6	11.6	17692000	3842600	3271200	4389000	3898200
sp|P10852|4 >sp|P10852|4F2_MOUSE 4F2 cell-surface antigen heavy chain OS=Mus r	21	20	21	21	21	21	20	21	21	21	41.8	41.8	41.8	41.8	41.8	1077200000	212000000	148450000	258440000	221290000
sp|Q6PCU2|\ >sp|Q6PCU2|VATE1_RAT V-type proton ATPase subunit E 1 OS=Rattus n	2	2	2	2	2	2	2	2	2	2	11.1	11.1	11.1	11.1	11.1	11808000	1557900	2124000	3716300	2300500
sp|P11103|P >sp|P11103|PARP1_MOUSE Poly [ADP-ribose] polymerase 1 OS=Mus m	3	3	3	3	3	1	1	1	1	1	18.6	18.6	20.4	18.6	20.4	56357000	6670700	3847800	21629000	12834000
sp|Q9D1R9|F >sp|Q9D1R9|RL34_MOUSE 60S ribosomal protein L34 OS=Mus muscu	2	2	2	2	2	2	2	2	2	2	14.5	14.5	14.5	14.5	14.5	36338000	5340900	5156600	11086000	7289300
sp|P11438|L >sp|P11438|LAMP1_MOUSE Lysosome-associated membrane glycoprot	5	5	5	5	5	5	5	5	5	5	11.8	11.8	11.8	11.8	11.8	98738000	14463000	13038000	28718000	20067000
sp|P11499|H >sp|P11499|HS90B_MOUSE Heat shock protein HSP 90-beta OS=Mus m	37	36	39	38	40	2	2	2	2	2	64.6	61.5	68.1	70	70.6	1.8914E+10	3089300000	2113800000	5229100000	3600400000
sp|P11835|I >sp|P11835|ITB2_MOUSE Integrin beta-2 OS=Mus musculus GN=Itgb2 P	7	6	7	7	7	7	6	7	7	7	13	11.3	13	13	13	66831000	11217000	7267900	18280000	12715000
sp|P11983|T >sp|P11983|TCPA_MOUSE T-complex protein 1 subunit alpha OS=Mus n	24	23	24	25	27	13	12	12	13	15	57	57.9	54.3	59.5	61	860880000	125530000	120710000	241600000	199020000
sp|P12265|B >sp|P12265|BGLR_MOUSE Beta-glucuronidase OS=Mus musculus GN=	3	3	3	3	2	3	3	3	3	2	5.7	5.7	5.7	5.7	4.3	17224000	3675600	2723000	4535800	4520200
sp|P12382|K >sp|P12382|K6PL_MOUSE 6-phosphofructokinase, liver type OS=Mus m	14	13	15	15	13	3	2	3	3	2	28.3	25.6	29.7	29.7	27.4	664630000	103090000	68544000	192130000	133920000
sp|P61257|R >sp|P61257|RL26_BOVIN 60S ribosomal protein L26 OS=Bos taurus GN=	3	2	3	3	3	3	2	3	3	3	20	13.8	20	20	20	22954000	2970700	1752400	7165900	6296700
sp|Q4R5C2|F >sp|Q4R5C2|RL7A_MACFA 60S ribosomal protein L7a OS=Macaca fascic	6	7	7	7	7	6	7	7	7	7	23.3	27.8	27.8	27.8	27.8	346400000	39409000	32436000	106770000	82075000
sp|P13020|G >sp|P13020|GELS_MOUSE Gelsolin OS=Mus musculus GN=Gsn PE=1 SV	14	12	13	11	13	6	5	5	5	5	28.3	21.9	25.5	25.5	25.5	367100000	60881000	45242000	100280000	69123000
sp|P13439|P >sp|P13439|PYR5_MOUSE Uridine 5-monophosphate synthase OS=Mus	6	6	6	6	6	4	4	4	4	4	16	16.6	16.6	13.9	13.9	70236000	10625000	7229200	23517000	14970000
sp|P62265|R >sp|P62265|RS14_CRIGR 40S ribosomal protein S14 OS=Cricetulus grise	5	4	5	5	5	5	4	5	5	5	33.1	31.8	33.1	33.1	33.1	95836000	14082000	12895000	27973000	22573000
sp|P13597|I >sp|P13597|ICAM1_MOUSE Intercellular adhesion molecule 1 OS=Mus	2	2	2	2	2	2	2	2	2	2	4.5	4.5	4.5	4.5	4.5	6407800	1259900	767100	1959700	904860
sp|P13705|N >sp|P13705|MSH3_MOUSE DNA mismatch repair protein Msh3 OS=Mu	3	1	3	3	3	2	1	2	2	2	5.4	2.3	5.4	5.4	5.4	19475000	1723400	732720	6322500	4762900
sp|P13864|D >sp|P13864|DNMT1_MOUSE DNA (cytosine-5)-methyltransferase 1 OS=	1	2	3	2	3	1	2	3	2	3	0.5	1.4	2.3	1.5	2.3	6748000	285030	477440	3126500	978990
sp|P14115|R >sp|P14115|RL27A_MOUSE 60S ribosomal protein L27a OS=Mus muscu	3	3	3	4	3	3	3	3	3	4	17.6	17.6	17.6	24.3	17.6	140250000	16903000	14370000	44506000	31610000
sp|Q3TOX6|R >sp|Q3TOX6|RS16_BOVIN 40S ribosomal protein S16 OS=Bos taurus GN	8	8	8	8	8	8	8	8	8	8	40.4	40.4	40.4	40.4	40.4	341030000	44231000	42176000	99837000	76108000
sp|P14148|R >sp|P14148|RL7_MOUSE 60S ribosomal protein L7 OS=Mus musculus G	10	10	10	10	10	10	10	10	10	10	31.1	31.1	31.1	31.1	31.1	347170000	36632000	31112000	112460000	94038000
sp|P14211|C >sp|P14211|CALR_MOUSE Calreticulin OS=Mus musculus GN=Calr PE=1	6	6	6	6	6	6	6	6	6	6	21.4	21.4	21.4	21.4	21.4	160710000	17980000	9780200	60871000	33164000
sp|Q6AYB5|S >sp|Q6AYB5|SRP54_RAT Signal recognition particle 54 kDa protein OS=F	6	5	5	6	6	6	5	5	6	6	18.7	17.3	17.3	18.7	18.7	28167000	4042700	3430100	7602600	6621900
sp|P14685|P >sp|P14685|PSMD3_MOUSE 26S proteasome non-ATPase regulatory su	17	16	16	17	16	17	16	16	17	16	38.7	38.7	40.9	38.7	39.2	296890000	40667000	30320000	95490000	63359000
sp|P14824|A >sp|P14824|ANXA6_MOUSE Annexin A6 OS=Mus musculus GN=Anxa6 P	22	23	20	22	19	16	17	15	16	15	38.2	41.6	36.7	40.4	33.3	300480000	51308000	41267000	84350000	62922000
sp|P14869|R >sp|P14869|RLA0_MOUSE 60S acidic ribosomal protein P0 OS=Mus mus	8	10	9	8	9	8	10	9	8	9	39.1	49.5	45.4	39.1	45.4	321050000	44000000	52018000	94128000	59640000
sp|Q8WNW3| >sp|Q8WNW3|PLAK_PIG Junction plakoglobin OS=Sus scrofa GN=Jup PE	3	3	3	2	2	3	3	3	2	2	5.6	5.6	5.6	3.2	4	8731900	2214600	2542400	2108900	491240
sp|P14963|E >sp|P14963|EF1A_EUGGR Elongation factor 1-alpha OS=Euglena gracilis	2	1	2	2	2	1	0	1	1	1	18.2	14.4	18.2	17.5	18.2	21159000	4105400	773370	5415200	7606100
sp|P15056|B >sp|P15056|BRAF_HUMAN Serine/threonine-protein kinase B-raf OS=Ho	1	1	3	1	1	1	1	2	1	1	3.9	3.9	7.6	3.9	5.2	9412500	871650	510390	3678400	815390
sp|Q9JKB1|U >sp|Q9JKB1|UCHL3_MOUSE Ubiquitin carboxyl-terminal hydrolase isoz	1	1	2	1	1	1	1	2	1	1	5.7	5.7	11.7	5.7	5.7	4551100	912410	477820	1420500	893730
sp|P15379|C >sp|P15379|CD44_MOUSE CD44 antigen OS=Mus musculus GN=Cd44 P	2	2	2	2	2	2	2	2	2	2	2.7	2.7	2.7	2.7	2.7	34780000	7173100	6049600	7577000	7530200
sp|P15532|N >sp|P15532|NDKA_MOUSE Nucleoside diphosphate kinase A OS=Mus m	3	3	3	3	3	2	2	2	2	2	30.3	30.3	30.3	30.3	30.3	135800000	22148000	17778000	39507000	31148000
sp|P15702|L >sp|P15702|LEUK_MOUSE Leukosialin OS=Mus musculus GN=Spn PE=1	2	2	2	2	2	2	2	2	2	2	9.6	9.6	9.6	9.6	9.6	46086000	5559500	7089100	13470000	7999000
sp|P15924|D >sp|P15924|DESP_HUMAN Desmoplakin OS=Homo sapiens GN=DSP PE	3	4	2	2	2	3	4	2	2	2	1.5	2.1	1.3	0.8	1.3	8463500	1093500	4483200	1279500	953570
sp|P43276|H >sp|P43276|H15_MOUSE Histone H1.5 OS=Mus musculus GN=Hist1h1b	3	3	3	3	3	3	3	3	3	3	17.9	17.9	17.9	17.9	17.9	29882000	5347500	4388000	9387900	6015700
sp|P16546|S >sp|P16546|SPTA2_MOUSE Spectrin alpha chain, brain OS=Mus muscul	29	36	49	46	48	10	10	15	15	13	15.2	17.7	27.2	25.3	26.1	603540000	26800000	33703000	238100000	127390000
sp|P16858|G >sp|P16858|G3P_MOUSE Glyceraldehyde-3-phosphate dehydrogenase (	15	14	15	17	16	4	3	4	6	5	49.8	49.8	61.3	69.7	61.3	2556000000	281450000	264250000	660590000	495990000
sp|P16879|F >sp|P16879|FES_MOUSE Tyrosine-protein kinase Fes/Fps OS=Mus musc	2	2	2	2	2	2	2	2	2	2	5.7	5.7	5.7	5.7	5.7	12029000	1417600	816490	3625800	2629200
sp|Q9JKB3|D >sp|Q9JKB3|DBPA_MOUSE DNA-binding protein A OS=Mus musculus GN	2	1	2	1	1	2	1	2	1	1	14.1	14.4	14.1	14.4	14.4	4828100	1017400	457030	2313900	585820
sp|P17047|L >sp|P17047|LAMP2_MOUSE Lysosome-associated membrane glycoprot	2	2	2	2	2	2	2	2	2	2	5.8	5.8	5.8	5.8	5.8	47498000	6989900	6220500	11375000	9666000
sp|Q9CZX8|R >sp|Q9CZX8|RS19_MOUSE 40S ribosomal protein S19 OS=Mus muscu	5	6	6	6	6	5	6	6	6	6	32.4	33.8	33.8	33.8	33.8	114240000	15567000	13117000	36691000	28423000
sp|Q98TF7|R >sp|Q98TF7|RL35_CHICK 60S ribosomal protein L35 OS=Gallus gallus GN	1	1	3	2	1	1	1	3	2	1	8.1	8.1	22.8	12.2	8.1	33150000	2650200	2426200	15058000	8533800
sp|P17182|E >sp|P17182|ENOA_MOUSE Alpha-enolase OS=Mus musculus GN=Eno1	26	24	26	27	25	4	2	4	5	3	62.4	53.7	64.7	63.8	59.4	4027400000	542100000	509260000	1289600000	778930000
sp|Q3T0Y5|P >sp|Q3T0Y5|PSA2_BOVIN Proteasome subunit alpha type-2 OS=Bos taur	2	2	2	2	1	2	2	2	2	1	17.5	17.5	17.5	17.5	9.4	11222000	2141500	1564500	3436200	3180600
sp|P17426|A >sp|P17426|AP2A1_MOUSE AP-2 complex subunit alpha-1 OS=Mus mus	16	16	18	16	16	16	16	18	16	16	32.5	31.5	35.2	29.7	32.1	379950000	44430000	30733000	121660000	74123000
sp|P25977|U >sp|P25977|UBF1_RAT Nucleolar transcription factor 1 OS=Rattus norve	1	2	2	2	2	1	2	2	2	2	1.6	3.7	3.7	3.7	3.7	18482000	1522600	2845300	4677500	4973600
sp|P17563|S >sp|P17563|SBP1_MOUSE Selenium-binding protein 1 OS=Mus musculu	6	6	4	6	6	6	6	4	6	6	17.4	17.4	10.6	17.4	17.4	36196000	5157700	5222100	8283800	9113400
sp|Q3T0L7|R >sp|Q3T0L7|RL28_BOVIN 60S ribosomal protein L28 OS=Bos taurus GN=	2	2	2	2	2	2	2	2	2	2	9.5	9.5	9.5	9.5	9.5	18510000	2211000	2795300	6449700	3281400
sp|P17710|H >sp|P17710|HXK1_MOUSE Hexokinase-1 OS=Mus musculus GN=Hk1 PE	12	11	10	12	12	12	11	10	12	12	17.8	15.7	14.6	16.5	17.8	190910000	24057000	19505000	52912000	41214000
sp|P17742|P >sp|P17742|PPIA_MOUSE Peptidyl-prolyl cis-trans isomerase A OS=Mus	7	8	6	7	7	3	4	4	3	3	56.1	64	48.8	56.1	56.1	664040000	108840000	118450000	193280000	144020000
sp|Q5E956|T >sp|Q5E956|TPIS_BOVIN Triosephosphate isomerase OS=Bos taurus GN	10	10	8	9	9	10	10	8	9	9	48.6	48.6	43.8	48.2	44.2	262770000	41526000	31362000	73814000	53049000
sp|P17918|P >sp|P17918|PCNA_MOUSE Proliferating cell nuclear antigen OS=Mus m	6	6	6	6	5	2	2	3	2	2	31.8	31.8	40.2	31.8	29.1	179880000	28916000	35713000	41516000	37946000
sp|Q63569|P >sp|Q63569|PRS6A_RAT 26S protease regulatory subunit 6A OS=Rattus	9	9	9	10	7	8	8	8	9	7	36.7	33	33	41.2	25.7	111080000	15358000	12515000	36775000	24694000
sp|P41216|A >sp|P41216|ACSL1_MOUSE Long-chain-fatty-acid--CoA ligase 1 OS=Mus	3	2	2	2	2	3	2	2	2	2	6	4.7	4.7	4.7	4.7	8454200	1536200	1180400	2674200	1576600
sp|P18242|C >sp|P18242|CATD_MOUSE Cathepsin D OS=Mus musculus GN=Ctsd PE=	3	3	2	2	2	3	3	2	2	2	13.4	13.4	9	9	9	28933000	5634000	4020200	8846400	4163300
sp|Q9WV60| >sp|Q9WV60|GSK3B_MOUSE Glycogen synthase kinase-3 beta OS=Mus	1	2	1	2	2	1	2	1	2	2	5.7	7.9	5.7	7.9	7.9	12428000	1521200	1611400	3884900	2950700
sp|Q5R5H1|T >sp|Q5R5H1|METK2_PONAB S-adenosylmethionine synthase isoform ty	8	8	8	8	8	8	8	8	8	8	24.8	24.8	24.8	24.8	24.8	360410000	55508000	46834000	105170000	75678000
sp|P18484|A >sp|P18484|AP2A2_RAT AP-2 complex subunit alpha-2 OS=Rattus norve	23	23	23	25	24	18	18	18	20	19	27.8	30.8	31.3	34.9	32.1	718160000	90781000	65846000	199700000	170470000

Accession	#	Description	Gene	Database	C1	C2	C3	C4	C5	C6	I1	I2	I3	I4	I5	I6	I7	I8	I9
Q99JR1	9	Sideroflexin-1	Sfxn1	>sp|Q99JR1|	7	8	8	7	8	8	101930000	169680000	89754000	6795400	11312000	5983600	346000000	458660000	337020000
Q8BGQ7	25	Alanine--tRNA ligase, cytoplasmic	Aars	>sp|Q8BGQ7|	17	23	24	17	23	24	150760000	249750000	164300000	2956000	4897000	3221500	242470000	321600000	327770000
Q9DBJ1;O70... 13;3		Phosphoglycerate mutase 1	Pgam1	>sp|Q9DBJ1|	10	13	12	10	13	12	185100000	255270000	463430000	14238000	19636000	35648000	602170000	799540000	1151000000
P25206	17	DNA replication licensing factor MCM3	Mcm3	>sp|P25206|	7	16	13	7	16	13	26985000	75389000	28101000	539700	1507800	562010	65312000	86799000	73895000
Q8JZR0	10	Long-chain-fatty-acid--CoA ligase 5	Acsl5	>sp|Q8JZR0|	5	9	7	4	7	5	12395000	30430000	9828600	364550	895000	289080	26910000	35832000	34859000
G3UZ34;A2A... 15;15;1...		116 kDa U5 small nuclear ribonucleoprotein component	Eftud2	>tr|G3UZ34|	6	15	11	6	15	11	19350000	52258000	14973000	386990	1045200	299460	31202000	41643000	44294000
Q8C3V4;P42... 5;5		**Signal transducer and activator of transcription;Signal transducer and activator of transcription 1**	**Stat1**	**>tr|Q8C3V4|**	**3**	**4**	**4**	**3**	**4**	**4**	**5804100**	**9939400**	**3181500**	**152740**	**261560**	**83724**	**9969900**	**13316000**	**10415000**
Q9Z0N1;Q9Z... 12;9;7		Eukaryotic translation initiation factor 2 subunit 3, X-linked;Eukaryotic translation initiation factor 2 subunit 3...	Eif2s3x;Eif2s3...	>sp|Q9Z0N1|	10	11	8	10	11	8	98956000	116840000	72997000	4712000	5563900	3476000	197720000	264170000	203250000
Q8BH69	4	Selenide, water dikinase 1	Sephs1	>sp|Q8BH69|	3	4	3	3	4	3	3377900	11297000	11280000	259840	868980	867660	22087000	29538000	24690000
Q3TUE1;Q91... 9;8;8		Far upstream element-binding protein 1	Fubp1	>tr|Q3TUE1|	6	9	8	6	9	8	43713000	45039000	29740000	1410100	1452900	959350	59145000	79114000	85861000
Q8C605;Q9W... 21;21;1...		6-phosphofructokinase;ATP-dependent 6-phosphofructokinase, platelet type	Pfkp	>sp|Q8C605|	17	21	20	14	18	18	146560000	235480000	126450000	4441100	7135700	3831700	265450000	355130000	336110000
Q99M87-3;Q... 5;5;4		DnaJ homolog subfamily A member 3, mitochondrial	Dnaja3	>sp|Q99M87...	3	4	4	3	4	4	5545400	15082000	14491000	264070	718200	690070	25550000	34237000	34559000
G3X9V0;P97... 7;7;3		Proteasome activator complex subunit 2	Psme2	>tr|G3X9V0|	7	7	4	7	7	4	15631000	35275000	6422800	1042100	2351700	428190	63050000	84533000	21372000
H3BKN0;Q1H... 16;16;1...		tRNA (cytosine(34)-C(5))-methyltransferase	Nsun2	>sp|H3BKN0|	9	16	12	9	16	12	42360000	68146000	35844000	1059000	1703700	896100	71904000	96438000	96368000
O89053;G3U... 13;9;3;1		Coronin-1A;Coronin	Coro1a	>sp|O89053|	9	12	12	9	12	12	203570000	266000000	125180000	10714000	14000000	6588400	428650000	574970000	329870000
Q9D0I8;A2A... 7;6;1		mRNA turnover protein 4 homolog	Mrto4	>sp|Q9D0I8|	2	7	5	2	7	5	4198300	13462000	2504100	262400	841390	156510	19295000	25922000	10853000
Q8K1R3;Q8K... 11;5		Polyribonucleotide nucleotidyltransferase 1, mitochondrial	Pnpt1	>sp|Q8K1R3|	7	11	11	7	11	11	20527000	40825000	17538000	488740	972020	417580	40691000	54671000	42646000
Q91VD9	13	NADH-ubiquinone oxidoreductase 75 kDa subunit, mitochondrial	Ndufs1	>sp|Q91VD9|	9	13	13	9	13	13	42859000	62341000	41447000	1020500	1484300	986840	77724000	104430000	98460000
Q62167;P163... 18;15		ATP-dependent RNA helicase DDX3X;Putative ATP-dependent RNA helicase PI10	Ddx3x;D1Pas...	>sp|Q62167|	14	17	15	2	3	3	128530000	213620000	104490000	3295600	5477500	2679300	254770000	342720000	327850000
Q3U741;Q50... 9;9;5		Probable ATP-dependent RNA helicase DDX17	Ddx17	>sp|Q3U741|	8	9	7	8	9	7	53634000	75284000	53681000	1676100	2352700	1677500	104430000	140560000	133550000
P48036	19	Annexin A5	Anxa5	>sp|P48036|	14	16	18	14	16	18	156670000	257200000	226910000	6811900	11182000	9865700	620910000	835790000	732390000
F6YY69;F6V... 4;4;4;4		14-3-3 protein theta	Ywhaq	>tr|F6YY69|	4	3	2	4	3	2	10757000	19488000	14712000	632790	1146400	865420	42799000	57616000	29435000
K3W4T3;Q9Z 3;3;3;3		V-type proton ATPase 116 kDa subunit a isoform 1	Atp6v0a1	>tr|K3W4T3|	2	3	2	2	3	2	4210400	7372100	3765300	123830	216830	110740	5516900	7435800	6742900
F7DEU6;P50... 7;7;6;5		Inosine-5-monophosphate dehydrogenase;Inosine-5-monophosphate dehydrogenase 1	Impdh1	>tr|F7DEU6|	6	6	5	6	6	5	13859000	17582000	8974800	602580	764450	390210	31848000	42998000	34025000
Q9Z1F9;H3B... 9;2;1;1		SUMO-activating enzyme subunit 2	Uba2	>sp|Q9Z1F9|	4	8	7	4	8	7	8779800	33678000	13249000	283220	1086400	427380	29605000	40064000	33541000
Q9R0E1	2	Procollagen-lysine,2-oxoglutarate 5-dioxygenase 3	Plod3	>sp|Q9R0E1|	2	2	2	2	2	2	7983300	9513800	3331900	210090	250360	87682	10041000	13604000	10339000
P26041	39	Moesin	Msn	>sp|P26041|	34	38	38	24	28	28	604970000	730290000	513070000	18332000	22130000	15548000	868080000	1176800000	1352300000
P70290;B7Z... 8;7;7;4;		55 kDa erythrocyte membrane protein	Mpp1	>sp|P70290|	8	8	7	8	8	7	24680000	38382000	14176000	949320	1476200	545230	57088000	77465000	38701000
Q8CI94;E9PU 9;2;2;2;...		Glycogen phosphorylase, brain form	Pygb	>sp|Q8CI94|	4	6	5	4	6	5	13218000	16992000	14807000	281240	361530	315040	22153000	30065000	18544000
Q9Z2U0;Q9C 7;4		Proteasome subunit alpha type-7;Proteasome subunit alpha type-7-like	Psma7;Psma...	>sp|Q9Z2U0|	5	5	7	5	5	5	24869000	33861000	104200000	1776400	2418700	7443000	91317000	124370000	215720000
Q99MR6-3;Q 6;6;6;6		Serrate RNA effector molecule homolog	Srrt	>sp|Q99MR6|	2	6	6	2	6	6	4375900	18096000	9889400	101760	420580	229990	13590000	18573000	18026000
Q922D8	16	C-1-tetrahydrofolate synthase, cytoplasmic;Methylenetetrahydrofolate dehydrogenase;Methenyltetrahydrof...	Mthfd1	>sp|Q922D8|	13	16	11	13	16	11	42495000	103810000	60186000	849910	2076200	1203700	103290000	141270000	129390000
Q7M6Y3-2;Q 2;2;2;2;...		Phosphatidylinositol-binding clathrin assembly protein;Clathrin coat assembly protein AP180	Picalm;Snap9...	>sp|Q7M6Y3|	2	2	2	2	2	2	3649100	7950600	6093900	152050	331280	253910	12147000	16632000	14739000
P62137	7	Serine/threonine-protein phosphatase PP1-alpha catalytic subunit	Ppp1ca	>sp|P62137|	7	5	5	4	2	3	22085000	22384000	13453000	1227000	1243600	747370	71116000	97595000	48041000
G5E902;Q8VI 10;10		Phosphate carrier protein, mitochondrial	Slc25a3	>tr|G5E902|	8	9	10	8	9	10	254190000	376470000	231850000	13378000	19814000	12203000	723650000	993410000	624910000
Q3UE92;S4R 14;13;1...		Xaa-Pro aminopeptidase 1	Xpnpep1	>tr|Q3UE92|	8	14	13	8	14	13	47953000	104370000	65916000	1332000	2892000	1831000	116310000	159710000	171370000
Q8K363;F6Z 6;1		ATP-dependent RNA helicase DDX18	Ddx18	>sp|Q8K363|	5	6	5	5	6	5	16641000	31539000	11012000	489430	927620	323880	28701000	39411000	37864000
Q91V61;Q3U 7;6;6		Sideroflexin-3	Sfxn3	>sp|Q91V61|	5	7	7	5	7	7	14982000	27053000	14258000	788550	1428800	750430	60712000	83770000	64126000
Q8BGH2	4	Sorting and assembly machinery component 50 homolog	Samm50	>sp|Q8BGH2|	3	4	2	3	4	2	6106300	17588000	4091100	203540	586260	136370	21224000	29352000	15194000
Q91VM5;Q9 5;4;3;3;		RNA binding motif protein, X-linked-like-1;RNA-binding motif protein, X chromosome;RNA-binding motif prot...	Rbmxl1;Rbm...	>sp|Q91VM5|	3	5	5	3	5	5	13506000	39372000	32491000	540260	1574900	1299600	59174000	81837000	78406000
Q7TNV0;E9Q 8;6;6		Protein DEK	Dek	>sp|Q7TNV0|	5	8	6	5	8	6	11549000	24073000	13078000	549950	1146400	622760	35935000	49725000	33849000
Q9DBR1-2;Q 10;10		5-3 exoribonuclease 2	Xrn2	>sp|Q9DBR1-|	4	10	6	4	10	6	12257000	31539000	12298000	266460	685640	267350	21658000	30007000	31310000
Q9D0R2;Q8B 18;1		Threonine--tRNA ligase, cytoplasmic	Tars	>sp|Q9D0R2|	14	18	14	14	18	14	96628000	115610000	61598000	2356800	2819700	1502400	145310000	201550000	123620000
Q9Z1J3-2;Q9 4;4;1;1;		Cysteine desulfurase, mitochondrial	Nfs1	>sp|Q9Z1J3-|	2	4	4	2	4	4	2276400	9277400	8951200	91055	371090	358050	12347000	17128000	20857000
Q9Z2W0	8	Aspartyl aminopeptidase	Dnpep	>sp|Q9Z2W0|	6	7	7	6	7	7	19155000	55933000	20536000	957730	2796700	1026800	68015000	94431000	65994000
Q3TWW8	6	Serine/arginine-rich splicing factor 6	Srsf6	>sp|Q3TWW|	4	5	5	2	2	3	66024000	61112000	22354000	4401600	4074100	1490200	103370000	143670000	93804000
A1BN54;Q7TI 14;14;0;		Alpha-actinin-1	Actn1	>tr|A1BN54|	12	14	12	11	13	11	41088000	76584000	29307000	790150	1472800	563600	64121000	89187000	72928000
F8WIT2;P148 16;16		Annexin;Annexin A6	Anxa6	>tr|F8WIT2|	13	16	15	13	16	15	48452000	106700000	56796000	1101200	2425000	1290800	110250000	153840000	178390000
P09411;S4R2 25;19		Phosphoglycerate kinase 1;Phosphoglycerate kinase	Pgk1	>sp|P09411|	18	21	25	13	15	18	1094500000	1490100000	2013100000	42097000	57313000	77428000	2609000000	3651300000	5335600000
Q9WU78;Q9 16;15;1		Programmed cell death 6-interacting protein	Pdcd6ip	>sp|Q9WU78|	14	16	13	14	16	13	61619000	115770000	40013000	1339500	2516700	869840	119490000	167230000	102830000
Q99KI0	25	Aconitate hydratase, mitochondrial	Aco2	>sp|Q99KI0|	23	25	24	23	25	24	275000000	380060000	240540000	7236900	10002000	6330000	451500000	631910000	529820000
A2AMW0;P4 9;9;9;7;		F-actin-capping protein subunit beta	Capzb	>tr|A2AMW0|	7	8	7	7	8	7	73835000	104550000	55329000	4922300	6970000	3688600	229660000	321800000	203830000
F2Z456;Q9D 5;5;5		NADH-cytochrome b5 reductase 3;NADH-cytochrome b5 reductase 3 membrane-bound form;NADH-cytochr...	Cyb5r3	>tr|F2Z456|	4	5	3	4	5	3	11705000	19517000	12587000	557370	929380	599390	42404000	59456000	44193000
Q61035;G5E 11;3;3		Histidine--tRNA ligase, cytoplasmic	Hars	>sp|Q61035|	11	11	8	11	11	8	60632000	57253000	29189000	2090800	1974300	1006500	102970000	144530000	98237000
P08003	27	Protein disulfide-isomerase A4	Pdia4	>sp|P08003|	19	25	23	19	25	23	212830000	310260000	193070000	6080800	8864600	5516400	328690000	461530000	438580000
Q60932-2;Q6 13;13;1...		Voltage-dependent anion-selective channel protein 1	Vdac1	>sp|Q60932-|	10	13	10	10	13	10	75916000	229720000	101580000	4465700	13513000	5975200	319620000	449830000	443780000
Q9R1P0;E9P 5;3;2		Proteasome subunit alpha type-4;Proteasome subunit alpha type	Psma4	>sp|Q9R1P0|	3	5	5	3	5	5	19904000	35962000	26183000	1531100	2766300	2014100	66465000	93381000	95973000
Q8BIJ6;E9PW 6;4;3		Isoleucine--tRNA ligase, mitochondrial	Iars2	>sp|Q8BIJ6|	2	6	6	2	6	6	5048800	34515000	15341000	117410	803510	356760	23228000	28769000	28769000
A2A6U3;Q80 19;19;1...		Septin-9	Sep-09	>tr|A2A6U3|	10	17	17	10	17	17	75681000	111240000	64480000	1892000	2780900	1612000	128880000	181880000	202560000
Q9JKR6;F6TR 29;11;6		Hypoxia up-regulated protein 1	Hyou1	>sp|Q9JKR6|	25	26	24	25	26	24	304750000	301380000	173710000	6484000	6423200	3695900	389510000	550830000	353940000
P63087;P630 2;2		Serine/threonine-protein phosphatase PP1-gamma catalytic subunit	Ppp1cc	>sp|P63087|	2	2	2	1	1	1	3597500	7091900	2603700	224840	443240	162730	15316000	21686000	12690000
P26043;Q7TS 8;2		Radixin	Rdx	>sp|P26043|	4	7	7	4	7	7	19178000	42771000	24116000	618640	1379700	777920	41567000	58887000	64866000
O09131;D3Z1 12;1;1		Glutathione S-transferase omega-1	Gsto1	>sp|O09131|	9	10	9	9	10	9	38473000	109020000	66064000	2404600	6813800	4129000	196490000	278720000	129640000
E9PYT3;Q91 7;7;4;1		Atlastin-3	Atl3	>tr|E9PYT3|	4	6	5	4	6	5	8595600	12564000	4568300	343830	502580	182730	17494000	24919000	10514000
A2AL85;Q88 12;12;1		Aspartyl/asparaginyl beta-hydroxylase	Asph	>tr|A2AL85|	9	10	9	9	10	9	29545000	45524000	28314000	1055200	1625900	1011200	47749000	68023000	72898000
P97379-2;P97 3;3		Ras GTPase-activating protein-binding protein 2	G3bp2	>sp|P97379-|	3	2	1	3	2	1	3612400	2136100	518360	190120	112430	27282	4563600	6504500	0

Accession	Count	Description	Gene	ID																
Q91YY4	3	ATP synthase mitochondrial F1 complex assembly factor 2	Atpaf2	>sp|Q91YY4|	0	3	3	0	3	3	0	3651400	6658100	0	243430	443870	0	7319200	19285000
Q921I9	3	Exosome complex component RRP41	Exosc4	>sp|Q921I9|	0	3	3	0	3	3	0	3534100	9002400	0	392670	1000300	0	15306000	20443000
Q922H4;D3Z	3;1;1;1	Mannose-1-phosphate guanyltransferase alpha	Gmppa	>sp|Q922H4|	0	2	3	0	2	3	0	2211900	5110900	0	110600	255550	0	3303700	14746000
Q923B1;F6U	2;1;1	Lariat debranching enzyme	Dbr1	>sp|Q923B1|	0	2	2	0	2	2	0	3556700	661630	0	169370	31506	0	4657600	3382200
Q924M7	2	Mannose-6-phosphate isomerase	Mpi	>sp|Q924M7|	0	2	2	0	2	2	0	3726500	2945000	0	186330	147250	0	8060600	7417900
Q99JZ4;P365	2;1	GTP-binding protein SAR1a	Sar1a	>tr|Q99JZ4|	0	2	2	0	2	2	0	14511000	4950900	0	1451100	495090	0	23253000	12915000
Q99LH1;B1A	2;1	Nucleolar GTP-binding protein 2	Gnl2	>sp|Q99LH1|	0	2	1	0	2	1	0	6068400	455930	0	173380	13027	0	9140000	0
Q99MJ9	2	ATP-dependent RNA helicase DDX50	Ddx50	>sp|Q99MJ9|	0	2	1	0	2	1	0	3148300	96573	0	82851	2541.4	0	5033600	0
Q9D3F3;Q99	3;3	39S ribosomal protein L1, mitochondrial	Mrpl1	>sp|Q9D3F3|	0	3	0	0	3	0	0	3287000	0	0	234790	0	0	7942100	0
Q99P58;Q9E	2;1	Ras-related protein Rab-27B;Ras-related protein Rab-27A	Rab27b;Rab2	>sp|Q99P58|	0	2	2	0	2	2	0	2140900	3632800	0	178410	302730	0	4817800	10223000
Q9CQ02	2	COMM domain-containing protein 4	Commd4	>sp|Q9CQ02|	0	2	0	0	2	0	0	2253800	0	0	204890	0	0	3094900	0
Q9CQA1	2	Trafficking protein particle complex subunit 5	Trappc5	>sp|Q9CQA1|	0	2	0	0	2	0	0	3145200	0	0	285930	0	0	4318900	0
Q9CQC9	6	GTP-binding protein SAR1b	Sar1b	>sp|Q9CQC9|	0	6	1	0	4	0	0	27718000	5686900	0	2771800	568690	0	38062000	0
Q9CQF0	2	39S ribosomal protein L11, mitochondrial	Mrpl11	>sp|Q9CQF0|	0	2	0	0	2	0	0	2584800	0	0	198830	0	0	3549400	0
Q9CQJ7;A2CE	3;2	U2 small nuclear ribonucleoprotein B	Snrpb2	>sp|Q9CQJ7|	0	3	3	0	3	3	0	7341400	19139000	0	734140	1913900	0	20736000	50788000
Q9CQW1	5	Synaptobrevin homolog YKT6	Ykt6	>sp|Q9CQW1|	0	5	1	0	5	1	0	8641600	910980	0	617260	65070	0	11867000	0
Q9CWI3	3	BRCA2 and CDKN1A-interacting protein	Bccip	>sp|Q9CWI3|	0	3	3	0	3	3	0	4894400	7461900	0	271910	414550	0	10537000	19219000
Q9CWQ0;Q8I	2;1;1	Diphthine synthase	Dph5	>sp|Q9CWQ0|	0	2	0	0	2	0	0	3487900	0	0	268300	0	0	8427400	0
Q9CWU9	2	Nucleoporin Nup37	Nup37	>sp|Q9CWU9|	0	2	2	0	2	2	0	4257600	912820	0	283840	60855	0	13256000	4410600
Q9CXI0	2	2-methoxy-6-polyprenyl-1,4-benzoquinol methylase, mitochondrial	Coq5	>sp|Q9CXI0|	0	2	2	0	2	2	0	2287600	563760	0	152500	37584	0	5509000	2324200
Q9CXU4;Q9W	2;2	Mitochondrial import inner membrane translocase subunit Tim23	Timm23	>tr|Q9CXU4|	0	2	1	0	2	1	0	5251700	1534200	0	583530	170460	0	7211600	0
Q9CZP5	3	Mitochondrial chaperone BCS1	Bcs1l	>sp|Q9CZP5|	0	3	3	0	3	3	0	4864100	4222200	0	202670	175920	0	5316000	15775000
Q9D125	2	28S ribosomal protein S25, mitochondrial	Mrps25	>sp|Q9D125|	0	2	0	0	2	0	0	3567300	0	0	396370	0	0	4898600	0
Q9D1H6	2	NADH dehydrogenase [ubiquinone] 1 alpha subcomplex assembly factor 4	Ndufaf4	>sp|Q9D1H6|	0	1	1	0	1	1	0	1048100	1896800	0	87345	158060	0	1439300	0
Q9D1N9;Q9D	3;1	39S ribosomal protein L21, mitochondrial	Mrpl21	>sp|Q9D1N9|	0	3	1	0	3	1	0	7114500	789270	0	547270	60713	0	9769600	0
Q9D6J6;Q9D	4;2;1	NADH dehydrogenase [ubiquinone] flavoprotein 2, mitochondrial	Ndufv2	>sp|Q9D6J6|	0	4	4	0	4	4	0	15080000	10642000	0	1077100	760140	0	26230000	30902000
Q9D753;F6S	2;1;1	Exosome complex component RRP43	Exosc8	>sp|Q9D753|	0	2	1	0	2	1	0	3651100	603580	0	331920	54871	0	10366000	0
Q9D7X8	3	Gamma-glutamylcyclotransferase	Ggct	>sp|Q9D7X8|	0	3	0	0	3	0	0	2923700	0	0	265790	0	0	4014800	0
Q9D892	2	Inosine triphosphate pyrophosphatase	Itpa	>sp|Q9D892|	0	2	1	0	2	1	0	4175800	1046700	0	417580	104670	0	5734100	0
Q9DBL9-2;Q9	3;3	1-acylglycerol-3-phosphate O-acyltransferase ABHD5	Abhd5	>sp|Q9DBL9|	0	3	2	0	3	2	0	3919100	1288000	0	391910	128800	0	7162700	5742400
Q9DBZ5;Q9D	4;1	Eukaryotic translation initiation factor 3 subunit K	Eif3k	>sp|Q9DBZ5|	0	3	3	0	3	3	0	14689000	5742300	0	1335400	522030	0	22131000	21874000
Q9DC23	2	DnaJ homolog subfamily C member 10	Dnajc10	>sp|Q9DC23|	0	2	2	0	2	2	0	4050900	1082500	0	115740	30928	0	5189800	3909300
Q9DC70	4	NADH dehydrogenase [ubiquinone] iron-sulfur protein 7, mitochondrial	Ndufs7	>sp|Q9DC70|	0	4	2	0	4	2	0	6565700	2886400	0	596880	262400	0	8584200	10923000
Q9DCA5	2	Ribosome biogenesis protein BRX1 homolog	Brix1	>sp|Q9DCA5|	0	2	2	0	2	2	0	3539000	1737500	0	176950	86784	0	7436000	5929400
Q9DCM0	2	Persulfide dioxygenase ETHE1, mitochondrial	Ethe1	>sp|Q9DCM0|	0	2	2	0	2	2	0	9720000	15604000	0	648000	1040300	0	26127000	40427000
Q9DCV4;A2A	3;1	Regulator of microtubule dynamics protein 1	Rmdn1	>sp|Q9DCV4|	0	3	3	0	3	3	0	4688900	8040000	0	246780	423160	0	13936000	21909000
Q9EPE9	3	Manganese-transporting ATPase 13A1	Atp13a1	>sp|Q9EPE9|	0	3	2	0	3	2	0	3756800	2969100	0	67086	53019	0	5070600	5193600
Q9EQQ9;Q9E	2;2	Bifunctional protein NCOAT;Protein O-GlcNAcase;Histone acetyltransferase	Mgea5	>sp|Q9EQQ9|	0	2	1	0	2	1	0	3665100	596120	0	79676	12959	0	4925300	0
Q9ES56	3	Trafficking protein particle complex subunit 4	Trappc4	>sp|Q9ES56|	0	3	0	0	3	0	0	2783600	0	0	198830	0	0	3822400	0
Q9JI13-2;Q9J	2;2	Something about silencing protein 10	Utp3	>sp|Q9JI13-2|	0	2	1	0	2	1	0	3921300	1931200	0	261420	128750	0	6180200	0
Q9JI75	2	Ribosyldihydronicotinamide dehydrogenase [quinone]	Nqo2	>sp|Q9JI75|	0	2	1	0	2	1	0	6834100	4155600	0	488150	296830	0	10518000	0
Q9JIK9	5	28S ribosomal protein S34, mitochondrial	Mrps34	>sp|Q9JIK9|	0	5	5	0	5	5	0	4863000	9651600	0	374080	742430	0	10461000	27332000
Q9JJ28	4	Protein flightless-1 homolog	Flii	>sp|Q9JJ28|	0	3	2	0	3	2	0	3968600	3976800	0	64009	64142	0	4584700	0
Q9JKX4-2;Q9	3;2	Protein AATF	Aatf	>sp|Q9JKX4-2|	0	2	3	0	2	3	0	1298100	4205200	0	61815	200250	0	1832300	11555000
Q9JLZ3;E9Q6	2;1;1;1	Methylglutaconyl-CoA hydratase, mitochondrial	Auh	>sp|Q9JLZ3|	0	2	2	0	2	2	0	2538000	658240	0	141000	36569	0	5992000	2832800
Q9QYF9;Q8V	3;2;1	Protein NDRG3	Ndrg3	>sp|Q9QYF9|	0	3	2	0	3	2	0	9399500	6189300	0	626630	412620	0	16596000	19196000
Q9QZH6;J3K	2;1	Evolutionarily conserved signaling intermediate in Toll pathway, mitochondrial	Ecsit	>sp|Q9QZH6|	0	2	2	0	2	2	0	1890200	2864500	0	72699	110170	0	4362500	7591000
Z4YN97;Q9R	2;2;2	Adenylate kinase isoenzyme 1	Ak1	>tr|Z4YN97|	0	2	2	0	2	2	0	3164500	510620	0	632890	102120	0	4313500	1397500
Q9R1C7-2;Q9	3;3;1	Pre-mRNA-processing factor 40 homolog A	Prpf40a	>sp|Q9R1C7-2|	0	3	3	0	3	3	0	6356400	7380800	0	198640	230650	0	8034400	12539000
Q9WUL7	4	ADP-ribosylation factor-like protein 3	Arl3	>sp|Q9WUL7|	0	4	1	0	4	1	0	10435000	994040	0	948630	90368	0	14329000	0
Q9WUR9;F6T	7;4;3	Adenylate kinase 4, mitochondrial	Ak4	>sp|Q9WUR9|	0	6	7	0	6	7	0	7793800	19781000	0	556700	1412900	0	24534000	52173000
Q9Z0W3-2;Q	4;4	Nuclear pore complex protein Nup160	Nup160	>sp|Q9Z0W3|	0	4	3	0	4	3	0	6363400	1359200	0	181810	38834	0	6811300	4738500
Q9Z1M8	4	Protein Red	Ik	>sp|Q9Z1M8|	0	4	2	0	4	2	0	5178100	1057100	0	235370	48050	0	6571600	6256500
Q9Z1T1	2	AP-3 complex subunit beta-1	Ap3b1	>sp|Q9Z1T1|	0	1	2	0	1	2	0	4703400	3148700	0	83989	56227	0	9604700	0
S4R1W8	2		Gapdh	>tr|S4R1W8|	0	2	2	0	2	2	0	23477000	447170	0	7825600	149060	0	82213000	2491900
A0A023T672;	4;3;3	RNA-binding protein 8A	RBM8;Rbm8a	>tr	A0A023T	1	4	2	1	4	2	251030	17844000	6999600	31379	2230500	874960	0	26478000	21434000
D3YYK9;A2A5	2;2;2;1	Brefeldin A-inhibited guanine nucleotide-exchange protein 2;Brefeldin A-inhibited guanine nucleotide-exchan	Arfgef1;Arfge	>tr|D3YYK9|	1	1	1	1	1	1	1055200	833170	0	19909	15720	0	0	1030800	0
A2A6G6;A2A	4;4;4;4	LIM and SH3 domain protein 1	Lasp1	>tr|A2A6G6|	1	4	3	1	4	3	12971000	12908000	10493000	2594200	2581600	2098600	0	47463000	17598000
A2AFQ9;E9PL	2;2;2	Gem-associated protein 5	Gemin5	>tr|A2AFQ9|	1	2	1	1	2	1	1062400	3311700	428660	13448	41920	5426.1	0	3701800	0
Q3U8S1;A2A1	2;2;2;2;	CD44 antigen	Cd44	>tr|Q3U8S1|	1	2	2	1	2	2	11041000	17007000	7674900	849300	1308200	590380	0	25744000	24398000
E9Q8N1;E9Q	2;2;2;1;	Titin	Ttn	>tr|E9Q8N1|	1	1	0	1	1	0	8007800	16044000	0	4431.5	8879	0	0	40906000	0
A2BFF8;Q3TP	3;3;3;3;	Cytoplasmic dynein 1 intermediate chain 2	Dync1i2	>tr|A2BFF8|	1	3	3	1	3	3	2272600	6168600	2686400	113630	308430	134320	0	8941400	8658500
A6H6E9;F6SJ	2;1	Tetratricopeptide repeat protein 23-like	Ttc23l	>tr|A6H6E9|	1	2	1	1	2	1	699530	1686300	623690	29147	70263	25987	0	2680400	0
B1AV77;B1A1	2;2;2	Aldehyde dehydrogenase;Fatty aldehyde dehydrogenase	Aldh3a2	>tr|B1AV77|	1	2	1	1	2	1	1207700	3696700	1321300	60385	184840	66063	0	7691900	0
B1ATP7;Q80Y	7;7;7;1	Zinc phosphodiesterase ELAC protein 2	Elac2	>tr|B1ATP7|	1	7	4	1	7	4	2303100	12392000	7868500	51181	275380	157520	0	15367000	19895000
B1AV14;Q78I	3;3	MICOS complex subunit Mic27	Apool	>tr|B1AV14|	1	3	3	1	3	3	2474400	2984900	8508500	176740	213210	607750	0	16495000	23029000
B1AXN9;P18	3;3;1;1	Ribosomal protein S6 kinase alpha-3	Rps6ka3	>tr|B1AXN9|	1	3	3	1	3	3	2802900	5888500	3893700	63702	133830	88492	0	9203700	12038000
B2C3G8;P42	2;1;1	Signal transducer and activator of transcription;Signal transducer and activator of transcription 5B;Signal	Stat5a;Stat5	>tr|B2C3G8|	1	2	1	1	2	1	986600	4651400	314920	24063	113450	7681.1	0	10678000	0

Accession	Protein name	Gene	Entry																
E0CYH4;Q8C6 3;3;1	WD repeat-containing protein 26	Wdr26	>tr|E0CYH4|E	1	3	3	1	3	3	918260	5391700	2556600	31664	185920	88158	0	8193600	8352800
E9PWE9;P48(2;2	Tyrosine-protein kinase;Tyrosine-protein kinase SYK	Syk	>tr|E9PWE9|	1	2	2	1	2	2	1427800	7615400	2271900	43265	230770	68844	0	9828400	8693100
E9PYA3;G5E8 2;2;2;2;	Hydroxyacylglutathione hydrolase, mitochondrial	Hagh	>tr|E9PYA3|E	1	2	2	1	2	2	68064	2758500	724880	4861.7	197030	51777	0	6483200	3750300
E9PZ88;F8WI 3;3;3;2	Alpha-mannosidase 2C1	Man2c1	>tr|E9PZ88|E	1	3	3	1	3	3	3755600	6501700	2809800	87340	151200	65344	0	6082900	8249300
E9PZC3;Q923 4;4;2	Flavin reductase (NADPH)	Blvrb	>tr|E9PZC3|E	1	4	3	1	4	3	337270	20251000	12202000	28106	1687600	1016800	0	33785000	36575000
E9Q066;G3X9 2;2;2	La-related protein 4	Larp4	>tr|E9Q066|I	1	2	2	1	2	2	1234400	10058000	1566700	47478	386840	60258	0	13889000	6206300
E9Q2A6;Q3U 4;4;4;2	Protein-tyrosine kinase 2-beta	Ptk2b	>tr|E9Q2A6|	1	4	4	1	4	4	2439300	5992300	2961900	38113	93630	46279	0	6706300	5266500
E9Q2X6;Q8C(2;2;1	Structural maintenance of chromosomes protein;Structural maintenance of chromosomes protein 4	Smc4	>tr|E9Q2X6|	1	2	2	1	2	2	4287400	5845500	3532900	63991	87246	52730	0	6978400	6162100
E9Q6Q4;E9Q 2;2		Rap1gds1	>tr|E9Q6Q4|	1	2	2	1	2	2	843650	2894300	1869500	29091	99803	64467	0	5372800	5517500
E9Q8N5;Q08(2;2;2;2	CLIP-associating protein 2	Clasp2	>tr|E9Q8N5|	1	1	1	1	1	1	1605000	1183700	385250	21690	15996	5206	0	1890900	0
E9Q9H2;P541 4;4;3;2	DnaJ homolog subfamily C member 2;DnaJ homolog subfamily C member 2, N-terminally processed	Dnajc2	>tr|E9Q9H2|	1	4	3	1	4	3	1066500	8892400	3431400	41018	342020	131980	0	10364000	13143000
E9Q9M5;J3KI 2;2;2;2	Ubiquitin carboxyl-terminal hydrolase;Ubiquitin carboxyl-terminal hydrolase 19	Usp19	>tr|E9Q9M5|	1	2	2	1	2	2	911190	3719500	2216700	14237	58117	34636	0	4138500	3966900
E9QKE4;Q8BI 2;2	Rab3 GTPase-activating protein non-catalytic subunit	Rab3gap2	>tr|E9QKE4|	1	2	2	1	2	2	3867800	4070900	2575100	63407	66736	42214	0	5103600	4032700
E9QKT1;O08; 2;1	Ubiquitin-protein ligase E3A	Ube3a	>tr|E9QKT1|	1	2	2	1	2	2	1765300	2502600	860010	44133	62565	21500	0	4097600	2568800
E9QM21;O08 3;3;1;1	Bcl-2 homologous antagonist/killer	Bak1	>tr|E9QM21|	1	3	3	1	3	3	1240500	5953800	5310100	112770	541250	482740	0	10695000	15221000
F6QKK2;Q8VI 3;3	ADP-ribosylation factor-like protein 8A	Arl8a	>tr|F6QKK2|	1	3	1	1	2	1	6210600	8841700	7140400	621060	884170	714040	0	22806000	0
F6VQH5;Q9Z 2;2	Heterogeneous nuclear ribonucleoprotein D-like	Hnrnpdl	>tr|F6VQH5|	1	2	1	1	2	1	3313900	4935900	413240	207120	308490	25827	0	16272000	0
G3UWV3;O35 5;5;4;3;	Calumenin	Calu	>tr	G3UWV3	1	2	5	1	2	5	411690	1926500	19592000	51461	240810	2449100	0	12237000	44592000
G3X972 8		Sec24c	>tr|G3X972|	1	8	6	1	8	6	2793600	17755000	5646200	71632	455260	144770	0	18824000	13695000
G3X9Q0;Q8C 2;2;2;2;	Muscleblind-like protein 2;Muscleblind-like protein 1;Muscleblind-like protein 3	Mbnl1;Mbnl2	>tr|G3X9Q0|	1	2	1	1	2	1	1251400	3802300	1938500	139040	422470	215390	0	7911400	0
G3XA17;F7CE 5;4;4;3;	Eukaryotic translation initiation factor 4 gamma 2	Eif4g2	>tr|G3XA17|	1	4	4	1	4	4	1312400	12536000	2276500	26248	250710	45530	0	15962000	9003700
Q5JC28;H3BK 3;3;3;2	Epidermal growth factor receptor substrate 15	Eps15	>tr|Q5JC28|(	1	3	2	1	3	2	1208200	3137300	1374700	30979	80444	35248	0	3013300	3187300
S4R1L5;H9KU 7;7;7;7;	Baculoviral IAP repeat-containing protein 6	Birc6	>tr|S4R1L5|S	1	7	3	1	7	3	2085900	10338000	2667900	10864	53846	13895	0	9685600	6866400
J3QJX3;Q9Z(3;3;3	Protein sel-1 homolog 1	Sel1l	>tr|J3QJX3|J	1	3	1	1	3	1	1168100	5010400	817280	30740	131850	21507	0	8003800	0
Q8BHX6;J3Q 3;3;3	Nucleolar complex protein 2 homolog	Noc2l	>tr|Q8BHX6|	1	3	2	1	3	3	2513800	6068200	3216600	96686	233390	123710	0	7739400	8033800
M0QWS4;Q9 2;2	Ubiquitin-fold modifier-conjugating enzyme 1	Ufc1	>tr	M0QWS4	1	2	1	1	2	1	496220	3132400	376080	82703	522060	62680	0	4301400	0
Q9CQM8;O0! 3;3	60S ribosomal protein L21	Rpl21	>tr	Q9CQM8	1	3	1	1	3	1	23150000	100390000	69751000	3858400	16731000	11625000	0	150580000	0
O09172;F6VN 4;2;2	Glutamate--cysteine ligase regulatory subunit	Gclm	>sp|O09172|	1	4	3	1	4	3	6843600	17421000	12826000	622150	1583700	1166000	0	46704000	36261000
O35604 2	Niemann-Pick C1 protein	Npc1	>sp|O35604|	1	2	2	1	2	2	3584600	5733000	1992500	108630	173730	60378	0	6446000	3510600
Q5SVG5;Q55\ 5;5;5;0	AP-1 complex subunit beta-1	Ap1b1	>tr|Q5SVG5|	1	5	5	1	5	5	6334800	22659000	11822000	137710	492580	257000	0	22670000	27778000
O54824-2;O5 3;3	Pro-interleukin-16;Interleukin-16	Il16	>sp	O54824-	1	2	2	1	2	2	1018500	4753600	2518300	29956	139810	74066	0	7592500	7815600
O54941 2	SWI/SNF-related matrix-associated actin-dependent regulator of chromatin subfamily E member 1	Smarce1	>sp|O54941|	1	2	1	1	2	2	915630	5741500	1297500	45781	287070	64873	0	13166000	0
Q7TMG8;O5! 5;5	Protein NipSnap homolog 2	Gbas	>sp	Q7TMG8	1	5	5	1	5	5	861340	7570800	13968000	53834	437180	872970	0	10870000	40710000
O70145 2	Neutrophil cytosol factor 2	Ncf2	>sp|O70145|	1	2	2	1	2	2	1867200	5128400	2722900	60234	165440	87834	0	8043300	8196900
O88325 2		Naglu	>sp|O88325|	1	2	2	1	2	2	2040500	3896000	2174400	65822	125680	70142	0	5739200	7035100
O88587-2;O8 4;4;1	Catechol O-methyltransferase	Comt	>sp	O88587-	1	4	4	1	4	4	98906	4805600	5192000	7064.7	343260	370860	0	8879900	16937000
O88796 3	Ribonuclease P protein subunit p30	Rpp30	>sp|O88796|	1	3	2	1	3	2	1214100	6820100	1495400	80942	454670	99691	0	13585000	8953100
O89079;D3Z3 6;5;2;1;	Coatomer subunit epsilon	Cope	>sp|O89079|	1	6	5	1	6	5	2842200	23713000	9778000	189480	1580900	651870	0	51785000	56523000
Q7JCZ1;P004 3;3	Cytochrome c oxidase subunit 2	mt-Co2;Mtco	>tr|Q7JCZ1|(	1	3	3	1	3	3	2548700	29928000	21261000	318580	3741000	2657600	0	44754000	75008000
P00687;P006 3;2;1;1;	Alpha-amylase 1;Pancreatic alpha-amylase	Amy1;Amy2	>sp|P00687|	1	3	2	0	1	1	11698000	10738000	479340	467940	429530	19174	0	37031000	0
P03975 2	IgE-binding protein	Iap	>sp|P03975|	1	2	1	1	2	1	1670300	6504800	3173500	61862	240920	117540	0	11313000	0
P04202 5	Transforming growth factor beta-1;Latency-associated peptide	Tgfb1	>sp|P04202|	1	3	5	1	3	5	2787000	5806500	8689700	126680	263930	394990	0	13092000	21576000
P10639 3	Thioredoxin	Txn	>sp|P10639|	1	1	3	1	1	3	5750800	11356000	12713000	821540	1622300	1816100	0	23741000	0
Q8K1M3;P12 3;3	cAMP-dependent protein kinase type II-alpha regulatory subunit	Prkar2a	>tr|Q8K1M3|	1	3	3	1	3	3	1706700	3860400	3040600	81272	183830	144790	0	8006700	8001200
P15864 4	Histone H1.2	Hist1h1c	>sp|P15864|	1	4	2	0	2	1	164140000	349270000	162740000	18237000	38808000	18082000	0	635680000	1114600000
P16332 2	Methylmalonyl-CoA mutase, mitochondrial	Mut	>sp|P16332|	1	2	2	1	2	2	940170	3813800	1927100	26116	105940	53532	0	5516600	6272000
P17426-2;P17 3;3;2	AP-2 complex subunit alpha-1	Ap2a1	>sp	P17426-	1	3	2	1	3	2	1529100	8338000	2675500	28851	157320	50482	0	11358000	7655500
P22907-2;P22 4;4	Porphobilinogen deaminase	Hmbs	>sp	P22907-	1	3	4	1	3	4	2504600	5798300	5240000	156540	362390	327500	0	12296000	13513000
P27048;P631 4;4	Small nuclear ribonucleoprotein-associated protein B;Small nuclear ribonucleoprotein-associated protein N	Snrpb;Snrpn	>sp|P27048|	1	3	4	1	3	4	121410	9430400	16388000	8094	548690	1092600	0	19422000	44013000
P28076;G3U\ 2;1	Proteasome subunit beta type-9	Psmb9	>sp|P28076|	1	2	1	1	2	1	430130	3443400	308370	39103	313030	28033	0	4728400	0
P35123 2	Ubiquitin carboxyl-terminal hydrolase 4	Usp4	>sp|P35123|	1	2	1	1	2	1	14899000	4147900	1820300	310400	86415	37922	0	7222700	0
P35279 7	Ras-related protein Rab-6A	Rab6a	>sp|P35279|	1	7	6	0	1	1	42027000	80800000	72150000	3232800	6215300	5550000	0	129330000	178820000
P35293 4	Ras-related protein Rab-18	Rab18	>sp|P35293|	1	3	2	1	3	2	172080	6110000	3447700	13237	470000	265210	0	9052500	0
P35991;A2BD 4;3	Tyrosine-protein kinase BTK	Btk	>sp|P35991|	1	3	3	1	3	3	2157400	5025500	2884300	53936	125640	72108	0	7562900	8871700
P41245 4	Matrix metalloproteinase-9	Mmp9	>sp|P41245|	1	4	3	1	4	3	1190500	16990000	3104100	34015	484830	88690	0	17779000	13684000
P41731 2	CD63 antigen	Cd63	>sp|P41731|	1	2	2	1	2	2	10169000	6668400	5709600	1271100	833580	713700	0	11335000	16996000
P42227;P4. 5;5;5;4	**Signal transducer and activator of transcription 3;Signal transducer and activator of transcription**	**Stat3**	**>sp	P42227-**	**1**	**4**	**4**	**1**	**4**	**4**	**3426600**	**10516000**	**4227200**	**87860**	**269640**	**108390**	**0**	**15002000**	**12019000**
Q9DBX5;P47. 3;3	Cytosolic phospholipase A2;Phospholipase A2;Lysophospholipase	Pla2g4a	>tr|Q9DBX5|	1	3	3	1	3	3	2159400	9589700	5368800	58363	259180	145100	0	14776000	16289000
P47941 3	Crk-like protein	Crkl	>sp|P47941|	1	3	3	1	3	3	619160	5130600	990770	38698	320660	61923	0	12543000	4354300
P47968 2	Ribose-5-phosphate isomerase	Rpia	>sp|P47968|	1	2	2	1	2	2	509300	2046300	3506500	31831	127890	219160	0	6890300	9014600
P53995;A2AT 4;3	Anaphase-promoting complex subunit 1	Anapc1	>sp|P53995|	1	4	3	1	4	3	1267100	4954600	1086300	13625	53275	11680	0	4546900	3592900
P55264-2;P55 6;6	Adenosine kinase	Adk	>sp	P55264-	1	4	5	1	4	5	1455500	7889800	10635000	80860	438320	590850	0	19048000	24940000
P57716 5	Nicastrin	Ncstn	>sp|P57716|	1	5	3	1	5	3	1073600	12209000	6117600	33551	381530	191180	0	16122000	13960000
P59325 5	Eukaryotic translation initiation factor 5	Eif5	>sp|P59325|	1	3	3	1	3	3	2039700	16840000	9043900	92714	765570	411090	0	32032000	25103000
P60670-2;P6(2;2	Nuclear protein localization protein 4 homolog	Nploc4	>sp	P60670-	1	1	1	1	1	1	2001000	2574800	1076100	71466	91956	38433	0	3763400	0
P61028 2	Ras-related protein Rab-8B	Rab8b	>sp|P61028|	1	2	2	1	2	2	588410	4453200	2484100	49034	371100	207010	0	11048000	4510800
P61087;D3Z4 8;5;1	Ubiquitin-conjugating enzyme E2 K	Ube2k	>sp|P61087|	1	8	5	1	8	5	599580	31075000	12589000	49965	2589600	1049100	0	38563000	48714000
P61089 2	Ubiquitin-conjugating enzyme E2 N	Ube2n	>sp|P61089|	1	2	2	1	2	2	4806000	2778800	7995200	480600	277880	799520	0	9470500	20221000
P61759;Q3TII 3;2	Prefoldin subunit 3	Vbp1	>sp|P61759|	1	3	2	1	3	2	108960	3758300	2872000	7264.3	250550	191470	0	5553200	8245200
P62830 2	60S ribosomal protein L23	Rpl23	>sp|P62830|	1	2	2	1	2	2	12731000	19105000	16382000	1414600	2122800	1820200	0	28222000	46860000
P62849-2;P62 2;2;2	40S ribosomal protein S24	Rps24	>sp	P62849-	1	2	2	1	2	2	2360500	6112500	9927800	393410	1018700	1654600	0	12213000	32236000
P62855 2	40S ribosomal protein S26	Rps26	>sp|P62855|	1	2	2	1	2	2	5500800	13055000	17861000	1100200	2610900	3572200	0	25748000	43915000

Appendix Table 6: Identification of STAT5b in mouse BaF3 cells and competitive displacement of peptide **27** by STAT5 inhibitor, **10** followed by Neutravidin pull down.

Protein IDs	Fasta headers	Razor + unique peptides A	Razor + unique peptides B	Razor + unique peptides C	Razor + unique peptides D	Razor + unique peptides E	Sequence coverage A [%]	Sequence coverage B [%]	Sequence coverage C [%]	Sequence coverage D [%]	Sequence coverage E [%]	Intensity	Intensity A	Intensity B	Intensity C
sp|P42232|STA5B_MOUSE;4|165932366|sign:	>sp|P42232|STA5B_MOUSE Signal transducer and activator of transcr	11	12	10	12	13	16.8	18.3	14.4	18.3	21.1	1.06E+08	14294000	15145000	25826000

Intensity D	Intensity E	iBAQ	iBAQ A	iBAQ B	iBAQ C	iBAQ D	iBAQ E	LFQ intensity A	LFQ intensity B	LFQ intensity C	LFQ intensity D	LFQ intensity E
19576000	31463000	2725700	366500	388320	662210	501940	806740	24188000	28316000	22069000	22650000	30071000

Vergleich der LFQ Intensitäten
Protein STA5B MOUSE
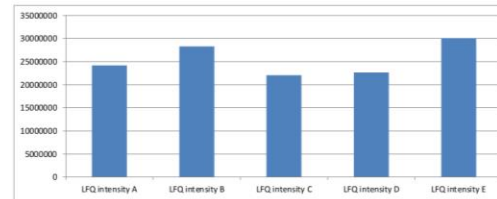
Fasta headers	Razor + unique peptides B1	Razor + unique peptides D1	Razor + unique peptides F1	Razor + unique peptides H1	Razor + unique peptides J1	Unique peptides B1	Unique peptides D1	Unique peptides F1	Unique peptides H1	Unique peptides J1	Sequence coverage B1 [%]	Sequence coverage D1 [%]	Sequence coverage F1 [%]	Sequence coverage H1 [%]	Sequence coverage J1 [%]
>5|MBP-STAT5b|MBP-STAT5b	13	25	57	59	18	3	8	26	26	5	14	27.5	57.6	58.3	23.5

Intensity	Intensity B1	Intensity D1	Intensity F1	Intensity H1	Intensity J1	iBAQ	iBAQ B1	iBAQ D1	iBAQ F1	iBAQ H1	iBAQ J1	LFQ intensity B1	LFQ intensity D1
2546900000	4680300	29953000	1057800000	1312800000	141690000	46307000	85096	544590	19233000	23869000	2576100	3651700	15102000

LFQ intensity F1	LFQ intensity J1	LFQ intensity H1
990800000	7090600	1105800000
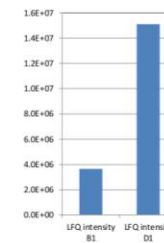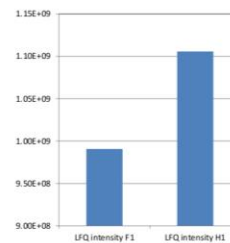
Appendix Table 7: Determination of maximum tolerated dose (MTD) and toxicity of compound **16** in non-xenografted mice.

Dr. Iduna Fichtner
Dr. Jens Hoffmann

Body Weight Statistics [g]
Study: 15084 Date: 24/7/2017

	Meas.		1	2	3	4	5
	Date:		25/7/17	28/7/17	1/8/17	3/8/17	7/8/17
Group	**Day:**		**1**	**4**	**8**	**10**	**14**
A	(n)		5	5	5	5	4
	Body Weight	Median	16.450	15.970	17.550	16.970	17.660
	[g]	Mean	16.536	16.182	17.336	17.270	17.728
		[S.D.]	0.5572	0.6237	1.0120	0.6213	0.8220
	BWC [%]		100	97.9	104.8	104.4	107.2
	Meas.		Gr. B M1	Gr. B M2	Gr. B M3	Gr. B M4	Gr. B M5
B	(n)		5	5	5	5	5
	Body Weight	Median	17.840	17.790	18.540	18.080	18.000
	[g]	Mean	17.650	17.894	18.552	17.874	17.506
		[S.D.]	0.7235	1.4395	1.4003	1.0150	1.0631
	BWC [%]	Mean	100	101.4	105.1	101.3	99.2
	Meas.		Gr. C M1	Gr. C M2	Gr. C M3	Gr. C M4	Gr. C M5
C	(n)		5	5	5	5	5
	Body Weight	Median	15.350	15.540	16.830	17.240	16.880
	[g]	Mean	15.584	15.654	16.960	17.246	17.180
		[S.D.]	0.9028	0.6043	0.5100	0.4203	0.5834
	BWC [%]	Mean	100	100.4	108.8	110.7	110.2
	Meas.		Gr. D M1	Gr. D M2	Gr. D M3	Gr. D M4	Gr. D M5
D	(n)		5	5	5	5	4
	Body Weight	Median	17.240	17.070	17.450	16.870	15.295
	[g]	Mean	17.022	16.454	17.644	17.590	15.670
		[S.D.]	1.0576	1.3556	0.9760	1.3595	0.8775
	BWC [%]	Mean	100	96.7	103.7	103.3	92.1

Table for Graph: BW Mean

Day	1	4	8	10	14
A -Vehicle	16.536	16.182	17.336	17.270	17.728
B -EN-30 100	17.650	17.894	18.552	17.874	17.506
C -EN-30 200	15.584	15.654	16.960	17.246	17.180
D -EN-30 300	17.022	16.454	17.644	17.590	15.670

Table for Graph: BW Change

Day	1	4	8	10	14
A -Vehicle	100.000	97.859	104.838	104.439	107.205
B -EN-30 100	100.000	101.382	105.110	101.269	99.184
C -EN-30 200	100.000	100.449	108.830	110.665	110.241
D -EN-30 300	100.000	96.663	103.654	103.337	92.057

Table for Graph: S.D.

Day	1	4	8	10	14
A -Vehicle	0.557	0.624	1.012	0.621	0.822
B -EN-30 100	0.723	1.440	1.400	1.015	1.063
C -EN-30 200	0.903	0.604	0.510	0.420	0.583
D -EN-30 300	1.058	1.356	0.976	1.359	0.878

(Mean) Body weight MV15084

- A -Vehicle
- B -EN-30 100 mg/kg
- C -EN-30 200 mg/kg
- D -EN-30 300 mg/kg
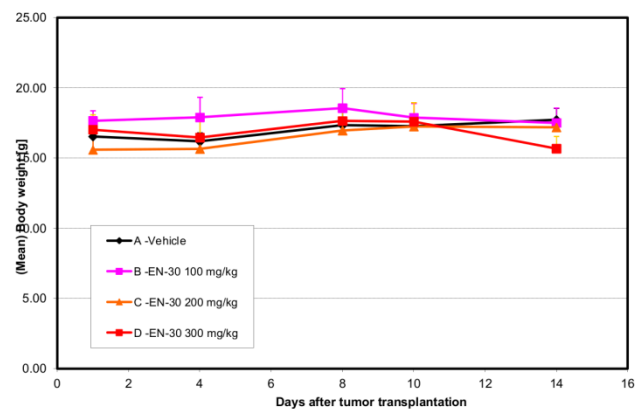
Appendix Table 8: Raw data tabulated for the corresponding body weight changes in non-xenografted mice and the tumor volume reduction upon treatment using compound **16**.

Body Weight Statistics [g]
Study: 15224   Date: 9/10/2017

	Meas.		1	2	3	4	5	6	7
	Date:		9/10/17	12/10/17	16/10/17	18/10/17	20/10/17	23/10/17	25/10/17
Group	Day:		0	3	7	9	11	14	16
A	(n)		6	6	6	6	6	5	
	Body Weight	Median	15.485	16.295	16.455	16.995	16.840	17.560	
	[g]	Mean	15.685	16.487	16.565	17.130	17.213	17.166	
		[S.D.]	1.5730	1.3216	1.4176	1.5782	1.3319	1.1876	
	BWC [%]		100	105.1	105.6	109.2	109.7	109.4	
	Meas.		Gr. B M1	Gr. B M2	Gr. B M3	Gr. B M4	Gr. B M5	Gr. B M6	Gr. B M7
B	(n)		7	7	7	7	7	7	6
	Body Weight	Median	15.900	17.070	17.510	16.980	16.680	17.160	17.425
	[g]	Mean	16.016	17.111	17.759	17.379	17.013	17.526	17.542
		[S.D.]	0.4932	0.8213	1.2486	0.9209	0.8442	1.1207	1.2499
	BWC [%]	Mean	100	106.8	110.9	108.5	106.2	109.4	109.5

Table for Graph: BW Mean

Day		0	3	7	9	11	14	16
	A -Vehicle	15.685	16.487	16.565	17.130	17.213	17.166	
	B -16 (200 mg	16.016	17.111	17.759	17.379	17.013	17.526	17.542

Table for Graph: BW Change

Day		0	3	7	9	11	14	16
	A -Vehicle	100.000	105.111	105.610	109.213	109.744	109.442	
	B -16 (200 m	100.000	106.841	110.882	108.509	106.226	109.428	109.528

Table for Graph: S.D.

Day		0	3	7	9	11	14	16
	A -Vehicle	1.573	1.322	1.418	1.578	1.332	1.188	
	B -EN-30	0.493	0.821	1.249	0.921	0.844	1.121	1.250

Tumor Volume Statistics (all values in cm³)
Study: 15224   Date: 9/10/2017

	Meas.		1	2	3	4	5	6	7
	Date:		9/10/17	12/10/17	16/10/17	18/10/17	20/10/17	23/10/17	25/10/17
Group	Day:		0	3	7	9	11	14	16
A	(n)		6	6	6	6	6	5	
	Tumor Volume	Median	0.001	0.001	0.129	0.657	1.348	1.796	
	[cm³]	Mean	0.001	0.001	0.162	0.652	1.260	1.676	
		[S.D.]	0.0000	0.0000	0.1555	0.2767	0.2532	0.5398	
	RTV	Median	1.0000	1.0	128.5	657.0	1348.0	1796.0	
		Mean	1.0000	1.0	162.2	652.3	1259.8	1675.6	
	Meas.		Gr. B M1	Gr. B M2	Gr. B M3	Gr. B M4	Gr. B M5	Gr. B M6	Gr. B M7
B	(n)		7	7	7	7	7	7	6
	Tumor Volume	Median	0.001	0.001	0.004	0.004	0.013	0.297	0.403
	[cm³]	Mean	0.001	0.001	0.003	0.004	0.073	0.474	0.424
		[S.D.]	0.0000	0.0000	0.0016	0.0000	0.0869	0.3783	0.2025
	RTV	Median	1.0000	1.0	4.0	4.0	13.0	297.0	402.5
		Mean	1.0000	1.0	2.7	4.0	73.1	474.0	423.7
	T/C [%]		100.0	100.0	1.7	0.6	5.8	28.3	#VALUE!

Table for Graph: TV Mean

DAY		0	3	7	9	11	14	16
	A -Vehicle	0.001	0.001	0.162	0.652	1.260	1.676	
	B -16 (200 m	0.001	0.001	0.003	0.004	0.073	0.474	0.424

Table for Graph: RTV Median

DAY		0	3	7	9	11	14	16
	A -Vehicle	1.000	1.000	128.500	657.000	1348.000	1796.000	
	B -EN-30	1.000	1.000	4.000	4.000	13.000	297.000	402.500

Table for Graph: RTV Mean

DAY		0	3	7	9	11	14	16
	A -Vehicle	1.000	1.000	162.167	652.333	1259.833	1675.600	
	B -EN-30	1.000	1.000	2.714	4.000	73.143	474.000	423.667

SEM for	Meas.	1	2	3	4	5	6	7
Tumor	Date:	9/10/17	12/10/17	16/10/17	18/10/17	20/10/17	23/10/17	25/10/17
Volume	Day:	0	3	7	9	11	14	16
A -Vehicle	[SEM]			0.063	0.113	0.103	0.241	
B -EN-30	[SEM]			0.001		0.033	0.143	0.083

- 194 -

List of Abbreviations

TKI	Tyrosine Kinase Inhbitor
DNA	Deoxyribonucleic acid
mAbs	monoclonal antibodies
5-FU	5-Fluorouracil
FBDD	Fragment Based Drug Design
NMR	Nuclear Magnetic Resonancce
STD-NMR	Saturation Transfer Difference
MST	Microscale Thermophoresis
ITC	Isothermal Titration Calorimetry
DSF	Differential Scanning Fluorimetry
TSA	Thermal Shift Assay
CETSA	Cellular Thermal Shift Assay
ITDRF	Isothermal dose-response fingerprints
FP	Fluorescence Polarization
SPR	Surface Plasmon Resonance
HTS	High Throughput Screening
STAT	Signal Transducers and Activator of Transcription factor
PTFL	Protein-Template Fragment Ligations
PPI	protein-protein interaction
ALL	acute lymphoblastic leukemia
CML	chronic myelogenous leukemia
AML	acute myelogenous leukemia
LGL	large lymphocytic leukemia
LSC	leukemic stem cell
SH2	Src-homology-2
FLT3	Fms related tyrosine kinase 3
ITD	Internal Tandem Duplication
BCR	Breakpoint cluster region
ABL	Abelson murine leukemia viral oncogene homolog
JAK	Janus Kinase
MBP	maltose binding protein
SOCs	suppressors of cytokine signalling

IL	interleukin
EPO	erythropoietin
TPO	thrombopoietin
PRL	prolactin
GM-CSF	granulocyte macrophage colony-stimulating factors
GH	growth hormones
HPLC	High Performance Liquid Chromatography
LC-MS	Liquid chromatography–mass spectrometry
QTOF	Quadrupole time-of-flight
CF	carboxyfluorescein
pcF	phosphonocarboxy-phenylalanine
CD	cooperative domain
DNA-BD	DNA-binding domain
TAD	transactivation domain
Ph	Philadelphia
LGA	Lamarckian Genetic Algorithm
DMSO	Dimethyl sulfoxide
PBS	Phosphate-buffered saline
TBS	Tris-buffered saline
EDTA	ethylenediaminetetraacetic acid
HEPES	4-(2-hydroxyethyl)-1-piperazineethanesulfonic acid
FBS	fetal bovine serum
ATP	adenosine triphosphate
cDNA	complementary deoxyribonucleic acid
mRNA	messenger RNA
PCR	polymerase chain reaction
PMSF	phenylmethylsulfonyl fluoride
qPCR	quantitative real-time PCR
SDS	sodium dodecyl sulfate
PAGE	poly acryl amide electrophoresis
siRNA	small interfering RNA
UV	ultraviolet
RT-PCR	reverse transcription PCR

FA	formaldehyde
AIDS	autoimmnunodeficiency diseases
Fa	fractional growth inhibition
Fc	fractional concentration
TC-PTP	T cell protein tyrosine phosphatase
OC_{50}	in-cell occupancy
FSC	forward scatter area
SSC	side scatter area
FITC	fluorescein isothiocyanate
WDI	World Drug Index
HRP	Horseradish Peroxidase
PVDF	Polyvinylidine fluoride
SEM	standard error of mean
SD	standard deviation
T_m	melting temperature
BSA	Bovine serum albumin
HRMS	High resolution mass spectrometry
PE	phycoerythrin
BSA	Bovine serum albumin
co-IP	co-immunoprecipitation
DiFMUP	6,8-difluoro-4-methylumbelliferyl phosphate
PIAS3	protein inhibitor of activated STAT3
CIS	cytokine-induced SH2-domain
SILAC	Stable Isotope Labeling with Amino Acids in Cell Culture
PTP1B	phosphotyrosines phosphatase IB
IgG	immunoglobulin G
ROS	reactive oxygen species
TMZ	temozolomide

List of Figures

List of Tables

List of Schemes

References

1   Hopkins, A. L., Keserü, G. M., Leeson, P. D., Rees, D. C. & Reynolds, C. H. The role of ligand efficiency metrics in drug discovery. *Nat Rev Drug Discov* **13**, 105 (2014).

2   Jiao, Q. *et al.* Advances in studies of tyrosine kinase inhibitors and their acquired resistance. *Mol Cancer* **17**, 36 (2018).

3   Rahman, M. & Hasan, M. Cancer metabolism and drug resistance. *Metabolites* **5**, 571-600 (2015).

4   Shewach,D.S. & Kuchta, R.D., 2009. Introduction to cancer therapeutics.

5   Diasio, R. B. & Harris, B. E. Clinical pharmacology of 5-fluorouracil. *Clin Pharmacokinet* **16**, 215-237 (1989).

6   Kaye, S. B. New antimetabolites in cancer chemotherapy and their clinical impact. *Br J Cancer* **78**, 1 (1998).

7   Sternberg, C. N. & Vogelzang, N. J. Gemcitabine, paclitaxel, pemetrexed and other newer agents in urothelial and kidney cancers. *Crit Rev Oncol Hematol* **46**, 105-115 (2003).

8   Weber, G. & Prajda, N. Targeted and non-targeted actions of anti-cancer drugs. *Adv Enzyme Regul* **34**, 71-89 (1994).

9   Conklin, K. A. Cancer chemotherapy and antioxidants. *J Nutr* **134**, 3201S-3204S (2004).

10 Cornelissen, J. *et al.* MDR-1 expression and response to vincristine, doxorubicin, and dexamethasone chemotherapy in multiple myeloma refractory to alkylating agents. *J Clin Oncol* **12**, 115-119 (1994).

11 Gao, Y.-g. & Wang, A. H.-J. Crystal structures of four morpholino-doxorubicin anti-cancer drugs complexed with d (CGTACG) and d (CGATCG): implications in drug-DNA crosslink. *J Biomol Struct Dyn* **13**, 103-117 (1995).

12 Carter, N. J. & Keam, S. J. Trabectedin. *Drugs* **67**, 2257-2276 (2007).

13 D'Incalci, M. & Galmarini, C. M. A review of trabectedin (ET-743): a unique mechanism of action. *Mol Cancer Ther* **9**, 2157-2163 (2010).

14 Rowe, J. M. & Tallman, M. S. How I treat acute myeloid leukemia. *Blood* **116**, 3147-3156 (2010).

15 Reynolds, C. H., Bembenek, S. D. & Tounge, B. A. The role of molecular size in ligand efficiency. *Bioorg Med Chem Lett* **17**, 4258-4261 (2007)

16 Erlanson, D. A., Fesik, S. W., Hubbard, R. E., Jahnke, W. & Jhoti, H. Twenty years on: the impact of fragments on drug discovery. *Nat Rev Drug Discov* **15**, 605 (2016).

17 Hann, M. M., Leach, A. R. & Harper, G. Molecular complexity and its impact on the probability of finding leads for drug discovery. *J Chem Inf Comput Sci* **41**, 856-864 (2001).

18 Whittaker, M., Law, R. J., Ichihara, O., Hesterkamp, T. & Hallett, D. Fragments: past, present and future. *Drug Discov Today Technol* **7**, e163-e171 (2010).

19 Andrews, P., Craik, D. & Martin, J. Functional group contributions to drug-receptor interactions. *J Med Chem* **27**, 1648-1657 (1984).

20 Shuker, S. B., Hajduk, P. J., Meadows, R. P. & Fesik, S. W. Discovering high-affinity ligands for proteins: SAR by NMR. *Science* **274**, 1531-1534 (1996).

21 Handling, S. F. The Virtual Elaboration of Fragment Ideas: Growing, Merging and Linking Fragments with Realistic Chemistry.

22   Velvadapu, V., Farmer, B. T. & Reitz, A. B. in *The Practice of Medicinal Chemistry*   161-180 (Elsevier, 2015)

23   Bowling, John J., et al. "Going Small: Using Biophysical Screening to Implement Fragment Based Drug Discovery." *Special Topics in Drug Discovery*, 25 (2016).

24   Herrmann, A. Dynamic combinatorial/covalent chemistry: a tool to read, generate and modulate the bioactivity of compounds and compound mixtures. *Chem Soc Rev* **43**, 1899-1933 (2014).

25   Huc, I. & Lehn, J.-M. Virtual combinatorial libraries: dynamic generation of molecular and supramolecular diversity by self-assembly. *Proc Natl Acad Sci* **94**, 2106-2110 (1997).

26   Ramström, O. & Lehn, J. M. In situ generation and screening of a dynamic combinatorial carbohydrate library against concanavalin A. *ChemBioChem* **1**, 41-48 (2000).

27   Lewis, W. G. *et al.* Click chemistry in situ: acetylcholinesterase as a reaction vessel for the selective assembly of a femtomolar inhibitor from an array of building blocks. *Angew Chem Int Ed Engl* **41**, 1053-1057 (2002).

28   Kubota, Y., Sakamoto, S., Yamaguchi, K. & Fujita, M. Guest-induced organization of an optimal receptor from a dynamic receptor library: Spectroscopic screening. *Proc Natl Acad Sci* **99**, 4854-4856 (2002).

29   Jahnke, W. *et al.* Second-site NMR screening and linker design. *Curr Top Med Chem* **3**, 69-80 (2003).

30   Larsson, R., Pei, Z. & Ramström, O. Catalytic self-screening of cholinesterase substrates from a dynamic combinatorial thioester library. *Angew Chem Int Ed Engl* **43**, 3716-3718 (2004).

31   Congreve, M. S. *et al.* Detection of ligands from a dynamic combinatorial library by X-ray crystallography. *Angew Chem Int Ed Engl* **42**, 4479-4482 (2003).

32   Gelin, M. *et al.* Screening and in situ synthesis using crystals of a NAD kinase lead to a potent antistaphylococcal compound. *Structure* **20**, 1107-1117 (2012).

33   Bourne, Y., Sharpless, K. B., Taylor, P. & Marchot, P. Steric and dynamic parameters influencing in situ cycloadditions to form triazole inhibitors with crystalline acetylcholinesterase. *J Am Chem Soc* **138**, 1611-1621 (2016).

34   Edink, E., Jansen, C., Leurs, R. & de Esch, I. J. The heat is on: thermodynamic analysis in fragment-based drug discovery. *Drug Discov Today Technol* **7**, e189-e201 (2010).

35   Hesterkamp, T., Barker, J., Davenport, A. & Whittaker, M. Fragment based drug discovery using fluorescence correlation spectroscopy techniques: challenges and solutions. *Curr Top Med Chem* **7**, 1582-1591 (2007).

36   Schmidt, M. F., El-Dahshan, A., Keller, S. & Rademann, J. Selective Identification of Cooperatively Binding Fragments in a High-Throughput Ligation Assay Enables Development of a Picomolar Caspase-3 Inhibitor. *Angew Chem Int Ed Engl* **48**, 6346-6349 (2009)

37   Schmidt, M. F. & Rademann, J. Dynamic template-assisted strategies in fragment-based drug discovery. *Trends Biotechnol* **27**, 512-521 (2009).

38   Retra, K., Irth, H. & van Muijlwijk-Koezen, J. E. Surface Plasmon Resonance biosensor analysis as a useful tool in FBDD. *Drug Discov Today Technol* **7**, e181-e187 (2010).

39   Pellecchia, M. *et al.* Perspectives on NMR in drug discovery: a technique comes of age. *Nat Rev Drug Discov* **7**, 738 (2008)

38   Schmidt, M. F., Groves, M. R. & Rademann, J. Dynamic Substrate Enhancement for the Identification of Specific, Second-Site-Binding Fragments Targeting a Set of Protein Tyrosine Phosphatases. *ChemBioChem* **12**, 2640-2646 (2011).

39   Retra, K., Irth, H. & van Muijlwijk-Koezen, J. E. Surface Plasmon Resonance biosensor analysis as a useful tool in FBDD. *Drug Discov Today Technol* **7**, e181-e187 (2010).

40   Jaegle, M. *et al.* Protein-Templated Fragment Ligations—From Molecular Recognition to Drug Discovery. *Angew Chem Int Ed Engl* **56**, 7358-7378 (2017).

41   Mondal, M. *et al.* Fragment Linking and Optimization of Inhibitors of the Aspartic Protease Endothiapepsin: Fragment-Based Drug Design Facilitated by Dynamic Combinatorial Chemistry. *Angew Chem Int Ed Engl* **55**, 9422-9426 (2016).

42   Ramström, O. & Lehn, J.-M. Drug discovery by dynamic combinatorial libraries. *Nat Rev Drug Discov* **1**, 26 (2002).

43   Jaegle, M., Nawrotzky, E., Wong, E. L., Arkona, C. & Rademann, J. Protein-Templated Fragment Ligation Methods: Emerging Technologies in Fragment-Based Drug Discovery. *Fragment-based Drug Discovery: Lessons and Outlook* (2015).

44   Hajduk, P. J. & Greer, J. A decade of fragment-based drug design: strategic advances and lessons learned. *Nat Rev Drug Discov* **6**, 211 (2007).

45   Congreve, M., Chessari, G., Tisi, D. & Woodhead, A. J. Recent developments in fragment-based drug discovery. *J Med Chem* **51**, 3661-3680 (2008).

46   Latchman, D. S. Transcription factors: an overview. *Int J Biochem Cell Biol* **29**, 1305-1312 (1997).

47   Bode, A. M. & Dong, Z. Post-translational modification of p53 in tumorigenesis. *Nat Rev Cancer* **4**, 793 (2004).

48   Levy, D. E. & Darnell Jr, J. Signalling: Stats: transcriptional control and biological impact. *Nat Rev Mol Cell Biol* **3**, 651 (2002).

49   Jacob, F. & Monod, J. Genetic regulatory mechanisms in the synthesis of proteins. *J Mol Biol* **3**, 318-356 (1961).

50   Verdier, F. *et al.* A sequence of the CIS gene promoter interacts preferentially with two associated STAT5A dimers: a distinct biochemical difference between STAT5A and STAT5B. *Mol Cell Biol* **18**, 5852-5860 (1998).

51   Adelman, K. & Lis, J. T. Promoter-proximal pausing of RNA polymerase II: emerging roles in metazoans. *Nat Rev Genet* **13**, 720 (2012).

52   Bannister, A. J. & Kouzarides, T. Regulation of chromatin by histone modifications. *Cell Res* **21**, 381 (2011).

53   Bromberg, J. Stat proteins and oncogenesis. *J Clin Invest* **109**, 1139-1142 (2002).

54   Bar-Natan, M., Nelson, E. A., Xiang, M. & Frank, D. A. STAT signaling in the pathogenesis and treatment of myeloid malignancies. *Jak-Stat* **1**, 55-64 (2012)

55   Yu, H., & Jove, R. The STATs of cancer—new molecular targets come of age. *Nat Rev Cancer* **4**(**2**), 97 (2004).

56   Cumaraswamy, A. A. *et al.* Nanomolar-Potency Small Molecule Inhibitor of STAT5 Protein. *ACS Med Chem Lett* **5**, 1202-1206, doi:10.1021/ml500165r (2014).

57   Cumaraswamy, A. A., Todic, A., Resetca, D., Minden, M. D., & Gunning, P. T. Inhibitors of Stat5 protein signalling. *MedChemComm*, **3**(**1**), 22-27 (2012).

58   Page, B. D. *et al.* Small molecule STAT5-SH2 domain inhibitors exhibit potent antileukemia activity. *J Med Chem* **55**(**3**), 1047-1055 (2012).

59   Tan, S.-H. & Nevalainen, M. T. Signal transducer and activator of transcription 5A/B in prostate and breast cancers. *Endocr Relat Cancer* **15**, 367-390 (2008).

60   Akira, S. Functional roles of STAT family proteins: lessons from knockout mice. *Stem cells* **17**, 138-146 (1999).

61   Schust, J., Sperl, B., Hollis, A., Mayer, T. U., & Berg, T. Stattic: a small-molecule inhibitor of STAT3 activation and dimerization. *Chem Biol*, **13**(**11**), 1235-1242 (2006).

62   Elumalai, N., Berg, A., Natarajan, K., Scharow, A. & Berg, T. Nanomolar Inhibitors of the Transcription Factor STAT5b with High Selectivity over STAT5a. *Angew Chem Int Ed Engl* **54**, 4758-4763 (2015).

63   Grimley, P. M., Dong, F. & Rui, H. Stat5a and Stat5b: fraternal twins of signal transduction and transcriptional activation. *Cytokine Growth F R* **10**, 131-157 (1999).

64   Neculai, D. *et al.* Structure of the unphosphorylated STAT5a dimer. *J Biol Chem* **280**, 40782-40787 (2005).

65   Shin, H. Y. & Reich, N. C. Dynamic trafficking of STAT5 depends on an unconventional nuclear localization signal. *J Cell Sci* **126**, 3333-3343 (2013).

66   Endo, T. A. *et al.* A new protein containing an SH2 domain that inhibits JAK kinases. *Nature* **387**, 921 (1997).

67   Verdier, F. *et al.* Proteasomes regulate erythropoietin receptor and signal transducer and activator of transcription 5 (STAT5) activation Possible involvement of the ubiquitinated Cis protein. *J Biol Chem* **273**, 28185-28190 (1998).

68   Vinkemeier, U., Moarefi, I., Darnell, J. E. & Kuriyan, J. Structure of the amino-terminal protein interaction domain of STAT-4. *Science* **279**, 1048-1052 (1998).

69   Soldaini, E. *et al.* DNA binding site selection of dimeric and tetrameric Stat5 proteins reveals a large repertoire of divergent tetrameric Stat5a binding sites. *Mol Cell Biol* **20**, 389-401 (2000).

70   de Araujo, E. D. *et al.* A functional in vitro assay for screening inhibitors of STAT5B phosphorylation. *J Pharm Biomed Anal* **162**, 60-65 (2019).

71   Elumalai, N. *et al.* Rational development of Stafib-2: a selective, nanomolar inhibitor of the transcription factor STAT5b. *Sci Rep* **7**, 819 (2017).

72   Groner, B., & von Manstein, V. Jak Stat signaling and cancer: Opportunities, benefits and side effects of targeted inhibition.1-14 (2017).

73   Kiu, H. & Nicholson, S. E. Biology and significance of the JAK/STAT signalling pathways. *Growth factors* **30**, 88-106 (2012).

74   Quintás-Cardama, A., Kantarjian, H., Cortes, J. & Verstovsek, S. Janus kinase inhibitors for the treatment of myeloproliferative neoplasias and beyond. *Nat Rev Drug Discov* **10**, 127 (2011).

75   Heine, A. *et al.* The JAK-inhibitor ruxolitinib impairs dendritic cell function in vitro and in vivo. *Blood* **122**, 1192-1202 (2013).

76   Recio, Carlota, et al. "JAK, an Oncokinase in Hematological Cancer." *Function of Tyrosine Kinases and Related Network in Cancer*. IntechOpen, 2019..

77   Pardanani, A. *et al.* Safety and efficacy of TG101348, a selective JAK2 inhibitor, in myelofibrosis. *J Clin Oncol* **29**, 789 (2011).

78   Yoshimoto, G. *et al.* FLT3-ITD up-regulates MCL-1 to promote survival of stem cells in acute myeloid leukemia via FLT3-ITD–specific STAT5 activation. *Blood* **114**, 5034-5043 (2009).

79   Kottaridis, P. D. *et al.* The presence of a FLT3 internal tandem duplication in patients with acute myeloid leukemia (AML) adds important prognostic information to cytogenetic risk group and response to the first cycle of chemotherapy: analysis of 854 patients from the United Kingdom Medical Research Council AML 10 and 12 trials. *Blood* **98**, 1752-1759 (2001).

80   Choudhary, C. *et al.* AML-associated Flt3 kinase domain mutations show signal transduction differences compared with Flt3 ITD mutations. *Blood* **106**, 265-273 (2005).

81   Levis, M. *et al.* Results from a randomized trial of salvage chemotherapy followed by lestaurtinib for patients with FLT3 mutant AML in first relapse. *Blood* **117**, 3294-3301 (2011).

82   Zhang, W. *et al.* Mutant FLT3: a direct target of sorafenib in acute myelogenous leukemia. *J Natl Cancer Inst* **100**, 184-198 (2008).

83   Turhan, A. G. STAT5 as a CML target: STATinib therapies? *Blood* **117**, 3252-3253 (2011).

84   Nelson, E. A. *et al.* The STAT5 inhibitor pimozide decreases survival of chronic myelogenous leukemia cells resistant to kinase inhibitors. *Blood* **117**, 3421-3429 (2011).

85   Grunwald, M. R. & Levis, M. J. FLT3 inhibitors for acute myeloid leukemia: a review of their efficacy and mechanisms of resistance. *Int J Hematol* **97**, 683-694 (2013).

86   Knapper, S. FLT3 inhibition in acute myeloid leukaemia. *Br J Haematol* **138**, 687-699 (2007).

87   Shuai, K., Halpern, J., Rao, X. & Sawyers, C. Constitutive activation of STAT5 by the BCR-ABL oncogene in chronic myelogenous leukemia. *Oncogene* **13**, 247-254 (1996).

88   Warmuth, M., Danhauser-Riedl, S. & Hallek, M. Molecular pathogenesis of chronic myeloid leukemia: implications for new therapeutic strategies. *Ann Hematol* **78**, 49-64 (1999).

89   Hantschel, O. & Superti-Furga, G. Regulation of the c-Abl and Bcr–Abl tyrosine kinases. *Nat Rev Mol Cell Biol* **5**, 33 (2004).

90   Druker, B. J. STI571 (Gleevec™) as a paradigm for cancer therapy. *Trends Mol Med* **8**, S14-S18 (2002).

91   Weisberg, E. *et al.* AMN107 (nilotinib): a novel and selective inhibitor of BCR-ABL. *Br J Cancer* **94**, 1765 (2006).

92   Kantarjian, H. M. *et al.* Nilotinib (formerly AMN107), a highly selective BCR-ABL tyrosine kinase inhibitor, is effective in patients with Philadelphia chromosome–positive chronic myelogenous leukemia in chronic phase following imatinib resistance and intolerance. *Blood* **110**, 3540-3546 (2007).

93   Rix, U. *et al.* Chemical proteomic profiles of the BCR-ABL inhibitors imatinib, nilotinib, and dasatinib reveal novel kinase and nonkinase targets. *Blood* **110**, 4055-4063 (2007).

94   Hantschel, O., Rix, U. & Superti-Furga, G. Target spectrum of the BCR-ABL inhibitors imatinib, nilotinib and dasatinib. *Leuk Lymphoma* **49**, 615-619 (2008).

95   Weber, A. *et al.* Stat5 Exerts Distinct, Vital Functions in the Cytoplasm and Nucleus of Bcr-Abl+ K562 and Jak2 (V617F)+ HEL Leukemia Cells. *Cancers* **7**, 503-537 (2015).

96   Mizuki, M. *et al.* Flt3 mutations from patients with acute myeloid leukemia induce transformation of 32D cells mediated by the Ras and STAT5 pathways. *Blood* **96**, 3907-3914 (2000).

97   Shuai, K. & Liu, B. Regulation of JAK–STAT signalling in the immune system. *Nat Rev Immunol* **3**, 900 (2003).

98   Nosaka, T. *et al.* STAT5 as a molecular regulator of proliferation, differentiation and apoptosis in hematopoietic cells. *EMBO J* **18**, 4754-4765 (1999).

99   Chen, Y. *et al.* Identification of Shp-2 as a Stat5A phosphatase. *J Biol Chem* **278**, 16520-16527 (2003).

100   Chughtai, N., Schimchowitsch, S., Lebrun, J.-J. & Ali, S. Prolactin induces SHP-2 association with Stat5, nuclear translocation, and binding to the β-casein gene promoter in mammary cells. *J Biol Chem* **277**, 31107-31114 (2002).

101   Kawashima, T. *et al.* A Rac GTPase-activating protein, MgcRacGAP, is a nuclear localizing signal-containing nuclear chaperone in the activation of STAT transcription factors. *Mol Cell Biol* **29**, 1796-1813 (2009).

102   Rycyzyn, M. A. & Clevenger, C. V. The intranuclear prolactin/cyclophilin B complex as a transcriptional inducer. *Proc Natl Acad Sci* **99**, 6790-6795 (2002).

103   Pham, H. T. T. *et al.* STAT5B N642H is a driver mutation for T cell neoplasia. *J Clin Invest* **128**, 387-401 (2018).

104   Mi, T., Wang, Z. & Bunting, K. The Cooperative Relationship between STAT5 and Reactive Oxygen Species in Leukemia: Mechanism and Therapeutic Potential. *Cancers* **10**, 359 (2018).

105   de Araujo, E. D. *et al.* Structural and functional consequences of the STAT5B N642H driver mutation. *Nat Commun* **10**, 2517 (2019).

106   Pham, H. T. T., Hengstschläger, M. & Moriggl, R. A haunted beast: Targeting STAT5BN642H in T-Cell Neoplasia. *Mol Cell Oncol* **5**, e1435181 (2018).

107   Nelson, E. A. *et al.* The STAT5 Inhibitor Pimozide Displays Efficacy in Models of Acute Myelogenous Leukemia Driven by FLT3 Mutations. *Genes Cancer* **3**, 503-511(2012).

108   Müller, J., Schust, J. & Berg, T. A high-throughput assay for signal transducer and activator of transcription 5b based on fluorescence polarization. *Anal Biochem* **375**, 249-254 (2008).

109   Liu, L.-J. *et al.* Antagonizing STAT5B dimerization with an osmium complex. *Sci Rep* **6**, 36044 (2016).

110   Wingelhofer, B. *et al.* Pharmacologic inhibition of STAT5 in acute myeloid leukemia. *Leukemia* **32**, 1135 (2018).

111   Erlanson, D. A. *et al.* Site-directed ligand discovery. *Proc Natl Acad Sci* **97**, 9367-9372 (2000)

112   Suzuki, T. *et al.* An unexpected example of protein-templated click chemistry. *Angew Chem Int Ed Engl* **49**, 6817-6820 (2010).

113   Hu, X., Sun, J., Wang, H.-G. & Manetsch, R. Bcl-XL-templated assembly of its own protein− protein interaction modulator from fragments decorated with thio acids and sulfonyl azides. *J Am Chem Soc* **130**, 13820-13821 (2008).

114   Jaegle, M., Steinmetzer, T. & Rademann, J. Protein-Templated Formation of an Inhibitor of the Blood Coagulation Factor Xa through a Background-Free Amidation Reaction. *Angew Chem Int Ed Engl* **56**, 3718-3722 (2017).

115   Kraskouskaya, D., Duodu, E., Arpin, C. C. & Gunning, P. T. Progress towards the development of SH2 domain inhibitors. *Chem Soc Rev* **42**, 3337-3370 (2013).

116   Wong, E. L. *et al.* The transcription factor STAT5 catalyzes Mannich ligation reactions yielding inhibitors of leukemic cell proliferation. *Nat Commun* **10**, 66 (2019)

117   Horatscheck, A. *et al.* Benzoylphosphonate-Based Photoactive Phosphopeptide Mimetics for Modulation of Protein Tyrosine Phosphatases and Highly Specific Labeling of SH2 Domains. *Angew Chem Int Ed Engl* **51**, 9441-9447 (2012).

118   Krishna, S. N. *et al.* A fluorescence-based thermal shift assay identifies inhibitors of mitogen activated protein kinase kinase 4. *PloS one* **8**, e81504 (2013).

119   Lin, J.-X. *et al.* Critical Role of STAT5 transcription factor tetramerization for cytokine responses and normal immune function. *Immunity* **36**, 586-599 (2012).

120   Barr, A. J. *et al.* Large-scale structural analysis of the classical human protein tyrosine phosphatome. *Cell* **136**, 352-363 (2009).

121   Hirsch, A. K., Fischer, F. R. & Diederich, F. Phosphate recognition in structural biology. *Angew Chem Int Ed Engl* **46**, 338-352 (2007).

122   Trott, O. & Olson, A. J. AutoDock Vina: improving the speed and accuracy of docking with a new scoring function, efficient optimization, and multithreading. *J Comput Chem* **31**, 455-461 (2010).

123   Goodsell, D. S., Morris, G. M. & Olson, A. J. Automated docking of flexible ligands: applications of AutoDock. *J Mol Recognit* **9**, 1-5 (1996).

124   Durrant, J. D. & McCammon, J. A. BINANA: a novel algorithm for ligand-binding characterization. *J Mol Graph Model* **29**, 888-893 (2011).

125   Nam, S. *et al.* Indirubin derivatives induce apoptosis of chronic myelogenous leukemia cells involving inhibition of Stat5 signaling. *Mol Oncol* **6**, 276-283 (2012).

126   Qian, Y.-H., Xiao, Q., Chen, H. & Xu, J. Dexamethasone inhibits camptothecin-induced apoptosis in C6-glioma via activation of Stat5/Bcl-xL pathway. *Biochim Biophys Acta Mol Cell Res* **1793**, 764-771 (2009).

127   Almqvist, H. *et al.* CETSA screening identifies known and novel thymidylate synthase inhibitors and slow intracellular activation of 5-fluorouracil. *Nat Commun* **7**, 11040 (2016).

128   Blumert, C. *et al.* Analysis of the STAT3 interactome using in-situ biotinylation and SILAC. *J Proteomics* **94**, 370-386 (2013).

129   Motulsky, H. *Analyzing data with GraphPad prism.* (GraphPad Software Incorporated, 1999).

130   Schneider, C. A., Rasband, W. S. & Eliceiri, K. W. NIH Image to ImageJ: 25 years of image analysis. *Nat Methods* **9**, 671 (2012).

131   Mann, M. Innovations: Functional and quantitative proteomics using SILAC. *Nat Rev Mol Cell Biol* **7**, 952 (2006).

132   Ong, S.-E. & Mann, M. A practical recipe for stable isotope labeling by amino acids in cell culture (SILAC). *Nat Protoc* **1**, 2650 (2006).

133   Mizuki, M. *et al.* Flt3 mutations from patients with acute myeloid leukemia induce transformation of 32D cells mediated by the Ras and STAT5 pathways. *Blood* **96**, 3907-3914 (2000).

134   Kindler, T., Lipka, D. B. & Fischer, T. FLT3 as a therapeutic target in AML: still challenging after all these years. *Blood* **116**, 5089-5102 (2010).

135   Mandal, P. K. *et al.* Potent and Selective Phosphopeptide Mimetic Prodrugs Targeted to the Src Homology 2 (SH2) Domain of Signal Transducer and Activator of Transcription 3. *J Med Chem* **54**, 3549-3563 (2011).

136   Fang, F., Antico, G., Zheng, J. & Clevenger, C. V. Quantification of PRL/Stat5 signaling with a novel pGL4-CISH reporter. *BMC Biotechnol* **8**, 11 (2008).

137   Silva, M. *et al.* Erythropoietin can induce the expression of bcl-xlthrough stat5 in erythropoietin-dependent progenitor cell lines. *J Biol Chem* **274**, 22165-22169 (1999).

138   Jafari, R. *et al.* The cellular thermal shift assay for evaluating drug target interactions in cells. *Nat Protoc* **9**, 2100 (2014).

139   Molina, D. M. *et al.* Monitoring drug target engagement in cells and tissues using the cellular thermal shift assay. *Science* **341**, 84-87 (2013).

140   Krutzik, P. O., Crane, J. M., Clutter, M. R. & Nolan, G. P. High-content single-cell drug screening with phosphospecific flow cytometry. *Nat Chem Biol* **4**, 132 (2008).

141   Chou, T.-C. Drug combination studies and their synergy quantification using the Chou-Talalay method. *Cancer Res* **70**, 440-446 (2010).

142   Chou, T.-C. & Talalay, P. Quantitative analysis of dose-effect relationships: the combined effects of multiple drugs or enzyme inhibitors. *Adv Enzyme Regul* **22**, 27-55 (1984).

143   Chong, S. J. F., Lai, J. X. H., Eu, J. Q., Bellot, G. L. & Pervaiz, S. Reactive oxygen species and oncoprotein signaling-a dangerous liaison. *Antioxid Redox Signal* **29**, 1553-1588 (2018).

144   Bourgeais, J., Gouilleux-Gruart, V. & Gouilleux, F. Oxidative metabolism in cancer: A STAT affair? *Jak-Stat* **2**, e25764 (2013).

145   Stupp, R. *et al.* Radiotherapy plus concomitant and adjuvant temozolomide for glioblastoma. *New England Journal of Medicine* **352**, 987-996 (2005).

146   Fabbro, D. *et al.* PKC412-a protein kinase inhibitor with a broad therapeutic potential. *Anti-cancer drug design* **15**, 17-28 (2000).

147   Weisberg, E. *et al.* Inhibition of mutant FLT3 receptors in leukemia cells by the small molecule tyrosine kinase inhibitor PKC412. *Cancer cell* **1**, 433-443 (2002).

148   Page, B. D. *et al*. Inhibiting aberrant signal transducer and activator of transcription protein activation with tetrapodal, small molecule Src homology 2 domain binders: promising agents against multiple myeloma. *J Med Chem* **56**(**18**), 7190-7200 (2013).

149   Lim, J. S. J. *et al.* Extended cohort study of OPB51602, a novel inhibitor of STAT3/5 activation, in non-small cell lung carcinoma. *J Clin Oncol* 8028-8028 (2014).

150   Brewer, T. F. & Chang, C. J. An aza-cope reactivity-based fluorescent probe for imaging formaldehyde in living cells. *J Am Chem Soc* **137**, 10886-10889 (2015).

151   LaRochelle, J. R. *et al.* Identification of an allosteric benzothiazolopyrimidone inhibitor of the oncogenic protein tyrosine phosphatase SHP2. *Bioorg Med Chem* **25**, 6479-6485 (2017).

152   Krutzik, P. O. & Nolan, G. P. Fluorescent cell barcoding in flow cytometry allows high-throughput drug screening and signaling profiling. *Nat. Methods* **3**, 361 (2006).

153   Wagner, S., Schütz, A. & Rademann, J. Light-switched inhibitors of protein tyrosine phosphatase PTP1B based on phosphonocarbonyl phenylalanine as photoactive phosphotyrosine mimetic. *Bioorg Med Chem* **23**, 2839-2847 (2015).

Publications

Peer reviewed articles

E.L Wong., E. Nawrotzky., C. Arkona., B.G.Kim, S.Beligny., X.Wang,…,J. Rademann. The transcription factor STAT5 catalyzes Mannich ligation reactions yielding inhibitors of leukemic cell proliferation. *Nat. Commun* **10(1)**, 66 (2019).

M. Jaegle, **E. L. Wong**, C. Tauber, E. Nawrotzky, C. Arkona, J. Rademann "Protein-templated fragment ligations: from molecular recognition to drug discovery", *Angew. Chem. Int. Ed.*, **56**, 7358-7378 (2017).

F. Müller, S. Hönzke, W.-O. Luthardt, **E. L. Wong**, M. Unbehauen, J. Bauer, R. Haag, S. Hedtrich, E. Rühl, J. Rademann "Rhamnolipids form drug-loaded nanoparticles for dermal drug delivery", *Eur. J. Pharm. Biopharm.*, **116**, 31-37.(2017)

Patent

J. Rademann, **E. L. Wong**, C. Arkona, B. G. Kim, E. Nawrotzky "Novel furazan-3-carboxylic acid derivatives and use thereof in treatment of cancer" Europäische Patentanmeldung 16192394.1 (Europe: EP 17 787 891.5)

Book chapter

M. Jaegle, E. Nawrotzky, **E. L. Wong**, C. Arkona, J. Rademann "Protein-templated fragment ligation methods: emerging technologies in fragment-based drug discovery", In: Fragment-based drug discovery (W. Jahnke, D. Erlanson, eds.), Wiley-VCH, Weinheim 2016, 292-326.